June 21, 2017

U.S. Forest Service
ATTN: Joby P. Timm
5162 Valleypointe Parkway
Roanoke, VA 24019

Re: United States Forest Service letter Comments
        on the Hydrological Analysis of Sedimentation dated April 25, 2017
        OEP/DG2E/Gas3
        Mountain Valley Pipeline, LLC
        Docket No. CP16-10-000

Dear Mr. Timm:

Mountain Valley Pipeline, LLC (Mountain Valley or MVP) received comments from the United States Forest Service (USFS) in a letter dated April 25, 2017 regarding MVP's Hydrological Analysis of Sedimentation. On May 9, 2017, a conference call was held between the USFS, the Bureau of Land Management (BLM), and MVP to discuss and clarify various aspects of the comments. As a follow-up, MVP committed to providing USFS with additional information supporting the sedimentation analysis.

This additional information included the reference documents cited in the analysis including: The Performance Evaluation of Two Silt Fence Geosynthetic Fabrics During and After Rainfall Event by Gregg Steven Dubinski (Attachment 1); a turbidity monitoring study completed by the United States Geological Survey (Attachment 2); details regarding site specific erosion control measures to be employed along Craig Creek (Attachment 3); and additional details supporting various aspects of the analysis (Attachment 4). The Hydrological Analysis on Sedimentation was updated to reflect this additional information and was provided to the USFS and BLM on June 9, 2017. As a follow up to the May 9, 2017 conference call and the comment letter, MVP has provided responses to each of the USFS comments in detail below.

USFS Recommendation No. 1: Section 2.1 (page 3) is written from the perspective of large watershed basins located within the Jefferson National Forest (JNF). The focus of the assessment should not be on the percentage of a stream's watershed area within the JNF; rather, the emphasis should be on what percentage of a stream's watershed is within the proposed Limit of Disturbance (LOD) for the MVP Project.

As an example, Table 1 indicates the subwatersheds that have a portion of their area within the LOD, and documents the portion of the subwatershed area that is within the JNF. This is extraneous information that does not help create an overall understanding of the impacts of the MVP Project. Update the analysis to include a LOD comparison.

Mountain Valley Response No. 1: The text in this section has been revised, including Table 1, to include Project area requirements within watersheds and baseline conditions.

USFS Recommendation No. 2: Section 2.2 (page 7). The report indicates that temporary access roads are converted to "established but not mature" vegetation four weeks after recovery. This is an unreasonable time scale for establishment of suitable vegetation, depending on soil type, season, rainfall, etc. It is more appropriate to err on the side of the worst case scenario, rather than the best case. Update the analysis to reflect a reasonable time scale for revegetation.

Mountain Valley Response No. 2: The estimated timeframe for establishment of herbaceous erosion controls on temporary access roads is a reasonable expectation based on knowledge of the species selected for this purpose. Mountain Valley understands that environmental factors can influence germination and establishment, such as shade, temperature, precipitation, and time of year, but temporary cover species are selected for their abilities to rapidly germinate and establish, as well as tolerate drought and infertile soils. In comparison to other plant species, grasses are among the quickest to establish with high daily root biomass growth and high total biomass growth (Gross et al. 1992). Many state erosion control manuals reflect this high growth rate. For example, the New Hampshire Stormwater Manual requires vegetated growth covering at least 85% within a four- to eight- week time frame (Comprehensive Environmental Inc. and NHDES 2008). This far exceeds the ground cover expectations used for the sedimentation analysis for the Project (10-50% coverage within four weeks [see Table 2 in the report]). Furthermore, the erosion control instructional modules provided by the Virginia Department of Environmental Quality state that grasses can establish a ground cover within just one or two weeks. This is reflected in the inspections requirement that typically occur two to six weeks after seeding. Therefore, four weeks does not represent an unreasonable time scale, but rather the median of a range that is generally accepted by agencies as the norm.

The suggestion to use a worst-case scenario is inconsistent with case law and regulations for implementing the impact analysis under the National Environmental Policy Act (NEPA). At one point, the Council on Environmental Quality's (CEQ's) NEPA regulations contained a requirement to prepare a worst-case analysis when complete information was lacking. CEQ rescinded this regulation, finding that the worst-case analysis requirement was "an unproductive and ineffective method" of achieving NEPA's disclosure goals and could "breed endless hypothesis and speculation." The current regulation directs agencies to provide "a summary of existing credible scientific evidence which is relevant to evaluating the reasonably foreseeable significant adverse impacts on the human environment" and "the agency's evaluation of such impacts based upon theoretical approaches or research methods generally accepted in the scientific community." The U.S. Supreme Court has confirmed that the NEPA analysis should focus on "reasonably foreseeable impacts" and that no worst-case scenario is required. Other courts have likewise stressed that NEPA does not require a worst-case analysis. Because the four weeks is supportable and represents the reasonably foreseeable timeframe for establishing ground cover, using this timeframe is appropriate for evaluating potential impacts.

References:
Comprehensive Environmental Inc. and the NHDES. 2008. New Hampshire Stormwater Manual. Volume: Erosion and Sediment Controls During Construction.

Gross, K. L., D. Maruca, and K.S. Pregitzer. 1992. Seedling growth and root morphology of plants with different life histories. The New Phytologist 120(4): 535-542.

USFS Recommendation No. 3: Section 2.2 (page 8). The effects of tree clearing are considered by using a cover and management factor of "bare soil land class scraped at the surface." An estimate of bare soil scraped at the surface may underestimate the sediment generated from the activity if the tree clearing will be

performed by machines rather than manually. Further, a portion of the LOD will have topsoil segregation impacts. Update analysis to reflect a cover factor equal to or greater than 0.250.

Mountain Valley Response No. 3: The cover and management factor for tree clearing (0.15) was selected because vegetation would generally be cut or scraped flush with the surface of the ground during tree clearing, leaving rootstock in place where possible. The density of this root system is expected to inhibit erosive forces. This fact was reflected in the Office of Surface Mining's "Guidelines for the Use of the Revised Universal Soil Loss Equation Revised Universal Soil Loss Equation Version 1.06 on Mined Lands, Construction Sites, and Reclaimed Lands" (see Galetovic 1998), which was the source for the cover and management factor. It should also be noted that after tree clearing, the limits of disturbance (LOD) for MVP will not be entirely bare soil; the LOD will include soil stockpiles that will be mulched and tree root structures will remain until crews being trenching the right-of-way. Soil loss will be inhibited by remaining roots and vegetative residue on the soil surface (Wischmeier and Smith 1978).

Dissmeyer and Foster (1992) suggest that soil loss in cleared areas is a function of remaining roots, canopy, steps, depression storage, and organic content. For untilled soils, the potential for erosion is likely less than or equal to the 0.15 value used in the MVP analysis. This is based on the limits of disturbance containing 80 percent or less of bare soil and the bare soil containing at least 20 percent fine roots in the top 3 centimeters of soil (Dissmeyer and Foster 1992). A larger percentage of bare soil (90-100%) may also result in similar erosion if fine roots are present at a higher percentage (60-100%).

Topsoil segregation is not expected to occur until right-of-way grubbing and grading occur. Therefore, no bare soils due to topsoil segregation are expected during the tree clearing phase. However, once the topsoil is segregated, it will be seeded and mulched by the end of the working day.

References:

Dissmeyer, G. E. and G. E. Foster. 1980. A guide for predicting sheet and rill erosion on forest land. U.S. Department of Agriculture, U.S. Forest Service, Southeastern Area, Technical Publication SA-TP 11, Atlanta, GA. 40 pp.

Galetovic, J. R. 1998. Guidelines for the use of the Revised Universal Soil Loss Equation (RUSLE) version on mined lands, construction sites, and reclaimed lands. T. J. Toy and G. R. Foster, eds. The Office of Technology Transfer, Western Regional Coordinating Center, Office of Surface Mining, Denver, Colorado. 148 pp.

Wischmeier, W. H. and D. D. Smith. 1965. Predicting rainfall-erosion losses from cropland east of the Rocky Mountains. USDA Agricultural Handbook 282. 47 pp.

USFS Recommendation No. 4: Section 2.3.5 (pages 12-13). This section clearly demonstrates the wide variety of effectiveness, even citing as low as 10% (EPA 1993). Yet the assumption chosen for the practice factor is very high. p=0.21 such that containment is 79%. Since many of the literature citations are laboratory based and proper installation is widely understood in the industry to be a limiting factor for effectiveness in the field, this is a vast overestimate of containment. It is more appropriate to err on the side of the worst case scenario, rather than the best case. Update the analysis to reflect a conservative p factor, equal to or less than 48% containment.

Mountain Valley Response No. 4: Mountain Valley participated on a conference call with USFS on May 9, 2017 to discuss the chosen practice factor. Following the meeting Mountain Valley provided the USFS with The Performance Evaluation of Two Silt Fence Geosynthetic Fabrics During and After Rainfall Event by Gregg Steven Dubinski (Attachment 1), a turbidity monitoring study completed by the United States

Geological Survey (Attachment 2), details regarding site specific erosion control measures to be employed along Craig Creek (Attachment 3), and additional details supporting various aspects of the analysis (Attachment 4).

The studies cited in this section use both field and laboratory investigations (e.g., Farias et al. [2006], Faucette et al. [2008], Faucette et al. [2009]) and these studies were used in tandem with information from the Dubinsky 2014 study describing field-scale tests to provide a range of efficiencies that are reasonably attainable. The 79% containment is not the best-case scenario, but rather the mean reported value for both silt fences and compost filter socks, two predominant controls proposed to be used on the Project ROW.

USFS Recommendation No. 5: Section 2.4 (page 14). There are coefficients and exponents used in Eq. 4 that are referenced to the 1983 National Engineering Handbook. The reference does not include the coefficients. The report should provide the source of the coefficients for verification.

Mountain Valley Response No. 5: Mountain Valley understands that the NRCS (1983) citation does not have coefficients. This curve has been converted to Eq. 4 in previous sources, and these coefficients have been used by many agencies and authors in several publications and reports, most notably it is a component of the EPA's BASIN tool (USEPA 2006). Please see the references listed below for verification of the coefficients. The NRCS (1983) citation was used because it was the original source for the curve.

References:
ADEM. 2002. Siltation TMDL development for 22 segments in the Lower Tennessee River Basin. Alabama Department of Environmental Management (ADEM), Water Quality Branch, Montgomery, Alabama.

ICPRB. 2012. Modeling framework for simulating hydrodynamics and water quality in the Liberty Reservoir, Baltimore and Carroll Counties, Maryland. Final report prepared for the Maryland Department of the Environment. Interstate Commission on the Potomac River Basin (ICPRB), Rockville, MD.

Jackson, C.R., J. K. Martin, D. S. Leigh, and L.T. West. 2005. A southeastern piedmont watershed sediment budget: evidence for a multi-millennial agricultural legacy. Journal of Soil and Water Conservation 60(6): 298-310.

McKee, L.J., M. Lewicki, D.H. Schoellhamer, and N.K. Ganju. 2013. Comparison of sediment supply to San Francisco Bay from watersheds draining the Bay Area and the Central Valley of California. Marine Geology 345: 47-62.

MDE. 2010. Water quality analysis of sediment in Middle Patuxent River, Howard County, Maryland. Final Report submitted to the U.S. Environmental Protection Agency, Maryland Department of the Environment (MDE), Baltimore, Maryland.

USEPA. 2006. EPA BASINS Technical Note 8: sediment parameter and calibration guidance for HSPF. U.S. Environmental Protection Agency (USEPA), Office of Water, Washington, D.C.

USFS Recommendation No. 6: Section 2.4 (pages 14-15). The report states that sediment will not be transported downstream of impoundments. While this is generally true, small impoundments may pass sediment during high flow events. The size of the impoundment relative to the surrounding watershed should be reviewed prior to issuing a general statement.

Mountain Valley Response No. 6: The sedimentation report states that instream impoundments can arrest the "majority" of sediments, but that the ultimate fate of sedimentation will be estuarine and/or marine environments. MVP acknowledges that sediment may pass impoundments during high-flow events, however, during normal flows, it is the nature of the reservoir to reduce flow velocity, thus encouraging sediment deposition. Incorporation in the model creates a more realistic estimate of both baseline and proposed effects. This was expressed within the USFS's Final Environmental Impact Statement (FEIS) for the Revised Land and Resource Management Plan (RLRMP) for the Jefferson National Forest (USFS 2004). The USFS recognized that within the soil loss analysis performed for the FEIS, not incorporating the effect of dams as sediment traps led to a "non-perfect representation" of current and future annual sediment yields. As implied in the comment, there are methods to estimate the trapping efficiency. However, even the most basic models require information about storage capacity (see Brown 1943 cited in Verstraeten and Poesen 2000) or annual inflow (Brune 1953), which is not available for most impoundments within the National Hydrography Dataset. More accurate models require even more information, including, but not limited to, particle-size distribution, runoff volume, peak discharge, base flow, pond typology, surface area, shape, outlet dimensions, outlet type, location of the outlet, and properties of the bottom surface (Verstraeten and Poesen 2000). Despite the inability to model sediment transport through impoundments due to data limitations, incorporating impoundments into the analysis provides a more realistic expectation regarding sediment transport.

References:
Brune, G.M. 1953. Trap efficiency of reservoirs. Transactions of the American Geophysical Union 34: 407-418.

USFS. 2004. Final Environmental Impact Statement for the Revised Land and Resource Management Plan: Jefferson National Forest. U.S. Department of Agriculture, Forest Service Southern Region, Management Bulletin R8-MB 115B, Atlanta, Georgia. 588 pp.

Verstraeten, G. and J. Poesen. 2000. Estimating trap efficiency of small reservoirs and ponds: methods and implications for the assessment of sediment yield. Progress in Physical Geography 24(2): 2519-251.

USFS Recommendation No. 7: Section 2.5 (pages 15-16). Stream power gradient is presented as change in unit stream power over length (Equation 8), referenced from Lea and Legleiter. The equation is provided, but the variable "s" as used be Lea and Legleiter is not defined and is therefore easily confused with the variable "S" presented earlier in Equation 6.

MVP's report suggests that a negative stream power gradient indicates deposition and a positive stream power gradient indicates erosion. Lea and Legleiter indicate that this is generally true, but that there is a critical stream power that needs to be considered to indicate magnitude of erosion and deposition. No consideration is given to this critical value and no reference is made about stream flow discharge (cfs) assumptions.

Channel geometry and morphology can also influence erosion and deposition potential within a stream reach. The equation presented does not include effects of such items as meander pools, which would have sufficient energy to mobilize sediment but not necessarily a steep slope.

Provide clarification and further define how the stream power gradient factor, discharge, and channel geometry/morphology were utilized or incorporate updates appropriately in the analysis.

Mountain Valley Response No. 7: The function $-\frac{\partial \omega}{\partial s}$ represents mean stream power gradient.

Although not technically a parameter, the "*ssss*" represents space, which is approximated by the length of the stream segment. Mountain Valley has updated this in the text to provide clarification.

No "critical value" was provided for the stream power gradient, because this relationship is relative and not absolute. Therefore, values cannot be attributed to critical thresholds, but can be compared among each other to provide a relative degree of erosion or deposition (see Figure 1 from Lea and Legleiter [2016]). Power gradients within the document were estimated using bankfull discharges and widths (as discussed in the last paragraph of Section 2.5). Table 6 (now referenced as Table 7), has been updated to include these power gradient values, and the determinations have been expanded to include sources of the regional curves (i.e., Keaton et al. 2005).

Mountain Valley agrees that channel geometry and morphology can also influence erosion. However, limited information is available within publically available datasets regarding channel geometry and morphology. These attributes are beyond the scale of the dataset used to derive sediment loads and stream power using a digital elevation model and the national hydrograph dataset.

Section 3.3 of the report has been adapted to reflect that other depositional areas may be present beyond those identified using stream gradient, but these areas were not identified due to the scale of the analysis and data available.

References:
Keaton, J. N., T. Messinger, and E. J. Doheny. 2005. Development and analysis of regional curves for streams in the non-urban Valley and Ridge Physiographic Province, Maryland, Virginia, and West Virginia. U.S. Department of the Interior, U.S. Geological Survey, Scientific Investigations Report 2005-5076, Reston, Virginia. 116 pp.

Lea, D. M. and C. J. Legleiter. 2016. Mapping spatial patterns of stream power and channel change along a gravel-bed river in northern Yellowstone. Geomorphology 252:66-79.

USFS Recommendation No. 8: <u>Section 2.6 (page 16). Regional curves for streams – typo – missing an 's'.</u>

Mountain Valley Response No. 8: This error has been corrected.

USFS Recommendation No. 9: <u>Section 2.6 (page 16). The analysis method is discussed but no examples of how the analysis was performed are provided. A full review of the RUSLE methodology should include an example of how soil, cover, slope length, etc. were utilized to develop a soil loss estimate. Please provide raw data sheets and descriptive analysis methods as appendices to this report.</u>

Mountain Valley Response No. 9: The analysis was performed within a Geographic Information Systems (GIS) environment and the report was generated with a level of detail such that one could replicate the methods used. Because the soil loss and sedimentation was estimated using a 10-meter cell resolution, the data output is so large that providing datasheets is not feasible. Instead, a descriptive appendix detailing the analysis methods applied within the GIS is provided as Appendix A in the Hydrological Analysis of Sedimentation Report. Appendix A includes Python, R, and Raster Calculator programing scripts used to generate soil loss and sediment delivery. Appendix A also discusses the inputs used to estimate erodibility, erosivity, management impacts, and slope length.

USFS Recommendation No. 10: Section 2.6 (page 17). The commonly used threshold of 10% may be a valid assumption for reaches meeting water quality standards or do not contain sensitive aquatic biota. However, in downstream areas where TES aquatic species are present, it is important to further evaluate cumulative impacts less than 10% increase in sediment load, particularly if construction may coincide with low flow conditions.

For example, Stony Creek with the presence of Candy Darter and Craig Creek with several TES species. Update the analysis to include cumulative effects delineation for Stony Creek and Craig Creek, and track updates (where appropriate) in the tables and figures.

Sensitive species must receive special management emphasis to ensure their viability and to preclude trends toward endangerment that would result in the need for Federal listing. If there are impacts to sensitive species the FS must analyze the significance of adverse effects on the populations, its habitat, and on the viability of the species as a whole. (FSM 2672.1)

The agency is required to document in the BE activities in sufficient detail to determine how an action may affect sensitive species. Thus, project actions taken on private property that may affect these species must be analyzed to determine any and all direct, indirect, and cumulative impacts of the propose action.

Mountain Valley Response No. 10: Mountain Valley participated on a conference call with USFS on May 9, 2017 to discuss the 10% threshold for sedimentation increases from baseline. Following the meeting Mountain Valley provided USFS: a report title "The Performance Evaluation of Two Silt Fence Geosynthetic Fabrics During and After Rainfall Event" by Gregg Steven Dubinski (Attachment 1); a turbidity monitoring study completed by the United States Geological Survey (Attachment 2); details regarding site specific erosion control measures to be employed along Craig Creek (Attachment 3); and additional details supporting various aspects of the analysis (Attachment 4). The Sedimentation Analysis explains that no nationally accepted sedimentation standard or exceedance threshold for sediment is available. The level of 10 percent was chosen because it was a commonly used impact threshold for sediment metrics in a review conducted by the U.S. Environmental Protection Agency (USEPA 2003). Additional detail is provided in Section 2.6 of the Sedimentation Analysis.

USFS Recommendation No. 11: Section 3.0 (pages 17). We understand that a broad evaluation of the full sub- watersheds has been used to develop the estimate of percentage increase in sediment load to the water bodies of interest. However, it is more beneficial to evaluate and compare the effects of construction on a scale equal to the LOD. This would allow a comparison of potential sediment increase in the local environs immediately downgradient of the construction activities. Update analysis to include a LOD comparison.

Mountain Valley Response No. 11: A full subwatershed evaluation was not used for the analysis. Instead, Mountain Valley estimated soil loss, under both baseline and proposed action conditions, within each unique catchment belonging to a stream segment within the 1:24,000 National Hydrograph Dataset (NHD), using the Revised Universal Soil Loss Equation (RUSLE). In addition to estimating soil loss, sediment loads and yields were estimated for all stream segments within the NHD using estimated soil loss and a sediment delivery ratio.

USFS Recommendation No. 12: Table 3 (page 18). A more appropriate impact analysis would compare the pre and post construction sedimentation across the LOD, not broadly across the entire sub-watershed. Include this additional LOD analysis across years here.

Mountain Valley Response No. 12: Please see Table 3, which provides sediment yields for unique, intersecting catchments draining stream segments from the NHD rather than broad estimates across respective subwatersheds.

This is an appropriate scale for the analysis given that it enables the estimation of sediment reaching the first downgradient stream segment and all stream segments downstream of that point. Thus, impacts to aquatic TES species are able to be evaluated and determined.

In addition to the sediment yields and sediment loads provided in Tables 3 and 4 of the report (now Tables 4 and 5), MVP has updated the analysis to include an additional table (Table 3) reporting baseline and proposed action soil loss within the limits of disturbance of intersecting catchments.

USFS Recommendation No. 13: Table 4 (page 19). Clarify data results for Kimbalton Creek, Curve Branch, and Clendennin Creek. Please describe how/why load above baseline would increase, decrease, then increase further or stay the same in years 3-5. Please explain this pattern. If related to active construction schedule, describe fully in text. If these loads reflect pipeline construction occurring in later years 3-5 then additional years and loads need to be calculated to reflect at what point new equilibrium values are achieved.

Mountain Valley Response No. 13: This pattern is related to the removal of temporary sedimentation controls surrounding Pocahontas and Mystery Ridge Roads after construction is completed and the road is graveled. The major increases in sediment loss occur during the improvement phase of these roads. Take note that after the road is graveled, it will continue to have greater soil loss than an equivalent area of forest (see Gaffer et al. 2008). The pattern observed in these streams represents: (1) the initial pulse of sediment from construction and improvement (i.e., initial increase); (2) a period of limited sediment delivery when temporary erosion controls are still in place following construction (i.e., the decreased loads); and (3) a period of higher sediment delivery once temporary erosion controls are removed (i.e., second increase). The pattern within these latter two periods represents a change in sediment delivery due to temporary erosion controls being in place and then removed once adequate vegetation is in place. This pattern is not due to increased soil loss within the limits of disturbance. No construction will occur three to five years from the Project's start date. Please take note that sediment estimates for year 5 represents the expected new sediment equilibrium during the operational phase of the Project.

References:
Gaffer, R. L., D. C. Flanagan, M. L. Denight, and B. A. Engel. 2008. Geographical information system erosion assessment at a military training site. Journal of Soil and Water Conservation 63:1-10.

USFS Recommendation No. 14: Tables 4, 5, and Figure 4 (page 21). There is discussion regarding the large increase in sediment load in Kimbalton Branch being related to Pocahontas Road, but there is no discussion as to why Rich Creek loads are so high. Please explain if this related to construction of access roads on private lands.

Mountain Valley Response No. 14: The description of the study area has been expanded to include acreage requirements for both private and JNF lands by USGS HUC 12 subwatersheds. As reported in the revised Table 1, acreage requirements within the Rich Creek subwatershed are largely private, with only one acre occurring on JNF lands. These increases in sediment loads can be attributed to actions occurring on private lands, and this has been included within the revised document. As requested by the USFS, disturbances taken on private lands were incorporated in order to assess the "direct, indirect, and cumulative effects from the proposed action."

USFS Recommendation No. 15: Section 3.2 (page 21). Existing roads are not represented in the baseline modeling. As noted, this could lead to an overestimate of sediment generated as a result of construction. Please include provisions for existing roads.

Mountain Valley Response No. 15: The analysis submitted in March 2017 did not contain provisions for pre-existing roads unless the feature was identified in the 2011 National Land Cover Database. Due to the analysis identifying an increases in sediment loads tied to the access roads during the construction and post-construction phase, changes were made to incorporate the existing footprint of both Pocahontas and Mystery Ridge roads (Forest Road 972 and 11080, respectively). These features were treated as improved roads within the revised analysis (see Gaffer et al. 2008) for the baseline treatment, and Table 4 (sediment yields), Table 5 (sediment loads), and Figure 4 (cumulative effect boundaries) were updated. All figures and tables were regenerated using this baseline treatment, and the text was updated.

References:
Gaffer, R. L., D. C. Flanagan, M. L. Denight, and B. A. Engel. 2008. Geographical information system erosion assessment at a military training site. Journal of Soil and Water Conservation 63:1-10.

USFS Recommendation: Section 3.3 (page 24). The unit of Stream Length presented in Table 6 is in yards. This is not a common unit. Please use miles.

Mountain Valley Response: Mountain Valley has updated the measurement unit to miles within the referenced table. Please note that Table 6 is now referenced as Table 7.

USFS Recommendation No. 16: Section 4.0 (page 25). Table 4 data does not track with statement that a new equilibrium is reached 4-5 years out for Kimbalton Creek, Curve Branch, and Clendennin Creek. Update the analysis to reflect more accurate estimates. It is not appropriate to indicate a new equilibrium in out years with 29-68% increases above baseline, then make a statement that it's an "overestimate." Explain by what factor it is an overestimate. Describe the new expected load for these locations.

Mountain Valley Response No. 16: Based on the methods used in the analysis, the statement that a new equilibrium is reached in four to five years is accurate. For most watersheds (68%), the new equilibrium is reached in year 4. However, for certain areas along the route, this equilibrium is not reached until there is a full year where vegetation is acting as a maturing crop. This timeframe varies among construction spreads resulting in variability in reaching this new equilibrium. Since no pre-existing roads were incorporated into the initial analysis submitted on March 1, 2017, sediment loads above baseline were overestimated in catchments containing access roads, which includes Kimballton Creek, Curve Branch and Clendennin Creek.

Mountain Valley's initial approach was to only use the National Land Cover Dataset (NLCD) for the baseline treatment. However, roads within the JNF were not represented due to the resolution of the NLCD and forest canopy. As a result, the baseline and proposed action treatments were reanalyzed with the incorporation of the current conditions of Pocahontas and Mystery Ridge roads (see Mountain Valley Response No. 15). Based off this analysis, new equilibriums in out years (i.e., years 4 and/or 5) are 20-44% above baseline.

USFS Recommendation No. 17: Overall. The number of significant figures used in the data and results are excessive, especially when considering the approximate methods used to generate data and the approximate method of both the soil loss generator and the stream deposition/erosion determinations. Use of less significant figures would also help identify the study as an estimate (example – in Table 4, the tons per year baseline load is estimated to be 18,463.99 tons per year). Please update accordingly.

Mountain Valley Response No. 17: Mountain Valley has made changes per your comment and all tables have been updated to use integers when appropriate to reflect the approximate methods used to generate the data.

Please feel free to contact me if you have questions or need any additional information. Thank you for your time and consideration.

Sincerely,

Megan Neylon
Supervisor – Environmental Permitting
(724) 873-3645

Attachment 1

PERFORMANCE EVALUATION OF TWO SILT FENCE GEOSYNTHETIC FABRICS
DURING AND AFTER RAINFALL EVENT

by

GREGG STEVEN DUBINSKY, E.I.
B.S. University of Central Florida, 2012

A thesis submitted in partial fulfillment of the requirements
for the degree of Masters of Science in Environmental Engineering
in the Department of Civil, Environmental, Construction Engineering
in the College of Engineering & Computer Science
at the University of Central Florida
Orlando, Florida

Spring Term
2014

Major Professor: Manoj Chopra

ABSTRACT

Silt fence is one of the most widely used perimeter control devices and is considered an

industry standard for use in the control of sediment transport from construction sites. Numerous

research studies have been conducted on the use of silt fence as a perimeter control, including a

number of studies involving controlled laboratory flume tests and outdoor tests performed in the

field on construction sites with actual monitored storm events. In field tests, due to the random

and uncontrollable nature of real storm events and field conditions, studies have shown difficulty

in evaluating silt fence performance. These field studies have shown the need for performance

testing of silt fence in a more controlled environment, which can also simulate the actual use and

performance in the field. This research, which is a continuation of ongoing research on silt fence

fabrics at UCF Stormwater and Management Academy, was conducted in order to evaluate silt

fence performance under simulated field conditions. Presented in this thesis are evaluation of

two silt fence fabrics, a woven (ASR 1400) fabric and nonwoven (BSRF) fabric. Both fabrics

were installed separately on a tilted test bed filled with a silty-sand soil and subjected to

simulated rainfall.

Previous field studies on the performance of silt fence fabrics have evaluated the

turbidity and sediment removal efficiencies only after the rain event, with the assumption that the

efficiency values represent the true overall performance of silt fence. The results of this study

revealed that the turbidity and suspended sediment performance efficiencies of silt fence were

significantly affected by the time of sampling. The performance efficiencies during rainfall

remained less than 55 percent, however, after the rainfall event ended, the performance

efficiencies increased over time, reaching performance efficiency upwards of 90 percent. The

increase in efficiency after rainfall was due to the constant or decreasing ponding depth behind the silt fence, increased filtration due to fabric clogging, and sedimentation of suspended particles.

The nonwoven fabric was found to achieve higher removal efficiencies and flow-through rates both during and after the rain event when compared with the woven fabric. However, over the entire test duration (during and after rainfall combined), the projected overall efficiencies of both fabrics were similar. The projected overall average turbidity performance efficiencies of the woven and nonwoven silt fence fabrics was 80 and 78 percent, respectively. Both fabric types also achieved comparable overall average suspended sediment concentration efficiencies of 79 percent.

This result leads to the conclusion that silt fence performance in the field is dependent on three main processes: filtration efficiency occurring during the rain event, filtration and sedimentation efficiency occurring after the rainfall event, and flow-through rate of the silt fence fabrics. Decreases in the flow-through rate lead to increases in the overall efficiency. This thesis quantifies the different mechanisms by which these processes contribute to the overall efficiency of the silt fence system and shows how these processes are affected by different conditions such as the degree of embankment slope and rainfall intensity.

Dedicated to my family and friends, in memory of my father, Leon

ACKNOWLEDGMENTS

TABLE OF CONTENTS

LIST OF FIGURES

LIST OF TABLES

ABBREVIATIONS

AOS = apparent opening size (mm)

AR = after rainfall

b_{TB} = test bed width (m)

d_p = particle diameter (m)

DR = during rainfall

E = efficiency (%)

EFF = effluent

g = gravitational constant (m/s^2)

INF = influent

K = hydraulic conductivity (cm/s)

mg/L = milligrams per liter

n = number of samples taken during the rain event

NTU = nephelometric turbidity unit

m = number of samples taken after the rain event

PD = ponding depth at face of silt fence (cm)

q = flow-through rate of silt fence (L/m^2/h)

S = embankment slope (%)

SSC = suspended sediment concentration (mg/L)

t = time (h)

T = turbidity (NTU)

TS = total solids (mg/L)

V = volume of water (L)

v_c = critical settling velocity (cm/min)

v_s = particle settling velocity (m/s)

WMEC = weighted mean influent concentration (mg/)

WMET = weighted mean effluent turbidity (NTU)

WMIC = weighted mean influent concentration (mg/L)

WMIT = weighted mean influent turbidity (NTU)

ρ = density (kg/m^3)

τ = hydraulic detention time (min)

μ = dynamic viscosity (kg/m/s)

CHAPTER 1: INTRODUCTION

Problem Statement

According to the United States Environmental Protection Agency (USEPA 2012), soil

erosion is the largest contributor to nonpoint source pollution in the United States. It is estimated

that over 4 billion tons of sediment are discharged into ponds, rivers, and lakes in the United

States each year and approximately 10 percent of this amount is due to erosion occurring from

land undergoing construction activities or land development (FDEP 2008). Eroded sediment can

cause a number of environmental and economic problems. Eroded sediments that carry nutrients

such as phosphorus and nitrogen can lead to the development of algal blooms and lake

eutrophication. If the eroded sediments are small and remain suspended in the water body, they

can block sunlight from penetrating the water body, disrupting photosynthesis. If, however, the

eroded sediments are large, they may settle to the bottom of the water body, reducing its storage

capacity and possibly increasing its flood frequency (Harbor 1999).

On construction sites, the erosion rate and the potential for sediment discharge are

greatest during the active construction phase of the project (Owens et al. 2000). Active

construction causes increase in the erosion rates when compared to the pre- and post-

construction conditions due to the loss of protective vegetative cover. Due to large erosion rates

during active construction, the soil loss from these sites over even a short period can rival losses

that would have taken decades to erode naturally (EPA 2007). For this reason it is important to

limit the sediment load that has the potential to be discharged from the construction site during

the active phase. A number of technologies including both erosion and perimeter control are

used for this purpose. However, silt fence in particular, is considered an industry standard for use on construction sites (Faucette et al. 2008)

Numerous research studies have been conducted on the use of silt fence as a perimeter sediment control. Majority of studies involve controlled laboratory flume tests (Britton et al. 2000, Farias et al. 2006, Risse et al. 2008) and outdoor tests performed in the field on construction sites with real monitored storm events (Barrett et al. 1995, Faucette et al. 2008). Although flume studies have shown that silt fence performs well in removing sediment from concentrated flows, these tests do not correctly simulate the field conditions of the use and performance of silt fence. In the field, the composition of the eroded soil is different from the parent soil and will contain more silt and less sand particles due to the higher erosion rate of these particles in comparison to sand particles (FDEP 2008). Rainfall collision with the ponding volume upstream of the silt fence will also disrupt settling within the pond during rainfall. These difference between the flume tests and actual field conditions lead to an overestimation of the silt fence performance.

The field studies evaluated the discharge concentration through the silt fence by comparing either to the known erosion rate of the soil or to the upstream concentration in the ponding volume after the rain event. Evaluating silt fence on a time dependent basis during rainfall however is not possible during these tests. For this reason, and due to the random and uncontrollable nature of real storm events and field conditions, it has been difficult to evaluate silt fence performance in the field. Both flume and field studies have shown the need to further evaluate silt fence in conditions which cannot only simulate the actual use and performance of silt fence in the field but can do so in a controlled environment.

Objective

The research presented in this thesis has been conducted in order to evaluate silt fence performance under varying field conditions. The study was performed on a tilted test bed filled with a silty-sand soil (AASHTO classification type A-2-4) set to different degrees of slope and subjected to varying intensities of simulated rainfall. The research is a continuation of previous research project conducted by Gogo-Abite and Chopra (2013) at UCF Stormwater Laboratory. Performance evaluation was completed on two silt fence fabrics, a woven (ASR 1400) fabric and a nonwoven (BSRF) fabric. These silt fence fabrics were installed separately on the tilted test bed and subjected to simulated rainfall events of 27, 76, and 127 mm/h (1, 3, 5 in/h) and to differing embankment slopes of 10, 25, and 33 percent.

The objective of this study is to evaluate the performance of both silt fence fabrics under field conditions and to quantify the turbidity and suspended solids performance efficiency as well as the flow-through rates of the fabrics under different embankment slope and rainfall intensity. Additional objective will also be to compare the performance of both silt fence fabrics. The woven fabric used in this study is the traditional monofilament geosynthetic typically used on construction sites. Previous studies on this fence have shown its inability to achieve required water quality performance targets (Barrett et al. 1995, Faucette et al. 2008, Gogo-Abite and Chopra 2013). The nonwoven fabric was designed to reduce turbidity and suspended solids and permit a greater flow-through rate of the fabric than the traditional woven monofilament silt fence (Risse et al. 2008). The performance efficiency of the nonwoven fabric should be greater than the woven fabric due to the pore sizes of both fabrics. Previous studies by Gogo-Abite and Chopra (2013) show that the apparent opening sizes (AOS) of the woven and nonwoven fabrics

17

are 0.70 mm and 0.21 mm, respectively. This thesis aims to study if the difference in AOS between the silt fence materials causes a significant difference in the performance efficiency. It is also of interest to see if any removal occurs by filtration at all with the woven fabric, as the AOS of this fabric is actually larger than 100 percent of the soil particle sizes used in the study.

The study further seeks to evaluate silt fence on a time dependent basis and determine if a difference in performance exists between removal encountered during and after rainfall. It will be interesting to see if changes in the embankment slope and rainfall intensity affect the removal mechanisms occurring for each of these processes over the entire duration of treatment.

Thesis Organization

The research was conducted in order to investigate the performance of silt fence materials under field scale conditions and to quantify the differences in performance occurring both during and after rainfall events. In order to present the research, an introduction is presented in Chapter 1 that discusses the significance of the study, objectives of the research, and the thesis organization.

Provided in Chapter 2 is a review of literature related to silt fence. The review discusses index properties of geotextiles that are relevant to silt fence, the theory that forms the basis for the types of filtration and sedimentation that occurs in silt fence treatment, and a review of previous flume, field, bench-scale, and field-scale studies that have been completed on silt fence.

After the literature review, the methodology is discussed in Chapter 3. In this chapter, details of the properties of the soil type, the properties of the silt fence, the field scale testing procedure, and the limitations of this testing procedure are presented.

Following the methodology, the results of the field scale performance testing of silt fence fabrics is presented in Chapter 4. The chapter is divided into three main sections; discussions on the performance evaluation of silt fence during the rain event, after the rain event, and over the entire duration of treatment.

The fifth and final chapter presents summary, conclusions, and recommendations of the field scale results of the study.

CHAPTER 2: LITERATURE REVIEW

Introduction

Erosion and soil losses from unprotected construction sites are one of the leading sources of sediments found in water bodies across the U.S. (Hayes et al. 2005). Due to the natural vegetative cover being remove from the soil, it is not uncommon for these sites to have soil erosion rates as high as 2 to 40,000 times greater than the preconstruction conditions (Harbor 1999). The increase in erosion has led to approximately 80 million tons per year of sediment being deposited to lakes, rivers and waterways in the United States due in part to inadequate preventive measures during the construction phase (Harbor 1999).

To control sediment transfer from construction sites, the prevention of erosion should be the primary focus. The common erosion control practices are temporary seeding, mulching, geotextile matting, chemical stabilization, and many other erosion control practices (USEPA 2011). These practices are the first line of defense in controlling sediment detachment from the exposed soil in construction sites by preventing erosion. The last line of defense in controlling sediment emissions from leaving the construction site are perimeter controls. These devices are used on the perimeters of construction sites and are used to intercept concentrated runoff water and remove its sediment. Thus, retaining the sediments on site and keeping them from entering offsite areas such as water bodies, roadways, and storm drains. Some of the sediment control measures include silt fence, filter socks, temporary diversion berms, temporary fill diversions, temporary slope drains, and floating turbidity barriers (FDEP 2008).

Of the perimeter control devices, silt fence is considered the current industry standard for perimeter control on construction sites (Faucette et al. 2008). Silt fence is defined as, "a temporary sediment barrier consisting of a filter fabric stretched across and attached to supporting posts and entrenched" (FDEP 2008). The supporting posts are usually made of wood, at least 2.5 x 5.0 centimeter (1 x 2 inch) in cross sectional area, and are a minimum of 0.9 meter (3 feet) in length. The posts are buried a minimum of 0.3 meter (1 foot) into the ground, but they may not exceed 0.9 meter (3 feet) in height above the surface. This maximum height requirement is because larger fence heights may cause the silt fence to impound a volume of water great enough to cause the stakes to fail. The stake posts are then installed at a maximum of 3 meter (10 feet) apart if the fence is used without a wire support. If no wire support is used, then the stakes are spaced a maximum of 1.8 meter (6 feet) apart.

In most cases, silt fence is installed around the perimeter of the construction site so that it can intercept all runoff water which has the potential to flow off of the site. The silt fence works by first acting as a physical barrier that reduces the velocity of the runoff water. Then, depending on the type of silt fence geotextile and the soil characteristics, the silt fence filters the sediment from the concentrated runoff water. As the silt fence starts to filter the sediment, the particles begin to clog the fabric, decreasing the ability of the silt fence to transmit water. When the flow-through rate of the silt fence starts to decrease, the runoff water starts to pond upstream of the silt fence, creating a ponding volume of accumulated runoff. Then, depending on the flow-through rate of the fabric, the suspended particles within the ponding volume may settle out of suspension before the water is discharged through silt fence. Thus, silt fence removes

sediment by two mechanisms, filtration through the fabric and sedimentation of suspended particles.

The remainder of this literature review discusses the types and properties of geotextiles used in silt fence applications, the theory of the sediment removal mechanisms of silt fence, and previous research which has been completed on silt fence.

Geotextile Characterization

ASTM (1987) defines geotextile as "any permeable textile used with foundation, soil, rock, or any other geotechnical engineering related material as an integral part of a manmade product, structure, or system." Silt fence therefore qualifies as a geotextile. These permeable textiles can be categorized as either woven or nonwoven. The woven geotextiles have relatively uniform rectangular openings and are manufactured by weaving synthetic fibers into flexible and porous fabrics (Koerner 2012). The fibers are interwoven perpendicular to each other; the horizontal elements are referred to as weft fibers and the longitudinal elements are referred to as warp fibers (Zhang et al. 2013). Unlike woven fabrics, which have relatively uniform openings, the pore structure and morphology of nonwoven geotextiles can be highly complex (Rawal and Saraswat 2011). These geotextiles are manufactured by needle punching or melt bonding (Lamy et al. 2013) with their fibers oriented in multidirectional and random arrangements (Fisher and Jarrett 1984).

Geotextile Index Testing

With the broad use of silt fence geotextiles in the industry, it is necessary to determine the properties of individual fabrics in reference to other fabrics and to recommended values. In

this regard ASTM D6461 (2007) has provided a list of current standard test methods in order to determine the index properties of silt fence fabrics. These index properties which are of interest in silt fence are: grab-tensile strength, ultraviolet (UV) stability, apparent opening size (AOS), and fabric permittivity. The recommended specifications for these index properties for silt fence are listed in Table 1. The details of these tests were not discussed in this thesis, however, a brief discussion of how these parameters affect silt fence performance in the field is discussed below.

TABLE 1 ASTM SPECIFICATIONS FOR SILT FENCE FABRICS

Property	Direction	ASTM Test Methods	Units	ASTM D6461
Grab strength	Machine	D 4632	N	400
	X-Machine			400
Permittivity		D 4491	sec^{-1}	0.05
AOS		D 451	mm	0.6
Ultraviolet stability		D 4355	% Retained strength	70% after 500 h of exposure

Permittivity is an indicator of the amount of water that can pass through a geotextile and is defined as the "volumetric flow rate of water per unit cross sectional area per unit head under laminar flow conditions, in the normal direction through a geotextile" (ASTM D4491 2009). Permittivity has been shown to be a good indicator of the clogging potential for nonwoven geotextiles where less clogging of the geotextile is observed with increasing permittivity (Aydilek and Edil 2003). However, permittivity is not a good indicator of the potential flow-through rate of the geotextile that will be encountered in the field (Weggel and Ward 2012). In the field, the permittivity of silt fence has been shown to decrease due to the impingement of sediment on the fabric.

The AOS of the fabric is a measure of the largest pore sizes of the fabric. AOS is found by running beads of a certain diameter through the fabric; and the AOS is the bead size for which 5% or less of the beads pass through. AOS may give an indication of the particle size that can be removed through filtration by the fabric. However in the field, pressure brought on by ponding water induces tensile strain on the silt fence that can result in larger pore openings (Gogo-Abite and Chopra 2013). Since AOS has been shown to have a proportional linear relationship to tensile strain (Wu et al. 2008), AOS may not give an accurate representation of the sediment removal potential of silt fence fabrics in the field.

UV stability is a very important property for silt fence. It is not uncommon for silt fence to remain on construction sites for long periods of time. Sunlight has been shown to be a dominant degradation factor for many geotextiles (Suits and Hsuan 2003), and as such, solar radiation has the potential to degrade silt fence, reducing its ability to function properly. Solar radiation, in the form of photons, has energies, which range from 300 to 390 kJ/mol. Making them sufficiently strong enough to degrade polymer carbon (C-C) and hydrogen (C-H) bonds of the silt fence fabric, which range from 340 to 420 kJ/mol (Suits and Hsuan 2003). For this reason, UV stabilizers are added to protect polymers and prolong their lifetimes when they are used in exposed applications. In silt fence, ultraviolet ray inhibitors and stabilizers are used, and must be designed to provide a minimum of 6 months solar radiation protection (FDEP 2008). Even when silt fences are UV stabilized, it has still been shown that their tensile strength and strain at break continue to decrease with exposer to UV, however, the rate of degradation is greatly reduced (Dierickx and Van Den Berghe 2004).

Sediment Removal Mechanisms of Silt Fence

The two major mechanisms of sediment removal by silt fence occurs by particle sedimentation by gravity and by filtration of particles through the fabric. Knowledge of both sedimentation and filtration theory is necessary in order to understand the mechanisms of sediment removal by silt fence. Discussed in the following two sections is the basic theory behind these mechanisms.

Sedimentation Theory

One of the most important, cost effective, and widespread treatments of suspended solids removal from water is by sedimentation (Barrett et al. 1995). Sedimentation during silt fence treatment occurs due to the formation of a ponding water volume caused by the flow rate of runoff water being greater than the flow rate of water through the silt fence. The ponding water volume, which is concentrated with eroded sediments, acts as a small dynamic sedimentation pond. Sedimentation will occur if the suspended particles in the pond are large and dense enough to settle out by gravitational forces in a time that is less than the critical settling velocity of the system (Howe et al. 2012). The critical particle settling velocity is related to both the ponding depth and the hydraulic detention time and is given by the following expressions in Equations 1 and 2:

$$v_c = \frac{PD}{\tau} \tag{1}$$

$$\tau = \frac{3(10^4)*PD}{q*S} \tag{2}$$

where v_c is the critical settling velocity (cm/min); PD is the ponding depth at the fence face

(cm); τ is the hydraulic detention time (min); q is the flow-through rate of the fence (L/m²-hr);

and S is the slope percent of the ground which is in contact with the ponding water volume (%).

The hydraulic detention time refers to the amount of time it would take for the entire ponding

volume to flow through the silt fence.

In order for sedimentation to occur, the particle settling velocity must be greater than

the critical settling velocity. The particle settling velocity is dependent on a number of factors,

one of which is the type of particle suspension within the pond. In total, there are four particle

suspension classifications, however only two are relevant to silt fence. They are, Type 1

(Discrete) particle settling and Type III (Hindered) settling.

<u>Type I Particle Settling</u>

Type 1 particle settling occurs in dilute solutions where individual particles do not

interact with each other. Under these conditions each individual particle settles based on their

own size and density (Howe et al. 2012). Assuming laminar flow conditions, the settling

velocity is given by Stokes' Law as

$$v_s = \frac{g*d_p^2*(\rho_p - \rho_w)}{18*\mu} \tag{3}$$

where v_s is the particle settling velocity (m/s); g is the gravitational constant (m/s²); d_p is the

particle diameter (m); ρ_p is the density of particle (kg/m³); ρ_w is the density of water (kg/m³);

and μ is the dynamic viscosity (kg/m-s). Based on Equation 3, settling velocity is proportional to

both the particle diameter and density. For this reason it is unlikely that very small particles such

as silts and clays will be removed by settling in silt fence applications due to their low settling velocities (Arjunan et al. 2006).

<u>Type III Settling</u>

In the literature it is common for stokes law to be referred to in discussions on silt fence in conjunction with sedimentation mechanisms even when the solids concentrations are large. Under high concentrations however, solutions are not dilute enough, and particle interactions restrict the settling potential of the solution. Under these conditions, Type 1 settling and stokes law are not justified, and the governing settling mechanism is instead Type III, or hindered settling.

In type III settling, the settling velocities of particles are affected by the presence of other particles due to particle collisions and frictional forces (Howe et al. 2012). During this type of settling, a blanket of particles forms with a distinct interface due to particle aggregation (Howe et al. 2012). This causes the settling velocity of larger particles to be reduced, however the settling velocity of smaller particles, such as silts and clays, are likely to be increased if they are caught within the settling blanket. Under Type III settling, the settling velocity is also dependent on the soil type and the solids concentration. As the solids concentration increases, the settling velocity decreases (Howe et al. 2012). Therefore, as the solids concentration increases, the potential removal by sedimentation will decrease. However, a larger solids concentration will increase the potential for removal by filtration.

An understanding of the basic theory of filtration and how it applies to silt fence applications is presented in this section. The discussion is broken up into three parts; how the filtration mechanism occurs in geotextiles, how filtration of the fabric affects the flow-through rate of the geotextile, and a brief discussion on different types of geotextile/soil interactions.

Filtration Mechanism

A discussion on the mechanics of filtration in geotextile applications is described by Faure et al. (2006), a summary of this discussion is presented below.

In a silt fence fabric, small openings in the fabric act as small pipes. Many of these openings in the fabric make up a pipe network where water and fine particles can flow through. The flow-through rate of this system is equal to the sum of the flow-through rates in each individual pipe in the network. Depending on the geotextile properties such as pore opening size and fabric thickness, as well as soil characteristics of the slurry, particles in suspension may settle or be caught within the individual pipes. Filtering of this nature is referred to as parallel filtering (Figure 1a). Different pipes will undergo parallel filtration at different rates depending on the properties of each pipe. Some pipes may experience an excessive amount of parallel filtration and become obstructed; causing additional particles to pile up in the pipe. This is called series filtration (Figure 1b). If series filtration causes a pipe to become entirely filled with particles, additional particles will start to accumulate on the outside of the fabric and will form a filter cake (Figure 1c).

As particles continue to be filtered by the fabric, the impinged particles reduce the pore sizes of the pipes. The reduction in pore size limits the ease with which water can flow through the fabric and also increases the filtration ability of the fabric. These mechanism are discussed in more detail in the following sections.
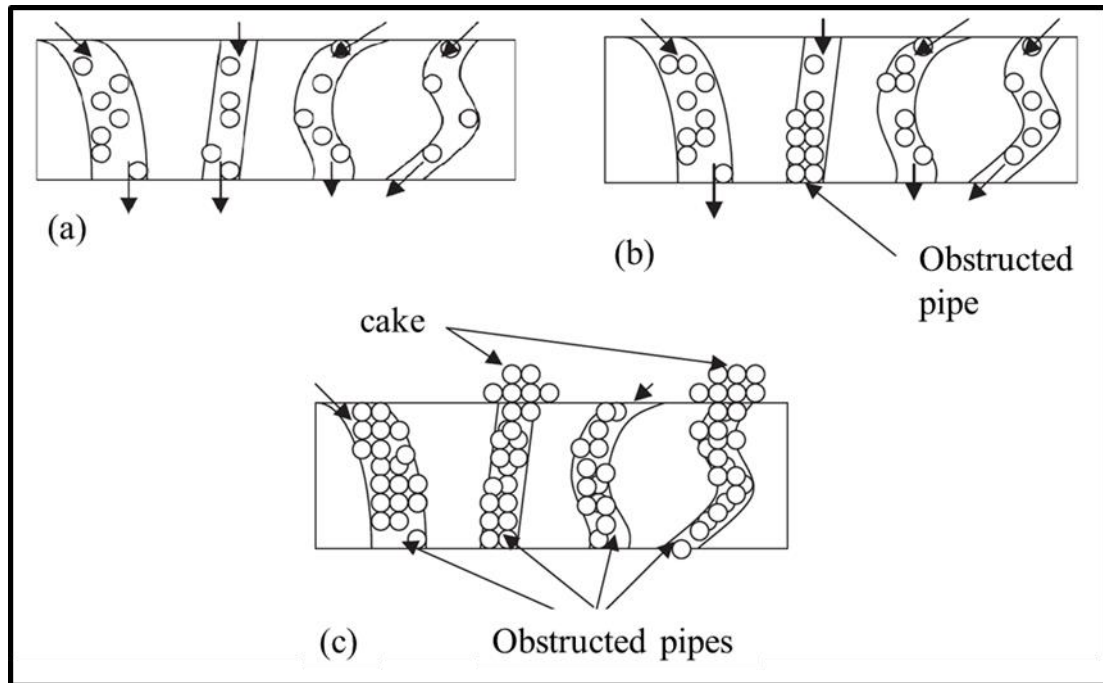
FIGURE 1 MECHANISM OF PARTICLE ACCUMULATION: (A) ALL PIPES ARE OPENED (SERIES FILTRATION), (B) FEW PIPES ARE OBSTRUCTED (SERIES AND PARALLEL FILTRATION), (C) FILTER CAKE FORMATION ABOVE COMPLETELY OBSTRUCTED PIPES (FAURE ET AL. 2006)

Effect of Filtration on Flow Rate

The purpose of silt fence is to remove soil particles from a concentrated slurry, while still permitting the flow of water through it. However, as soil particles accumulate both within and on the fabric, both the pore sizes of the fabric and the ability of the fabric to transmit water are reduced (Fisher and Jarrett 1984, Britton et al. 2000, Risse et al. 2008). The decrease in flow-through rate causes an increase in the accumulation of ponding water upstream of the silt

fence. Although this will increase the hydraulic detention time of the system, allowing

additional time for the sedimentation mechanism to take place, excessive ponding could also

cause the ponding water to overtop the silt fence (Farias et al. 2006). The additional pressure

brought on by large ponding depths could also cause the silt fence to fail. For these reason silt

fence must be prevented from becoming clogged with sediment and there must exist a

compromise between the fabrics ability to retain soil and its ability to transmit water (Fisher and

Jarrett 1984).

Sansone and Koerner (1992) defined clogging of the fabric due to particle filtering as,

"the reduction of the geotextile's permeability to the point where flow through it results in the

hydraulic system's nonperformance." The potential of a filter to become clogged depends on

both the fabric characteristics and the parent/eroded soil characteristics. Studies by Aydilek and

Edil (2003) have shown that the permittivity of the geotextile is the "main pore structure

parameter" that affects its clogging. Where increases in the initial permittivity of the geotextile

lead to a decrease in the potential of the fabric to become clogged with sediment. However,

according to Weggel and Dortch (2012) the permittivity of the geotextile is only important

initially. What controls the flow-through rate of the fabric and the ability of the fabric to become

clogged is the geotextile/soil characteristics and the nature of the filter cake that forms on the

fabric. In general, greater reductions in flow rate also occur in heavier and thicker geotextiles

due to the increased available volume for binding and impregnation in these fabrics (Farias et al.

2006).

Geotextile/Soil Interaction

Overall, the soil characteristics relative to the geotextile's characteristics are the most important parameters affecting both the potential for fabric clogging and the ability of the fabric to filter the concentered slurry. In general, soils that contain particles that are for the most part larger than the geotextiles opening pores will operate with high efficiency and will not clog, but will build a stable filter cake on the geotextile (Sansone and Koerner 1992). The filter cake will continue to thicken over time as additional particles adhere to the filter cake, however, the flow rate will remain relatively constant and will be dependent on the permittivity of the accumulated filter cake (Sansone and Koerner 1992, Weggel and Ward 2012).

For soils where all the particles are smaller than the pore size of the fabric, the silt fence will operate with a low filtering efficiency, but clogging is not likely to occur (Sansone and Koerner 1992). Soils consisting of primarily silts and clays fall into this category. For this reason silt fence is generally not an effective filter of silty and clayey soils (Fisher and Jarrett 1984).

The last soil type consists of particles that are both larger (i.e. sands) and smaller (i.e. silts and clays) than the pore size openings of the fabric. These types of soils can lead to excessive clogging of the geotextile depending on how well graded the soil is (Sansone and Koerner 1992). Initially the larger sand particles are filtered by the fabric, decreasing the pore sizes of the fabric. This leads to smaller particles also being filtered by the fabric. As the pore size of the fabric continues to decreases due to smaller and smaller particles being filtered, the ability of the system to transmit water also decreases. In this fashion, the fabric may become

completely clogged over time, and the flow-through rate of the fabric will be severely diminished.

Previous Silt Fence Research

This section describes previous research that has been conducted on the performance efficiency of silt fence. These studies were conducted in a number of ways, including; monitoring silt fence in the field under actual storm events, bench and field scale studies with simulated rainfall, and flume studies. A summary of previous research on silt fence that has been conducted these three types of studies is presented in this section.

Flume Studies

A flume study is a controlled test performed in the laboratory. The test is conducted by mixing a mass of parent soil with a certain volume of water to create concentrated slurry. The concentration of the slurry becomes the influent concentration to the flume. The slurry is pumped into the flume and flows down the flume, where it is exposed to a silt fence that sits at the bottom of the flume. The concentration that is discharged through the silt fence is the effluent concentration. The efficiency of the silt fence is then calculated by comparing the effluent concentration to the initial influent concentration.

Farias et al. (2006) tested four nonwoven silt fence fabrics of various opening sizes and thicknesses using flume tests. The slope of the flume was not stated. The opening sizes of the geotextiles ranged from 0.11 mm to 0.60 mm and the thickness of the geotextiles ranged from 0.8 mm to 4.5 mm. Three soil types were used with a sediment concentration of 10,000 mg/L; namely two silty soils and one sandy soil. Results showed that sediment reduction under these

32

conditions ranged from 93 to 96 percent for all fabrics and soil combination pairs tested. The opening size and thickness of the fabrics did not affect the reduction efficiencies; however, these parameters did affect the flow rate. The thicker and less opened geotextiles had the greatest flow rate reductions, whereas the lighter and more opened geotextile presented the smallest reductions in flow rate (Farias et al. 2006). Thus, the study concluded that the thicker and less opened the geotextile, the easier it would be for the fabric to become clogged; reducing its ability to transmit water. Results from this study also showed that silt fence, even those with large opening sizes of 0.60 mm could efficiently remove silty soils.

Risse et al. (2008) also tested silt fence fabrics using flumes. The flume was raised to a grade of 8 percent, and both a woven and a nonwoven fabric were tested. The nonwoven fabric was a polyester silt fence that was introduced by Silt-Saver Inc. and is called a Belted Silt Retention Fence (BSRF). Three soils, Tifton sand, Fannin silt, and Cecil clay loam, were used at concentrations of approximately 3000 mg/L and 6000 mg/L. Sediment removal efficiencies under all test conditions were at least 87 percent, indicating high removal for both fabrics under all soil conditions. Risse et al. (2008) concluded that the high sediment removal efficiencies were attributed to the low slope gradient and the extended holding time created under these conditions, and that much of the released sediment settled out of suspension prior to reaching the silt fence. Risse et al. (2008) also investigated the performance of silt under a large slope of 58%, and found that sediment removal still remained high (upwards of 80%). So it seems the low slope gradient did not have that large of an effect on reduction after all. Although sediment removals were high, turbidity reduction was significantly lower and ranged from 25 to 58 percent for the woven fabric and 55 to 90 percent for the nonwoven fabric.

Risse et al. (2008) also found that the flow rate through the fabrics decreased with increasing influent concentration. These results indicate that soil particles have an influence on the flow rate and suggested that the sediment trapped behind the fence was controlling the flow rate more than the fence itself (Risse et al. 2008). Note that flow rates were significantly higher with the sandy soil than the silty or clayey soils. The reason for this may be that the silty and clayey soils have better graded distribution of soil particle sizes than the sandy soil; which consisted mostly of sand sized particles. As was discussed in the section on filtering theory, the well-graded soils can progressively clog silt fence fabrics due to progressively smaller sediments clogging the pores of the filter.

Results from this study show that silt fence is capable of high sediment removals of silt, sand, and clay loams. However, it is less effective in removing turbidity from these soil types. The lower turbidity removal shows that the larger sediment particles most likely settled out of suspension, while the smaller particles did not, and were discharged through the silt fence. While the large sediment particles that settled out affect the mass of sediment discharged and to some extent the turbidity, the smaller silt and clay particles affect the turbidity to a larger extent (Bilotta and Brazier 2008). However, due to their small size, they do not contribute to the total solid mass to the extent that the larger particles do. This explains why turbidity removal was lower.

Field Testing

Barrett et al. (1995) investigated the performance of silt fences under controlled conditions in an outdoor flume as well as in the field under actual rainfall on active construction sites. The flume slope was 0.33% and a slurry was made using Austin silty clay soil at a

34

concentration of 3000 mg/L. Sediment removal efficiencies ranged from 68 to 90 percent. The high removal efficiencies were attributed to the geometry of the upstream ponding volume; the low slope allowed adequate detention time for the suspended solids to settle out before reaching the silt fence. Barrett et al. (1995) was able to show that silt fence was capable of removing silt and clay sized particles under low sloped conditions. The mechanism for removal however was not due to filtering through the silt fence, but through settling.

Barrett et al. (1995) also investigated silt fence performance in the field by monitoring installations on active highway construction sites. However, information regarding the intensity, duration, or quantity of each rainfall event was not obtained due to limited equipment. In total six different sites were monitored, two of which used nonwoven fabrics and four of which used woven fabrics. Over the course of seven rainfall events, the average removal efficiencies ranged from negative 61 to 54 percent with a median of 0 percent and negative 32 to 49 percent with a median of 2 percent for sediment and turbidity, respectively. According to Britton et al. (2000), due to the magnitude and random nature of the measured concentration, the instantaneous comparison of these values were not valid. An accurate estimate of the overall operation efficiency would need to be approximated by collecting samples over the entire duration of a storm event in order to determine the total load into and out of the control device over time.

Bench Scale Testing

Faucette et al. (2008) investigated the performance of silt fence using bench scale tests. The bench scale testing bed was 100 cm length by 35 cm width by 25 cm depth (39 in × 14 in × 10 in). The test beds were filled with a silt loam and raised to a 10 percent slope and exposed to rainfall intensity of 7.45 mm/h (2.93 in/h). Removal efficiencies ranged from 78 to 87 percent

and from 54 to 76 percent for sediment concentration and turbidity, respectively. This result shows further that silt fence does not reduce turbidity as well as it does sediment. The results also showed that even though silt fence removed sediment from 78 to 87 percent, effluent concentrations were still high. Effluent sediment concentrations ranged from 9,000 mg/L to 14,000 mg/L despite the large reduction efficiencies, which indicates that the erosion rate of the soil was high during the bench scale testing.

Field Scale Testing

Due to the uncontrollable nature of actual field testing on construction sites and the need to further investigate the performance of silt fences under these conditions, Gogo-Abite and Chopra (2013) studied the performance of both woven and nonwoven (BSRF) silt fence fabrics. The study was done using a tilted test bed filled with a sandy soil and rainfall simulator in order to simulate field conditions in a controlled environment. In order to simulate worst case conditions that would be found in the field, high slopes of 10 and 25 percent, and high intensities of 27, 76, 127 millimeter per hour (1, 3, and 5 inches per hour) were evaluated. The woven fabric reduced turbidity by 18 percent and reduced sediment by 28 percent. The nonwoven fabric achieved reductions of 52 and 57 percent for turbidity and sediment, respectively. The low removal percentages were caused by inadequate time for settling due to the large slopes and because a large portion of the suspended sediment was smaller than the AOS of either fabric. Gogo-Abite and Chopra (2013) concluded that due to the low removal efficiencies, silt fence as a standalone process installed at the toes of high slopes of 10% and greater would not be adequate enough to meet the reductions of turbidity and sediment as required by regulatory agencies.

Summary

Literature related to silt fence show that sediment removal is by gravity settling and by filtration of the fabric. The performance efficiency of the fabrics is dependent on the particle size characteristics as well as the geotextile properties such as opening pore size and thickness. The flow-through rate of these fabrics in the field is also a function of the ease with which the fabric can become clogged and is therefore a function of the soil characteristics, the gradation of the soil, and the geotextiles opening pore size.

It is common for silt fence to be characterized by both its permittivity and apparent opening size, however, this literature review has shown that both these properties do not correctly describe silt fence performance under field conditions. The initial permittivity in particular will not give indication to the expected hydraulic performance of the fabric in the field due to filter clogging when exposed to concentrated flows. The apparent opening size can give an indication of what particle sizes may be intercepted by the fabric in the field, however, ponding water upstream of the silt fence creates a load on the silt fence that induces a strain that can result in an increase in the opening size of the fabric. This would increase the particle sizes that could pass through the fabric and decrease the fabric efficiency.

Previous research on silt fence performance has been conducted on active construction sites under monitored storm events, in flume studies, and in both pilot and field scale test beds. Results from flume studies have shown that silt fence reduces sediment concentrations of sandy soils as well as silty and clayey loams at high efficiencies upwards of 70 percent. However, silt fence did not reduce turbidity to this extent due to the difficulty of silt fence in removing small silt and clay sized particles.

37

While flume studies have shown high removal efficiencies, field tests and field scale tests have shown that silt fence does not reduce turbidity or sediment as well under field conditions. In particular, field scale testing with tilted test beds and active rainfall have shown that silt fence reduces sediment and turbidity in the range of only 20 to 50 percent depending on the type of geotextile used. These studies have shown a need for additional field scale testing of silt fence geotextiles in order to further evaluate their performance in the field.

CHAPTER 3: METHODOLOGY

Introduction

This project compared and evaluated the performance of two silt fence geotextiles exposed to a simulated rain event over a silty-sand-soil. The evaluation and comparison was performed using a field scale tilted test bed and rainfall simulator located at University of Central Florida's Stormwater Management Academy Research and Testing Laboratory (SMARTL). This chapter will describe the soil type that was used in the study, the types of silt fence geotextiles used, the test preparation and set up, the field scale testing method, and the limitations encountered during the study.

Soil Characteristics

A series of bench scale tests were used in order to characterize the soil that was loaded in the test bed. Testing was done in order to determine the soils particle size distribution, maximum compaction, and permeability. Brief discussions on the results of these tests are the topic of the next few sections.

Soil Classification and Particle Size Distribution

Defining the soils classification and particle size distribution is particularly important when evaluating the performance of silt fence fabrics. The ability of the geotextile to filter the concentrated slurry and the settling velocity of the suspended particles are primarily dependent on both the soil particle sizes and on the distribution and uniformity of these particle sizes. Due to this dependence, the AASHTO Classification system was used because this system distinguishes between clay and silt particles based on grain diameter. The AASHTO

39

Classification system was also used because it is the common classification system for construction sites for roadway and stormwater management. The AASHTO Classification system also takes into account the plastic and liquid limits of the soil. The results of these tests showed that the soil type was non-plastic. The soil classification was therefore based solely on its grain size distribution. The grain size classification used in the AASHTO Classification system is shown in Table 2.

TABLE 2 SUMMARY OF SOIL PARTICLE CLASSIFICATION ANALYSES

Particle Type	AASHTO Classification, grain diameter (mm)	Percentage of Soil (%)
Gravel	76.2 to 2	0
Sand	2 to 0.075	84
Silt	0.075 to 0.002	4
Clay	< 0.002	12

Particle size distribution

Three tests were completed in order to determine the particle size distribution of the soil. These tests were the standard test method for materials finer than 75 μm (No. 200) sieve in mineral aggregates by washing (ASTM C117-13 2013), sieve analysis of fine and coarse aggregates (ASTM C136-06 2013), and standard test method for particle-size analysis of soils by hydrometer analysis (ASTM D422-63 2013). The method for materials finer than 75 μm was performed first in order to determine the percentage of the soil that was finer than 75 μm (No. 200 mesh). Following the method for materials finer than 75 μm, those particles with diameters that were greater than 75 μm and that were retained on the number 200 sieve were used in the sieve analysis in order to determine the distribution of those particles which were greater than 75

μm. Finally, a hydrometer analysis was conducted in order to determine the soil distribution of those particles which had diameters less than 75 μm.

The results for material finer than 75 μm by washing, sieve for fine and coarse aggregates, and particle size analysis using hydrometer are shown in Table 21, Table 22 and Table 23, respectively, of Appendix A. A summary of these results and the particle-size distribution curve for this soil are also shown in Table 2 and Figure 2, respectively.
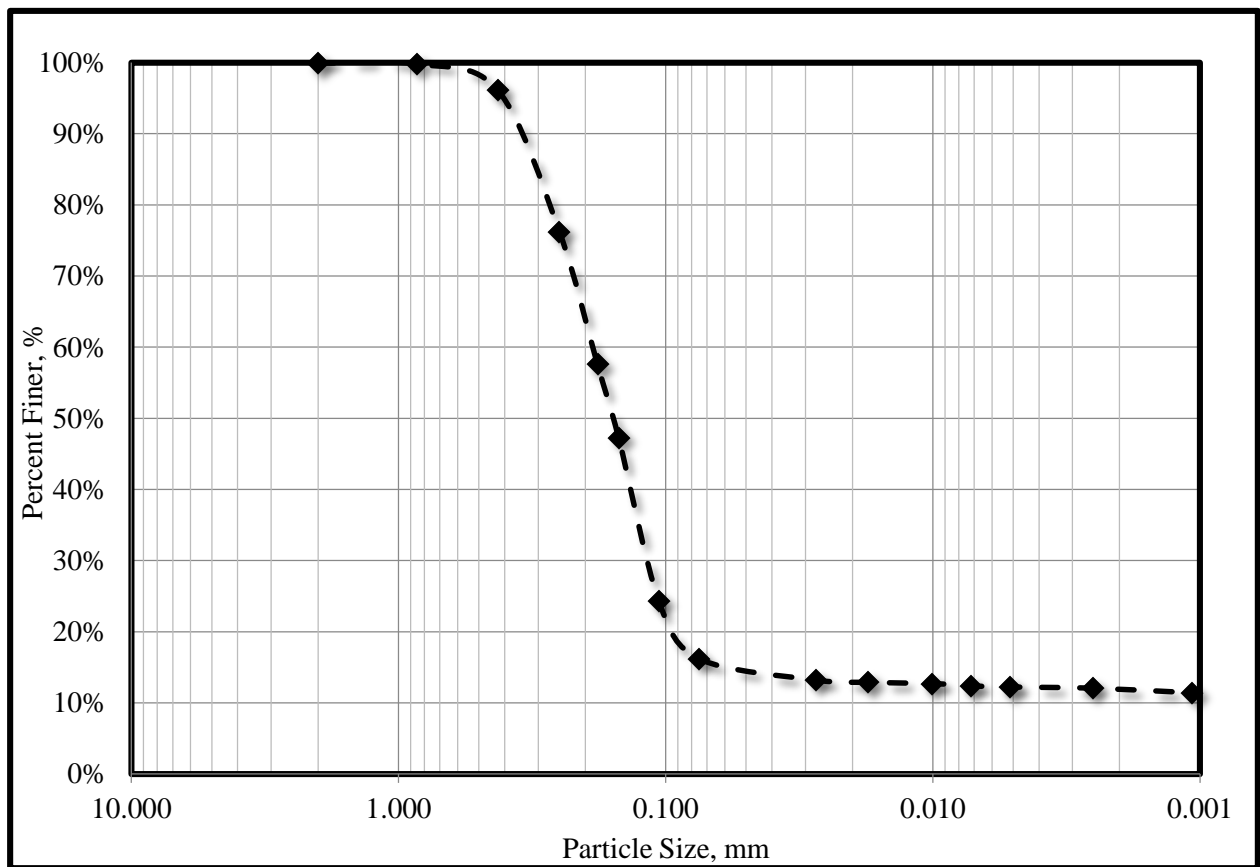
FIGURE 2 PARTICLE SIZE DISTRIBUTION CURVE

The silty-sand soil is made primarily of sand particles (84 percent sand) in the range of 0.075 mm to 4.0 mm. The remaining 16 percent of the soil distribution is made of clay particles

41

with diameters of less than 0.001 mm (12 percent) and silt sized particles in the range of 0.075 to 0.002 (4 percent). It will be interesting to see if silt fence is able to achieve removal efficiencies of greater than 84 percent from this soil type. Silt fence is well known for being unable to remove silt and clay sized particles due to their very small particle sizes (Fisher and Jarrett 1984). It is also well known however that the erosion rate of clay particles is lower than the erosion rate of small sands and silts (FDEP 2008). Thus, the soil composition of particles that actually erode from this parent soil may be different from the parent soil composition itself.

Proctor (Laboratory) Compaction Test

The compaction level of the soil affects both the permeability and the erodibility of the soil. The additional compaction reduces the permeability and increases the erodibility of the soil (European Commission 2012). The in situ compaction level of the soil in the test bed is therefore an important characteristic that will affect both the erodibility of the soil and the volume of sheet flow over the soil. For this reason, during testing, a constant compaction level of the soil at the beginning of each test is maintained in order to best simulate constant soil conditions from test to test. Originally, that compaction level prior to each test was 95 percent of maximum dry density of the soil, however, it was too difficult to achieve this level of compaction in the field. The difficultly in achieving this compaction level in the field is discussed in further detail in the section, Test Bed Preparation and Setup, of this chapter. Instead, the soil was compacted to 80 percent of the maximum dry density prior to each new test.

The maximum dry density and the moisture content at which this density occurs is determined using the standard proctor test Method A as described in D698-12 (2013). The results of the laboratory compaction test and compaction curve are presented in Table 24 and

42

Figure 20 of Appendix A. The results of the proctor test show that the maximum dry unit weight of the soil is 1.86 g/cm^3 (116 lb/ft^3) and occurs at a moisture content of 11.5%. With a compaction level of 80% in the field, an initial field density of 1.5 g/cm^3 (92 lb/ft^3) was the compaction goal prior to each field test.

Permeability Test

The permeability of the soil measures the ability of the soil to pass water through it. The permeability and hydraulic conductivity of the soil are found using the constant head method in ASTM D2434-68 (2006). The hydraulic conductivity of the soil describes the ease with which water can move through pore spaces of the soil. It is related to the permeability of the soil, the dynamic viscosity and density of the fluid, and the gravitational constant.

The results of the constant head permeability test are shown in Table 25 of Appendix A. The results of the test show that the permeability and hydraulic conductivity of the soil are 1.41E-08 cm^2 and 0.0014 cm/s, respectively, at a temperature of 20°C and a soil density of 1.45 g/cm^3 (91 lb/ft^3). This value of permeability is in the range for silty-sands (Geotechdata.info 2008).

Silt Fence Geotextiles

Two silt fence fabrics were evaluated in this study. The first silt fence is a woven monofilament geosynthetic which was donated by Absolute Erosion Control, Incorporated and is referred to as an ASR 1400 silt fence. This woven fabric is shown in Figure 3.

FIGURE 3 WOVEN (ASR 1400) SILT FENCE INSTALLED ON A TILTED TEST BED (GOGO-ABITE 2012)

This type of silt fence is well known for being commonly used on construction sites, however, previous studies on this type of silt fence have shown the fences inability in achieving desired performance targets (Gogo-Abite 2012). For this reason, Silt Savers, Inc. introduced a polyester nonwoven belted silt retention fence (BSRF) as shown in Figure 4. The BSRF was designed to both retain more silt and reduce turbidity and suspended sediment more than the traditional woven monofilament silt fence fabric (Risse et al. 2008).

FIGURE 4 NONWOVEN (BSRF) SILT FENCE INSTALLED ON A TILTED TEST BED

Both silt fence fabrics have been tested in a previous study by Gogo-Abite and Chopra (2013) to determine the grab strength, permittivity, and AOS of both the woven (ASR 1400) and nonwoven (BSRF) fabrics. The results from this study were compared with the ASTM D6461 (2007) recommended index test values as shown in Table 3.

TABLE 3 COMPARISON OF WOVEN AND NONWOVEN FABRICS

Property	Direction	ASTM Test Methods	Units	ASTM D6461	Woven Fabric	Nonwoven Fabric
Grab strength	Machine	D 4632	N	400	539	591
	X-Machine			400	637	726
Permittivity		D 4491	sec^{-1}	0.05	0.11	2.5
AOS		D 451	mm	0.6	0.7	0.212

Results of the index testing show that both fabrics, for the most part, surpassed the recommended standards set by ASTM D6461 (2007). The grab strengths of both fabrics were higher than the recommended values, however, the nonwoven fabric was slightly stronger than the woven fabric. The permittivity of both fabrics were also higher than the recommended value, with the woven fabric having a permittivity over a magnitude greater than the recommended value and the nonwoven fabric having a permittivity over two magnitudes greater. The AOS of the woven fabric was the only standard that was not met. The AOS was slightly higher than the maximum value recommended. It will be interesting to see the filtering abilities of the woven and nonwoven fabrics will be affected by this difference in AOS. Recall from Figure 2 that the AOS of the nonwoven fabric (0.212 mm) is smaller than approximately 40% of the soil distribution and that the woven fabric, which AOS is 0.70 mm, is actually larger than 100 percent of the soil distribution used in this study.

<div align="center">Test Bed Preparation and Setup</div>

The investigations on silt fence performance were carried out using the tilted test bed and rainfall simulator at the UCF SMARTL. The aluminum tilted test bed measures 2.4 meter (8 feet) wide by 9.1 meter (30 feet) long by 30.5 centimeter (1 foot) deep and can be set to embankment slopes ranging from 0 to 50 percent. Due to the initial test bed depth of only 30.5 centimeters, the test bed was modified by the construction of a plywood apron on its perimeter in order to increase the depth to 50.8 centimeter (20 inches) to accommodate the minimum required post embedment of 45.7 centimeter (18 inches) as shown in Figure 5a (Gogo-Abite 2012). Following the plywood apron construction a visqueen was placed over the plywood apron in order to protect it from water damage (Figure 5b). The bed was then loaded with the silty-sand

soil (84 percent sand, 12 percent clay, and 4 percent silt, AASHTO Classification Type A-2-4) in

three layers of 15.2 centimeter (6 inch), and compacted to achieve 80 percent Standard Proctor

compaction effort of 7 kilogram per cubic meter (92 pounds per cubic feet) maximum dry unit

weight.
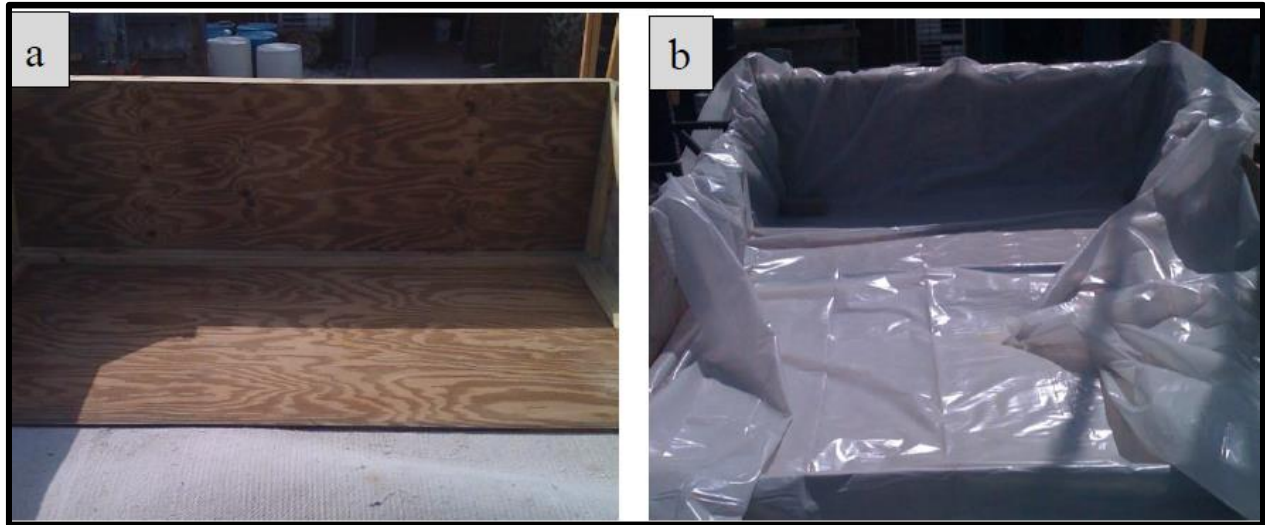
FIGURE 5 PICTURES OF TEST BED MODIFICATIONS (A) PLYWOOD FOR DEPTH, AND (B)
VISQUEEN TO PROTECT PLYWOOD (GOGO-ABITE 2012)

Prior to each field scale test, a silt fence was installed along the perimeter of the test bed

in an "L" shape as shown in Figure 6a. The test bed soil was then graded and compacted as

shown in Figure 6b. Initially, the compaction goal prior to each test was 95% maximum dry unit

weight, however, there was a difficulty in achieving this compaction goal with the silty-sand soil

in the field. Instead a compaction effort of only 80 percent was able to be achieved prior to each

test. A lower compaction effort would cause more percolation of water into the soil and would

also reduce the erosion rate of the soil in comparison with a higher compaction effort. However,

it was more important to have a compaction effort, which could be achieved on a consistent basis

at the beginning of each test, so that all tests would be subjected to the same initial conditions.

For this reason, 80 percent soil compaction was chosen. After test bed soil compaction, rain gages were placed on the test bed in order to measure the rainfall intensity over the test bed, and a meter stick was installed at the face of the silt fence in order to measure the ponding depth of water behind the fence (Figure 6a). The test bed was then raised to the proper embankment slope and the rainfall simulator was placed over the tilted test bed (Figure 6c).

FIGURE 6 TEST BED SETUP (A) WOVEN FABRIC, RAIN GAGES, AND METER STICK INSTALLED, (B) TEST BED COMPACTION, (C) RAINFALL SIMULATOR AND TILTED TEST BED WITH NONWOVEN FABRIC INSTALLED

49

Field Scale Testing Procedure

Both the woven and nonwoven fabrics were field tested under three different

embankment slopes (33, 25, and 10 percent) and three different simulated rainfall intensities –

25, 76, and 127 mm/h (1, 3, and 5 inches per hour). For each embankment slope, each rainfall

intensity was simulated four times for each fabric. The testing matrix for a typical case of 10%

embankment slope is shown in Figure 7.
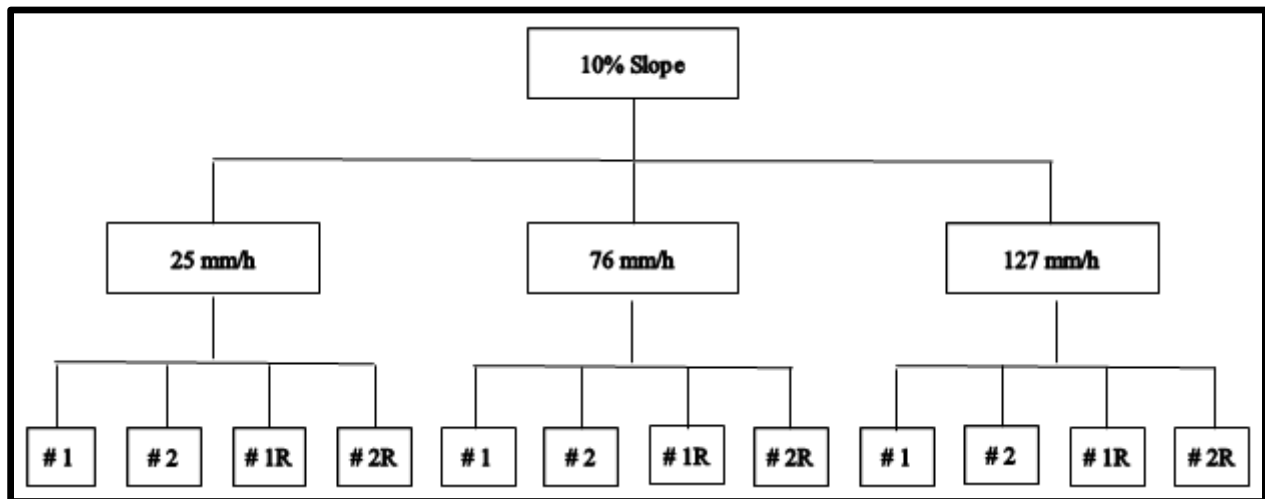
FIGURE 7 SAMPLE FIELD TEST MATRIX FOR 10 PERCENT SLOPE (REPEATED FOR 33 AND 10 PERCENT SLOPES)

Four rainfall events were simulated for each pair of embankment slope and rainfall

intensity. These four rainfall events were broken up into two pairs of two rainfall events each.

The first rainfall event, denoted as #1, evaluated the performance of a newly installed silt fence.

After the commencement of Test #1, a minimum of three-hour interval was given before the

initiation of Test #2. The second rainfall event, denoted as #2, was then simulated without

performing any maintenance or retrofit to the silt fence or soil surface in order to test the silt

fences performance when subjected to an additional rainfall event without having any

50

maintenance performed on it. When Test #2 was completed, a new silt fence was installed and the soil surface was re-graded and compacted to its initial condition of 80 percent maximum dry unit weight. Tests #1 and #2 were then repeated under the same slope and intensity as in the previous two tests. The repeated tests are referred to as # 1R and # 2R as shown in Figure 7.

For each rainfall event, simulated rainfall was allowed to fall over the tilted test bed for 30 minutes after the initiation of downstream runoff through the silt fence. During the 30-minute rainfall event, six grab samples (one grab sample every five minutes for 30 minutes) were collected both upstream (influent) of the silt fence and downstream (effluent) of the silt fence.

Figure 8 shows the downstream collection system used during testing. Runoff water flowed through the silt fence and over a white visqueen where the runoff water was channeled into two separate troughs. Water then flowed through each trough and into a white PVC pipe that connected both troughs. The water then exited the PVC pipe and flowed into a bucket as shown in Figure 8. The bucket was changed every minute and the mass of water that flowed through the fence in that one-minute interval was recorded. In addition, a grab sample was taken from the bucket as well as upstream of the silt fence every five minutes as discussed previously. The upstream sample was taken from the middle of the ponding water depth and close to the silt fence.

FIGURE 8 FIELD SCALE TESTING: DOWNSTREAM COLLECTION SYSTEM

At the end of the 30-minute rainfall event, the concentrated ponded water behind the silt fence was given an additional 30 minutes to flow through the silt fence in order to evaluate the performance of the fabric after the rain event had ended. During this time, six more grab samples (one grab sample every five minutes) were taken both upstream and downstream of the silt fence. All collected grab samples were then tested for both sediment concentration (total solids) and turbidity according to the Standard Methods for the Examination of Water and Wastewater (APHA et al. 2005). In addition to collected grab samples that were tested for turbidity and sediment concentration, downstream runoff was also collected at one-minute intervals from the start of when runoff first occurred to either the conclusion of the one hour test or until runoff stopped, which ever occurred first. Downstream runoff was collected in one-minute intervals in order to measure the flow rate of water with time through the silt fence fabrics.

Limitations of Field Scale Testing

There were certain limitations of the field scale testing procedure used in this study. For the most part, as will be discussed in Chapter 4, the field scale testing method was not repeatable between tests. Many factors contributed to the performance of silt fence from test to test. Changes in the initial field density and moisture content affected both the erosion rate of the soil and percolation of water through the soil. It was not possible to obtain the same exact initial conditions from test to test.

For the upstream collection, a grab sample is taken by hand from the middle of the ponding volume behind the silt fence. The sample was taken from the middle of the pond and close to the silt fence. It is assumed that the turbidity and sediment concentration of this sample represented the average concentration of suspended sediment of the entire ponding volume. However, due to human error in taking sample by hand and the unknown vertical concentration gradient of suspended solids within the pond, this sample may not have adequately represented the concentration within the ponding volume.

The samples that were taken both upstream and downstream of the silt fence also had relatively high turbidity values. Turbidity values were high enough that in order to calculate the turbidity multiple dilutions were needed. The accuracy of the turbidity measurement decreases as the dilution factor is increased.

CHAPTER 4: RESULTS AND DISCUSSION

Introduction

Results of the field scale performance of woven and nonwoven fabrics installed on a silty-sand soil are presented in this section. Both fabrics were tested on three embankment slopes (33, 25, and 10 percent) and under three rainfall intensities – 25, 76, and 125 millimeters per hour (1, 3, 5 inches per hour). In total, 78 rainfall events were simulated over the course of 15 months on both fabrics, starting from June 4, 2012 to September 20, 2013. Although 78 rainfall events were simulated, only 62 of those rainfall events were used in analysis, with the results of the other 16 tests being discarded. These 16 tests were discarded due to a series of testing errors, which led to the results from these tests being unusable. These testing errors involved errors in the upstream collection behind the fence, which yielded average efficiency values of negative 30 to negative 50 percent for both turbidity and suspended sediment concentration. These results were deemed erroneous and the tests were thrown out. The results of these tests are not presented or analyzed in this thesis. All 16 tests that were discarded occurred during testing with the woven fabric; so in total, only 27 rainfall events were used for the woven fabric and 35 rainfall events for the nonwoven fabric.

The tests that were thrown out are four tests from 10 percent slope and 127 mm/h rainfall intensity, four tests from 25 percent slope and 25 mm/h rainfall intensity, four tests from 25 percent slope and 76 mm/h rainfall intensity, and four tests from 25 percent slope and 127 mm/h rainfall intensity. If time had permitted, all 16 tests that were thrown out would have been repeated, however, due to time constraints there was only enough time to complete two additional tests instead of the usual four tests for each of the slope and intensity pairs discussed

above. More tests on the nonwoven fabric than on the woven fabric were analyzed because of the observed errors in the tests on the woven fabric.

The performance evaluation on these silt fence fabrics involve the analysis of fabric efficiency in both turbidity and suspended sediment removal as well as fabric flow-through rate of each geotextile, both during rain events and after rainfall stops. For the woven fabric, 294 grab samples were taken during the rain event and 254 grab samples after the rain event. In the case of the nonwoven fabric, 418 grab samples were taken during the rain event and 380 grab samples after the rain event. There are two discrepancies with these numbers. The first is that over 200 more grab samples were taken overall for the nonwoven fabric than for the woven fabric. The second being that more grab samples were taken during the rain event than after the rain event for both fabrics.

The reason that more samples were taken for the nonwoven fabric was discussed previously and was due to the 8 tests that were not able to be completed due to time constraints. For the second discrepancy there were more grab samples taken during the rain event than after the rain event due to overtopping of the silt fence or fence failure occurring during some of the rainfall events. The overtopping events or fence failures, such as stake breaking and fabric pullout of the fence from the staples, caused the test to be cancelled during the rain event, and no post rainfall samples were collected. In particular, no post rainfall samples were taken for the woven fabric for test on a 33 percent slope and a 127 millimeter per hour (5 inches per hour) rainfall event due to overtopping of the silt fence during all testing. For the nonwoven fabric, a stake breaking in half on a 33 percent slope and a 76 millimeter per hour (3 inches per hour)

56

rainfall also caused no after rain event samples taken. Fence failures that occurred during testing are discussed in more detailed in this chapter in the section: Silt Fence Failure.

For each embankment slope and intensity pair, four tests were completed for each fabric, except for the tests on the woven fabric on 10 percent and 127 mm/h rainfall and each pair on 25 percent embankment slope, as discussed previously. Of these four tests, two were repeated tests using a new fabric on the same slope and intensity as was previously tested. The tests were repeated in order to obtain additional data for each slope and intensity pair and to determine if the field-scale testing procedure was repeatable. In order to show if there was a significant difference in the upstream and downstream turbidity and suspended sediment concentrations between both sets of tests, a Wilcoxon rank sum test was performed on the samples taken during the rain event between both sets of tests. Results of these tests are shown in Table 26 and Table 27 in Appendix B for the woven and nonwoven fabrics, respectively. The tests show that initial conditions and silt fence performance between the initial test and the repeat tests were statistically different with 95 percent confidence in 20 of the 52 tests. These results show that it was difficult to obtain the constant initial conditions sought after for each test and that the erosion rate and the downstream discharge concentrations varied from test to test; and were thus, not very repeatable

Additional statistical analysis is performed throughout this chapter in order to significantly quantify the data. Three types of statistical tests were used; single factor ANOVA, Wilcoxon rank sum test, and Wilcoxon rank sum test on difference. All statistical tests were completed with a confidence level of 95 percent ($\alpha = 0.05$) and are located in the appropriate appendixes.

Tables of results of all time dependent efficiency and flow-through rates from field scale testing are presented in Table 46 through Table 48 for the woven fabric and Table 49 through Table 51 for the nonwoven fabric in Appendix D. The remainder of this chapter discusses all results pertaining to this research with field scale testing of silt fence fabrics used in conjunction with a silty-sand soil. The chapter is broken into four main sections; fabric performance during the rain event, fabric performance after the rain event, overall silt fence performance based on measured samples, and overall silt fence performance based on projection. The first section is further broken down into discussions on fabric efficiency, fabric flow-through rate, and silt fence failure; and the second section is broken into discussions on fabric efficiency and flow-through rate.

Fabric Performance during Rain Events

Fabric Reduction Efficiency during Rain Events

This section presents results of fabric performance efficiency in both turbidity and suspended sediment concentrations (SSC), which occurred during the rainfall event. On every test, both the turbidity and SCC values were obtained from all collected grab samples both downstream and upstream of the silt fence. Downstream turbidity and SCC values were weighted by the volume of runoff water which transmitted through the silt fence for that sample. Upstream values were weighted by the volume of ponding water upstream of the silt fence when the sample was taken. The volume-weighted downstream and upstream values were then compared to each other to determine a mean efficiency value. These computations are expressed in Equations 4 through 9

$$WMIT = \frac{\sum_{i=0}^{n}[T_{\text{INF}} * V_{upstream}]}{\sum_{i=0}^{n} V_{upstream}} \tag{4}$$

$$WMIC = \frac{\sum_{i=0}^{n}[TS_{\text{INF}} * V_{upstream}]}{\sum_{i=0}^{n} V_{upstream}} \tag{5}$$

$$(WMET)_{\text{DR}} = \frac{\sum_{i=0}^{n}[T_{\text{EFF}} * V_{downstream}]}{\sum_{i=0}^{n} V_{downstream}} \tag{6}$$

$$(WMEC)_{DR} = \frac{\sum_{i=0}^{n}[TS_{\text{EFF}} * V_{downstream}]}{\sum_{i=0}^{n} V_{downstream}} \tag{7}$$

$$E_T(\%)_{DR} = 100 * \left[1 - \frac{(WMET)_{DR}}{WMIT}\right] \tag{8}$$

$$E_{SSC}(\%)_{DR} = 100 * \left[1 - \frac{(WMEC)_{DR}}{WMIC}\right] \tag{9}$$

where, WMIT is the volume-weighted mean influent turbidity (NTU); $(WMET)_{DR}$ is the volume-weighted mean effluent turbidity during the rain event (NTU); T_{inf} is the influent turbidity value collected for sample i (NTU); $V_{upstream}$ is the upstream ponding volume when sample i was taken (L); WMIC is the volume-weighted mean influent concentration (mg/L); $(WMEC)_{DR}$ is the volume-weighted mean effluent concentration during the rain event (mg/L); SSC is the suspended sediment concentration in runoff collected for sample i (mg/L); $V_{downstream}$ is the volume of collected runoff which discharged through the silt fence in interval between sample i and sample $i-1$ (L); n is the number of samples collected during the rain event; $E_T(\%)_{DR}$ is the mean turbidity performance efficiency during the rain event; and $E_{SSC}(\%)_{DR}$ is the mean suspended sediment concentration performance efficiency during the rain event. Table 4 and TABLE 5 present the volume-weighted turbidity and suspended sediment concentration and the respective performance efficiency that occurred during the rain event for both the ASR-1400 and BSRF silt fence fabrics. Note that from this point forward, woven fabric will be used to refer to the ASR-1400 silt fence and nonwoven fabric will be used to refer to the BSRF silt fence.

TABLE 4 WOVEN FABRIC TEST VOLUME-WEIGHTED MEAN TURBIDITY AND SSC RESULTS DURING THE RAIN EVENT

Slope % (Ratio)	Rainfall Intensity (mm/h)	Rainfall Events	Volume-Weighted Mean Turbidity			Volume-Weighted Mean SSC		
			Up-stream (NTU)	Down-stream (NTU)	Performance Efficiency (%)	Up-stream (mg/L)	Down-stream (mg/L)	Performance Efficiency (%)
33% (3:1) Slope	25	#1	50171	25054	50	32616	14186	57
		#2	33573	16998	49	23412	15867	32
		#1R	28738	19743	31	21001	13728	35
		#2R	30096	17200	43	25614	13299	48
	76	#1	43339	19359	55	40099	13496	66
		#2	--	--	--	--	--	--
		#1R	41442	20644	50	21641	12620	42
		#2R	27811	15466	44	17641	11928	32
	127	#1	48311	18760	61	31212	12121	61
		#2	--	--	--	--	--	--
		#1R	57945	27442	53	46322	21086	54
		#2R	40266	28031	30	35427	21355	40
25% (4:1) Slope	25	#1	29396	22130	25	19585	14185	28
		#2	21551	15465	28	13875	11893	14
	76	#1	19080	14532	24	13462	11312	16
		#2	25891	20995	19	11361	9797	14
	127	#1	47590	22583	53	15744	12260	22
		#2	30530	18983	38	12755	8541	33
10% (10:1) Slope	25	#1	12357	7782	37	10959	6558	40
		#2	10839	3293	70	10743	2409	78
		#1R	13365	5176	61	10468	3544	66
		#2R	9453	5113	46	5920	3621	39
	76	#1	5358	4132	23	4215	3089	27
		#2	3707	2802	24	3426	2196	36
		#1R	6036	4472	26	4610	3491	24
		#2R	2619	2092	20	2117	1681	21
	127	#1	4886	3129	36	3982	2363	41
		#2	4321	2644	39	3763	2171	42

Table entries that appear with "--" indicate that no samples were collected during those tests due to previous test failures

TABLE 5 NONWOVEN FABRIC TEST VOLUME-WEIGHTED MEAN TURBIDITY AND SSC RESULTS DURING THE RAIN EVENT

Slope % (Ratio)	Rainfall Intensity (mm/h)	Rainfall Events	Volume-Weighted Mean Turbidity			Volume-Weighted Mean SSC		
			Up-stream (NTU)	Down-stream (NTU)	Performance Efficiency (%)	Up-stream (mg/L)	Down-stream (mg/L)	Performance Efficiency (%)
33% (3:1) Slope	25	#1	29690	13544	54	27767	9356	66
		#2	39009	2467	94	25079	3001	88
		#1R	46765	24193	48	33356	16805	50
		#2R	18628	9623	48	22205	8753	61
	76	#1	40355	18276	55	31706	14155	55
		#2	32081	11134	65	24753	9700	61
		#1R	26588	20144	24	19271	12361	36
		#2R	24696	12370	50	19142	9423	51
	127	#1	37989	21601	43	31958	17041	47
		#2	--	--	--	--	--	--
		#1R	37008	16518	55	26679	13855	48
		#2R	18925	12308	35	13685	6012	56
25% (4:1) Slope	25	#1	24380	12494	49	21495	9037	58
		#2	20556	7308	64	17723	5361	70
		#1R	22906	16882	26	18459	11691	37
		#2R	22996	9191	60	17807	7024	61
	76	#1	8780	7861	10	6547	6682	-2
		#2	6976	5567	20	5256	4204	20
		#1R	8244	6002	27	5608	4274	24
		#2R	3915	2431	38	2720	1107	59
	127	#1	7772	6282	19	5544	4465	19
		#2	19213	10394	46	14032	8048	43
		#1R	14489	8965	38	13018	6301	52
		#2R	8384	4284	49	7123	3221	55
10% (10:1) Slope	25	#1	13512	1848	86	14449	1327	91
		#2	13824	2101	85	14555	2136	85
		#1R	6631	2512	62	5962	1891	68
		#2R	9973	3539	65	7318	2660	64
	76	#1	9472	4769	50	10330	3303	68
		#2	10282	2686	74	11088	2222	80
		#1R	7217	5072	30	5932	3611	39
		#2R	4736	1545	67	3441	1178	66

Slope % (Ratio)	Rainfall Intensity (mm/h)	Rainfall Events	Volume-Weighted Mean Turbidity			Volume-Weighted Mean SSC		
			Up-stream (NTU)	Down-stream (NTU)	Performance Efficiency (%)	Up-stream (mg/L)	Down-stream (mg/L)	Performance Efficiency (%)
	127	#1	12466	7966	36	7147	4606	36
		#2	14303	5764	60	10503	2715	74
		#1R	8629	5817	33	6416	4544	29
		#2R	6044	3298	45	4779	2457	49

Table entries that appear with "--" indicate that no samples were collected during those tests due to previous test failures

Table 4 and TABLE 5 show the volume-weighted mean influent and effluent, and efficiency values for both the turbidity and SSC for both fabrics for every test during the rain event. These results show that overall for the woven fabric, turbidity performance efficiency during the rain event for all slopes and intensities tested ranged from 19 to 70 percent with a mean and median of 40 and 38 percent, respectively. The SCC performance efficiency ranged from 14 to 78 percent with a mean and median of 39 and 37 percent, respectively. For the nonwoven fabric, performance efficiency during the rain event ranged from 10 to 94 percent with a mean and median of 49 percent, and from negative 2 to 91 percent with a mean of 53 percent and a median of 55 percent for the turbidity and SCC, respectively. From these results, a Wilcoxon rank sum test was performed to determine if the nonwoven fabric performance efficiencies were significantly higher than those occurring with the woven fabric. The test was completed using the volume-weighted mean efficiencies that were shown in Table 4 and TABLE 5 for each embankment slope. The results of these tests are shown in Table 28 of Appendix B. The statistical analysis showed that the nonwoven fabric significantly reduced both turbidity and SSC to a greater extent than the woven fabric over the combination of all embankment slopes.

The greater reduction by the nonwoven fabric can be attributed to the smaller pore size of this fabric when compared to the woven fabric.

Fabric Reduction Efficiency based on Embankment Slope

For each fabric, testing was completed on three embankment slopes; 10, 25, and 33 percent slopes. Comparison between the efficiency values occurring between slopes can give insight into a possible relation of silt fence effectiveness with change in slope. The comparison was done using a single factor ANOVA analysis in order to test if the efficiency values occurring on each slope stem from the same underlying distribution. If the ANOVA test were to be significant, it would indicate that the efficiency values occurring on at least one of the slopes differed significantly from the others. The analyses were done on the volume-weighted mean efficiency values for all embankment slopes (that is, 10, 25 and 33 percent) during the rainfall event. The results and discussion of these tests are presented in the following two sections for the woven and nonwoven fabrics.

Woven Fabric Performance Efficiency based on Embankment Slope

Results showed that during rainfall, the woven fabric had 40 and 39 percent turbidity and SSC performance efficiencies, respectively, for all embankment slopes and rainfall intensities. Statistical analysis shows however that the efficiency values of both turbidity and SSC were significantly different when compared on different embankment slopes as shown in Table 32 of Appendix B. The changes in the turbidity and SSC performance efficiency with changes in slope are shown graphically in Figure 9 and FIGURE 10, respectively.

64
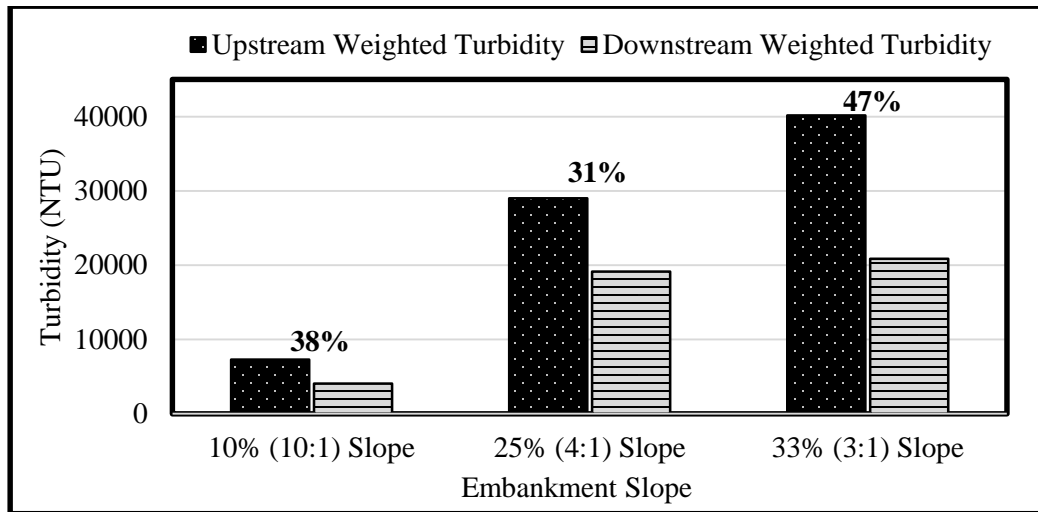
FIGURE 9 WOVEN FABRIC VOLUME-WEIGHTED MEAN TURBIDITY PERFORMANCE EFFICIENCY
WITH EMBANKMENT SLOPE

Shown directly above both bars on each embankment slope is the average performance

efficiency on the respective embankment slope. The highest mean performance efficiency

occurred on the 33 percent embankment slope and the lowest efficiency occurred on the 25
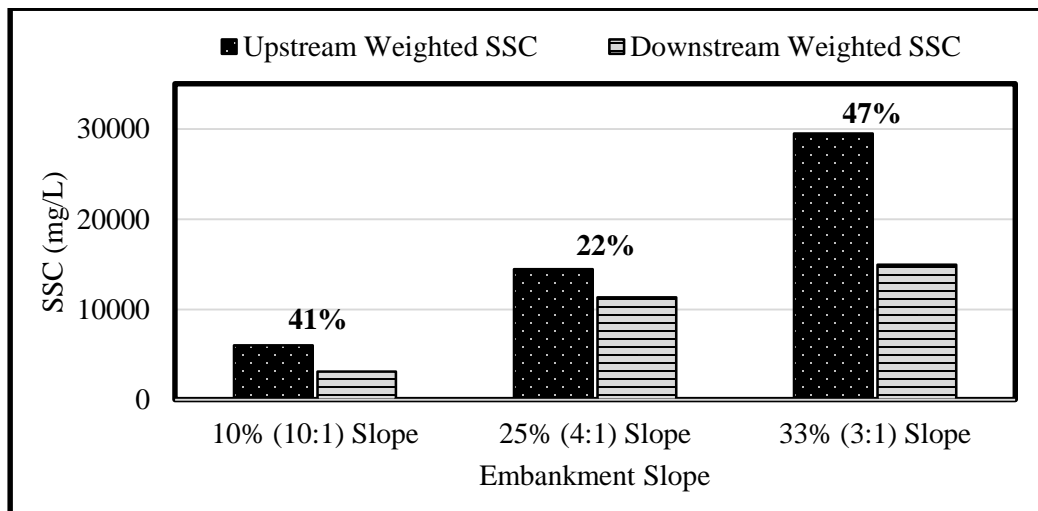
percent slope.

FIGURE 10 WOVEN FABRIC VOLUME-WEIGHTED MEAN SSC PERFORMANCE EFFICIENCY WITH
EMBANKMENT SLOPE

Results for the SCC performance efficiency show a similar trend to those of the turbidity, with efficiencies of 41 and 47 percent on 10 and 33 percent slopes, respectively, but with mean performance efficiency of only 21 percent on the 25 percent slope. Once again, the lowest mean efficiencies occurred on the 25 percent slope. It is not completely understood why the performance efficiency decreased on the 25 percent slope, however, a possible theory is given in the following section.

Although there was not much of a trend in performance efficiency with degree of slope, Figure 9 and FIGURE 10 show the significant increase in both upstream and downstream turbidity and sediment concentrations with increases in slope percent, respectively. The reason for the increasing trend was due to the increase in the rate of erosion caused by increasing degree of slope; as the degree of slope increased, erosion rate increased, and more particles were available to runoff through the silt fence. The trend shows that although performance efficiency was similar on 10 and 33 percent embankment slopes, the effluent turbidity and sediment concentrations were significantly higher on the 33 percent slope. It is also interesting that even though the lowest volume-weighted mean reduction efficiencies occurred on 25 percent embankment slopes, the volume-weighted mean effluent turbidity and concentration were still lower on the 25 percent slope when compared to the 33 percent slope due to the higher erosion rate occurring on the 33 percent slope.

Nonwoven Fabric Reduction Efficiency Based on Embankment Slope

For the nonwoven fabric, performance results during rainfall event showed that turbidity and SSC were reduced by a mean value of 49 and 53 percent, respectively, for all embankment slopes and rainfall intensities. Similar to the woven fabric, statistical analysis on

the nonwoven fabric as shown in Table 33 of Appendix B showed that the efficiency values of both turbidity and SSC were significantly different when compared on different embankment slopes. The changes in the turbidity and SSC performance efficiency with changes in slope are shown in Figure 11 and FIGURE 12, respectively.
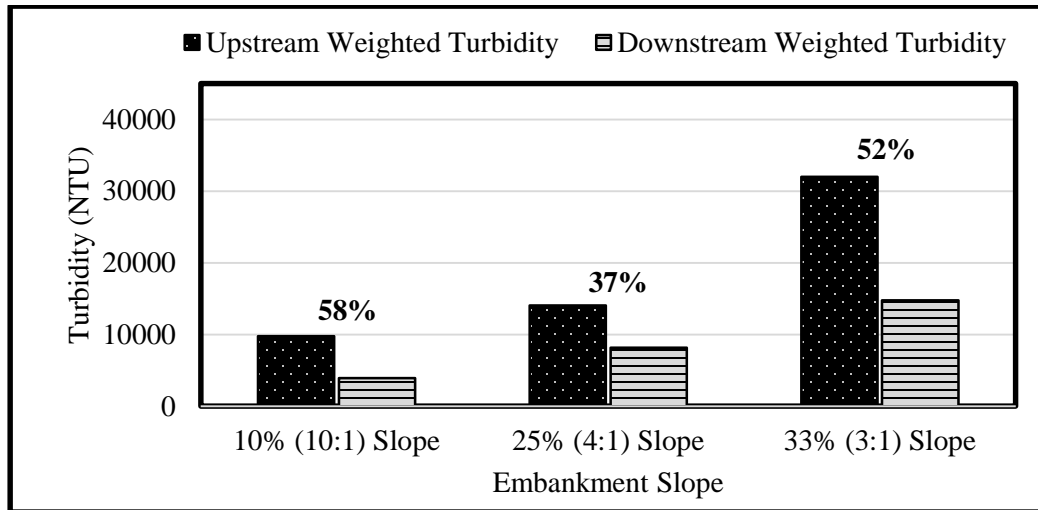
FIGURE 11 NONWOVEN FABRIC VOLUME-WEIGHTED MEAN TURBIDITY PERFORMANCE EFFICIENCY WITH EMBANKMENT SLOPE
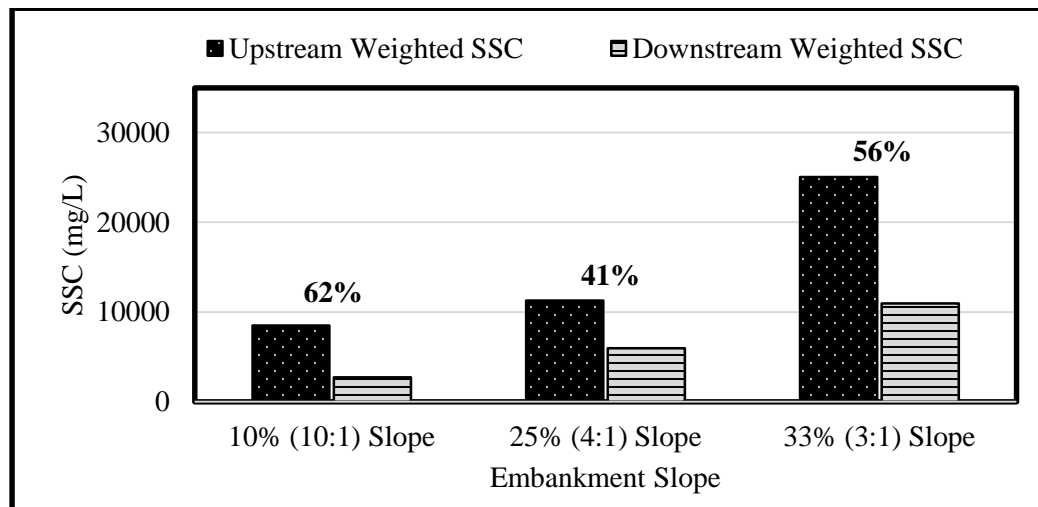
FIGURE 12 NONWOVEN FABRIC VOLUME-WEIGHTED MEAN SSC PERFORMANCE EFFICIENCY WITH EMBANKMENT SLOPE

For the nonwoven fabric the average volume-weighted performance efficiencies were 58 and 62 percent for the turbidity and SSC on the 10 percent slope, 37 and 41 percent for the turbidity and SSC on the 25 percent slope, and 52 and 56 percent for the turbidity and SSC on the 33 percent slope. These results show that the average performance efficiencies of both turbidity and SSC were higher on the nonwoven fabric than on the woven fabric for the three embankment slopes tested.

As was the case with the woven fabric, the 25 percent slope had the lowest performance efficiencies of both turbidity and SSC, and the efficiency on this slope was significantly different from the reduction on 10 and 33 percent slopes. A possible explanation for this trend, which occurred on testing with both silt fence fabrics, could be due to the effect of settling and filtering on these slopes. On the high slope of 33 percent, the erosion rate was very high, leading to a large amount of suspended sediment in the upstream ponding volume. Due to the large portion of suspended sediment, the filtering of the fabric was increased due to increased opportunity for particles to clog the pore spaces of the fabric; leading to a relatively high efficiency on the 33 percent slope. On the lower slope of 10 percent, the amount of suspended particles in the pond was much lower due to the decreased erosion rate. However, due to the low slope, the ponding volume height is also much lower; possibly allowing a large portion of the suspended solids within the ponding volume to settle before discharging through the silt fence and leading once again to a relatively high efficiency. On the 25 percent slope, based on geometry of the slope and assuming a constant flow-through rate, the ponding height would be 2.5 times that of the 10 percent slope, which would lead to a much smaller portion of the suspended mass settling out than was the case with the 10 percent slope. The ponding depth on the 25 percent slope would

be much closer to the case of the 33 percent slope, with the ponding depth on the 33 percent slope only being 1.3 times higher than on the 25 percent slope. Although the ponding depths would be similar, the added erosion caused from increasing the slope from 25 to 33 percent led to the upstream suspended solids concentration doubling as shown in Figure 10 and FIGURE 12. The settling taking place on the 25 and 33 percent slopes would therefore be similar but the filtering on the 33 percent slope would be much larger due to the much higher influent SSC. This is a possible explanation for why the performance efficiency is seen to decrease on the 25 percent slope when compared to the 10 and 33 percent slopes. This result also shows that it is likely that if a constant influent concentration were to be used for all three embankment slopes, there would most likely be a trend of decreasing efficiency with increasing embankment slope.

Fabric Reduction Efficiency from Test 1 to Test 2

For each rainfall intensity and embankment slope, four tests were completed on each fabric. Test 1 was performed on a new silt fence material and Test 2 was performed on the silt fence used in Test 1 without any maintenance being performed on the silt fence. These two tests were then repeated on a new silt fence under the same intensity and slope. Comparison between Test 1 and Test 2 can help show how silt fence fabric performance is affected by being used previously without having any maintenance performed. The comparison was done using a Wilcoxon signed rank test and was completed in order to determine if a change in performance efficiency was significant between Test 1 and Test 2 for both fabrics. The signed rank test was completed on the time dependent efficiency values between each test that occurred during the rain event. The results and discussion of these tests are shown in the following two sections for the woven fabric and the nonwoven fabric, respectively.

69

Woven Fabric Reduction Efficiency from Test 1 to Test 2

A summary of the volume-weighted mean turbidity and SCC performance efficiencies that occurred on the woven fabric from Test 1 to Test 2 are shown in Table 6.

TABLE 6 WOVEN FABRIC TURBIDITY AND SCC PERFORMANCE EFFICIENCY FROM TEST 1 TO TEST 2

Slope % (Ratio)	Rainfall Intensity (mm/h)	Rainfall Events	Volume-Weighted Mean Turbidity Efficiency (%)		Volume-Weighted Mean SSC Efficiency (%)	
			Test 1 (New Fabric)	Test 2 (Used Fabric)	Test 1 (New Fabric)	Test 2 (Used Fabric)
33% (3:1) Slope	25	#1, #2	51	50	58	34
		#1R, #2R	35	43	37	48
	76	#1, #2	55	--	67	--
		#1R, #2R	51	45	43	34
	127	#1, #2	64	--	67	--
		#1R, #2R	53	30	54	40
25% (4:1) Slope	25	#1, #2	24	28	26	13
	76	#1, #2	25	23	18	17
	127	#1, #2	53	41	22	35
10% (10:1) Slope	25	#1, #2	36	69	40	78
		#1R, #2R	61	49	66	42
	76	#1, #2	30	26	33	37
		#1R, #2R	33	24	31	25
	127	#1, #2	36	42	41	44

Table entries that appear with "--" indicate that no samples were collected during those tests due to previous test failures.

Overall, the volume-weighted mean turbidity efficiency for all tests from Test 1 to Test 2 showed a slighted decrease; having mean performance efficiency of 44 percent on Test 1 and mean efficiency of 39 percent on Test 2. The volume-weighted mean SSC for all tests was similar as well; having mean performance efficiency of 43 percent on Test 1 and mean efficiency of 37 percent on Test 2.

The statistical analysis however, showed that a change in fabric efficiency was not significant with 95 percent confidence from Test 1 to Test 2. The statistical analysis is shown in Table 34 and Table 35 of Appendix B for the turbidity and SSC, respectively.

The overall decrease in efficiency from Test 1 to Test 2 may indicate that the woven fabric pore spaces were stretched and enlarged from Test 1 to Test 2. The pore spaces could have been enlarged due to the stress brought on by the ponding volume on the silt fence from the previous test. The increase in pore size would have decreased the filtration ability of the fabric, decreasing the filtration mechanism of the woven fabric from Test 1 to Test 2. Previous studies by (Gogo-Abite 2012) have indicated a similar result of the pore sizes of the woven fabric increasing due to increased ponding depth on the upstream side of the silt fence. However, results from this study show that a change in efficiency between Test 1 to Test 2 was not significant with the woven fabric.

Nonwoven Fabric Reduction Efficiency from Test 1 to Test 2

Statistical analysis on the change in turbidity and SSC performance efficiency from Test 1 to Test 2 of nonwoven fabrics is shown in Table 36 and Table 37 of Appendix B. Table 7 shows a summary of the performance efficiencies that occurred from Test 1 to Test 2 for the nonwoven fabric.

TABLE 7 NONWOVEN FABRIC TURBIDITY AND SSC PERFORMANCE EFFICIENCY FROM TEST 1 TO TEST 2

Slope % (Ratio)	Rainfall Intensity (mm/h)	Rainfall Events	Volume-Weighted Mean Turbidity Efficiency (%)		Volume-Weighted Mean SSC Efficiency (%)	
			Test 1 (New Fabric)	Test 2 (Used Fabric)	Test 1 (New Fabric)	Test 2 (Used Fabric)
33% (3:1) Slope	25	#1, #2	56	94	67	88
		#1R, #2R	49	49	50	61
	76	#1, #2	56	66	58	62
		#1R, #2R	27	50	38	50
	127	#1, #2	47	--	48	--
		#1R, #2R	58	38	51	58
25% (4:1) Slope	25	#1, #2	49	64	59	70
		#1R, #2R	27	58	37	59
	76	#1, #2	13	20	1	20
		#1R, #2R	32	39	30	59
	127	#1, #2	35	48	23	45
		#1R, #2R	40	51	55	57
10% (10:1) Slope	25	#1, #2	86	85	91	85
		#1R, #2R	64	65	71	64
	76	#1, #2	50	74	68	80
		#1R, #2R	32	67	42	66
	127	#1, #2	39	60	39	74
		#1R, #2R	34	46	30	49

Table entries that appear with "--" indicate that no samples were collected during those tests due to previous test failures.

The overall volume-weighted mean efficiency values that occurred for the nonwoven fabric from Test 1 to Test 2 were 44 to 57 percent and 48 to 62 percent for the turbidity and SSC efficiencies, respectively. The statistical analysis showed that there was a significant increase in the turbidity and sediment performance efficiencies from Test 1 to Test 2 on 10, 25, and 33 percent slopes for the nonwoven fabric. These results indicate that clogged particles within and on the fabric from previous tests influenced the performance of the nonwoven fabric and led to

the increase in efficiency from Test 1 to Test 2. The clogged particles would have increased the efficiency from Test 1 to Test 2 because they would decrease the pore size of the fabric and allowed additional filtration to occur.

In general, both impingement of particles on the fabric and pore space enlargement due to ponding water will affect the performance of silt fence from Test 1 to Test 2, as well as over the lifespan of the silt fence in the field over many rainfall events. Although both mechanisms will contribute to the future performance of the silt fence, from the results of the field scale testing of these two fabrics indicate that the dominate mechanism for the nonwoven fabric was the impingement of particles on the fabric which increased the efficiency of the silt fence. The dominating mechanism for the woven fabric however could not be determined with a significant degree of confidence.

Flow-through rate during the Rain Event

The water flux through the silt fence fabrics, herein referred to as flow-through rate, is a measure of the volume of water that flows through the silt fence per unit area of silt fence. In this study the flow-through rate is calculated as the volume of water which flowed through the fabric in time interval t, divided by the average area of submerged silt fence during the same time period as expressed in Equation 10. For each test, the calculated flow-through rate for each time interval during the rain event was then averaged to obtain a representative mean flow-through rate for each test as expressed in Equation 11. Table 8 presents summary results for the average flow-through rate encountered on each embankment slope during the rain event for each fabric.

$$q_i = \frac{V_{downstream}}{\left[\frac{1}{2}*(PD_{i-1}+PD_i)\right]*b_{TB}*\Delta t} \tag{10}$$

$$q_{DR} = \frac{\sum_{i=2}^{n} q_i}{n-1} \qquad\qquad (11)$$

where, i refers to the time dependent order with which the ponding depth upstream of the silt

fence is measured; n refers to the number of measurements taken; q_i is the flow-through rate of

the silt fence fabric during the rain event occurring during measurement i (L/m^2/h); q_{DR} is the

average flow-through rate occurring during the rain event; $V_{downstream}$ is the volume of

collected runoff which discharged through the silt fence in interval between measurement i - 1

and measurement i (L); PD_i is the ponding depth occurring at measurement i; b_{TB} is the width of

the test bed; and Δt is the time interval between measurement i - 1 and measurement i.

TABLE 8 SUMMARY RESULTS FOR FLOW-THROUGH RATE OF WOVEN AND NONWOVEN FABRICS
DURING THE RAIN EVENT

Embankment Slope (%)	Rainfall Intensity (mm/h)	Flow-through rate (L/m^2/h)					
		Woven Fabric			Nonwoven Fabric		
		Mean	Median	Standard Deviation	Mean	Median	Standard Deviation
33	25	60	57	42	310	293	176
	76	132	103	74	416	442	231
	127	72	64	27	460	419	289
25	25	125	128	26	880	973	460
	76	214	178	96	1512	1566	234
	127	397	377	177	1155	1136	624
10	25	830	902	408	1267	766	1018
	76	1494	1448	570	2377	2248	837
	127	1360	1376	209	2564	2686	1266

Results from Table 8 show that nonwoven fabric achieved a higher mean flow-through

rate during the rain event on every slope and intensity pair tested. Higher flow-through rates

would decrease the chances of developing high ponding depths which could lead to silt fence

failure or overtopping of the silt fence. Lower flow through rates, however, would decrease the volume of water that is discharged during the rain event. This would lead to a higher overall efficiency of the silt fence as will be discussed in this chapter in the section: Overall Performance Efficiency (Projected).

The results also suggest a trend of increasing flow-through rate with decreasing embankment slope. The mean flow-through rate is shown to increase by approximately a magnitude when comparing results on the 33 percent slope to those on the 10 percent slope. For the woven fabric, the flow-through rate is shown to range from 57 $L/m^2/h$ on a 33 percent slope to 1494 $L/m^2/h$ on a 10 percent slope, and in the case of the nonwoven fabric, from 310 $L/m^2/h$ on a 33 percent slope to 2564 $L/m^2/h$ on a 10 percent slope.

A statistical analysis was performed in order to determine if the trend of increasing flow-through rate with decreasing embankment slope was significant during the tests. The statistical analysis was completed by performing a Wilcoxon rank sum test between the time dependent flow-through rate values on 10 and 25 percent slopes and then again between the flow-through rate values on 25 and 33 percent slopes for both fabrics. The results of these statistical analyses are shown in Table 40 and Table 41 of Appendix C for the woven and nonwoven fabrics, respectively. Results revealed that the flow-through rate of both silt fence fabrics was significantly higher on the 10 percent slope when compared to the 25 percent slope and that the flow-through rates were also significantly higher on the 25 percent slope when compared to the 33 percent slope.

The results of this statistical analysis; decreases in flow-through rate with increases in embankment slope, goes against what would be commonly expected. In theory, given clean

water, an increase in embankment slope should cause an increase in the flow-through rate, not a decrease. The reason for this is that the ponding depth behind the silt fence will be higher on the higher slope if the influent water volume remains constant. Higher ponding depths would cause a larger force on the silt fence and would cause the pores of the fabric to be enlarged, increasing the flow-through rate of the fabric. The result from this study however shows the opposite; that increases in embankment slope caused a decrease in the flow-through rate.

The observed contradiction is because the flow-through rate is directly related to the concentration of suspended sediment in contact with each fabric. Recall from Figure 10 and Figure 12 that the erosion rate and the concentration of upstream suspended solids increased with increasing embankment slope. The increase in upstream SSC led to a decrease in the flow-through rate because the mass of particles that had the potential to be filtered by the fabric increased. Filtering of the soil particles by the fabric clogged the fabrics pores and decreased the ability of the fabric to transmit water. Risse et al. (2008) and Britton et al. (2000) also observed that increasing sediment concentration led to a decrease in flow-through rate of silt fence. Figure 13 shows the trend of decreasing flow-through rate with increasing upstream suspended sediment concentration encountered for both the woven and nonwoven fabrics for this soil type.
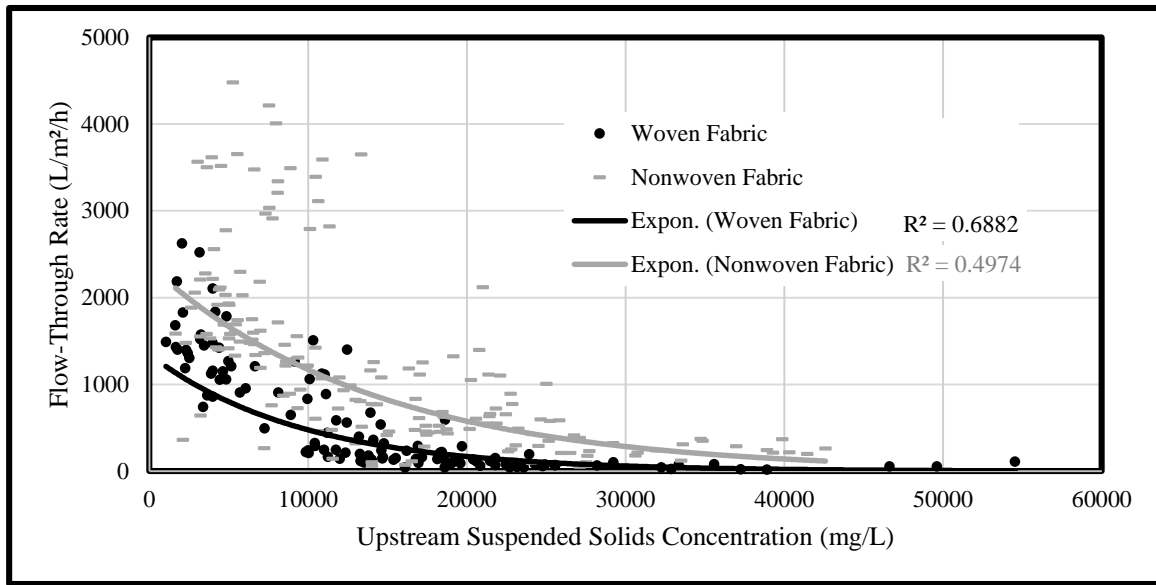
FIGURE 13 TREND OF DECREASING FLOW-THROUGH RATE WITH INCREASING UPSTREAM SSC
FOR BOTH WOVEN AND NONWOVEN FABRICS

Figure 13 is a plot of the SSC in the ponding water volume upstream of the silt fence (x-axis) verse the average flow-through rate of the silt fence (y-axis). Note that the plot is only of samples taken during the rain event. In total, 112 samples for the woven fabric and 163 samples for the nonwoven fabric. According to Figure 13, the flow-through rate tended to decrease exponentially with increases in the upstream solids concentration ($R^2 = 0.69$ for the woven fabric and $R^2 = 0.52$ for the nonwoven fabric). This trend was due to the increased filtering and impingement of soil particles on the fabric with increases in the SSC in contact with the silt fence. This increase in filtering caused reduction of the fabric pore size and limited the ability of water to flow through the silt fence. The plot shows how strongly influenced the flow-through rate of silt fence fabrics can be on the concentration of suspended solids in contact with them. The plot also shows that the flow-through rates encountered in the field are more a function of the upstream suspended solids concentration than the initial permittivity or AOS of the fabric.

77

It would have been interesting to test the effect of changing upstream SSC on the flow-through rate of used fabrics. For instance, testing the fabric under a high slope (high concentration) condition during Test 1. Then, during Test 2, testing the same silt fence under a lower slope (lower concentration) condition to see if the high influent concentration from Test 1 would have affected the flow-through rate encountered in Test 2. In this study, these tests were not conducted, however, changing rainfall intensity under the same embankment slope was, and is the topic of the next section.

Comparing flow-through rate from Test 1 to Test 2

Comparing the flow-through rate of the silt fence from Test 1 to Test 2 can give insight into how the fabric is affected by multiple rain events occurring without maintenance being performed. A Wilcoxon signed rank test on the difference between Test 1 and Test 2 was completed on the time dependent flow-through rate values to determine if a significant change in the flow-through rate occurred from Test 1 to Test 2 for each embankment slope. The test was conducted on the difference between Test 1 and Test 2 because the flow-through rate data show a trend of increasing with time during the rain event due to the increasing ponding depth. For this reason, the statistical analysis is performed by pairing the flow-through rates on a time dependent basis between Test 1 and Test 2. The statistical analysis is shown in Table 42 of Appendix C for both woven and nonwoven fabrics.

The mean flow-through rates for both fabrics occurring on Test 1 and Test 2 during the rain event are presented in Table 9 for each embankment slope and intensity pair tested.

TABLE 9 AVERAGE FLOW-THROUGH RATE OCCURRING DURING THE RAIN EVENT BETWEEN
TEST 1 AND TEST 2 FOR BOTH WOVEN AND NONWOVEN FABRICS

| Slope % (Ratio) | Rainfall Intensity (mm/h) | Rainfall Events | Average Flow-through rate During the Rain Event (L/m^2/h) | | | |
| | | | Woven Fabric | | Nonwoven Fabric | |
			Test 1 (New Fabric)	Test 2 (Used Fabric)	Test 1 (New Fabric)	Test 2 (Used Fabric)
33% (3:1) Slope	25	#1, #2	27	68	198	228
		#1R, #2R	44	102	340	476
	76	#1, #2	131	--	254	324
		#1R, #2R	97	167	583	504
	127	#1, #2	154	--	344	--
		#1R, #2R	51	--	389	648
25% (4:1) Slope	25	#1, #2	117	132	636	411
		#1R, #2R	--	--	1386	1085
	76	#1, #2	167	260	1620	1629
		#1R, #2R	--	--	1433	1368
	127	#1, #2	370	424	1985	652
		#1R, #2R	--	--	1091	892
10% (10:1) Slope	25	#1, #2	805	1279	464	604
		#1R, #2R	244	992	1142	2859
	76	#1, #2	2057	1516	3384	1293
		#1R, #2R	1129	1272	2690	2141
	127	#1, #2	1458	1262	1513	1265
		#1R, #2R	--	--	3774	3702

Table entries that appear with "--" indicate that the flow-through rate could not be calculated during these tests due to test failures

The statistical analysis showed that, for the woven fabric, there was a trend of increasing flow-through rate from Test 1 to Test 2 on the combination of all embankment slope tested. This trend was also significant on the 25 and 33 percent slopes, however, it was not significant on the 10 percent slope The increase in flow-through rate suggest that the pore spaces

of the fabric increased from Test 1 to Test 2, allowing an increase in the rate at which water was allowed to flow through the silt fence.

The statistical analysis also showed that, for the nonwoven fabric, there was a trend of decreasing flow through rate from Test 1 to Test 2 on 10 and 25 percent slopes, however the trend was only significant with 95 percent confidence on the 25 percent slope. The decrease in flow-through rate conforms with the results from the section: Nonwoven Fabric Reduction Efficiency from Test 1 to Test 2, in which the reduction efficiency was found to increase from Test 1 to Test 2. These tests suggest that it is likely that the impingement of particles within the fabric decreased the pore size of the fabric and caused both an increase in the reduction efficiency and a decrease in the flow-through rate from Test 1 to Test 2.

However, for the nonwoven fabric on the 33 percent slope, the statistical analysis showed that there was a trend of increasing flow-through rate from Test 1 to Test 2, but the result was not significant for 95 percent confidence interval. Although the trend suggest an increase in flow-through rate from Test 1 to Test 2, review of the time dependent flow-through rate results shown in Table 51 of Appendix C suggest that the impingement of particles within the fabric from Test 1 did decreased the flow-through rate of this fabric in Test 2. The decrease in flow-through rate however only occurred for the first couple of samples taken. The reason for this is shown graphically in Figure 14 below for testing done on a 33 percent slope and 76 mm/h rainfall event on the nonwoven fabric.
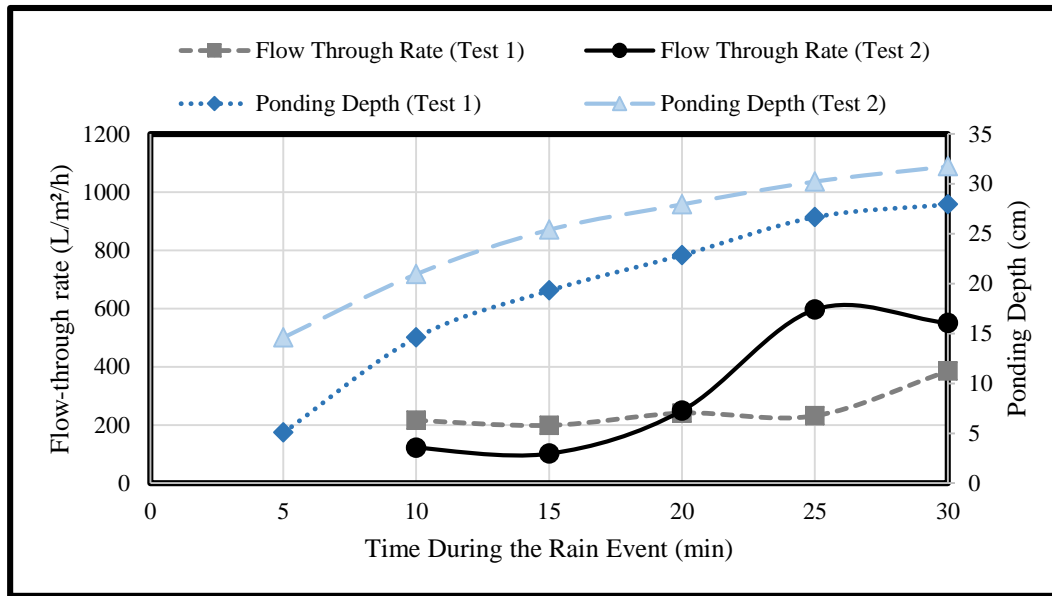
FIGURE 14 NONWOVEN FABRIC CHANGE IN FLOW RATE WITH CHANGE IN PONDING DEPTH
BETWEEN TEST 1 AND TEST 2 ON A 33 PERCENT SLOPE

Figure 14 shows the flow-through rate and ponding depth during Test 1 and Test 2 on a 33 percent slope and a 76 mm/h rainfall event for the nonwoven fabric. Results for other tests on the 33 percent slope show similar trends. Note the point where the ponding depth during Test 2 surpasses the maximum ponding depth that occurred during all of Test 1. This point occurs at minute 20 at a ponding depth of 30 cm. During Test 2, when the ponding depth is less than the maximum ponding depth that occurred during Test 1, the flow-through rate is less than the flow-through rate during Test 1. This indicates that impingement of particles within the fabric from Test 1 decreased the flow-through rate that occurred during Test 2. However, at minute 20 of Test 2, the ponding depth became higher than the maximum depth that occurred during Test 1 and the flow-through rate increased substantially. The increase in flow-through rate was because the ponding water was no longer influenced by the impinged particles from Test 1.

This trend and the overlying results with the nonwoven fabric show its susceptibility to forming a filter cake within and on its fabric. Although the woven fabric also filters the concentrated water, the impingement of particles within this fabric did not seem to affect its performance in future tests. It is possible that once the woven fabric is given time to dry, the impinged particles fall off the surface of the fabric. However, for the nonwoven fabric, the particles remained impinged within the fabric itself and affected its future performance.

Figure 15 shows the filter cake formation on the nonwoven fabric over the span of Test 1 and Test 2. When the concentrated water was in contact with the nonwoven fabric, a filter cake formed on its surface as shown in Figure 15b. During Test 2, when the ponding depth was in contact with the fabric with filter cake on it, the flow-through rate of the fabric was decreased and the efficiency of the fabric was increased. When the ponding depth during Test 2 became higher than the filter cake from Test 1, a new filter cake started to form on this new fabric. Figure 15c shows the increase in filter cake height from Test 1 to Test 2.
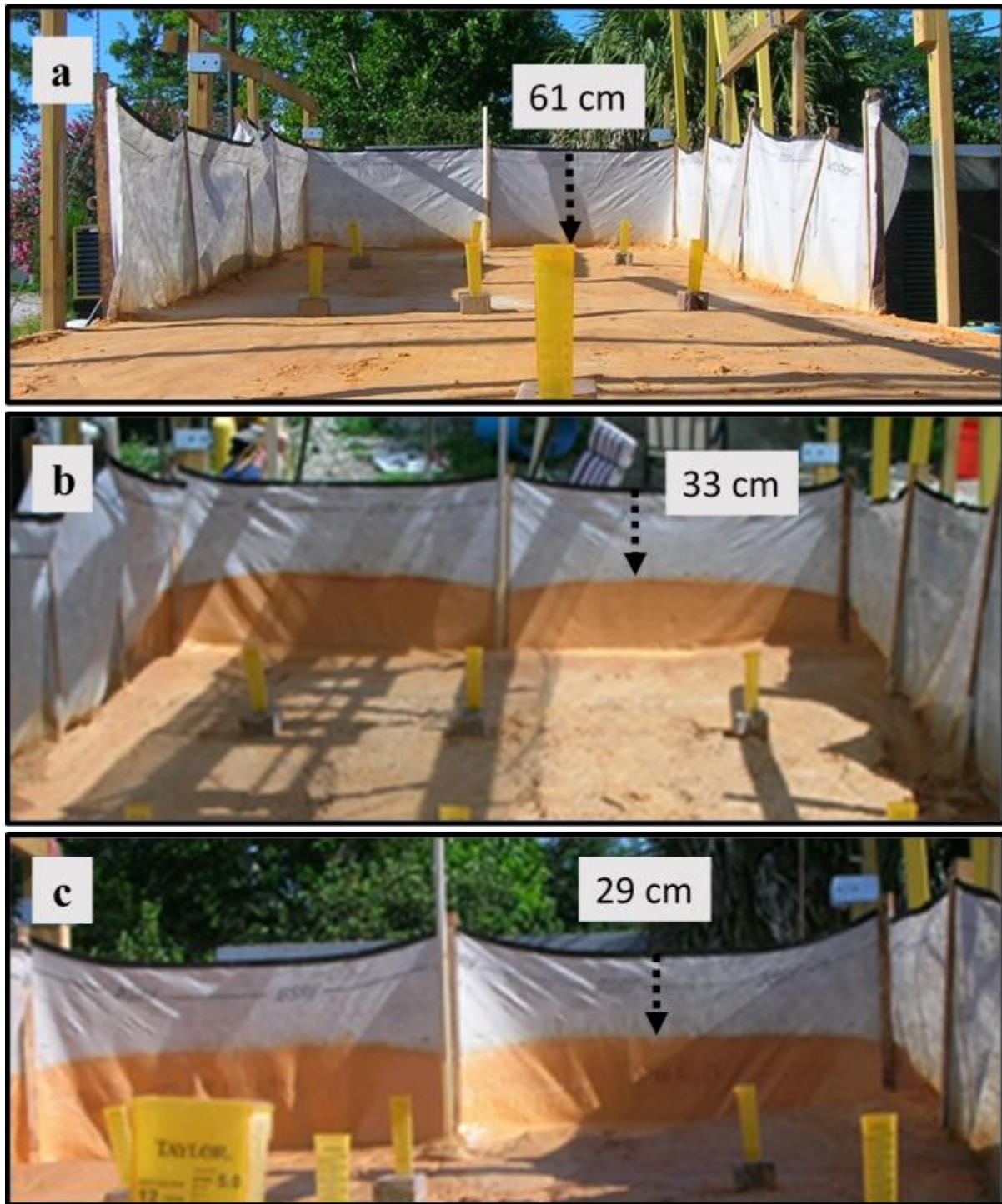
FIGURE 15 FILTER CAKE FORMATION ON NONWOVEN (A) UNTESTED FABRIC (B) CAKE FORMATION AFTER COMPLETION OF TEST 1 (C) CAKE FORMATION AFTER COMPLETION OF TEST 2

Overall, the results of the analyses show that the flow-through rate for both fabrics changed from Test 1 to Test 2. For the woven fabric, testing on the fabric caused an increase in the flow-through rate that is most likely caused by an increase in the pore size of the fabric. For the nonwoven fabric, previous testing on the fabric caused decreases in the flow-through rate due to impingent of particles within and on the fabric. It is interesting that even though the flow-through rate increased for the woven fabric and decreased for the nonwoven fabric from Test 1 to Test 2, the flow-through rates on the nonwoven fabric remained higher than the woven fabric during Test 2. It would have been interesting to test if this trend of increasing flow-through rate of the woven fabric and decreasing flow-through rate of the nonwoven fabric would have continue over additional testing on both fabrics.

Comparing flow-through rates due to changing rainfall intensity

A single factor ANOVA was performed on the flow-through rates to determine if changes in the rainfall intensity affected the flow-through rate of the fabrics on each embankment slope. Results of these tests are shown in Table 43 and Table 44 of Appendix C for the woven and nonwoven fabrics, respectively. Similar with results presented by Gogo-Abite and Chopra (2013), the rainfall intensity significantly affected the flow-through rate of the woven fabric with probabilities of 0.000, 0.000, and 0.002 for falsely rejecting the null hypotheses on 10, 25 and 33 percent slopes, respectively. The rainfall intensity also significantly affected the flow-through rate through the nonwoven fabric as well on 10 and 25 percent slopes, with probabilities of 0.001 and 0.000, respectively. The rainfall intensity however did not significantly affect the flow-through rate on the 33 percent slope for the nonwoven fabric, with probability of 0.176.

Results show that the lowest mean flow-through rates occurred on the lowest rainfall intensity of 25 mm/h for both fabrics on all embankment slopes tested. The reason for the higher flow-through rates occurring on the higher intensity rainfall events may be attributed to the fabrics stretching and elongation under stress caused by these higher intensity rainfall events. The higher rainfall intensity increases the upstream ponding volume, which causes a larger pressure on the silt fence. The increased water pressure may have caused a greater force to develop which pushed water through the fabric at a greater rate.

Silt Fence Failure

Due to the trend of decreasing flow-through rate with increasing embankment slope and the decreased storage volume on the higher slopes, the ponding depth behind the silt fence reached high levels during testing with both fabrics on the 33 percent slope. The high ponding depths increased the chance of silt fence failure by means of both tearing and ripping of the silt fence or by failure of the wooden stakes due to the increased hydrostatic pressure brought on by the high ponding depth. In addition, low flow-through rate of the silt fence caused it to fail by means of overtopping. Throughout the field scale testing with both fabrics, five silt fence failures and two overtopping events occurred over the span of all tests. The types of silt fence failures that occurred during testing are shown in Figure 16.

FIGURE 16 SILT FENCE FAILURES: (A) PULLOUT OF FABRIC FROM MIDDLE STAKE ON 33% SLOPE (B) OVERTOPPING ON 33% SLOPE (C) CORNER STAKE FAILURE ON 33% SLOPE (D) CORNER STAKE TEAR ON 25% SLOPE

For the woven fabric, it was observed that high slopes (33%) and high intensity (127 mm/h) caused the ponding water to overtop the silt fence during each rainfall event in less than 30 minutes. This failure is depicted in Figure 16b. Failures of this nature were not observed while testing the nonwoven fabric due to the ability of this fabric to transmit water at a large enough rate to avoid overtopping failures under the conditions evaluated in this study. Other failures that occurred during testing with the woven fabric include pullout of the fabric from the

stake and fabric tears occurring at corner stakes as shown in Figure 16a and Figure 16d. Pullout of the fabric from the stake occurred during only one test, on a 33 percent slope and 76 mm/h rainfall event, while the failures involving fabric tears at corner stakes occurred multiple times on 25 and 33 percent slopes. Once again, no such failures of this nature were observed for the nonwoven fabric. However, during testing on a 33 percent slope and a 127 mm/h rainfall event, a corner stake broke in half as shown on Figure 16c and caused failure to occur with the nonwoven fabric. It should be noted however, that during the repeat test on this same slope and intensity the nonwoven silt fence did not fail or overtop.

One of the reason that failures such as pullout of the fabric from the stake and fabric tearing at the corners occurred on the woven fabric and not on the nonwoven fabric was because the common woven silt fence used in this study did not come furnished with nailing strips attached to the stakes. These nailing strips are thin pieces of wood that sandwich the silt fence between the stake and the nailing strip itself. This construction helped to distribute the load caused by ponding water over the entire length of the post rather than at discrete points as would be the case if the material was just stapled without the nailing strips attached (Risse et al. 2008). The difference in strength between the fabrics may also have contributed, but it seems that the nailing strips were very helpful in preventing the nonwoven fabric from failing by pullout or tear.

Fabric Performance following Rain Events

Fabric Reduction Efficiency following Rain Events

Grab samples were collected both upstream and downstream of the silt fence for 30

minutes after rainfall ended. Samples were collected in order to determine the performance of

silt fence after rainfall stopped. Under high intensity rainfall as was simulated in these tests, the

flow rate of water that was transmitted through the silt fence was less than the flow rate of runoff

water. For this reason a ponding volume of runoff water accumulated on the upstream side of

the silt fence. When rainfall stopped, grab samples were taken both upstream and downstream of

the silt fence as the ponding volume continued to flow through the fabric, in order to evaluate the

performance of the silt fence after rainfall had stopped. It should be noted that samples were

taken for only 30 minutes after rainfall stopped, however, the estimated hydraulic detention time

of the ponding volume ranged from 1 hour to over 15 hours depending on the rainfall intensity,

embankment slope, and fabric type tested. Due to the large hydraulic detention times it was not

possible to collect samples over the entire time period. However, results show that performance

efficiency increased with time after rainfall ended and that downstream concentration values

decreased with time after rainfall ended. For this reason, the results discussed in this section,

which take into account only the first 30 minutes after rainfall ended, can be thought of as

conservative estimates of the true performance of silt fence after rainfall ends.

The efficiency values for after rainfall were calculated in a similar way as the during

rainfall calculations. Downstream samples were weighted by the volume of water which

discharged through the fabric in the time interval with which the sample was taken. The after

rainfall efficiency was then calculated by comparing the after rainfall volume-weighted mean

effluent concentration to the during rainfall volume-weighted mean influent concentration. The

expressions for the after rainfall efficiencies are shown in Equations 12 through 15.

$$(\text{WMET})_{AR} = \frac{\sum_{i=0}^{m}[T_{\text{eff}} * V_{downstream}]}{\sum_{i=0}^{m} V_{downstream}} \tag{12}$$

$$(WMEC)_{AR} = \frac{\sum_{i=0}^{m}[TS_{\text{eff}} * V_{downstream}]}{\sum_{i=0}^{m} V_{downstream}} \tag{13}$$

$$E_T(\%)_{AR} = 100 * \left[1 - \frac{(WMET)_{AR}}{WMIT}\right] \tag{14}$$

$$E_{SSC}(\%)_{AR} = 100 * \left[1 - \frac{(WMEC)_{AR}}{WMIC}\right] \tag{15}$$

where, $(\text{WMET})_{AR}$ is the volume-weighted mean effluent turbidity after rainfall (NTU);

$(\text{WMEC})_{AR}$ is the volume-weighted mean effluent concentration after rainfall (mg/L);

$V_{downstream}$ is the volume of collected runoff which discharged through the silt fence in interval

between sample i and sample $i-1$ (L); m is the number of samples collected after rainfall;

$E_T(\%)_{AR}$ is the mean turbidity performance efficiency after rainfall; and $E_{SSC}(\%)_{AR}$ is the mean

suspended sediment concentration performance efficiency after rainfall. WMIT and WMIC

where defined previously in Equations 4 and 5, respectively. The volume-weighted mean

turbidity and suspended sediment concentrations as well as the performance efficiencies that

occurred after the rain event for both fabrics are shown in Table 10 and TABLE 11, respectively.

TABLE 10 WOVEN FABRIC TEST VOLUME-WEIGHTED MEAN TURBIDITY AND SSC RESULTS AFTER THE RAIN EVENT

Slope % (Ratio)	Rainfall Intensity (mm/h)	Rainfall Events	Volume-Weighted Mean Turbidity			Volume-Weighted Mean SSC		
			Up-stream (NTU)	Down-stream (NTU)	Performance Efficiency (%)	Up-stream (mg/L)	Down-stream (mg/L)	Performance Efficiency (%)
33% (3:1) Slope	25	#1	50171	15791	69	32616	9010	72
		#2	33573	6159	82	23412	4973	79
		#1R	28738	5817	80	21001	4187	80
		#2R	30096	3800	87	25614	3034	88
	76	#1	43339	--	--	40099	--	--
		#2	--	--	--	--	--	--
		#1R	41442	11000	73	21641	6096	72
		#2R	27811	4579	84	17641	3677	79
	127	#1	48311	--	--	31212	--	--
		#2	--	--	--	--	--	--
		#1R	57945	--	--	46322	--	--
		#2R	40266	--	--	35427	--	--
25% (4:1) Slope	25	#1	29396	9426	68	19585	6422	67
		#2	21551	6689	69	13875	4558	67
	76	#1	19080	5993	69	13462	4380	67
		#2	25891	6760	74	11361	3558	69
	127	#1	47590	7676	84	15744	4123	74
		#2	30530	2942	90	12755	2042	84
10% (10:1) Slope	25	#1	12357	2104	83	10959	1722	84
		#2	10839	1093	90	10743	915	91
		#1R	13365	904	93	10468	787	92
		#2R	9453	1614	83	5920	1165	80
	76	#1	5358	1116	79	4215	1026	76
		#2	3707	1170	68	3426	920	73
		#1R	6036	932	85	4610	886	81
		#2R	2619	916	65	2117	789	63
	127	#1	4886	761	84	3982	781	80
		#2	4321	907	79	3763	1000	73

Table entries that appear with "--" indicate that no samples were collected during those tests due to previous test failures

TABLE 11 NONWOVEN FABRIC TEST VOLUME-WEIGHTED MEAN TURBIDITY AND SSC RESULTS AFTER THE RAIN EVENT

Slope % (Ratio)	Rainfall Intensity (mm/h)	Rainfall Events	Volume-Weighted Mean Turbidity			Volume-Weighted Mean SSC		
			Up-stream (NTU)	Down-stream (NTU)	Performance Efficiency (%)	Up-stream (mg/L)	Down-stream (mg/L)	Performance Efficiency (%)
33% (3:1) Slope	25	#1	29690	2775	91	27767	1479	95
		#2	39009	1538	96	25079	1227	95
		#1R	46765	3552	92	33356	2952	91
		#2R	18628	2103	89	22205	1914	91
	76	#1	40355	1681	96	31706	1835	94
		#2	32081	969	97	24753	851	97
		#1R	26588	802	97	19271	405	98
		#2R	24696	954	96	19142	1027	95
	127	#1	37989	--	--	31958	--	--
		#2	--	--	--	--	--	--
		#1R	37008	1312	96	26679	1075	96
		#2R	18925	460	98	13685	1235	91
25% (4:1) Slope	25	#1	24380	4230	83	21495	3298	85
		#2	20556	2981	85	17723	2053	88
		#1R	22906	1692	93	18459	1290	93
		#2R	22996	3509	85	17807	2752	85
	76	#1	8780	946	89	6547	768	88
		#2	6976	3210	54	5256	2729	48
		#1R	8244	729	91	5608	599	89
		#2R	3915	269	93	2720	237	91
	127	#1	7772	1016	87	5544	834	85
		#2	19213	4184	78	14032	319	98
		#1R	14489	1523	89	13018	1212	91
		#2R	8384	2326	72	7123	1732	76
10% (10:1) Slope	25	#1	13512	770	94	14449	647	96
		#2	13824	525	96	14555	660	95
		#1R	6631	1681	75	5962	1280	79
		#2R	9973	1812	82	7318	1476	80
	76	#1	9472	3765	60	10330	2224	78
		#2	10282	2031	80	11088	1497	87
		#1R	7217	823	89	5932	697	88
		#2R	4736	803	83	3441	696	80

Slope % (Ratio)	Rainfall Intensity (mm/h)	Rainfall Events	Volume-Weighted Mean Turbidity			Volume-Weighted Mean SSC		
			Up-stream (NTU)	Down-stream (NTU)	Performance Efficiency (%)	Up-stream (mg/L)	Down-stream (mg/L)	Performance Efficiency (%)
	127	#1	12466	3408	73	7147	1999	72
		#2	14303	1725	88	10503	1371	87
		#1R	8629	2104	76	6416	1642	74
		#2R	6044	1919	68	4779	1524	68

Table entries that appear with "--" indicate that no samples were collected during those tests due to previous test failures

The turbidity performance efficiency that occurred after the rain event in the first 30 minutes, for all slopes and intensities tested, for the woven and nonwoven fabrics had a mean of 79 and 86 percent; median of 81 and 89 percent, and ranged from 65 to 93 percent and from 54 to 98 percent, respectively. The SSC performance efficiency was similar, with mean of 77 and 87 percent; median of 77 and 89 percent; and ranged from 63 to 92 percent and from 48 to 98 percent for the woven and nonwoven fabrics, respectively.

Using the volume-weighted mean turbidity and SSC efficiencies shown in Table 10 and TABLE 11 a Wilcoxon rank sum test was completed in order to determine if the performance efficiencies on the nonwoven fabric were significantly greater than the efficiencies on the woven fabric. The results of the analysis are shown in Table 29 of Appendix B. As was the case of the results during rainfall, the after rainfall results also show that the nonwoven fabric significantly reduced both turbidity and SSC to a greater extent than did the woven fabric when analyzed on all embankment slopes combined. The greater removal by the nonwoven fabric can be attributed to the smaller pore size of the nonwoven fabric in comparison to the woven fabric.

The above performance efficiencies were normalized based on the volume-weighted mean influent turbidity and SCC occurring during the rain event. The efficiency after rainfall can also be calculated on a time dependent basis by comparing the downstream concentration that discharged through the fence at time t to the upstream concentration of the ponding volume at the same time t. In this calculation, the effect of particle settling has been largely ignored and the efficiency values are based on the filtering of the fabric at time t.

The results of these time dependent calculations are shown in Table 46 through Table 48 of Appendix D for the woven fabric and Table 49 through Table 51 of Appendix D for the nonwoven fabric. A Wilcoxon rank sum test on the difference between the during and after rainfall efficiencies was also conducted and is presented in Table 38 and Table 39 of Appendix B for the woven and nonwoven fabrics, respectively. The statistical test was conducted on both the during rainfall average performance efficiencies and the after rainfall average efficiencies in order to determine if there was a statistically significant change in performance efficiency from during rainfall to after rainfall on each embankment slope for each fabric. The results of the analysis show that the performance efficiency for both the turbidity and SSC increased significantly from during the rain event to after the rain event on all embankment slopes for both fabrics. The efficiency increase was dependent on time, as the time since rainfall ended increased, the efficiency of the fabric in removing turbidity and SSC increased. Figure 17 depicts the typical trend encountered for the increased mean turbidity performance efficiency and the decrease in effluent turbidity with time after rainfall stopped. The plot shows the average efficiencies and concentrations occurring on a 25 percent slope for both fabrics. This trend was similar on all embankment slopes and also was similar for the SSC efficiency and

concentrations. Plots associated with the other embankment slopes as well as the SSC reductions

are shown in Figure 21 through Figure 25 in Appendix D.
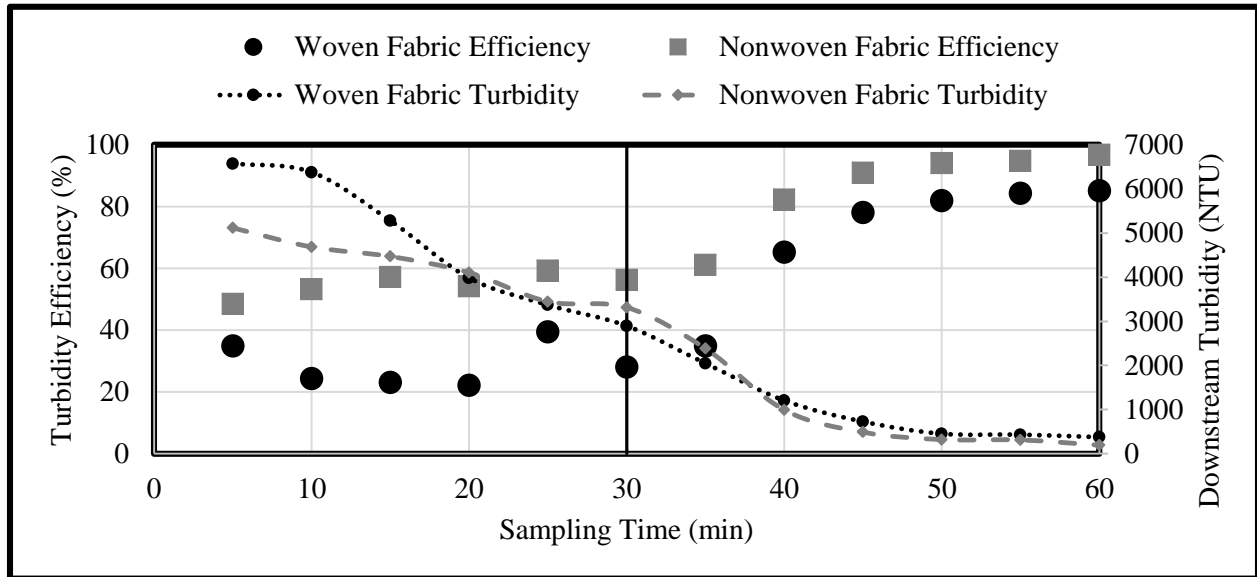
FIGURE 17 TIME DEPENDENT AVERAGE TURBIDITY REDUCTION EFFICIENCY AND
DOWNSTREAM VALUE ON 10 PERCENT SLOPE

The black vertical line indicates the point at which rainfall stops. Points to the left are

efficiency and turbidity values during the rain event and points to the right are efficiency and

turbidity values after the rain event. After rainfall stopped the efficiency of the silt fence

increased substantially with time before leveling off. The opposite is true for the downstream

effluent turbidity, which decreased with time after rainfall stopped.

The increase in efficiency after rainfall ended was perhaps due to a combination of the

filtration ability of the fabric and the settling of the suspended sediments. A possible theory as to

why the observed filtration efficiency increased after rainfall ended is the topic of the next

couple of sections. Filtration is discussed first and a discussion on sedimentation follows.

The ability of the silt fence fabric to filter the concentrated water volume is dependent on the opening of the pore sizes of the fabric and on the relative size distribution of soil particles in the ponding volume. At first, only those particle sizes that are in close or larger than the opening size of the fabric will be filtered, while smaller particles will pass through. However, over time, the opening size of the fabric will decrease due to impregnation of soil particles on the fabric. The filtration efficiency of the fabric will therefore increase with time as it is exposed to the concentrated water volume. This process is taking place both during and after the rain event. The efficiency values remain somewhat low and do not increase during the rain event because the ponding water volume behind the fence is constantly increasing and exposing new fabric to the concentrated water volume with time. When the concentrated water volume reaches the new fabric, the process repeats (i.e. a large portion of the soil distribution will pass through this portion of the fabric until particles become impinged it). Figure 18 shows the typical relationship between the height of ponding water behind the fence and the time dependent efficiency values.
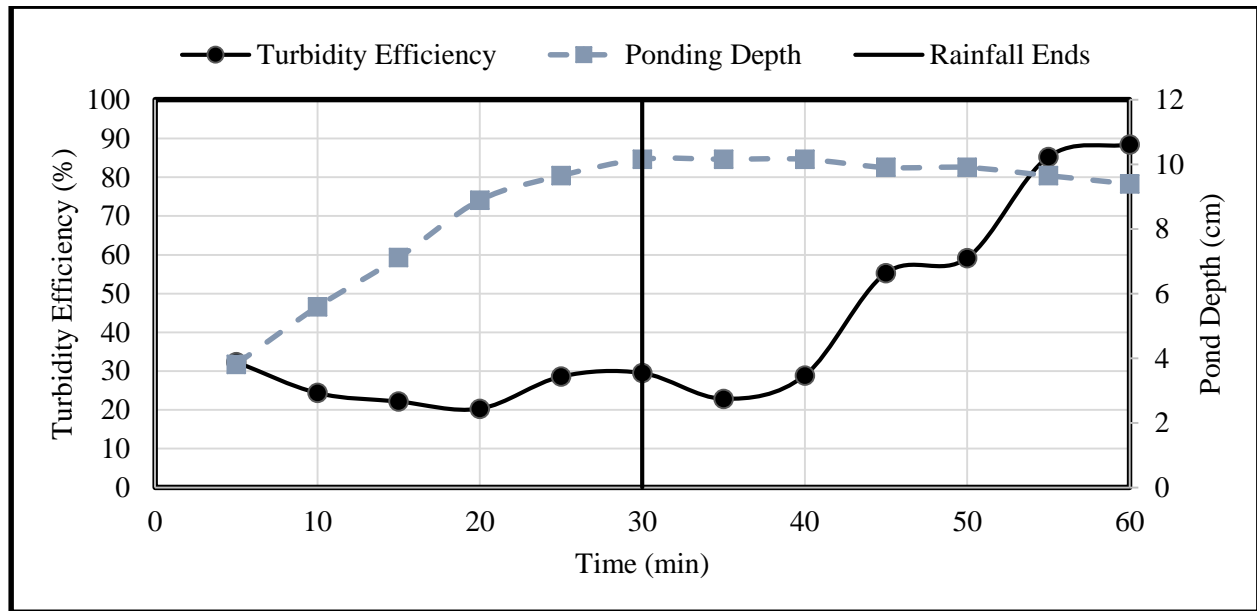
FIGURE 18 WOVEN FABRIC TIME DEPENDENT EFFICIENCY VALUES AND PONDING DEPTH ON 25 PERCENT SLOPE AND 25 MM/H RAINFALL INTENSITY

The plot shows that during the rain event, as the ponding depth is constantly increasing, exposing new fabric to the ponding water volume, the efficiency values remain relatively low and constant. When rainfall stopped, the efficiency of the silt fence system started to increase with time. This increase with time was due in part to the clogging mechanism described above, however, the main mechanism by which the efficiency increased was likely due to the concentration gradient which forms within the pond after rainfall ends. Settling and concentration gradient is discussed below.

Settling Mechanism

In the ponding volume upstream of the silt fence a vertical concentration gradient exists due to settling. The lowest concentration exists at the top of the pond and the concentration

96

increases as the depth increases. The increasing concentration gradient that forms after the rain

event ends is most likely main reason for the observed increasing efficiency.

During the rain event, the concentration gradient was not as noticeable as it was after

the rain event. Falling rainfall impacting the ponding volume as well as sheet flow colliding

with the ponding volume decreased the potential for the suspended sediments to settle.

Although, these collisions may disrupt sedimentation, the suspended particles will still settle

during the rain event. However, new sediment is constantly being introduced into the ponding

volume replacing particles which have settled. Therefore, during the rain event, a noticeable

concentration gradient did not form and the concentration throughout the vertical height of

ponding water remained relatively constant.

When rainfall stops, no new sediment is introduced into the ponding water volume and

a concentration gradient starts to form as suspended particles settle. Figure 19 shows a possible

trend of the concentration gradient which may form over time after rainfall ends.
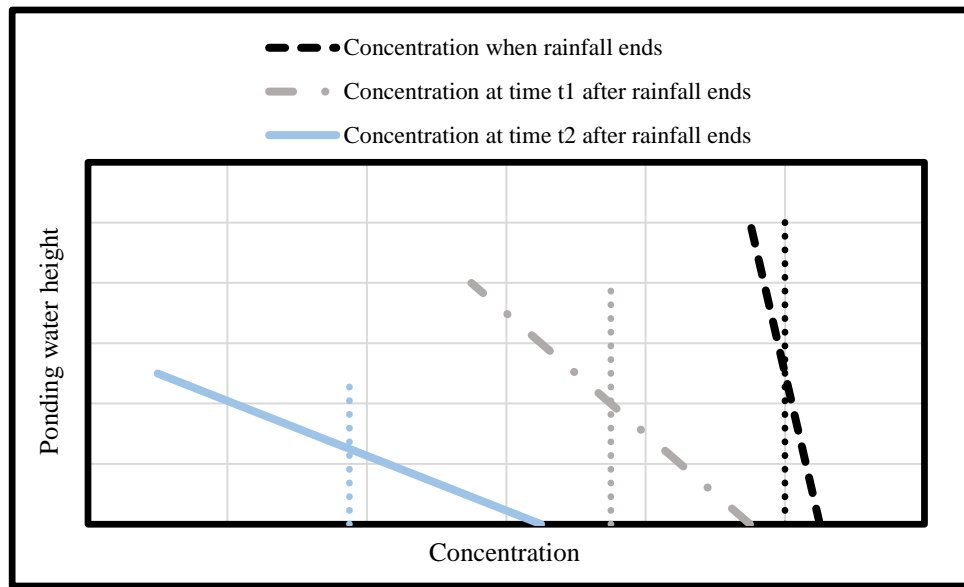
FIGURE 19 CONCEPTUAL EXAMPLE OF HOW CONCENTRATION GRADIENT IN PONDING VOLUME
MAY CHANGE OVER TIME AFTER RAINFALL ENDS

The slanting lines represent the concentration in the ponding volume with depth. The

vertical dotted lines indicate the average concentration in the pond at that time. Figure 19 shows

that over time, due to settling, the average concentration in the ponding volume decreases. As

settling occurs, a concentration gradient may start to become more spread out over time.

Recall from the previous section: Filtration Mechanism, that over time, particles clog the

silt fence fabric, reducing its pore size. The reduction in pore size not only increase the

reduction efficiency of the fabric, but also limit the ability of the fabric to transmit water. For

this reason, parts of the fabric at the bottom will be transmit flow at a lesser rate than parts near

the top of the ponding volume. The increase in efficiency is due to both this difference in flow-

through rate and the increasing spread of the concentration gradient.

For example, referring to Figure 19 and the far right lines, the concentration at the top of

pond is relatively close to the average concentration in the pond, leading to low efficiency.

When rainfall stops, the suspended particles settle and no new sediment is introduced into the system. The concentration gradient becomes more spread out, with the ratio between the concentrations at the top of the pond to the average concentration in the pond increasing. This leads to an observed increase in efficiency because a greater flow-through rate occurs near the top of the ponding volume when compared to lower portions due to filter clogging. Essentially, the increase in efficiency is because the rate of sedimentation at the top of the pond where the flow-through rate is highest is greater than the overall settling velocity of the ponding volume as a whole.

Flow-through rate after the Rainfall Event

The flow-through rate after the rain event decreased due to fabric clogging as was observed with the downstream turbidity and SSC. A Wilcoxon rank sum test on the difference between flow-through rates occurring during and after the rain event is shown in Table 45 in Appendix C for the woven and nonwoven fabrics. The statistical analysis showed that there was a significant decrease in the flow-through rate from during the rain event to after the rain event for both fabrics on all embankment slopes tested, except for the woven fabric on a 10 percent slope. The lower flow-through rate after rainfall ended is another indication that filter cake formation on both fabrics affects the performance. Table 12 shows the average flow-through rates that occurred during and after the rain event on all embankment slopes and rainfall intensities tested.

TABLE 12 AVERAGE FLOW-THROUGH RATES DURING AND AFTER RAIN EVENTS

Embankment Slope (%)	Rainfall Intensity (mm/h)	Mean Flow through rate (L/m²/h)			
		Woven Fabric		Nonwoven Fabric	
		During Rainfall	After Rainfall	During Rainfall	After Rainfall
33	25	60	32	310	130
	76	132	104	416	109
	127	72	--	460	132
25	25	125	75	880	295
	76	214	132	1512	386
	127	397	227	1155	262
10	25	830	771	1267	716
	76	1494	1467	2377	520
	127	1360	1084	2564	926

Table entries that appear with "--" indicate that no after rainfall samples were taken due to overtopping events

Due to the low flow-through rate encountered on the higher slopes and the decreasing flow-through rate after rainfall ended, the hydraulic detention time of the ponding volume increased for some of the tests. More hydraulic detention time of the ponding volume gives additional time for settling to occur. Thus, a high hydraulic detention time post rainfall would therefore lead to higher efficiency removal. In this section, the efficiency values are based on only the first 30 minutes after rainfall ended. However, the estimated hydraulic detention times of the pond show that water would have discharged through the silt fence anywhere from 1 hour to 15 hours depending on the embankment slope and fabric tested. The estimated hydraulic detention time of the pond was calculated using the equation expressed in Equation 16. A summary of the estimated average hydraulic detention times on each embankment slope for each fabric are shown in Table 13.

$$\tau_{HD} = \frac{(V_{pond})_{end\,test} * (PD)_{end\,test} * b_{TB}}{(q)_{end\,test}} + (t)_{end\,test} \qquad (16)$$

where, τ_{HD} is the hydraulic detention time of the ponding volume when rainfall stops (h); V_{pond} is

the ponding volume for the 30 minutes after rainfall test sampling was completed; PD is the

ponding depth for the 30 minutes after rainfall test sampling was completed; b_{TB} is the width of

silt fence perpendicular to flow; q is the measured flow-through rate for the 30 minutes after

rainfall test sampling was completed; and *t* is the 30 minutes after rainfall test event (h).

TABLE 13 ESTIMATED AVERAGE HYDRAULIC DETENTION TIME OF THE PONDING VOLUME

Embankment slope (%)	Rainfall intensity (mm/h)	Average Hydraulic Detention Time (h)	
		Woven Fabric	Nonwoven Fabric
33	25	15.2	4
	76	11.7	9.5
	127	--	10
25	25	4.2	2.2
	76	6.6	3.5
	127	7	6.3
10	25	1.1	1.8
	76	0.9	4.5
	127	1.3	4.7

Table entries that appear with "--" indicate that test failures occurred during the rain
event and the hydraulic detention time could not be calculated

In general the woven fabric had higher hydraulic detention times due to its low flow-

through rate. The exception occurs on the 10 percent slope where the nonwoven fabric had very

low measured flow-through rates at the end of the 30 minutes after rainfall test, leading to

relatively high estimated detention times on this slope in comparison with the woven fabric. The

reason for this is unknown. It can also be seen that the detention times, for the most part,

increased with increasing embankment slope. This was due to the trend of decreasing flow-through rate with increasing upstream suspended solids concentration caused by the increasing embankment slope.

Overall Performance Efficiency (Collected): Both During and After Rain events

In order to quantify the overall efficiency of silt fence, an overall weighted mean effluent value was calculated based on discharge volume. The overall weighted mean effluent value was then compared to the volume-weighted influent occurring during the rain event to obtain an overall performance efficiency of the silt fence. The expression for the overall efficiency is shown in Equations 17 through 20.

$$(WMET)_{\text{Overall}} = \frac{\sum_{i=0}^{n}\left[T_{\text{eff}_{DR}} * V_{down_{DR}}\right] + \sum_{i=0}^{m}\left[T_{\text{eff}_{AR}} * V_{down_{AR}}\right]}{\sum_{i=0}^{n} V_{down_{DR}} + \sum_{i=0}^{m} V_{down_{AR}}} \qquad (17)$$

$$(WMEC)_{\text{Overall}} = \frac{\sum_{i=0}^{n}\left[SSC_{\text{eff}_{DR}} * V_{down_{DR}}\right] + \sum_{i=0}^{m}\left[SSC_{\text{eff}_{AR}} * V_{down_{AR}}\right]}{\sum_{i=0}^{n} V_{down_{DR}} + \sum_{i=0}^{m} V_{down_{AR}}} \qquad (18)$$

$$E_T(\%)_{Overall} = 100 * \left[1 - \frac{(WMET)_{Overall}}{WMIT}\right] \qquad (19)$$

$$E_{SSC}(\%)_{Overall} = 100 * \left[1 - \frac{(WMEC)_{Overall}}{WMIC}\right] \qquad (20)$$

where, $(WMET)_{\text{Overall}}$ is the overall volume-weighted mean effluent turbidity (NTU); $(WMEC)_{\text{Overall}}$ is the overall volume-weighted mean effluent concentration (mg/L); V_{down} is the volume of collected runoff which discharged through the silt fence in interval between sample i and sample $i-1$ (L); n is the number of samples collected during rainfall; m is the number of samples collected after rainfall; EFF stands for effluent; DR stands for during rainfall; AR stands for after rainfall; $E_T(\%)_{Overall}$ is the overall mean turbidity performance efficiency; and $E_{SSC}(\%)_{Overall}$ is the mean suspended sediment concentration performance efficiency. WMIT and WMIC where defined previously in Equations 4 and 5, respectively.

Note that the calculation takes into account only those samples that were collected during the 1-hour test. Flow would have continued to discharged through the silt fence for upwards of 14 additional hours depending on the test type, and would have led to an increased overall efficiency value. Therefore, the results shown in this section can be thought of as conservative estimates of the performance efficiency of silt fence. The mean overall efficiency values under all embankment slope and intensity pairs for both the woven and nonwoven fabrics are shown in Table 14 and Table 15, respectively. Discussion of a projected overall efficiency calculation, which would take into account the entire hydraulic detention time of the test, is the topic of the next section.

TABLE 14 OVERALL PERFORMANCE EFFICIENCY OF WOVEN SILT FENCE (COLLECTED SAMPLES)

Slope % (Ratio)	Rainfall Intensity (mm/h)	Rainfall Events	Volume-Weighted Mean Turbidity			Volume-Weighted Mean SSC		
			Up-stream (NTU)	Down-stream (NTU)	Performance Efficiency (%)	Up-stream (mg/L)	Down-stream (mg/L)	Performance Efficiency (%)
33% (3:1) Slope	25	#1	50171	20002	60	32616	11363	65
		#2	33573	12059	64	23412	10902	53
		#1R	28738	13334	54	21001	9337	56
		#2R	30096	12518	58	25614	9712	62
	76	#1	43339	--	--	40099	--	--
		#2	--	--	--	--	--	--
		#1R	41442	16522	60	21641	9831	55
		#2R	27811	9668	65	17641	7534	57
	127	#1	48311	--	--	31212	--	--
		#2	--	--	--	--	--	--
		#1R	57945	--	--	46322	--	--
		#2R	40266	--	--	35427	--	--
25% (4:1) Slope	25	#1	29396	16928	42	19585	11006	44
		#2	21551	11151	48	13875	8287	40
	76	#1	19080	11187	41	13462	8597	36
		#2	25891	14189	45	11361	6815	40
	127	#1	47590	16708	65	15744	9053	42
		#2	30530	12383	59	12755	5867	54
10% (10:1) Slope	25	#1	12357	4719	62	10959	3950	64
		#2	10839	2164	80	10743	1642	85
		#1R	13365	2830	79	10468	2030	81
		#2R	9453	3478	63	5920	2473	58
	76	#1	5358	2678	50	4215	2095	50
		#2	3707	2160	42	3426	1694	51
		#1R	6036	2375	61	4610	1947	58
		#2R	2619	1668	36	2117	1359	36
	127	#1	4886	2227	54	3982	1761	56
		#2	4321	2024	53	3763	1753	53

Table entries that appear with "--" indicate that no samples were collected during those tests due to previous test failures

Table 15 OVERALL PERFORMANCE EFFICIENCY OF NONWOVEN SILT FENCE (COLLECTED SAMPLES)

Slope % (Ratio)	Rainfall Intensity (mm/h)	Rainfall Events	Volume-Weighted Mean Turbidity			Volume-Weighted Mean SSC		
			Up-stream (NTU)	Down-stream (NTU)	Performance Efficiency (%)	Up-stream (mg/L)	Down-stream (mg/L)	Performance Efficiency (%)
33% (3:1) Slope	25	#1	29690	9039	70	27767	6061	78
		#2	39009	2049	95	25079	2203	91
		#1R	46765	17232	63	33356	12133	64
		#2R	18628	6490	65	22205	5904	73
	76	#1	40355	11954	70	31706	9462	70
		#2	32081	7750	76	24753	6754	73
		#1R	26588	15692	41	19271	9609	50
		#2R	24696	9682	61	19142	7446	61
	127	#1	37989	--	--	31958	--	--
		#2	--	--	--	--	--	--
		#1R	37008	12601	66	26679	10563	60
		#2R	18925	9646	49	13685	4939	64
25% (4:1) Slope	25	#1	24380	9056	63	21495	6650	69
		#2	20556	5820	72	17723	4224	76
		#1R	22906	13817	40	18459	9592	48
		#2R	22996	7336	68	17807	5629	68
	76	#1	8780	6759	23	6547	5740	12
		#2	6976	5043	28	5256	3876	26
		#1R	8244	4979	40	5608	3561	37
		#2R	3915	2050	48	2720	954	65
	127	#1	7772	5546	29	5544	3958	29
		#2	19213	8063	58	14032	5147	63
		#1R	14489	6957	52	13018	4928	62
		#2R	8384	3513	58	7123	2635	63
10% (10:1) Slope	25	#1	13512	1615	88	14449	1180	92
		#2	13824	1248	91	14555	1338	91
		#1R	6631	2144	68	5962	1620	73
		#2R	9973	3136	69	7318	2384	67
	76	#1	9472	4518	52	10330	3033	71
		#2	10282	2526	75	11088	2045	82
		#1R	7217	4480	38	5932	3205	46
		#2R	4736	1415	70	3441	1093	68

Slope % (Ratio)	Rainfall Intensity (mm/h)	Rainfall Events	Volume-Weighted Mean Turbidity			Volume-Weighted Mean SSC		
			Up-stream (NTU)	Down-stream (NTU)	Performance Efficiency (%)	Up-stream (mg/L)	Down-stream (mg/L)	Performance Efficiency (%)
	127	#1	12466	6737	46	7147	3903	45
		#2	14303	4585	68	10503	2322	78
		#1R	8629	4872	44	6416	3805	41
		#2R	6044	2935	51	4779	2211	54

Table entries that appear with "--" indicate that no samples were collected during those tests due to previous test failures

The overall performance efficiency of the woven fabric ranged from 36 to 80 percent and from 36 to 85 percent with a mean of 57 and 54 percent for the turbidity and suspended sediment concentrations, respectively. For the nonwoven fabric, the overall performance efficiency ranged from 23 to 95 percent and 12 to 92 percent with a mean of 59 and 62 percent for the turbidity and sediment concentrations, respectively. These performance results show that the nonwoven fabric performed slightly better than the woven fabric in the overall removal of turbidity and suspended sediment concentrations.

Table 16 shows a summary of the above overall efficiency results as well as a summary of efficiency results from during and after the rain event.

TABLE 16 SUMMARY OF VOLUME-WEIGHTED MEAN TURBIDITY AND SCC PERFORMANCE
EFFICIENCY

Performance criteria	Slope (%)	Statistical parameter	Woven			Nonwoven		
			During rainfall	After rainfall	Overall	During rainfall	After rainfall	Overall
Turbidity Performance Efficiency (%)	All slopes	Mean	40	79	57	49	86	59
		Median	38	81	59	49	89	62
	33	Mean	47	79	60	52	95	66
		Median	50	81	60	50	96	66
	25	Mean	31	76	50	37	83	48
		Median	26	71	47	38	86	50
	10	Mean	38	81	58	58	80	63
		Median	36	83	58	61	81	68
SSC Performance Efficiency (%)	All slopes	Mean	39	77	54	53	87	62
		Median	37	77	54	55	89	64
	33	Mean	47	78	58	56	94	68
		Median	45	79	56	55	95	68
	25	Mean	21	71	43	41	85	52
		Median	19	68	41	47	88	63
	10	Mean	41	79	59	62	82	67
		Median	40	80	57	67	80	69

The overall efficiency values show that the nonwoven achieved slightly higher fabric
efficiency values for both the turbidity and SSC on every slope and intensity pair except on the
25 percent slope for turbidity. A statistical analysis in the form of a Wilcoxon rank sum test was
performed on the overall volume-weighted mean performance efficiencies in order to determine
if the nonwoven fabric significantly reduced turbidity and SSC to a greater extent than the woven
fabric. Presented in Table 30 of Appendix B are the results of this analysis. Results show that
there was not a significant difference in the overall turbidity performance efficiency of the
woven and nonwoven fabric on any embankment slope. However, there was a significant
difference in the overall SSC performance efficiency of the woven and nonwoven fabrics on 25

and 33 percent slopes. All other embankment slopes showed no significant difference between the performance efficiencies of either fabric.

The result of the woven and nonwoven not having statistically different performance efficiencies is interesting since the nonwoven fabric significantly removed both turbidity and SCC to a greater extent than the woven fabric on combination of all embankment slopes both during and after the rain event. The reason for the similar performance efficiencies was due to the flow-through rates of both fabrics. How the flow-through rate affects the overall efficiency is discussed in the following section: Overall Performance Efficiency (Projected).

Overall Performance Efficiency (Projected)

The field-scale testing procedure allowed for only 1-hour sampling time. However, as shown in Chapter 4, section: Flow-through rate after the rainfall event, the projected hydraulic detention time of the ponding volume was as high as 15 hours. Much of the turbidity and SCC removal will occur during the long hydraulic detention time after rainfall has ended due to settling and increased filtration. The focus of this section is to calculate an overall projected performance efficiency of silt fence which takes into the removal which occurs during the entire hydraulic detention time of the system.

Two assumptions are needed in order to calculate the projected performance efficiency. 1) The entire ponding volume upstream of the silt fence would have discharge through the silt fence. This assumption negates water losses through infiltration of the soil and evaporation. 2) The concentration of the last downstream measurement taken during sampling would have continued to discharge through the silt fence. This assumption can be considered conservative. Due to settling and increased filtration, the downstream discharge concentration was shown to decrease with time after rainfall ended as shown in Chapter 4, section: Fabric reduction efficiency following rain events. Noting these assumption, the overall projected efficiency is calculated as expressed in Equations 21 through 24.

$$(WMET)_{\text{Projected}} = \frac{\sum_{i=0}^{n}\left[T_{\text{eff}_{DR}} * V_{down_{DR}}\right] + \sum_{i=0}^{m}\left[T_{\text{eff}_{AR}} * V_{down_{AR}}\right] + \left[\left(T_{EFF_{AR}}\right)_m * (V_{up})_m\right]}{\sum_{i=0}^{n}V_{down_{DR}} + \sum_{i=0}^{m}V_{down_{AR}} + (V_{up})_m} \quad (21)$$

$$(WMEC)_{\text{Projected}} = \frac{\sum_{i=0}^{n}\left[SSC_{\text{eff}_{DR}} * V_{down_{DR}}\right] + \sum_{i=0}^{m}\left[SSC_{\text{eff}_{AR}} * V_{down_{AR}}\right] + \left[\left(SSC_{EFF_{AR}}\right)_m * (V_{up})_m\right]}{\sum_{i=0}^{n}V_{down_{DR}} + \sum_{i=0}^{m}V_{down_{AR}} + (V_{up})_m} \quad (22)$$

$$E_T(\%)_{Projected} = 100 * \left[1 - \frac{(WMET)_{Projected}}{WMIT}\right] \quad (23)$$

$$E_{SSC}(\%)_{Projected} = 100 * \left[1 - \frac{(WMEC)_{Projected}}{WMIT}\right] \qquad (24)$$

where (WMET)Projected is the projected weighted mean effluent turbidity (NTU); $\left(T_{EFF_{AR}}\right)_m$ is

the effluent turbidity of the last sample taken during the 1-hour test (NTU); $\left(V_{up}\right)_m$ is the volume

of ponding water upstream of the silt fence when the last sample during the test was taken (L);

(WMEC)Projected is the projected weighted mean effluent SCC (mg/L); $\left(SSC_{EFF_{AR}}\right)_m$ is the

effluent SSC of the last sample taken during the 1-hour test (mg/L); $E_T(\%)_{Projected}$ is the

projected turbidity performance efficiency; $E_{SSC}(\%)_{Projected}$ is the projected SSC performance

efficiency. All other terms have been describe previously. The mean overall projected volume-

weighted turbidity and SCC efficiencies are shown in Table 17 and Table 18 and for the woven

and nonwoven fabrics, respectively.

TABLE 17 PROJECTED OVERALL WOVEN FABRIC PERFORMANCE EFFICIENCY

Slope % (Ratio)	Rainfall Intensity (mm/h)	Rainfall Events	Volume-Weighted Mean Turbidity			Volume-Weighted Mean SSC		
			Up-stream (NTU)	Down-stream (NTU)	Performance Efficiency (%)	Up-stream (mg/L)	Down-stream (mg/L)	Performance Efficiency (%)
33% (3:1) Slope	25	#1	50171	1534	97	32616	1091	97
		#2	33573	1554	95	23412	1507	94
		#1R	28738	756	97	21001	709	97
		#2R	30096	1916	94	25614	1705	93
	76	#1	43339	--	--	40099	--	--
		#2	--	--	--	--	--	--
		#1R	41442	1755	96	21641	994	95
		#2R	27811	1331	95	17641	1282	93
	127	#1	48311	--	--	31212	--	--
		#2	--	--	--	--	--	--
		#1R	57945	--	--	46322	--	--
		#2R	40266	--	--	35427	--	--
25% (4:1) Slope	25	#1	29396	2803	90	19585	2007	90
		#2	21551	3199	85	13875	2487	82
	76	#1	19080	2168	89	13462	1776	87
		#2	25891	2926	89	11361	1640	86
	127	#1	47590	3950	92	15744	1700	89
		#2	30530	2509	92	12755	1420	89
10% (10:1) Slope	25	#1	12357	4399	64	10959	3693	66
		#2	10839	2005	82	10743	1531	86
		#1R	13365	1383	90	10468	1093	90
		#2R	9453	3167	66	5920	2273	62
	76	#1	5358	2605	51	4215	2044	52
		#2	3707	1889	49	3426	1513	56
		#1R	6036	1856	69	4610	1558	66
		#2R	2619	1297	50	2117	1091	48
	127	#1	4886	1873	62	3982	1523	62
		#2	4321	1713	60	3763	1516	60

Table entries that appear with "--" indicate that no samples were collected during those tests due to previous test failures

TABLE 18 PROJECTED OVERALL NONWOVEN FABRIC PERFORMANCE EFFICIENCY

Slope % (Ratio)	Rainfall Intensity (mm/h)	Rainfall Events	Volume-Weighted Mean Turbidity			Volume-Weighted Mean SSC		
			Up-stream (NTU)	Down-stream (NTU)	Performance Efficiency (%)	Up-stream (mg/L)	Down-stream (mg/L)	Performance Efficiency (%)
33% (3:1) Slope	25	#1	29690	1609	95	27767	1153	96
		#2	39009	758	98	25079	875	97
		#1R	46765	4222	91	33356	3135	91
		#2R	18628	2771	85	22205	2665	88
	76	#1	40355	1121	97	31706	1073	97
		#2	32081	1080	97	24753	1127	95
		#1R	26588	2750	90	19271	1886	90
		#2R	24696	1834	93	19142	1624	92
	127	#1	37989	--	--	31958	--	--
		#2	--	--	--	--	--	--
		#1R	37008	1364	96	26679	1296	95
		#2R	18925	2265	88	13685	1279	91
25% (4:1) Slope	25	#1	24380	3549	85	21495	2701	87
		#2	20556	2016	90	17723	1626	91
		#1R	22906	11037	52	18459	7684	58
		#2R	22996	5581	76	17807	4324	76
	76	#1	8780	3867	56	6547	3397	48
		#2	6976	2819	60	5256	2251	57
		#1R	8244	2648	68	5608	2032	64
		#2R	3915	1195	69	2720	614	77
	127	#1	7772	3061	61	5544	2269	59
		#2	19213	1955	90	14032	1410	90
		#1R	14489	2729	81	13018	2042	84
		#2R	8384	1354	84	7123	1115	84
10% (10:1) Slope	25	#1	13512	878	94	14449	714	95
		#2	13824	855	94	14555	971	93
		#1R	6631	1985	70	5962	1515	75
		#2R	9973	2889	71	7318	2215	70
	76	#1	9472	3831	60	10330	2599	75
		#2	10282	1751	83	11088	1480	87
		#1R	7217	3556	51	5932	2578	57
		#2R	4736	1152	76	3441	926	73
	127	#1	12466	4105	67	7147	2410	66

Slope % (Ratio)	Rainfall Intensity (mm/h)	Rainfall Events	Volume-Weighted Mean Turbidity			Volume-Weighted Mean SSC		
			Up-stream (NTU)	Down-stream (NTU)	Performance Efficiency (%)	Up-stream (mg/L)	Down-stream (mg/L)	Performance Efficiency (%)
		#2	14303	2638	82	10503	1450	86
		#1R	8629	4342	50	6416	3413	47
		#2R	6044	2466	59	4779	1890	60

Table entries that appear with "--" indicate that no samples were collected during those tests due to previous test failures

The overall projected turbidity performance efficiency for the woven fabric under all slopes and intensities tested ranged from 50 to 98 percent with a mean and median of 78 and 82 percent, respectively. The SCC performance efficiency ranged from 48 to 97 percent with a mean and median of 79 and 86 percent, respectively. For the nonwoven fabric, performance efficiency during the rain event ranged from 50 to 98 percent with a mean and median of 78 and 82 percent, respectively, and from 47 to 97 percent with a mean of 79 percent and a median of 85 percent for the turbidity and SCC, respectively.

Using the volume-weighted mean turbidity and SSC removals shown in Table 17 and Table 18, a Wilcoxon rank sum test was completed in order to determine if the performance efficiencies on the woven and nonwoven fabric were significantly different from each other. The results of the analysis are shown in Table 31 of Appendix B. The results show that there was only a significant difference between the performance efficiencies of either fabric on a 25 percent embankment slope; with the woven fabric significantly reducing turbidity to a greater extent than the nonwoven fabric. Table 19 shows summary results of the overall projected efficiencies for both fabrics.

TABLE 19 SUMMARY OF OVERALL PROJECTED PERFORMANCE EFFICIENCY

Performance criteria	Slope (%)	Statistical parameter	Projected Overall Performance	
			Woven Fabric	Nonwoven Fabric
Turbidity Performance Efficiency (%)	All slopes	Mean	80	78
		Median	89	82
	33	Mean	96	93
		Median	96	94
	25	Mean	89	73
		Median	90	73
	10	Mean	64	71
		Median	63	71
SSC Performance Efficiency (%)	All slopes	Mean	79	79
		Median	86	85
	33	Mean	95	93
		Median	94	93
	25	Mean	87	73
		Median	88	77
	10	Mean	65	74
		Median	62	74

Table 19 shows that the projected performance of the woven fabric is actually better than the nonwoven fabric on every slope except for 10 percent. This is interesting because during the rain event as well as after the rain event, the nonwoven significantly reduced both turbidity and SCC to a greater extent than the woven fabric.

The reason for the greater performance efficiency occurring on the woven fabric is due to the lower flow-through rate of this fabric. Lower flow through-rates lead to greater performance efficiencies because water discharges at a slower rate during the rain event where the performance efficiencies are low. The lower flow-through rate allows a greater portion of the influent water to discharge after the rain event where the performance efficiency is significantly

higher due to increased filtration and sedimentation. Comparing the woven and nonwoven fabrics, the woven fabric achieved overall greater performance efficiency because less flow discharged during rainfall in comparison with the nonwoven fabric. This explains why even though the nonwoven fabric achieved higher removals both during and after the rainfall event, the woven fabric still achieved an overall comparable performance efficiency.

The effect of how flow-through rate on performance efficiency can affect the overall performance can be seen in Table 19 by noting the trend of increasing efficiency with increasing embankment slope for both fabrics. Recall from Chapter 4, section: Flow-through rates during the rain event, that the flow-through rate of both fabrics decreased with increasing embankment slope. The decrease in flow-through rate with embankment slope is what led to the trend of increasing efficiency with increasing embankment slope.

The reason for the woven fabric having a higher performance efficiency in comparison with the nonwoven fabric and the trend of increasing performance efficiency with increasing embankment slope can be better explained by comparing the volumes of water which discharged through both fabrics both during and after the rain event, as presented in Table 20.

TABLE 20 DISCHARGE WATER VOLUME BOTH DURING AND AFTER RAINFALL

Embankment Slope (%)	Rainfall Intensity (mm/h)	Volume Discharged (L)					
		Woven Fabric			Nonwoven Fabric		
		During Rainfall	After Rainfall	Ratio, During/After	During Rainfall	After Rainfall	Ratio, During/After
33	25	9	155	0.06	24	63	0.38
	76	37	434	0.09	86	330	0.26
	127	16	--	--	128	468	0.27
25	25	10	50	0.2	48	34	1.41
	76	44	281	0.16	206	109	1.89
	127	124	616	0.2	230	269	0.86
10	25	47	53	0.89	69	72	0.96
	76	162	173	0.94	220	131	1.68
	127	111	264	0.42	240	193	1.24

Table 20 shows the volume of water discharged through both fabrics during and after the rain event. Additionally, presented is the ratio of during rainfall to after rainfall volume for both fabrics. Comparing the ratios between both fabrics, the nonwoven fabric had a greater ratio on each embankment slope and rainfall intensity tested because the nonwoven fabric allowed a greater volume of water to discharge through the silt fence during the rain event. The greater ratio of the nonwoven fabric is what helped lead to the lower overall projected efficiency. There is also a trend of decreasing ratio with increasing embankment slope, which helps to further explain the trend of increasing performance efficiency with increasing embankment slope.

Overall, projections show that both silt fences would have removed both turbidity and SSC with comparable efficiencies. The woven fabric removed more sediment through ponding of water and sedimentation than the nonwoven fabric did, while the nonwoven fabric removed more sediment through filtration than did the woven fabric. Although both fabrics removed

turbidity and SSC at similar rates, the nonwoven fabric did so with a higher flow-through rate, thus decreasing the chances of this fabric attaining high ponding depths, which could lead to failure or overtopping.

CHAPTER 5: CONCLUSION

This study presented an investigation on active field-scale performance of two silt fence fabrics, woven (ASR 1400) and nonwoven (BSRF). Both fabric types were evaluated in both turbidity and suspended sediment concentration performance efficiencies as well as flow-through rate for different simulated rainfall events and embankments slopes using a tilted test-bed and rainfall simulator.

Overall measured results showed that woven and nonwoven fabrics achieved performance efficiencies of 57 and 59 percent in turbidity, and 59 and 62 percent in suspended sediment concentrations, respectively. Projected results also showed that the woven and nonwoven fabrics would have achieved performance efficiencies of 80 and 78 percent in turbidity, and 78 and 79 percent in suspended sediment concentrations, respectively.

The overall efficiency was dependent on the filtration efficiency occurring during the rain event, the filtration and settling efficiencies occurring after the rain event, and the flow-through rate of the fabrics. The flow-through rate was found to affect the overall efficiency due to the performance efficiency after rainfall being significantly higher ($\alpha = 0.05$) than the performance efficiency during rainfall. Lower flow-through rates limited the volume of water discharged during the rain event where the performance efficiencies were relatively low. Thus, allowing additional hydraulic detention time for the settling mechanism to occur and for discharge to occur after the rainfall event where performance efficiencies were higher. There was therefore a tradeoff between the flow-through rate of the fabric and the overall efficiency of the silt fence.

The AOS of both fabrics affected their performance efficiencies. Due in part to the nonwoven fabrics smaller AOS, the nonwoven fabric achieved significantly ($\alpha = 0.05$) greater performance efficiencies both during and after the rain event when compared to the woven fabric. The woven fabric achieved average performance efficiencies of 40 and 78 percent, and the nonwoven fabric achieved average efficiencies of 50 and 85 percent during and after the rain event, respectively. Although AOS was found to influence the filtration and performance efficiency of the silt fence fabrics, AOS could not be used to predict particle size capture. The woven fabrics AOS was larger than 100% of the particle sizes used in the study, however, the filtration efficiency of this fabric during the rain event was 40 percent. It is therefore likely that the particle sizes captured by silt fence in the field can be smaller than the AOS of the silt fence.

Results of the field-scale study showed that silt fence was not adequate as a stand-alone treatment installed on a silty-sand soil at the toes of embankment slopes of 10 percent and greater. Due to the large erosion rate of the silty-sand soil, the effluent discharge turbidities of both fabrics were on average, at least 2 magnitudes greater than the regulated maximum discharge turbidity of 29 NTU above background. Additional treatment processes would need to be installed in conjunction with silt fence in order to form a treatment train if effluent discharge limits were to be met.

Both the woven and nonwoven fabrics performed similarly, however, there were differences in how they operated as silt fence. Both fabrics reduced the discharge of the silty-sand soil through filtration, with the nonwoven fabric achieving higher efficiency due to its smaller AOS. Both fabrics also reduced sediment through ponding of water and sedimentation; however, the woven fabric removed sediment to a greater extent using this mechanism due to its

lower flow-through rate. Overall, both fabrics reduce turbidity and suspended sediment

concentrations by approximately 60 percent. The nonwoven fabric however, achieved this

performance efficiency while maintaining a higher flow-through rate. Thus, decreasing the

chance of this fabric failing or overtopping due to high ponding ponds depths.

APPENDIX A: ANALYSES OF SOIL TESTING

Soil Particle Distribution

TABLE 21 MATERIALS FINER THAN 75-μm BY WASHING ANALYSIS

Parameter	Unit	Value
Total dry soil mass	g	715.2
Dry mass retained on number 200 sieve	g	601.7
Dry mass finer than number 200 sieve	g	113.5
Percent finer than number 200 sieve	%	16

TABLE 22 SIEVE ANALYSIS

Sieve Number	Sieve Opening (mm)	Mass of Sieve (g)	Mass of Soil and Sieve (g)	Mass Retained (g)	Retained (%)	Cumulative Percent Retained (%)	Percent Finer (%)
10	2	486.1	486.6	0.5	0	0	100
20	0.85	570.7	571.7	1	0	0	100
40	0.425	390.7	417	26.3	4	4	96
60	0.25	407.6	549.5	141.9	20	24	76
80	0.18	526	659.6	133.6	19	42	58
100	0.15	351.3	424.9	73.6	10	53	47
140	0.106	337	501.5	164.5	23	76	24
200	0.075	337.6	395.5	57.9	8	84	16

TABLE 23 HYDROMETER ANALYSIS

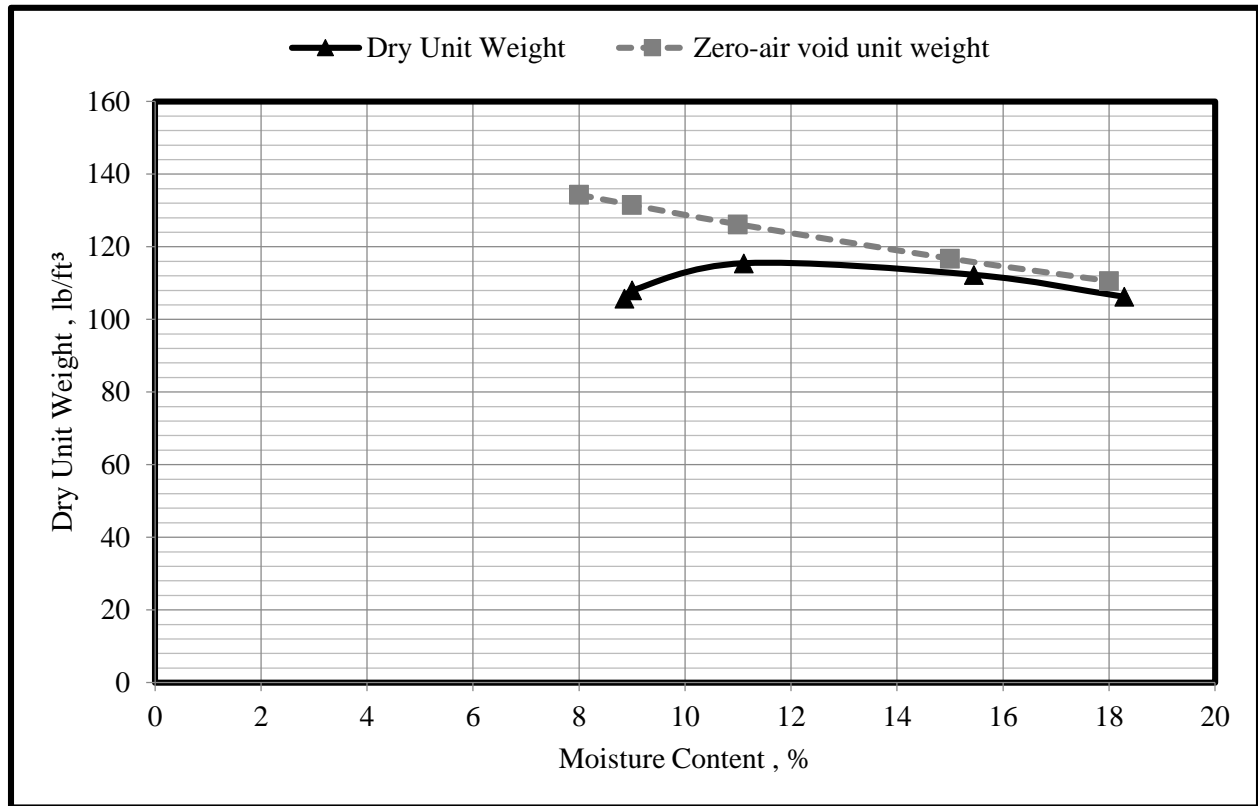| Time (min)	Reading	Rcp	Percent Finer (%)	Rcl	L (cm)	Particle Diameter (mm)
2	44.5	40.62	13.2	45.5	8.8	0.027
5	43.5	39.62	12.9	44.5	9	0.017
15	43	39.12	12.7	44	9.1	0.01
30	42	38.12	12.4	43	9.2	0.007
60	41.5	37.62	12.2	42.5	9.3	0.005
250	41	37.12	12.1	42	9.4	0.003
1440	39	35.12	11.4	40	9.7	0.001

FIGURE 20 MAXIMUM DRY UNIT WEIGHT OF SILTY-SAND SOIL

TABLE 24 MAXIMUM DRY UNIT WEIGHT FOR SILTY-SAND

Moisture Content Determination

Trial No.	Mass of Moist Specimen + Mold (kg)	Mass of Moist Specimen (kg)	Moist Density of Compacted Specimen (Mg/m3)	Theoretical Moisture Content (%)	Mass of Wet Soil + Can (g)	Mass of Dry Soil + Can (g)	Mass of Water (g)	Mass of Can (g)	Mass of Dry Soil (g)	Moisture Content (%)
1	6.02	1.74	1.84	8	162.9	153.74	9.16	50.37	103.37	8.86
2	6.06	1.78	1.89	9	126.25	119.92	6.33	49.65	70.27	9
3	6.22	1.94	2.06	11	187.8	174.01	13.79	49.92	124.09	11.11
4	6.24	1.96	2.08	15	133.11	122.02	11.09	50.24	71.78	15.46
5	6.18	1.9	2.01	18	151.19	135.58	15.61	50.21	85.37	18.29

Unit Weight Determination

Trial No.	Dry Density of Compacted Specimen (Mg/m^3)	Dry Unit Weight, (lb/ft^3)	Moist Density of Compacted Specimen, (Mg/m^3)	Moist Unit Weight, (lb/ft^3)	zero-air-void Unit Weight, (lb/ft^3)
1	1.69	105.73	1.84	115.1	134.37
2	1.73	108.02	1.89	117.74	131.54
3	1.85	115.49	2.06	128.33	126.22
4	1.8	112.29	2.08	129.65	116.78
5	1.7	106.25	2.01	125.68	110.57

Volume of Mold = 0.000944 m³

Specific Gravity = 2.60

Unit Weight of Water = 62.4 lb/ft³

Mass of Mold = 4.28 kg

Constant Head Permeability Testing

TABLE 25 SILTY-SAND SOIL PERMEABILITY

Test #	1			2		
	1A	1B	1C	2A	2B	2C
Volume Collected, cm^3	19.61	17.61	14.53	42.26	36.6	30.67
Time of Collection, sec		60			60	
Temperature of Water, °C	24.2	24.2	24.2	24.1	24.9	24.7
Head difference "h" (cm)	98.63	87.63	87.63	98.63	87.63	74.63
Diameter of Specimen, mm		75.62			75.62	
Length of Specimen, mm	130.69	130.07	130.04	137.2	138.48	139.8
Area of Specimen, cm^2		44.91			44.91	
Hydraulic Conductivity, cm/s	0.00096	0.00097	0.0008	0.00218	0.00215	0.00213
$\eta_{T°C}/\eta_{20°C}$	0.9058	0.9058	0.9058	0.9079	0.8911	0.8953
Corrected Hydraulic Conductivity, cm/s	0.000873	0.000879	0.000725	0.001981	0.001913	0.001909
Hydraulic Conductivity @ 20°C, cm/s	0.0014					
Permeability @ 20°C, cm^2	1.41E-08					

Dry Density Calculations

Mass of empty container, g	2096.1
mass of soil + container, g	3005.4
mass of soil, g	909.3
Volume of specimen, cm^3	625.4008
Dry Density, g/cm^3	1.453948
Dry Density, lb/ft^3	90.76699

Temperature, T (°C)	$\eta_{T°C}/\eta_{20°C}$	Temperature, T (°C)	$\eta_{T°C}/\eta_{20°C}$
15	1.135	23	0.931
16	1.106	24	0.910
17	1.077	25	0.889
18	1.051	26	0.869
19	1.025	27	0.850
20	1.000	28	0.832
21	0.976	29	0.814
22	0.953	30	0.797

APPENDIX B: STATISTICAL ANALYSES OF PERFORMANCE EFFICIENCY

Statistical Difference between Initial and Repeat Tests

TABLE 26 WILCOXON RANK SUM TEST: WOVEN FABRIC SIGNIFICANT P-VALUES BETWEEN
INITIAL AND REPEAT TESTS

Embankment Slope (%)	Rainfall Intensity (mm/h)	p-Value			
		Upstream Turbidity	Downstream Turbidity	Upstream SSC	Downstream SSC
33	25	0.045	0.810	0.013	0.575
	127	1.000	0.530	0.676	0.403
10	25	0.522	0.020	0.575	0.013
	76	0.810	0.940	1.000	0.936

TABLE 27 WILCOXON RANK SUM TEST: NONWOVEN FABRIC SIGNIFICANT P-VALUES BETWEEN
INITIAL AND REPEAT TESTS

Embankment Slope (%)	Rainfall Intensity (mm/h)	p-Value			
		Upstream Turbidity	Downstream Turbidity	Upstream SSC	Downstream SSC
33	25	0.013	0.013	0.298	0.008
	76	0.689	0.689	0.008	0.575
	127	0.523	0.523	0.410	0.411
25	25	0.005	0.005	0.020	0.013
	76	0.470	0.471	0.379	0.128
	127	0.066	0.093	0.005	0.128
10	25	0.031	0.031	0.013	0.031
	76	0.571	0.571	0.093	1.000
	127	0.045	0.045	0.047	0.575

Statistical Analysis of woven fabric performance efficiency verse nonwoven fabric performance efficiency

TABLE 28 WILCOXON RANK SUM TEST: SIGNIFICANT P-VALUES FOR NONWOVEN FABRIC HAVING GREATER PERFORMANCE EFFICIENCY THAN WOVEN FABRIC DURING THE RAIN EVENT

Embankment Slope (%)	p-Value	
	Volume-weighted Turbidity Efficiency	Volume-weighted SSC Efficiency
33, 25 and 10	0.041	0.001
33	0.252	0.049
25	0.303	0.010
10	0.016	0.009

TABLE 29 WILCOXON RANK SUM TEST: SIGNIFICANT P-VALUES FOR NONWOVEN FABRIC HAVING GREATER PERFORMANCE EFFICIENCY THAN WOVEN FABRIC AFTER THE RAIN EVENT

Embankment Slope (%)	p-Value	
	Volume-weighted Turbidity Efficiency	Volume-weighted SSC Efficiency
33, 25 and 10	0.003	0.000
33	0.000	0.000
25	0.050	0.004
10	0.435	0.383

TABLE 30 WILCOXON RANK SUM TEST: SIGNIFICANT P-VALUES FOR NONWOVEN FABRIC HAVING AN OVERALL GREATER PERFORMANCE EFFICIENCY THAN WOVEN FABRIC

Embankment Slope (%)	p-Value	
	Volume-weighted Turbidity Efficiency	Volume-weighted SSC Efficiency
33, 25 and 10	0.238	0.012
33	0.087	0.029
25	0.750	0.014
10	0.244	0.153

TABLE 31 WILCOXON RANK SUM TEST: SIGNIFICANT P-VALUES FOR WOVEN AND NONWOVEN
FABRIC HAVING SIGNIFICANTLY DIFFERENT PROJECTED OVERALL PERFORMANCE EFFICIENCY

Embankment Slope (%)	p-Value	
	Volume-weighted Turbidity Efficiency	Volume-weighted SSC Efficiency
33, 25 and 10	0.597	0.980
33	0.303	0.255
25	0.008	0.083
10	0.249	0.121

Performance Efficiency Based on Embankment Slope

TABLE 32 SINGLE FACTOR ANOVA: WOVEN FABRIC STATISTICAL DIFFERENCE OF VOLUME-WEIGHTED MEAN EFFICIENCY BETWEEN DIFFERENT SLOPES

Parameter	Embankment Slope (%)	No. Sample	Average (%)	Variance	p-Value	Significance ($\alpha = 0.05$)
Turbidity Efficiency	33	10	48	97	0.026	Significant
	25	6	32	149		
	10	10	37	121		
SSC Efficiency	33	10	48	162	0.003	Significant
	25	6	22	63		
	10	10	44	262		

TABLE 33 SINGLE FACTOR ANOVA: NONWOVEN FABRIC STATISTICAL DIFFERENCE OF VOLUME-WEIGHTED MEAN EFFICIENCY BETWEEN DIFFERENT SLOPES

Parameter	Embankment Slope (%)	No. Sample	Average (%)	Variance	p-Value	Significance ($\alpha = 0.05$)
Turbidity Efficiency	33	11	54	285	0.030	Significant
	25	12	40	235		
	10	12	58	342		
SSC Efficiency	33	11	58	166	0.026	Significant
	25	12	43	430		
	10	12	63	368		

Performance Efficiency Change of Test 1 to Test 2

TABLE 34 WILCOXON RANK SUM TEST: WOVEN FABRIC STATISTICAL DIFFERENCE OF TURBIDITY PERFORMANCE EFFICIENCY BETWEEN TEST 1 AND TEST 2

Embankment Slope (%)	Test	No. Samples	Median	p-Value	Significance ($\alpha = 0.05$)
33, 25, and 10	# 1	68	35.5	0.886	Not Significant
	# 2	68	35.5		
33	# 1	21	51	0.753	Not Significant
	# 2	21	54		
25	# 1	17	30	0.270	Not Significant
	# 2	17	29		
10	# 1	30	27	0.616	Not Significant
	# 2	30	30		

TABLE 35 WILCOXON RANK SUM TEST: WOVEN FABRIC STATISTICAL DIFFERENCE OF SEDIMENT PERFORMANCE EFFICIENCY BETWEEN TEST 1 AND TEST 2

Embankment Slope (%)	Test	No. Samples	Median	p-Value	Significance ($\alpha = 0.05$)
33, 25, and 10	# 1	68	32	0.407	Not Significant
	# 2	68	28		
33	# 1	21	49	0.178	Not Significant
	# 2	21	41		
25	# 1	17	22	0.318	Not Significant
	# 2	17	19		
10	# 1	30	32	0.842	Not Significant
	# 2	30	32		

TABLE 36 WILCOXON RANK SUM TEST: NONWOVEN FABRIC STATISTICAL DIFFERENCE OF TURBIDITY PERFORMANCE EFFICIENCY BETWEEN TEST 1 AND TEST 2

Embankment Slope (%)	Test	No. Samples	Median	p-Value	Significance ($\alpha = 0.05$)
33, 25, and 10	# 1	102	39	0.000	Significant
	# 2	102	63		
33	# 1	30	44.5	0.000	Significant
	# 2	30	65		
25	# 1	36	28.5	0.001	Significant
	# 2	36	54.5		
10	# 1	36	45.5	0.006	Significant
	# 2	36	66		

TABLE 37 WILCOXON RANK SUM TEST: NONWOVEN FABRIC STATISTICAL DIFFERENCE OF SEDIMENT PERFORMANCE EFFICIENCY BETWEEN TEST 1 AND TEST 2

Embankment Slope (%)	Test	No. Samples	Median	p-Value	Significance ($\alpha = 0.05$)
33, 25, and 10	# 1	102	46	0.000	Significant
	# 2	102	64		
33	# 1	30	57	0.006	Significant
	# 2	30	67.5		
25	# 1	36	32.5	0.006	Significant
	# 2	36	54.5		
10	# 1	36	52.5	0.032	Significant
	# 2	36	70		

Change in Efficiency from During Rainfall to After Rainfall

TABLE 38 WILCOXON RANK SUM TEST: WOVEN FABRIC STATISTICAL DIFFERENCE OF PERORMANCE EFFICIENCY DURING AND AFTER RAINFALL

Parameter	Embankment Slope (%)	No. Sample	Estimated Efficiency Difference, During - After (%)	p-Value	Significance (α = 0.05)
Turbidity Efficiency	33, 25, and 10	22	-30	0.000	Significant
	33	6	-28	0.036	Significant
	25	6	-29	0.036	Significant
	10	10	-31	0.006	Significant
SSC Efficiency	33, 25, and 10	22	-28	0.000	Significant
	33	6	-28	0.036	Significant
	25	6	-36	0.036	Significant
	10	10	-23	0.006	Significant

TABLE 39 WILCOXON RANK SUM TEST: NONWOVEN FABRIC STATISTICAL DIFFERENCE OF PERFORMANCE EFFICIENCY FROM DURING RAINFALL TO AFTER RAINFALL

Parameter	Embankment Slope (%)	No. Sample	Estimated Efficiency Difference, During - After (%)	p-Value	Significance (α = 0.05)
Turbidity Efficiency	33, 25, and 10	34	-40	0.000	Significant
	33	10	-43	0.006	Significant
	25	12	-48	0.003	Significant
	10	12	-27	0.003	Significant
SSC Efficiency	33, 25, and 10	34	-32	0.000	Significant
	33	10	-36	0.006	Significant
	25	12	-39	0.003	Significant
	10	12	-17	0.003	Significant

APPENDIX C: STATISTICAL ANALYSES OF FLOW-THROUGH RATE

Change in Flow Through Rate with Change in Embankment Slope

TABLE 40 WILCOXON RANK SUM TEST: WOVEN FABRIC STATISTICAL DIFFERENCE FOR FLOW THROUGH RATE BETWEEN SLOPES

Testing	Embankment Slope (%)	No. of Samples	Median	p-Value	Significance ($\alpha = 0.05$)
10% vs. 25%	10	50	1193	0.000	Significant
	25	30	169		
25% vs. 33%	25	30	169	0.000	Significant
	33	36	68		

TABLE 41 WILCOXON RANK SUM TEST: NONWOVEN FABRIC STATISTICAL DIFFERENCE FOR FLOW THROUGH RATE BETWEEN SLOPES

Testing	Embankment Slope (%)	No. of Samples	Median	p-Value	Significance ($\alpha = 0.05$)
10% vs. 25%	10	60	1975	0.000	Significant
	25	60	1234		
25% vs. 33%	25	60	1234	0.000	Significant
	33	53	324		

Change in Flow Through Rate from Test 1 to Test 2

TABLE 42 WILCOXON RANK SUM TEST: STATISTICAL DIFFERENCE OF FLOW-THROUGH RATE
BETWEEN TEST 1 AND TEST 2

Fabric Type	Embankment Slope (%)	No. Samples	Estimated Flow rate Difference, Test 1 - Test 2 (L/m²/h)	p-Value	Significance (α = 0.05)
Woven Fabric	33, 25, and 10	55	-48.5	0.010	Significant
	33	15	-40	0.001	Significant
	25	15	-43.5	0.003	Significant
	10	25	-128	0.226	Not Significant
Nonwoven Fabric	33, 25, and 10	85	64	0.227	Not Significant
	33	25	-93	0.060	Not Significant
	25	30	299	0.020	Significant
	10	30	138	0.399	Not Significant

Change in Flow-Through Rate due to Change in Rainfall Intensity

TABLE 43 SINGLE FACTOR ANOVA: WOVEN FABRIC STATISTICAL DIFFERENCE OF FLOW-THROUGH RATE BASED ON DIFFERENT RAINFALL INTENSITIES

Embankment Slope (%)	Rainfall Intensity (mm/h)	No. of Sample	Average Flow rate (L/m²/h)	p-Value	Significance (α = 0.05)
33	25	19	63	0.002	Significant
	76	9	139		
	127	--	--		
25	25	9	123	0.000	Significant
	76	9	220		
	127	9	427		
10	25	20	830	0.000	Significant
	76	20	1494		
	127	10	1360		

TABLE 44 SINGLE FACTOR ANOVA: NONWOVEN FABRIC STATISTICAL DIFFERENCE OF FLOW THROUGH RATE BASED ON DIFFERENT RAINFALL INTENSITIES

Embankment Slope (%)	Rainfall Intensity (mm/h)	No. of Sample	Average Flow rate (L/m²/h)	p-Value	Significance (α = 0.05)
33	25	20	310	0.176	Significant
	76	20	416		
	127	13	458		
25	25	20	860	0.000	Significant
	76	20	1512		
	127	20	1155		
10	25	19	1310	0.001	Significant
	76	19	2355		
	127	19	2652		

Change in Flow Through Rate from During Rainfall to After Rainfall

TABLE 45 WILCOXON RANK SUM TEST: STATISTICAL DIFFERENCE OF FLOW THROUGH RATE
BETWEEN DURING AND AFTER THE RAIN EVENT

Fabric Type	Embankment Slope (%)	No. Samples	Estimated Flow rate Difference, During - After (L/m²/h)	p-Value	Significance (α = 0.05)
Woven Fabric	33, 25, and 10	22	61	0.002	Significant
	33	6	24	0.036	Significant
	25	6	89	0.036	Significant
	10	10	74	0.103	Not Significant
Nonwoven Fabric	33, 25, and 10	34	752	0.000	Significant
	33	10	272	0.006	Significant
	25	12	896	0.003	Significant
	10	12	1278	0.003	Significant

APPENDIX D: MISCELLANEOUS

Time Dependent Efficiency and Flow Rate Results

TABLE 46 WOVEN FABRIC TIME DEPENDENT EFFICIENCY AND FLOW-THROUGH RATE RESULTS ON 10% SLOPE

Intensity (mm/h)	Test	During Rainfall				After Rainfall			
		time (min)	Turbidity Efficiency (%)	SSC Efficiency (%)	Flow Rate (L/m²/h)	time (min)	Turbidity Efficiency (%)	SSC Efficiency (%)	Flow Rate (L/m²/h)
25	# 1	5	37	47	--	35	39	59	1114
		10	46	11	584	40	71	83	1014
		15	29	52	670	45	92	94	873
		20	4	32	829	50	91	93	793
		25	27	39	884	55	94	95	673
		30	57	49	1058	60	96	96	709
	# 2	5	66	65	--	35	77	84	1570
		10	29	63	1111	40	84	89	1457
		15	69	77	1119	45	89	92	1311
		20	67	74	1262	50	94	95	1151
		25	80	84	1398	55	95	95	938
		30	72	80	1503	60	94	95	749
	# 1R	5	75	79	--	35	87	87	233
		10	50	56	236	40	84	85	277
		15	50	57	241	45	96	94	292
		20	67	67	241	50	95	93	238
		25	57	63	217	55	96	95	230
		30	79	83	286	60	96	95	190
	# 2R	5	34	6	--	35	57	57	1121
		10	33	26	903	40	72	75	902
		15	31	21	953	45	90	85	844
		20	44	45	902	50	93	87	756
		25	55	46	1055	55	87	87	606
		30	57	53	1147	60	90	86	477
76	# 1	5	17	15	--	35	9	13	2414
		10	1	-1	1206	40	60	53	2268
		15	-5	-5	1834	45	80	71	2122
		20	16	28	2103	50	80	76	1704
		25	21	27	2518	55	86	77	1638
		30	-3	13	2623	60	82	75	--
	# 2	5	0	-12	--	35	-14	17	1964
		10	0	-14	737	40	46	58	1296
		15	28	49	1265	45	69	73	999
		20	9	44	1571	50	74	70	768
		25	12	15	1825	55	76	70	626
		30	-19	5	2182	60	--	--	--
	# 1R	5	49	51	--	35	9	9	1937
		10	8	-20	489	40	59	39	1740
		15	-50	-55	855	45	73	56	1558

141

Intensity (mm/h)	Test	During Rainfall				After Rainfall			
		time (min)	Turbidity Efficiency (%)	SSC Efficiency (%)	Flow Rate (L/m²/h)	time (min)	Turbidity Efficiency (%)	SSC Efficiency (%)	Flow Rate (L/m²/h)
		20	-1	7	1155	50	81	72	1333
		25	26	32	1470	55	83	72	1032
		30	-15	-11	1677	60	84	74	856
	# 2R	5	9	12	--	35	9	5	1444
		10	29	34	870	40	37	34	1176
		15	16	17	1182	45	54	44	1002
		20	-41	6	1425	50	--	--	--
		25	38	22	1398	55	--	--	--
		30	-15	-26	1487	60	--	--	--
127	# 1	5	8	10	--	35	27	47	1450
		10	5	5	1122	40	72	60	1227
		15	27	39	1421	45	78	66	1017
		20	33	32	1518	50	49	28	895
		25	50	45	1446	55	56	66	690
		30	55	66	1782	60	48	24	552
	# 2	5	53	51	--	35	42	49	1570
		10	43	40	1051	40	67	54	1457
		15	35	56	1204	45	74	71	1311
		20	23	13	1302	50	79	72	1151
		25	28	31	1357	55	86	81	938
		30	13	22	1395	60	89	82	749

TABLE 47 WOVEN FABRIC TIME DEPENDENT EFFICIENCY AND FLOW-THROUGH RATE RESULTS ON 25% SLOPE

Intensity (mm/h)	Test	During Rainfall				After Rainfall			
		time (min)	Turbidity Efficiency (%)	SSC Efficiency (%)	Flow Rate (L/m²/h)	time (min)	Turbidity Efficiency (%)	SSC Efficiency (%)	Flow Rate (L/m²/h)
25	# 1	5	34	32	--	35	4	23	109
		10	15	24	135	40	11	29	62
		15	30	22	127	45	32	55	50
		20	11	20	87	50	65	59	41
		25	29	29	105	55	87	85	35
		30	22	29	133	60	89	88	42
	# 2	5	22	3	--	35	11	7	168
		10	17	10	129	40	33	33	113
		15	3	8	115	45	86	84	90
		20	92	14	96	50	91	87	78
		25	29	19	143	55	90	84	63
		30	1	14	176	60	87	81	47
76	# 1R	5	50	57	--	35	3	13	129
		10	41	44	156	40	-3	29	80
		15	28	28	148	45	38	35	74
		20	32	15	157	50	63	56	64
		25	4	-4	162	55	68	69	58
		30	18	3	212	60	72	68	62
	# 2R	5	41	28	--	35	14	10	379
		10	31	19	194	40	33	42	238
		15	31	14	139	45	77	73	184
		20	10	3	207	50	88	81	139
		25	8	2	322	55	92	86	103
		30	11	21	440	60	92	88	79
127	# 1	5	52	33	--	35	32	-3	402
		10	65	16	130	40	58	37	280
		15	60	5	237	45	65	44	208
		20	28	-3	358	50	63	53	160
		25	39	16	535	55	66	83	120
		30	59	43	590	60	--	--	--
	# 2	5	--	--	--	35	43	32	443
		10	41	25	232	40	82	79	318
		15	33	28	288	45	90	88	230
		20	21	23	395	50	94	61	159
		25	29	31	558	55	97	91	111
		30	40	31	644	60	95	84	72

TABLE 48 WOVEN FABRIC TIME DEPENDENT EFFICIENCY AND FLOW-THROUGH RATE RESULTS ON 33% SLOPE

Intensity (mm/h)	Test	During Rainfall				After Rainfall			
		time (min)	Turbidity Efficiency (%)	SSC Efficiency (%)	Flow Rate (L/m²/h)	time (min)	Turbidity Efficiency (%)	SSC Efficiency (%)	Flow Rate (L/m²/h)
25	# 1	5	67	75	--	35	12	41	58
		10	78	81	15	40	53	53	26
		15	71	76	18	45	88	87	17
		20	56	56	23	50	92	91	14
		25	42	43	41	55	93	93	13
		30	21	43	39	60	96	95	10
	# 2	5	84	73	--	35	4	24	73
		10	65	48	63	40	48	13	49
		15	52	21	65	45	80	65	36
		20	57	30	75	50	68	66	33
		25	35	16	76	55	73	66	35
		30	29	30	59	60	86	83	34
	# 1R	5	69	63	--	35	16	25	41
		10	32	30	42	40	62	64	26
		15	33	35	55	45	86	83	22
		20	39	47	44	50	90	87	24
		25	9	17	40	55	96	94	26
		30	24	32	39	60	96	93	20
	# 2R	5	-11	15	--	35	65	68	55
		10	67	55	217	40	73	75	34
		15	61	67	98	45	80	78	32
		20	70	72	67	50	85	84	31
		25	54	65	67	55	87	84	29
		30	72	72	64	60	91	89	22
76	# 1	5	84	90	--	35	--	--	--
		10	55	58	69	40	--	--	--
		15	10	24	192	45	--	--	--
		20	--	--	--	50	--	--	--
		25	--	--	--	55	--	--	--
		30	--	--	--	60	--	--	--
	# 2	5	--	--	--	35	--	--	--
		10	--	--	--	40	--	--	--
		15	--	--	--	45	--	--	--
		20	--	--	--	50	--	--	--
		25	--	--	--	55	--	--	--
		30	--	--	--	60	--	--	--
	# 1R	5	79	83	--	35	48	-27	150
		10	69	65	73	40	80	51	69
		15	51	49	77	45	90	77	45
		20	38	26	88	50	97	68	34
		25	45	33	114	55	94	84	24
		30	43	25	135	60	95	79	25

Intensity (mm/h)	Test	During Rainfall				After Rainfall			
		time (min)	Turbidity Efficiency (%)	SSC Efficiency (%)	Flow Rate (L/m²/h)	time (min)	Turbidity Efficiency (%)	SSC Efficiency (%)	Flow Rate (L/m²/h)
	# 2R	5	75	75	--	35	28	22	282
		10	65	57	87	40	78	63	187
		15	53	41	91	45	21	89	152
		20	42	27	131	50	94	93	119
		25	42	27	211	55	90	88	88
		30	29	17	316	60	97	95	69
	# 1	5	93	95	--	35	--	--	--
		10	98	98	108	40	--	--	--
		15	73	77	76	45	--	--	--
		20	33	24	147	50	--	--	--
		25	31	9	284	55	--	--	--
		30	--	--	--	60	--	--	--
	# 2	5	--	--	--	35	--	--	--
		10	--	--	--	40	--	--	--
		15	--	--	--	45	--	--	--
		20	--	--	--	50	--	--	--
		25	--	--	--	55	--	--	--
127		30	--	--	--	60	--	--	--
	# 1R	5	82	85	--	35	--	--	--
		10	82	84	51	40	--	--	--
		15	81	82	51	45	--	--	--
		20	40	51	143	50	--	--	--
		25	31	40	2429	55	--	--	--
		30	--	--	--	60	--	--	--
	# 2R	5	63	70	--	35	--	--	--
		10	35	37	220	40	--	--	--
		15	29	38	5325	45	--	--	--
		20	--	--	--	50	--	--	--
		25	--	--	--	55	--	--	--
		30	--	--	--	60	--	--	--

TABLE 49 NONWOVEN FABRIC TIME DEPENDENT EFFICIENCY AND FLOW-THROUGH RATE RESULTS ON 10% SLOPE

Intensity (mm/h)	Test	During Rainfall				After Rainfall			
		time (min)	Turbidity Efficiency (%)	SSC Efficiency (%)	Flow Rate (L/m²/h)	time (min)	Turbidity Efficiency (%)	SSC Efficiency (%)	Flow Rate (L/m²/h)
25	# 1	5	82	87	--	35	90	93	387
		10	88	93	453	40	94	95	234
		15	87	90	459	45	96	96	147
		20	90	93	475	50	--	--	--
		25	82	88	475	55	--	--	--
		30	86	91	457	60	--	--	--
	# 2	5	39	52	--	35	88	87	575
		10	78	71	321	40	93	94	623
		15	88	88	606	45	98	97	698
		20	84	86	772	50	98	96	768
		25	87	87	809	55	98	97	755
		30	86	89	511	60	99	97	632
	# 1R	5	49	56	--	35	42	48	1890
		10	70	88	774	40	77	79	1246
		15	70	71	725	45	91	88	557
		20	61	65	761	50	94	91	364
		25	56	57	1529	55	95	91	305
		30	54	59	1919	60	--	--	--
	# 2R	5	42	47	--	35	51	50	2526
		10	38	41	2560	40	83	80	933
		15	72	72	3033	45	85	77	431
		20	72	68	2912	50	95	88	295
		25	64	61	2969	55	95	90	236
		30	71	71	2820	60	--	--	--
76	# 1	5	29	-5	--	35	24	47	3239
		10	52	69	2792	40	78	81	993
		15	49	73	3651	45	91	89	327
		20	40	73	3593	50	94	93	192
		25	46	60	3491	55	96	94	144
		30	62	70	3394	60	97	94	119
	# 2	5	70	81	--	35	30	59	1103
		10	81	86	1216	40	81	86	368
		15	40	62	1331	45	91	92	152
		20	82	85	1396	50	93	91	123
		25	68	72	1307	55	95	93	103
		30	80	80	1217	60	96	94	87
	# 1R	5	18	31	--	35	75	70	1251
		10	30	41	3209	40	89	83	333
		15	47	62	3112	45	93	86	186
		20	21	27	2775	50	95	89	144
		25	45	49	2296	55	96	90	113
		30	25	22	2058	60	--	--	--

Intensity (mm/h)	Test	During Rainfall				After Rainfall			
		time (min)	Turbidity Efficiency (%)	SSC Efficiency (%)	Flow Rate (L/m²/h)	time (min)	Turbidity Efficiency (%)	SSC Efficiency (%)	Flow Rate (L/m²/h)
	# 2R	5	44	39	--	35	71	69	1551
		10	52	55	1885	40	83	78	449
		15	62	67	2278	45	90	82	239
		20	74	73	2117	50	93	87	125
		25	73	72	2218	55	95	88	92
		30	76	66	2208	60	--	--	--
	# 1	5	49	43	--	35	45	44	1764
		10	23	30	892	40	88	87	448
		15	31	30	1259	45	96	94	198
		20	28	20	1463	50	94	74	123
		25	35	22	1918	55	87	88	94
		30	26	37	2032	60	97	96	75
	# 2	5	75	73	--	35	67	74	1294
		10	59	42	605	40	92	92	501
		15	46	49	1287	45	96	95	276
		20	38	81	1422	50	98	96	201
		25	70	83	1556	55	98	96	157
127		30	52	79	1458	60	98	96	126
	# 1R	5	34	18	--	35	48	45	2932
		10	39	22	4215	40	71	68	1284
		15	32	37	4008	45	88	85	937
		20	25	22	3653	50	95	91	819
		25	40	42	3477	55	96	92	557
		30	25	23	3518	60	96	92	380
	# 2R	5	51	53	--	35	34	29	--
		10	28	40	4480	40	81	77	3774
		15	64	69	3340	45	88	84	1151
		20	37	38	3618	50	91	84	2344
		25	46	41	3505	55	94	88	--
		30	33	26	3567	60	94	88	--

TABLE 50 Nonwoven fabric time dependent efficiency and flow-through rate results on 25% slope

Intensity (mm/h)	Test	During Rainfall				After Rainfall			
		time (min)	Turbidity Efficiency (%)	SSC Efficiency (%)	Flow Rate (L/m²/h)	time (min)	Turbidity Efficiency (%)	SSC Efficiency (%)	Flow Rate (L/m²/h)
25	# 1	5	84	85	--	35	59	61	522
		10	49	64	1007	40	93	93	306
		15	50	64	776	45	97	96	156
		20	52	59	579	50	98	97	108
		25	43	44	458	55	99	97	94
		30	54	64	361	60	98	98	89
	# 2	5	78	83	--	35	64	74	504
		10	65	74	104	40	96	95	235
		15	63	63	418	45	98	98	116
		20	69	77	490	50	99	98	81
		25	66	70	522	55	99	98	62
		30	66	68	524	60	--	--	--
	# 1R	5	-15	-5	--	35	85	87	716
		10	35	39	2122	40	98	97	299
		15	26	37	1322	45	99	99	181
		20	33	32	1255	50	99	99	170
		25	32	34	1182	55	--	--	--
		30	27	54	1051	60	--	--	--
	# 2R	5	57	64	--	35	44	45	1086
		10	-4	4	939	40	96	94	562
		15	52	46	1161	45	99	97	271
		20	63	59	1114	50	99	97	188
		25	69	69	1112	55	99	97	156
		30	68	73	1101	60	--	--	--
76	# 1	5	14	-17	--	35	72	75	882
		10	61	1	1715	40	95	87	236
		15	-19	-8	1751	45	96	85	136
		20	13	9	1620	50	90	57	105
		25	16	11	1597	55	90	43	88
		30	-16	-4	1416	60	--	--	--
	# 2	5	16	16	--	35	11	6	1403
		10	6	6	1693	40	82	73	398
		15	21	19	1601	45	93	82	138
		20	26	28	1739	50	95	82	89
		25	26	28	1581	55	--	--	--
		30	28	21	1531	60	--	--	--
	# 1R	5	23	16	--	35	70	69	877
		10	13	7	1359	40	95	84	233
		15	30	30	1480	45	96	82	143
		20	27	32	1494	50	98	88	113
		25	39	25	1428	55	99	89	98
		30	33	36	1403	60	99	83	83

Intensity (mm/h)	Test	During Rainfall				After Rainfall			
		time (min)	Turbidity Efficiency (%)	SSC Efficiency (%)	Flow Rate (L/m²/h)	time (min)	Turbidity Efficiency (%)	SSC Efficiency (%)	Flow Rate (L/m²/h)
	# 2R	5	77	71	--	35	61	74	780
		10	71	70	642	40	88	81	227
		15	33	65	1581	45	92	81	145
		20	3	47	1479	50	95	80	106
		25	43	72	1552	55	97	80	92
		30	34	32	1586	60	97	85	85
	# 1	5	9	8	--	35	21	20	874
		10	13	17	2181	40	81	64	224
		15	16	20	2027	45	87	70	151
		20	6	8	2093	50	87	71	110
		25	27	28	1934	55	93	63	89
		30	36	31	1688	60	91	72	47
	# 2	5	96	95	--	35	47	96	987
		10	85	85	113	40	97	97	271
		15	56	42	613	45	99	97	145
		20	21	25	723	50	99	96	102
		25	39	35	821	55	99	95	80
127		30	47	46	988	60	99	95	66
	# 1R	5	25	46	--	35	77	81	835
		10	11	56	833	40	96	93	355
		15	26	46	1080	45	98	98	194
		20	51	60	1256	50	98	95	152
		25	33	44	1071	55	99	97	118
		30	52	54	1214	60	98	96	100
	# 2R	5	65	80	--	35	39	35	1414
		10	92	93	144	40	95	94	422
		15	54	61	267	45	97	95	207
		20	55	62	1192	50	97	93	141
		25	32	45	1515	55	96	91	116
		30	49	50	1340	60	98	96	105

TABLE 51 NONWOVEN FABRIC TIME DEPENDENT EFFICIENCY AND FLOW-THROUGH RATE RESULTS ON 33% SLOPE

Intensity (mm/h)	Test	During Rainfall				After Rainfall			
		time (min)	Turbidity Efficiency (%)	SSC Efficiency (%)	Flow Rate (L/m²/h)	time (min)	Turbidity Efficiency (%)	SSC Efficiency (%)	Flow Rate (L/m²/h)
25	# 1	5	57	60	--	35	72	88	170
		10	74	72	181	40	91	93	153
		15	58	63	214	45	98	98	89
		20	33	57	177	50	99	99	70
		25	64	70	208	55	99	99	48
		30	46	70	209	60	99	99	40
	# 2	5	81	94	--	35	91	92	370
		10	85	84	51	40	99	98	163
		15	86	81	96	45	99	98	107
		20	89	85	230	50	99	90	81
		25	92	93	349	55	99	99	56
		30	98	86	413	60	99	97	53
	# 1R	5	14	-24	--	35	84	81	298
		10	30	41	369	40	96	94	122
		15	41	47	287	45	98	97	71
		20	44	47	371	50	99	98	45
		25	60	57	349	55	99	98	35
		30	58	57	324	60	99	98	34
	# 2R	5	31	38	--	35	79	84	550
		10	57	71	586	40	94	94	223
		15	65	82	137	45	95	96	133
		20	71	80	300	50	99	98	91
		25	37	55	635	55	99	99	65
		30	47	55	722	60	100	98	56
76	# 1	5	17	62	--	35	88	70	267
		10	29	32	216	40	99	97	125
		15	49	59	198	45	99	97	71
		20	49	59	240	50	100	98	56
		25	57	58	231	55	100	98	44
		30	64	55	385	60	100	97	31
	# 2	5	82	82	--	35	90	91	332
		10	65	64	122	40	99	98	132
		15	69	61	101	45	99	98	88
		20	61	62	249	50	99	98	69
		25	65	57	596	55	100	98	57
		30	67	59	550	60	99	95	50
	# 1R	5	3	8	--	35	92	97	248
		10	12	12	891	40	98	96	121
		15	29	33	656	45	97	94	77
		20	38	31	484	50	98	95	60
		25	38	47	437	55	99	95	52
		30	40	92	447	60	98	93	52

Intensity (mm/h)	Test	During Rainfall				After Rainfall			
		time (min)	Turbidity Efficiency (%)	SSC Efficiency (%)	Flow Rate (L/m²/h)	time (min)	Turbidity Efficiency (%)	SSC Efficiency (%)	Flow Rate (L/m²/h)
127	# 2R	5	98	97	--	35	92	90	347
		10	89	75	61	40	99	97	110
		15	52	56	488	45	99	97	86
		20	49	48	683	50	99	96	63
		25	46	47	628	55	98	96	49
		30	51	55	660	60	99	93	39
	# 1	5	50	16	--	35	--	--	--
		10	55	63	261	40	--	--	--
		15	47	54	214	45	--	--	--
		20	28	31	291	50	--	--	--
		25	41	45	472	55	--	--	--
		30	--	--	480	60	--	--	--
	# 2	5	--	--	--	35	--	--	--
		10	--	--	--	40	--	--	--
		15	--	--	--	45	--	--	--
		20	--	--	--	50	--	--	--
		25	--	--	--	55	--	--	--
		30	--	--	--	60	--	--	--
	# 1R	5	62	59	--	35	87	86	280
		10	41	48	243	40	99	97	119
		15	47	52	310	45	99	97	81
		20	93	39	426	50	99	97	59
		25	33	33	419	55	99	97	47
		30	45	50	548	60	100	97	39
	# 2R	5	100	99	--	35	91	66	320
		10	97	98	73	40	99	95	232
		15	60	96	283	45	98	96	145
		20	26	46	933	50	98	93	110
		25	16	43	1082	55	99	95	86
		30	2	24	868	60	99	95	69

Change in Performance Efficiency and Discharge Concentration with Time
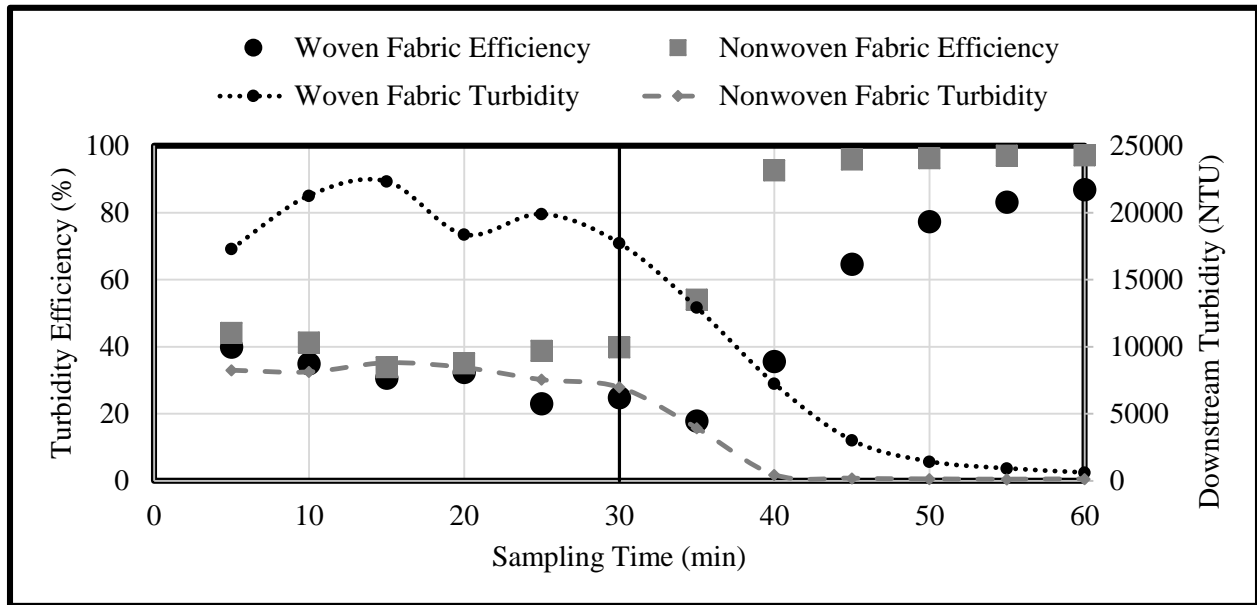
FIGURE 21 TIME DEPENDENT AVERAGE TURBIDITY PERFORMANCE EFFICIENCY AND
DOWNSTREAM VALUE ON 25 PERCENT SLOPE
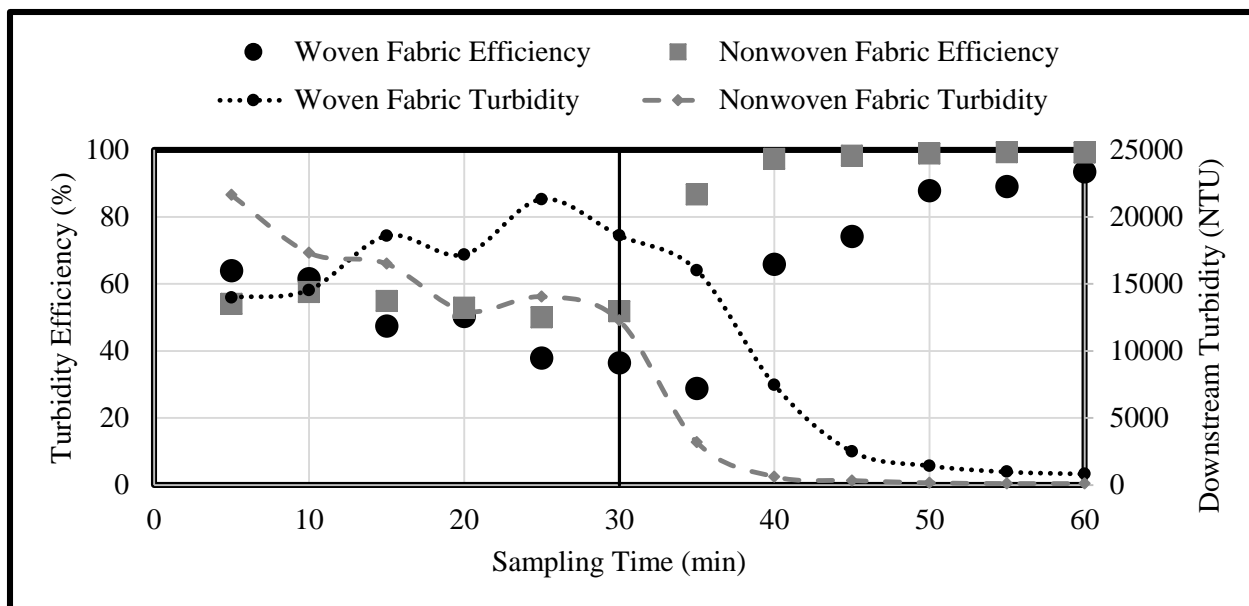
FIGURE 22 TIME DEPENDENT AVERAGE TURBIDITY PERFORMANCE EFFICIENCY AND
DOWNSTREAM VALUE ON 33 PERCENT SLOPE
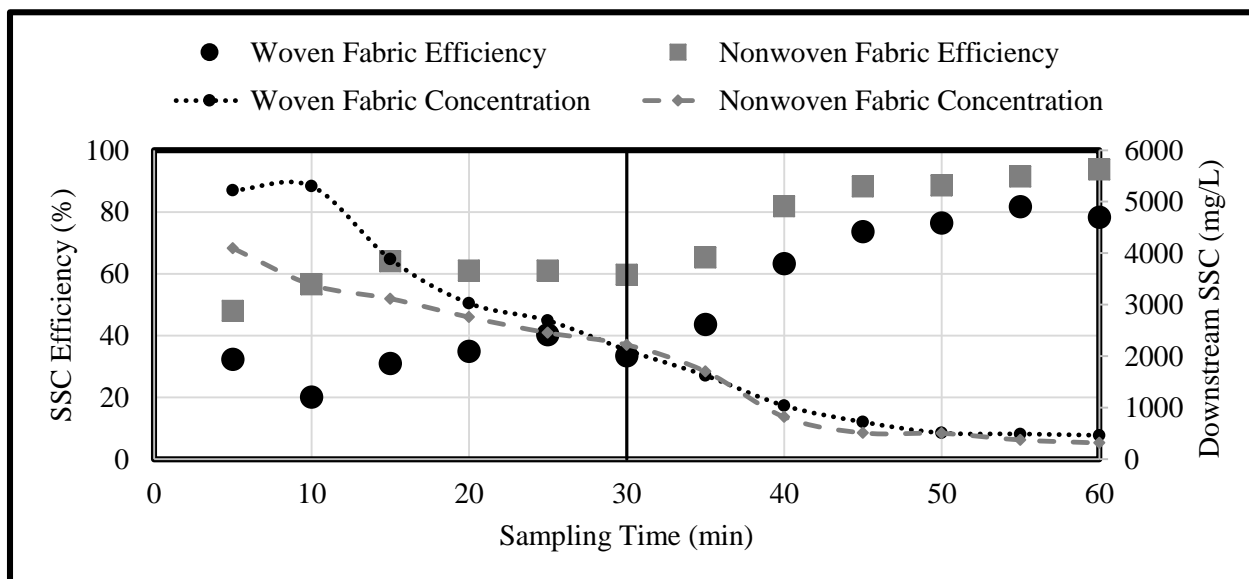
FIGURE 23 TIME DEPENDENT AVERAGE SSC PERFORMANCE EFFICIENCY AND DOWNSTREAM
VALUE ON 10 PERCENT SLOPE

153
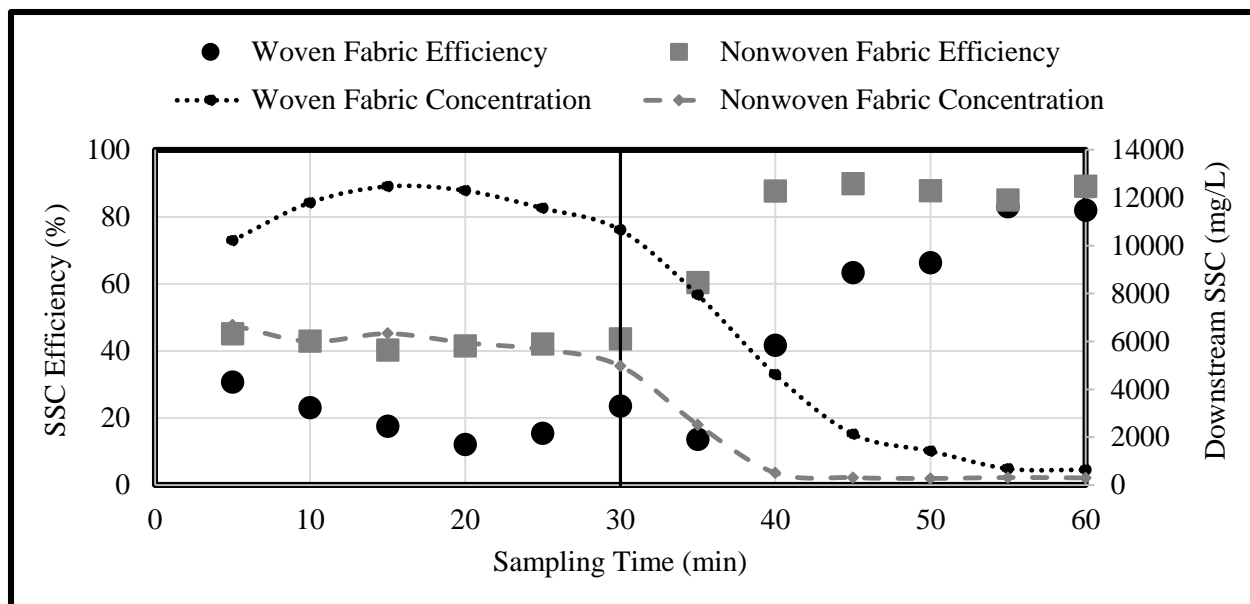
FIGURE 24 TIME DEPENDENT AVERAGE SSC PERFORMANCE EFFICIENCY AND DOWNSTREAM
VALUE ON 25 PERCENT SLOPE
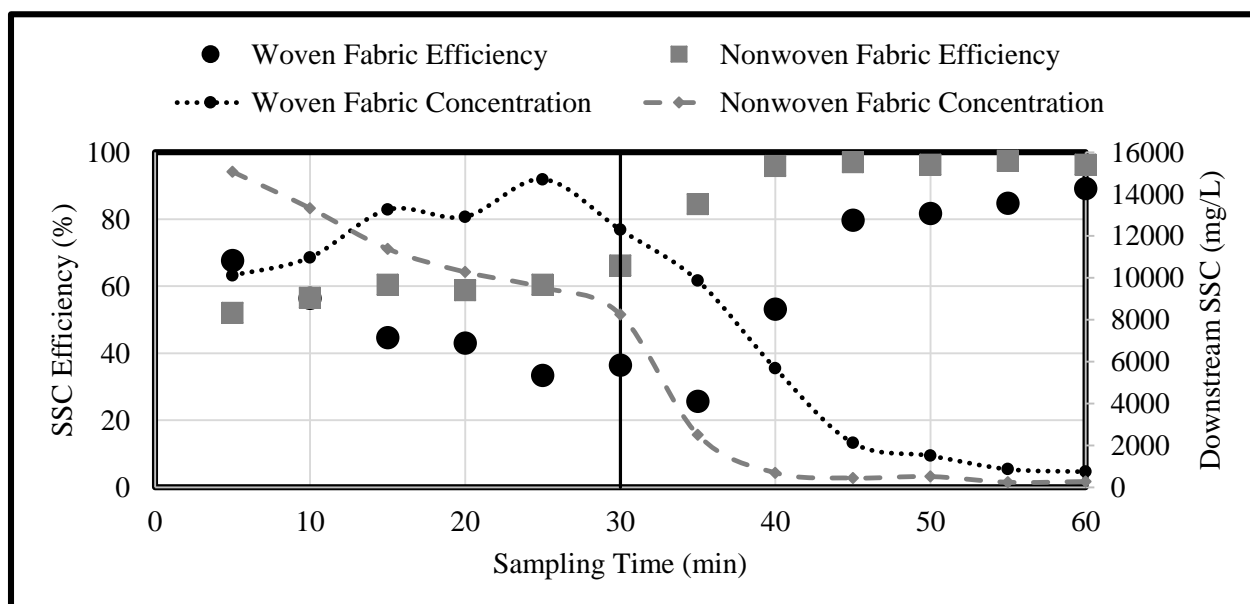
FIGURE 25 TIME DEPENDENT AVERAGE SSC PERFORMANCE EFFICIENCY AND DOWNSTREAM
VALUE ON 33 PERCENT SLOPE

LIST OF REFERENCES

APHA, AWWA and WEF (2005). Standard Method for the Examination of Water and Wastewater, A.D. Eaton, Washinton D.C.

Arjunan, J., S. Yeri, E. Stevens, B. Barfield and K. Gasem (2006). Application of Polyacrylamide to Enhance Silt Fence Performance, Oklahoma State University.

ASTM (1987). D 4632-86 Standard Test Method for Breaking Load and Elongation of Geotextiles. Annual Book of ASTM Standards, American Society for Testing and Materials. **Vol. 4.08**.

ASTM C117-13 (2013). Standard Test Method for Materials Finer than 75-um (No. 200) Sieve in Mineral Aggregates by Washing. ASTM Volue 04.02 Concrete and Aggregates.

ASTM C136-06 (2013). Standard Test Method for Sieve Analysis of Fine and Coarse Aggregates. ASTM Volume 04.02 Concrete and Aggregates.

ASTM D422-63 (2013). Standard Test Method for Particle-Size Analysis of Soils. ASTM Volue 04.08 Soil and Rock (I): D420-D5876.

ASTM D2434-68 (2006). Standard Test Method for Permeability of Granular Soils (Constant Head). ASTM Volume 04.08 Soil and Rock (I): D420-D5876.

ASTM D4491 (2009). "Test Methods for Water Permeability of geotextiles by Permittivity." West Conshohocken, PA, ASTM International. 04.13.

ASTM D6461 (2007). Standard Specification for Silt Fence Materials. ASTM Volume 04.09 Soil and Rock (II): D5877-latest.

Aydilek, A. and T. Edil (2003). "Long-term filtration performance of nonwoven geotextile-sludge systems." Geosynthetics International **10**(4): 110-123.

Barrett, M. E., J. E. Kearney, T. G. McCoy, J. F. Malina, R. Charbeneau and G. Ward (1995). An evaluation of the use and effectiveness of temporary sediment controls, Center for Research in Water Resources, University of Texas at Austin.

Bilotta, G. and R. Brazier (2008). "Understanding the influence of suspended solids on water quality and aquatic biota." Water research **42**(12): 2849-2861.

Britton, S. L., K. M. Robinson, B. J. Barfield and K. Kadavy (2000). Silt fence performance testing. 2000 ASAE Annual International Meeting, Milwaukee, Wisconsin, USA, 9-12 July 2000, American Society of Agricultural Engineers.

D698-12, A. (2013). Standard Test Methods for Laboratory Compaction Characteristics of Soil Using Standard Effort. ASTM Volume 04.08 Soil and Rock (I): D420-D5876.

Dierickx, W. and P. Van Den Berghe (2004). "Natural weathering of textiles used in agricultural applications." Geotextiles and Geomembranes **22**(4): 255-272.

EPA (2007). Developing Your Stormwater Pollution Prevention Plan: A Guide for Construction Sites**:** 46.

European Commission. (2012). "Soil Compaction." European Soil Portal - Soil Data and Information System Retrieved January 28, 2014, from http://eusoils.jrc.ec.europa.eu/library/themes/compaction/.

Farias, R., E. Palmeira and J. Carvalho (2006). "Performance of geotextile silt fences in large flume tests." Geosynthetics International **13**(4): 133-144.

Faucette, L., K. Sefton, A. Sadeghi and R. Rowland (2008). "Sediment and phosphorus removal from simulated storm runoff with compost filter socks and silt fence." Journal of soil and water conservation **63**(4): 257-264.

Faure, Y.-H., A. Baudoin, P. Pierson and O. Ple (2006). "A contribution for predicting geotextile clogging during filtration of suspended solids." Geotextiles and Geomembranes **24**(1): 11-20.

FDEP (2008). "Florida Stormwater Erosion and Sedimentation Control Inspector's Manual". Talahassee, Florida Department of Environmental Protection**:** 378.

Fisher, L. and A. Jarrett (1984). "Sediment retention efficiency of synthetic filter fabrics [Land management, erosion, flowing soil suspensions]." Transactions of the ASAE [American Society of Agricultural Engineers](USA).

Geotechdata.info. (2008, July 7, 2013). "Soil permeability coefficient."   Retrieved January 28, 2014, from http://www.geotechdata.info/parameter/permeability.html.

Gogo-Abite, I. (2012). Effluent Water Quality Improvement Using Silt Fences and Stormwater Harvesting. Doctor of Philosophy, University of Central Florida.

Gogo-Abite, I. and M. Chopra (2013). "Performance evaluation of two silt fence geotextiles using a tilting test-bed with simulated rainfall." Geotextiles and Geomembranes **39**: 30-38.

Harbor, J. (1999). "Engineering geomorphology at the cutting edge of land disturbance: erosion and sediment control on construction sites." Geomorphology **31**(1): 247-263.

Hayes, S. A., R. McLaughlin and D. Osmond (2005). "Polyacrylamide use for erosion and turbidity control on construction sites." Journal of soil and water conservation **60**(4): 193-199.

Howe, K. J., D. W. Hand, J. C. Crittenden, R. R. Trussell and G. Tchobandglous (2012). Principles of Water Treatment, John Wiley & Sons, Inc.

Koerner, R. M. (2012). Designing with geosynthetics, Xlibris Corporation.

Lamy, E., L. Lassabatere, B. Bechet and H. Andrieu (2013). "Effect of a nonwoven geotextile on solute and colloid transport in porous media under both saturated and unsaturated conditions." Geotextiles and Geomembranes **36**: 55-65.

Owens, D. W., P. Jopke, D. W. Hall, J. Balousek and A. Roa (2000). "Soil erosion from two small construction sites, Dane County, Wisconsin." USGS Fact Sheet, USGS, Madison, WI.

Rawal, A. and H. Saraswat (2011). "Pore size distribution of hybrid nonwoven geotextiles." Geotextiles and Geomembranes **29**(3): 363-367.

Risse, L., S. Thompson, J. Governo and K. Harris (2008). "Testing of new silt fence materials: A case study of a belted strand retention fence." Journal of soil and water conservation **63**(5): 265-273.

Sansone, L. and R. Koerner (1992). "Fine fraction filtration test to assess geotextile filter performance." Geotextiles and Geomembranes **11**(4): 371-393.

Suits, L. D. and Y. G. Hsuan (2003). "Assessing the photo-degradation of geosynthetics by outdoor exposure and laboratory weatherometer." Geotextiles and Geomembranes **21**(2): 111-122.

USEPA. (2011). "Sediment and Erosion Control." Retrieved March 10, 2014, from http://www.epa.gov/region6/6en/w/sw/sediment.pdf.

USEPA. (2012). "Nonpoint Source Pollution: The Nation's Largest Water Quality Problem." Water: Outreach & Communication Retrieved March 11, 2013, from http://water.epa.gov/polwaste/nps/outreach/point1.cfm.

Weggel, J. R. and J. Dortch (2012). "A model for filter cake formation on geotextiles: Experiments." Geotextiles and Geomembranes **31**: 62-68.

Weggel, J. R. and N. D. Ward (2012). "A model for filter cake formation on geotextiles: Theory." Geotextiles and Geomembranes **31**: 51-61.

Wu, C.-S., Y.-S. Hong and R.-H. Wang (2008). "The influence of uniaxial tensile strain on the pore size and filtration characteristics of geotextiles." Geotextiles and Geomembranes **26**(3): 250-262.

Zhang, Y., W. Liu, W. Shao and Y. Yang (2013). "Experimental study on water permittivity of woven polypropylene geotextile under tension." Geotextiles and Geomembranes **37**: 10-15.

Attachment 2

Continuous Turbidity Monitoring in the Indian Creek Watershed, Tazewell County, Virginia, 2006–08

U.S. Department of the Interior
U.S. Geological Survey

Continuous Turbidity Monitoring in the Indian Creek Watershed, Tazewell County, Virginia, 2006–08

By Douglas L. Moyer and Kenneth E. Hyer

Scientific Investigations Report 2009–5085

U.S. Department of the Interior
U.S. Geological Survey

U.S. Department of the Interior
KEN SALAZAR, Secretary

U.S. Geological Survey
Suzette M. Kimball, Acting Director

U.S. Geological Survey, Reston, Virginia: 2009

Contents

Figures

Tables

Conversion Factors and Vertical Datum

Multiply	By	To obtain
Length		
inch (in.)	2.54	centimeter (cm)
inch (in.)	25.4	millimeter (mm)
foot (ft)	0.3048	meter (m)
mile (mi)	1.609	kilometer (km)
square mile (mi^2)	2.590	square kilometer (km^2)
Volume		
ounce, fluid (fl. oz)	0.02957	liter (L)
gallon (gal)	3.785	liter (L)
gallon (gal)	0.003785	cubic meter (m^3)
cubic foot (ft^3)	0.02832	cubic meter (m^3)
foot per second (ft/s)	0.3048	meter per second (m/s)
cubic foot per second (ft^3/s)	0.02832	cubic meter per second (m^3/s)
Mass		
ounce, avoirdupois (oz)	28.35	gram (g)
pound, avoirdupois (lb)	0.4536	kilogram (kg)

Temperature in degrees Celsius (°C) may be converted to degrees Fahrenheit (°F) as follows:

$$°F=(1.8×°C)+32$$

Horizontal coordinate information is referenced to the North American Datum of 1983 (NAD 83).

Specific conductance is reported in microsiemens per centimeter at 25 degrees Celsius (µS/cm at 25 °C).

Water year is the 12-month period that extends from October 1 through September 30. The water year is designated by the calendar year in which it ends and which includes 9 of the 12 months. Thus, the year ending September 30, 2008, is called the 2008 water year.

Continuous Turbidity Monitoring in the Indian Creek Watershed, Tazewell County, Virginia, 2006–08

By Douglas L. Moyer and Kenneth E. Hyer

Abstract

Thousands of miles of natural gas pipelines are installed annually in the United States. These pipelines commonly cross streams, rivers, and other water bodies during pipeline construction. A major concern associated with pipelines crossing water bodies is increased sediment loading and the subsequent impact to the ecology of the aquatic system. Several studies have investigated the techniques used to install pipelines across surface-water bodies and their effect on downstream suspended-sediment concentrations. These studies frequently employ the evaluation of suspended-sediment or turbidity data that were collected using discrete sample-collection methods. No studies, however, have evaluated the utility of continuous turbidity monitoring for identifying real-time sediment input and providing a robust dataset for the evaluation of long-term changes in suspended-sediment concentration as it relates to a pipeline crossing.

In 2006, the U.S. Geological Survey, in cooperation with East Tennessee Natural Gas and the U.S. Fish and Wildlife Service, began a study to monitor the effects of construction of the Jewell Ridge Lateral natural gas pipeline on turbidity conditions below pipeline crossings of Indian Creek and an unnamed tributary to Indian Creek, in Tazewell County, Virginia. The potential for increased sediment loading to Indian Creek is of major concern for watershed managers because Indian Creek is listed as one of Virginia's Threatened and Endangered Species Waters and contains critical habitat for two freshwater mussel species, purple bean (*Villosa perpurpurea*) and rough rabbitsfoot (*Quadrula cylindrical strigillata*). Additionally, Indian Creek contains the last known reproducing population of the tan riffleshell (*Epioblasma florentina walkeri*). Therefore, the objectives of the U.S. Geological Survey monitoring effort were to (1) develop a continuous turbidity monitoring network that attempted to measure real-time changes in suspended sediment (using turbidity as a surrogate) downstream from the pipeline crossings, and (2) provide continuous turbidity data that enable the development of a real-time turbidity-input warning system and assessment of long-term changes in turbidity conditions.

Water-quality conditions were assessed using continuous water-quality monitors deployed upstream and downstream from the pipeline crossings in Indian Creek and the unnamed tributary. These paired upstream and downstream monitors were outfitted with turbidity, pH (for Indian Creek only), specific-conductance, and water-temperature sensors. Water-quality data were collected continuously (every 15 minutes) during three phases of the pipeline construction: pre-construction, during construction, and post-construction. Continuous turbidity data were evaluated at various time steps to determine whether the construction of the pipeline crossings had an effect on downstream suspended-sediment conditions in Indian Creek and the unnamed tributary. These continuous turbidity data were analyzed in real time with the aid of a turbidity-input warning system. A warning occurred when turbidity values downstream from the pipeline were 6 Formazin Nephelometric Units or 15 percent (depending on the observed range) greater than turbidity upstream from the pipeline crossing. Statistical analyses also were performed on monthly and phase-of-construction turbidity data to determine if the pipeline crossing served as a long-term source of sediment.

Results of this intensive water-quality monitoring effort indicate that values of turbidity in Indian Creek increased significantly between the upstream and downstream water-quality monitors during the construction of the Jewell Ridge pipeline. The magnitude of the significant turbidity increase, however, was small (less than 2 Formazin Nephelometric Units). Patterns in the continuous turbidity data indicate that the actual pipeline crossing of Indian Creek had little influence of downstream water quality; conversely, these data indicate upland runoff from the construction right-of-way was the primary source of turbidity detected in Indian Creek. Results from the analysis of continuous turbidity data collected during the three construction phases from the unnamed tributary indicate that the pipeline crossing did not adversely alter long-term water-quality conditions. Turbidity data collected during the active construction of the pipeline crossing through the unnamed tributary indicate that short-term turbidity increases did occur downstream; however, these increases were shown to be minimal compared to the turbidity values measured during natural runoff events.

Introduction

Elevated suspended-sediment concentrations are of major concern for water-resource managers because of the potential adverse impact on living resources and streams, rivers, and estuaries (Lloyd and others, 1987; Ryan, 1991; Waters, 1995; Wood and Armitage, 1997). Suspended sediments are derived from natural processes of upland erosion, lateral movement of channels into streambanks, and downcutting of streambeds (Waters, 1995). Human activities such as agriculture, logging, mining, and urbanization, however, increase the rate of sediment loading to these aquatic systems through accelerated soil and stream-channel erosion (Ryan, 1991; Waters, 1995). Anthropogenically derived sediment often overwhelms the natural assimilative capacity and alters the structure and function of the aquatic ecosystem (Cairns, 1977). Elevated suspended-sediment concentrations may impair the growth of aquatic vegetation by reducing light levels, burying filter-feeding organisms, reducing habitat available for macroinvertebrates, and contributing to decreased fish populations (Lenat and others, 1981; Dennison and others, 1993; Box and Mossa, 1999; Madsen and others, 2001). An ancillary and often overlooked impact of these elevated sediment concentrations is the transport of particle-associated contaminants, such as bacteria, nutrients, and metals (Griscom and others, 2000; Christensen, 2001).

Thousands of miles of natural gas pipelines are installed annually in the United States (True, 1998; Tobin, 2003). Streams, rivers, and other water bodies are routinely crossed during pipeline construction. Pipeline construction can lead to increased sediment loading to aquatic systems through trench excavation and backfilling, erosion and runoff from adjacent upland worksites, and discharge of water from hydrostatic pipe testing or trench dewatering (Reid and others, 2004).

Three possible pipeline-crossing techniques are typically used when installing pipeline beneath streams, rivers, or other water bodies: open-cut wet crossing, open-cut dry crossing, and horizontal-directional drilling (HDD) (Zwirn, 2002). The open-cut wet crossing approach involves trenching, pipe installation, and backfilling in the open stream channel while streamflow continues; sediment and pollutant runoff can be severe (Zwirn, 2002). The open-cut dry crossing approach involves trenching, pipe installation, and backfilling in the open stream channel while streamflow is diverted using a pump or flume; sediment and pollutant runoff is considerably reduced because of the lack of streamflow to transport sediment (Zwirn, 2002). HDD involves drilling a small-diameter tunnel at least 5 feet beneath the stream channel and subsequently pulling the preassembled pipeline through the tunnel. The HDD method is the least disruptive to the ecological integrity of the associated aquatic ecosystem (Zwirn, 2002).

Several studies have evaluated the impact on the aquatic ecosystem associated with various pipeline-crossing techniques. Many of these studies found that the open-cut wet crossing method had the greatest impact to the aquatic ecosystem through increased sediment loading downstream from the pipeline crossing (Phillip and others, 1981; Young and Mackie, 1991; Reid and others, 2004). Reid and others (2002) found that the open-cut dry crossing method, using either dam and pump or flume crossing, had considerably less downstream transport of sediment compared to the wet-crossing method; the greatest impact was observed when the dam/ flume was removed and stored sediment was mobilized. The HDD-crossing method has become the preferred method when crossing ecologically sensitive streams and rivers because of the lack of sediment mobilization; however, this crossing method is time-consuming and expensive (Reid and others, 2002; Lévesque and Dubé, 2007).

In 2005, East Tennessee Natural Gas filed an application with the Federal Energy Regulatory Commission (FERC) to install the Jewell Ridge Lateral natural gas pipeline in Smyth and Tazewell Counties in southwest Virginia. This 32-mile, 20-inch-diameter pipeline would connect the East Tennessee Natural Gas mainline to CNX Gas Company LLC's existing Cardinal States Gathering System (fig. 1). As part of the FERC permitting process, a Biological Opinion was prepared by the U.S. Fish and Wildlife Service (USFWS) to determine the effects of the Jewell Ridge pipeline on federally listed species and federally designated critical habitat (U.S. Fish and Wildlife Service, 2006). The USFWS determined that 45 water bodies would be crossed by the Jewell Ridge pipeline. Of these 45 water bodies, 4 are listed as State-designated Threatened and Endangered Species Waters because of documented occurrences of federally and State-listed endangered freshwater mussel species and (or) federally designated critical habitat for freshwater mussels. Although the Jewell Ridge pipeline will cross three other Threatened and Endangered Species Waters, Indian Creek was selected by the USFWS for intensive monitoring as a tool to help protect the critically endangered mussels or their required habitat. The USFWS requested that intensive turbidity and macroinvertebrate monitoring be performed prior to, during, and after pipeline crossing.

The USFWS was concerned about the Jewell Ridge pipeline construction because Indian Creek is listed as one of the Virginia Department of Game and Inland Fisheries' designated Threatened and Endangered Species Waters and contains federally designated critical habitat for two endangered freshwater mussel species, purple bean (*Villosa perpurpurea*) and rough rabbitsfoot (*Quadrula cylindrical strigillata*), and the last known reproducing population of the tan riffleshell (*Epioblasma florentina walkeri*). The purple bean, rough rabbitsfoot, and tan riffleshell are filter-feeding mussels that feed on algae and other microorganisms suspended in the water column. These mussels require relatively silt-free substrate for survival. The USFWS in accordance with Section 7 of the Endangered Species Act (ESA) of 1973 (87 Stat. 884, as amended; 16 U.S.C. 1531 et seq.) requested "sound and reasonable monitoring" to document potential water-quality impacts. The primary impact of concern is that instream suspended-sediment concentrations, due to pipeline-related construction activities, could be detrimental to the quality of the habitat required by these threatened and endangered species.
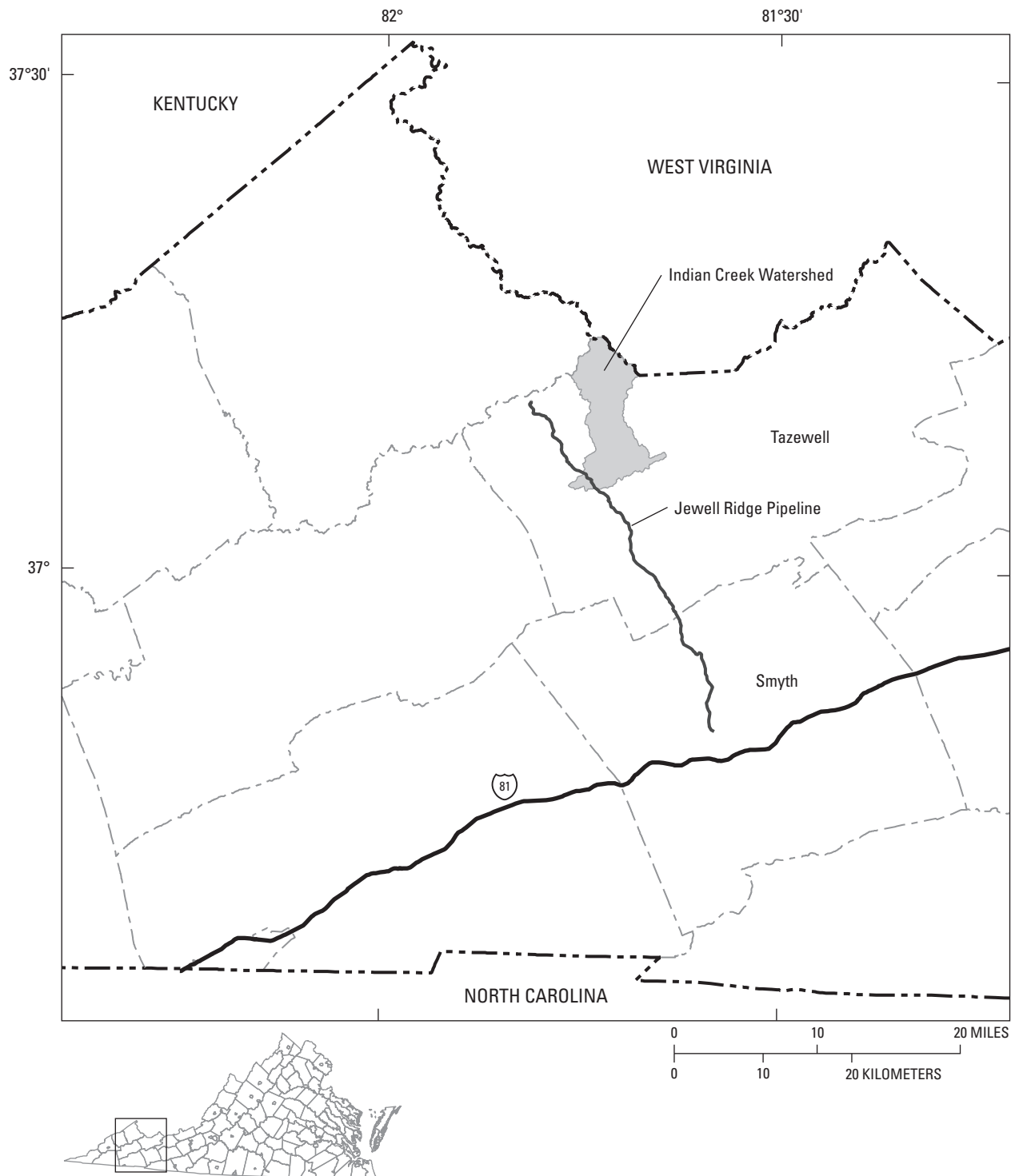
Figure 1.   The Jewell Ridge Lateral natural gas pipeline, Virginia.

In 2006, the U.S. Geological Survey (USGS), in cooperation with East Tennessee Natural Gas and the U.S. Fish and Wildlife Service, began a study to monitor water-quality conditions in Indian Creek and an unnamed tributary to Indian Creek. Turbidity, a well-documented surrogate for fine suspended sediment (Christensen, 2001), was the primary water-quality property to be monitored prior to, during, and after construction of the pipeline crossing of Indian Creek and the unnamed tributary to Indian Creek. The primary objective of the USGS monitoring effort was to identify whether the construction of the Indian Creek pipeline crossing would adversely impact the suspended-sediment concentrations in Indian Creek. The specific study objectives were to (1) develop a continuous turbidity monitoring network that attempted to measure real-time changes in suspended-sediment conditions (using turbidity as a surrogate) downstream from the pipeline crossing in Indian Creek and the unnamed tributary to Indian Creek, and (2) provide continuous turbidity data that allow for the development of a turbidity-input warning system and assessment of long-term changes in turbidity conditions.

Purpose and Scope

This report describes monitored turbidity conditions in Indian Creek and an unnamed tributary to Indian Creek prior to, during, and after construction of the Jewell Ridge Lateral natural gas pipeline crossing. Turbidity values were collected every 15 minutes upstream and downstream from the pipeline crossing in Indian Creek and an unnamed tributary to Indian Creek from April 2006 to April 2008. This report also describes the methods of collection and the results of using these continuous turbidity data as a near real-time and long-term indicator of elevated suspended sediment downstream from the pipeline crossings. This information will provide East Tennessee Natural Gas and USFWS with information on the influence of the Jewell Ridge Lateral natural gas pipeline crossings on instream turbidity conditions.

Description of Study Area

The Indian Creek watershed is located in Tazewell County, in southwest Virginia (fig. 1). The headwaters of Indian Creek originate in the primarily forested northernmost part of Tazewell County. Indian Creek flows to the southwest, where it joins the Clinch River near Cedar Bluff, Virginia (fig. 2). The Clinch River, which is known for its biodiversity and large number of imperiled species, flows southwest where it joins the Tennessee River and ultimately, the Mississippi River. Indian Creek has a drainage area of 33.9 square miles and is composed of forest (78.5 percent), agricultural (13.9 percent), and residential (7.6 percent) land use.

Indian Creek lies within the Appalachian Plateaus Physiographic Province, which is a narrow chain of westward-facing folded mountains that extend from southwestern Virginia to central New York (Fenneman, 1938). The Appalachian

Plateaus consist of the Allegheny Plateau and the Cumberland Plateau. The Cumberland Plateau is the dominant physiographic feature in the Indian Creek watershed. The underlying geology in the Appalachian Plateaus is dominated by shale, sandstone, and coal (Fenneman, 1938). Extensive erosion has resulted in topography consisting of steep slopes and narrow ridges and valleys (Hayes, 1991; Woods and others, 1999).

Jewell Ridge Pipeline Construction

The Jewell Ridge pipeline was brought into the Indian Creek watershed by employing overland- and stream-channel crossing methods in accordance with Federal regulations and guidelines. The overland pipeline construction required the creation of a 100-foot-wide construction right-of-way (ROW). The ROW measured 65 feet on the working side and 35 feet on the spoil side. The overland-pipeline construction method involved installing the pipeline as a moving assembly line with activities that proceeded in the following sequence: surveying and flagging of the ROW, clearing and grading, trenching, stringing and bending, welding, lowering-in, backfilling, hydrostatic testing, cleanup and restoration, and post-construction monitoring. Erosion- and sediment-control measures were employed along the entire length of the ROW.

Two stream-channel crossing techniques were utilized in the Indian Creek watershed. Indian Creek was crossed using HDD. This method allows for the installation of pipelines beneath roadways, railroads, and streams to minimize the potential impact of elevated sediment loading to the threatened and endangered mussel species and their associated habitat. The HDD method allowed for the installation of the pipeline more than 5 feet below the channel bottom of Indian Creek. The Indian Creek pipeline crossing is approximately 1.6 miles east-northeast of Cedar Bluff, Virginia, and is approximately 1,100 feet upstream from Route 631 (fig. 2). The borehole under Indian Creek was continually dewatered during the boring process. The water and associated constituents were captured and stored in settling tanks on site. Once the particles settled from suspension, the captured water was returned to Indian Creek. Impacts to vegetative cover on both streambanks were minimized by leaving a 50-foot buffer on the south bank and a 35-foot buffer on the north bank of undisturbed vegetation.

The pipeline route also crossed an unnamed tributary (fig. 2), which flows into Indian Creek downstream from the Route 631 bridge, but still upstream from several of the critical mussel populations residing on the main stem of Indian Creek. The open-cut dam and flume dry-crossing method was used to install the pipeline across the unnamed tributary because no critical mussel habitat exists at or immediately downstream from the unnamed tributary crossing. This technique isolates flow from the construction area while the pipeline is installed in the dry channel. The dry channel is trenched so that the pipeline is installed at a minimum of 5 feet beneath the active channel.
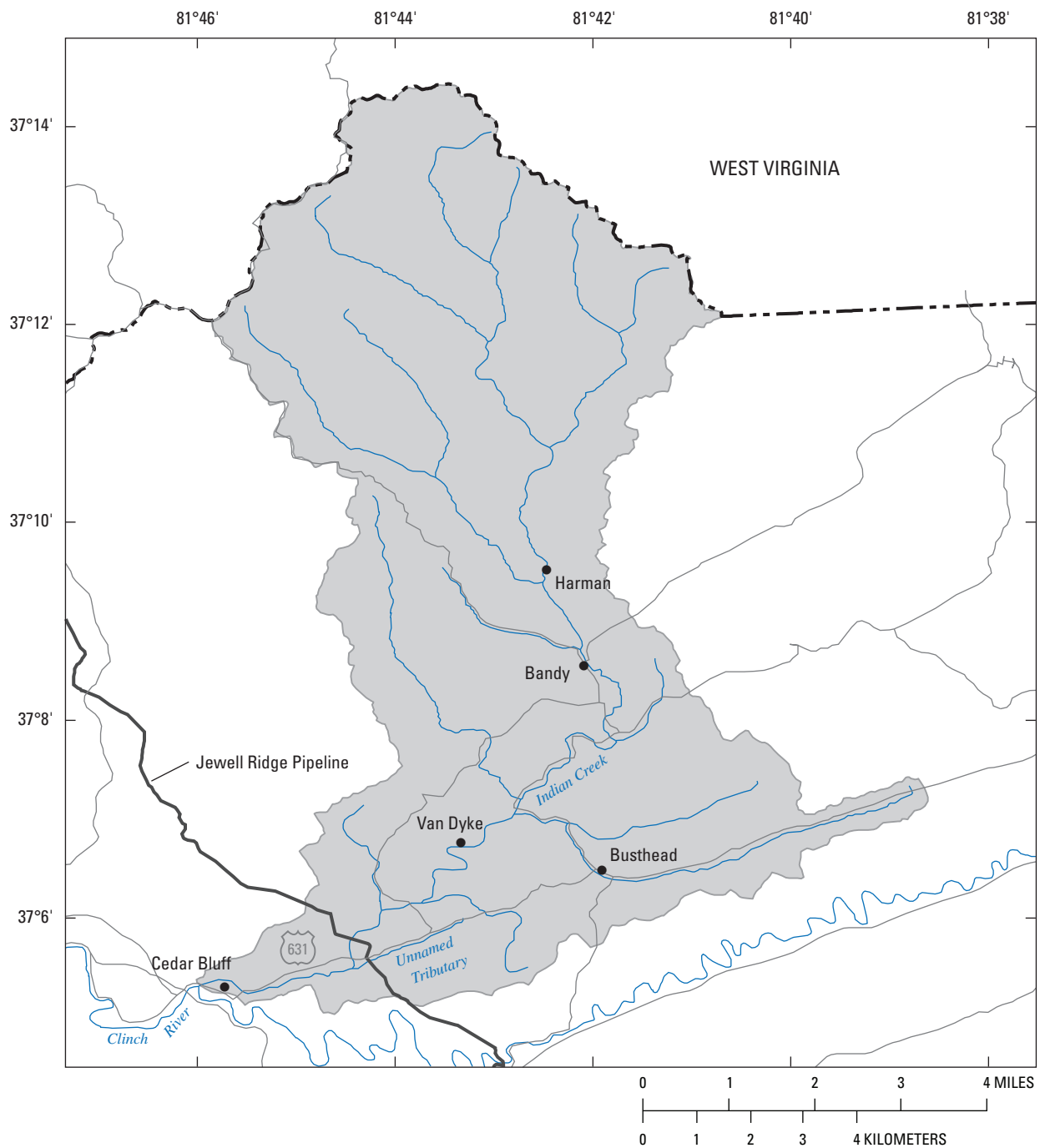
Figure 2. The Indian Creek watershed, Tazewell County, Virginia.

Methods of Investigation

In most streams, suspended sediments are generally transported during stormflow periods (Wolman and Miller, 1960), while rainfall-induced surface-runoff processes are active; however, during these runoff periods, the fewest suspended-sediment data are generally collected. One promising new technology for improved suspended-sediment determination involves the continuous monitoring of turbidity, using an in-situ sensor, as a surrogate for suspended-sediment concentrations. Turbidity measurements are usually well correlated to suspended-sediment concentrations; because turbidity represents an optical measure of water clarity, the presence of suspended sediment directly influences this measurement of clarity. Using turbidity values as a surrogate for suspended-sediment concentration is not new, but until recently, technological limitations have made this approach largely unusable. Walling (1977) described this surrogate approach using turbidity.

The development of continuous turbidity records has gradually become more feasible because of technical improvements to in-situ water-quality sensors and improved telecommunications equipment. Continuous turbidity measurement has now become a more common field approach because it provides substantially more detailed and more accurate information on suspended-sediment concentrations than previously possible.

Continuous Water-Quality Monitor Installation

The continuous water-quality monitoring network was designed to detect sediment inputs, as indicated by turbidity, directly associated with the construction and pipeline crossing activities on Indian Creek and the unnamed tributary while also minimizing the chance of detecting sediment inputs unrelated to the pipeline construction. Therefore, a paired upstream-downstream design was implemented around the Indian Creek and unnamed tributary pipeline crossings (fig. 3).
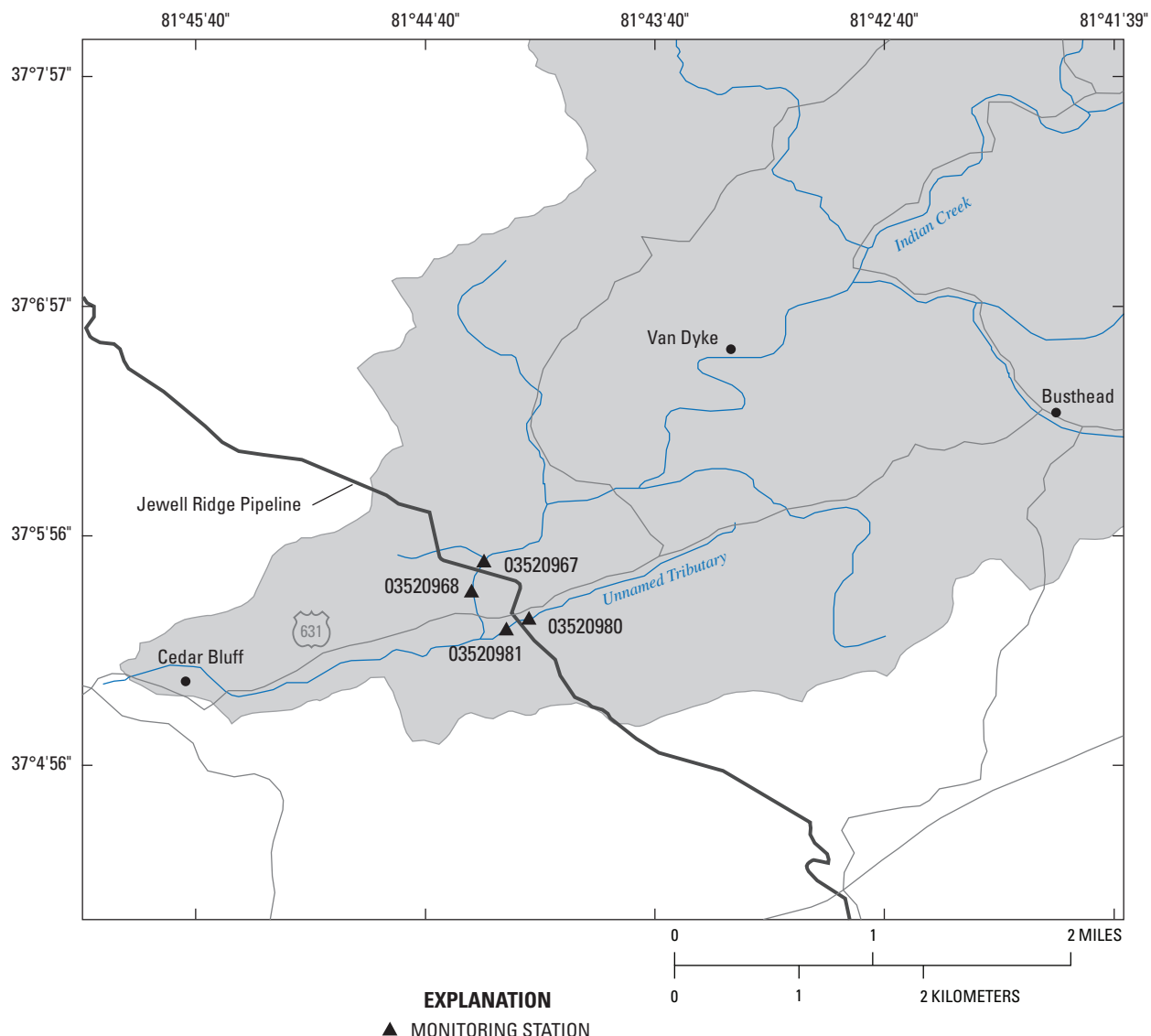
Figure 3.   The Indian Creek and unnamed tributary monitoring network, Tazewell County, Virginia.

An additional water-quality-monitoring concern in Indian Creek was incomplete water-column mixing in the monitoring reach. To address this concern, two additional monitors were added so that the paired upstream and downstream monitors consisted of a near left-bank and near right-bank design. The use of dual upstream monitors located off each bank of the stream is appropriate for two reasons. First, the use of monitors located only a short distance off the streambank provided a dataset that was directly comparable to the dataset from the downstream monitors and used to determine how conditions change within the monitoring reach. Secondly, an ephemeral unnamed tributary to Indian Creek is located approximately 350 feet above the pipeline crossing; the potential sediment contributions from this unnamed tributary needed to be documented to ensure that the potential sediment contributions were not erroneously interpreted as sediment inputs from the pipeline crossing. The monitoring stations on both Indian Creek and the unnamed tributary were instrumented and activated 1 month prior to the initiation of the Jewell Ridge pipeline construction within the Indian Creek watershed. The monitoring allowed for the establishment of a brief baseline understanding of the differences in turbidity levels upstream and downstream from the pipeline crossings.

Indian Creek Network

The effect of the Indian Creek pipeline crossing on water-quality conditions was monitored by four continuous water-quality monitors installed pair-wise upstream and downstream from the pipeline crossing. Two monitors were installed 120 feet upstream (USGS station 03520967) from the pipeline crossing (fig. 3). These two upstream monitors were suspended from a boom so that one monitor was submersed 10 feet from the left bank and the second monitor was submersed 10 feet from the right bank (fig. 4*A*, table 1). The remaining two monitors were suspended from a boom 200 feet downstream (USGS station 03520968) from the pipeline

crossing so that one monitor was submersed 10 feet from the left bank and the second monitor was submersed 10 feet from the right bank (fig. 4*B*, table 1). Each Indian Creek monitoring station was instrumented with a YSI Inc. Model 6920 multi-parameter sonde, which was outfitted with turbidity, pH, specific-conductance, and water-temperature sensors, and values for each of these water-quality properties were collected every 15 minutes. The water-quality values were stored and subsequently transmitted hourly using a Sutron SatLink2 GOES Satellite Transmitter and Logger. The hourly transmitted data were stored in and subsequently made publicly available via the USGS National Water Information System (NWIS) at *http://waterdata.usgs.gov/va/nwis*.

Unnamed Tributary Network

The effect of the unnamed tributary pipeline crossing on water-quality conditions was monitored by two continuous water-quality monitors installed upstream (USGS station 03520980) and downstream (USGS station 03520981) from the crossing (fig. 3). The upstream monitor was located approximately 100 feet above the pipeline crossing whereas the downstream monitor was located approximately 65 feet below the pipeline crossing (fig. 5, table 1). Each monitoring station was instrumented with a YSI Inc. Model 600 multi-parameter sonde. The YSI Inc. Model 600 multi-parameter sonde, which has a smaller diameter than the Model 6920 multi-parameter sonde, was selected for the unnamed tributary because of the shallow surface-water depths encountered. Each sonde was outfitted with turbidity, specific-conductance, water-temperature, and water-level sensors. Values for each of these constituents were collected every 15 minutes and then stored and subsequently transmitted hourly using a Sutron SatLink2 GOES Satellite Transmitter and Logger. These hourly transmitted data were stored in and subsequently made publicly available via NWIS at *http://waterdata.usgs.gov/va/nwis*.

Table 1. Water-quality monitoring stations, Indian Creek and unnamed tributary, Tazewell County, Virginia.

Station number	Station name	Latitude Longitude	Left- and right-bank water-quality monitors deployed
03520967	Indian Creek near Cedar Bluff, Va.	37°05'47" 81°44'27"	Yes
03520968	Indian Creek above Rt. 631 near Cedar Bluff, Va.	37°05'42" 81°44'28"	Yes
03520980	Indian Creek Tributary along Rt. 631 near Cedar Bluff, Va.	37°05'35" 81°44'13"	No
03520981	Indian Creek Tributary above mouth nr Cedar Bluff, Va.	37°05'32" 81°44'19"	No

(A)

(B)

Figure 4.   Indian Creek water-quality monitoring stations located (*A*) upstream (Station number 03520967) and (*B*) downstream (Station number 03520968) from the Jewell Ridge Lateral natural gas pipeline crossing, Tazewell County, Virginia.

Figure 5.   Water-quality monitors located on the unnamed tributary to Indian Creek, Tazewell County, Virginia. The monitoring station located in the foreground is the downstream monitor (Station number 03520980). The monitoring station in the background is the upstream monitor (Station number 03520981).

Continuous Water-Quality Monitor Maintenance

Approximately every 4 weeks, the water-quality monitors were serviced in the field to clean the equipment, evaluate the quality of the data being collected, and recalibrate the instrument (if necessary). This monitor servicing was performed using the methods described in the USGS guidelines for the operation and maintenance of continuous monitors (Wagner and others, 2000). A summary of the maintenance steps is presented here. In all cases, water-quality properties were measured before and after the instrument was cleaned of any algae or biofilm that may have developed. The differences before and after cleaning were used to evaluate whether the data needed to be corrected for instrument fouling. Following the fouling check, the calibration for pH, specific conductance, and turbidity were all checked using known standards. Discrepancies between the known values of the standards and the readings from the individual sondes were used to determine whether the data needed to be corrected for a drift in instrument calibration. Following the fouling and calibration checks, the instrument was re-calibrated if any of the measured water-quality properties were out of instrument tolerance (Wagner and others, 2000). Upon returning to the office from the field-maintenance visit, any necessary data corrections were applied to the data record and the data on the NWIS Web site were updated.

In addition to the monthly monitor maintenance, the entire water-quality record for each measured water-quality property was reviewed and finalized at the end of each water year. This annual review evaluated all the fouling and calibration drift checks, and screened the data for anomalous values, before the quality of the record was rated (either as excellent, good, fair, or poor). These ratings were determined on the basis of the corrections that had been applied to the record, and the criteria used for the ratings were those provided by Wagner and others (2000).

Continuous Stream Gage Operation

A standard USGS stream gage was installed, following established USGS procedures (Buchanan and Somers, 1968), at the upstream Indian Creek monitoring site (USGS station 03520967) (fig. 3) in October 2006 and maintained through April 2008 (table 1). Indian Creek water levels were measured at 15-minute intervals using a Keller-Pressure Systems, Incorporated (KPSI) pressure transducer. These water-level (stage) data were stored and subsequently transmitted hourly using a Sutron SatLink2 GOES Satellite Transmitter and Logger. The hourly transmitted data were stored in and subsequently made publicly available via NWIS at *http://waterdata.usgs.gov/va/nwis*. Stream discharge was measured routinely, during a variety of streamflow conditions, to establish a stage-discharge rating for Indian Creek. This stage-discharge rating was used to calculate stream discharge for each 15-minute interval of measured stage.

Data Analysis

The primary objective of the USGS monitoring effort was to identify whether the construction of the pipeline crossings would adversely impact the sediment-water quality in Indian Creek and the unnamed tributary. The specific study objectives were to (1) develop a continuous turbidity monitoring network that attempted to measure real-time changes in suspended-sediment conditions (using turbidity as a surrogate) downstream from the pipeline crossing in Indian Creek and the unnamed tributary to Indian Creek, and (2) provide continuous turbidity data that allow for the development of a turbidity-input warning system and assessment of long-term changes in turbidity conditions. The following sections document the approach that was used to monitor and evaluate water-quality conditions.

Continuous Water-Quality Data Collection

Turbidity, water temperature, specific conductance, and pH measurements were collected at the four water-quality monitoring stations on Indian Creek, and turbidity, water temperature, specific conductance, and water levels were collected at the two water-quality monitoring stations on the unnamed tributary. The primary objective for collecting these water-quality data was to enable East Tennessee Natural Gas, the USFWS, and the USGS to detect changes in water-quality conditions, more specifically sediment-water quality, immediately downstream from the pipeline crossings. These water-quality properties were collected during three phases of the pipeline construction: pre-construction, during construction, and post-construction. The time periods for these three phases were:

1. Pre-construction—April 28, 2006, through May 31, 2006;

2. Construction—June 1, 2006, through August 31, 2006; and

3. Post-construction—September 1, 2006, through April 9, 2008.

These data were essential for determining whether the construction of the Jewell Ridge pipeline crossing altered the short-term and long-term water quality in Indian Creek and the unnamed tributary.

Assessment of Long-Term Turbidity Patterns

The objective of the long-term water-quality assessment was to determine the influence of the pipeline crossing on downstream suspended-sediment conditions (using turbidity as a surrogate for suspended sediment) in Indian Creek and the unnamed tributary. Statistical analysis of the paired differences of the continuously collected upstream and downstream turbidity data is the most direct approach to determine whether turbidity conditions are changing downstream from the pipeline crossing. A signed-rank test (Helsel and Hirsch, 1992) was selected to test the null hypothesis for Indian Creek and

the unnamed tributary. The signed-rank test was performed on the paired differences obtained from the following Indian Creek paired monitors: upstream minus downstream left bank (USLB and DSLB, respectively); upstream minus downstream right bank (USRB and DSRB, respectively); and upstream minus downstream monitors in the unnamed tributary (USTR and DSTR, respectively). The null hypothesis associated with an analysis of paired differences is that the median paired difference is equal to zero. This null hypothesis is true when the number of positive paired differences (upstream turbidity is greater than downstream turbidity) is approximately equal to the negative paired differences (upstream turbidity is less than downstream turbidity). The alternative hypothesis is that the median paired difference value is not equal to zero. A test was considered statistically different if the p-value was less than 0.05. These paired differences were calculated for each of the three time periods (pre-construction, construction, and post-construction).

In addition to the statistical analysis of paired differences, graphical presentations of turbidity data were used to visually determine differences between upstream and downstream values of turbidity. Monthly boxplots of paired differences, obtained from the upstream, right-bank, and left-bank monitors on Indian Creek and the upstream and downstream monitors on the unnamed tributary, were used to determine if the variability within the monthly paired differences was associated with the phase of pipeline construction. Each boxplot shows the distribution of the monthly paired differences by identifying the 10th, 25th, 50th, 75th, and 90th percentiles, where each percentile represents the percentage of samples that reside below that designated value. If the median (50th percentile) turbidity paired difference is 1.0 Formazin Nephelometric Units (FNU), for example, then 50 percent of monthly paired differences are greater than 1.0 FNU and 50 percent of the monthly paired differences are less than 1.0 FNU. Exceedance plots also were used to identify differences in turbidity conditions upstream and downstream from the pipeline crossing. Exceedance plots are similar to boxplots because they are used to relate a given turbidity value to the frequency of occurrence. The shape of the exceedance plot, however, can assist in identifying processes that may be controlling turbidity in Indian Creek and the unnamed tributary. For example, exceedance plots for the pre-construction turbidity values collected at the USLB (red line) and the USRB (blue line) monitor are shown in figure 6. These plots show that the USLB and USRB turbidity values have similar distributions with similar medians (50th percentile) of 3.0 and 3.2 FNU, respectively. The black line represents a hypothetical condition obtained by doubling all turbidity values collected at the USRB monitor, which shows that increases in turbidity cause the exceedance plot to shift to the right.
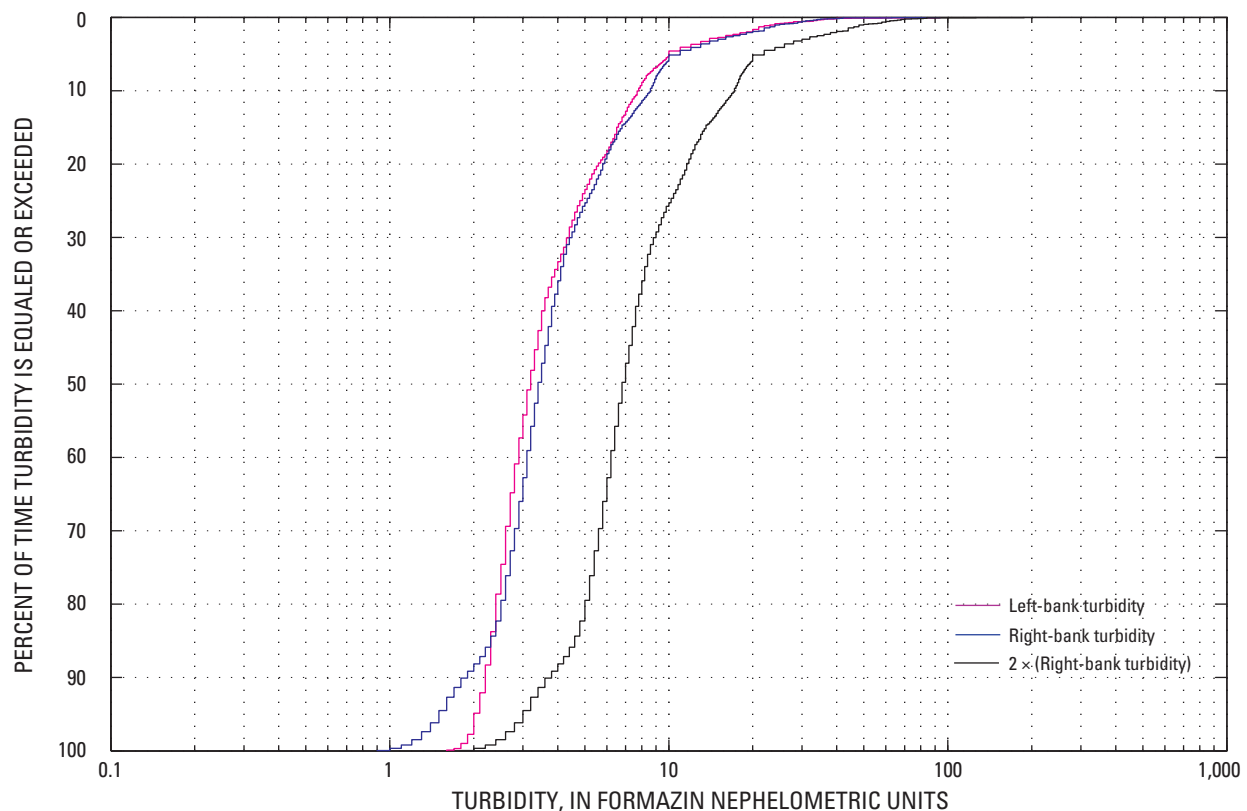
Figure 6. Exceedance plots for left-bank and right-bank turbidity collected at the upstream Indian Creek water-quality monitor (Station number 03520967) Tazewell County, Virginia. The black line represents the right-bank turbidity values multiplied by 2.

Turbidity-Input Warning System

The ability to detect real-time sediment input (using turbidity as a surrogate) downstream from the Indian Creek and unnamed tributary pipeline crossings was a primary requirement of the USFWS Biological Opinion (U.S. Fish and Wildlife Service, 2006). East Tennessee Natural Gas developed a real-time turbidity-input warning system in order to ensure that the water-quality requirement established by the USFWS was met. The thresholds for detecting changes in turbidity downstream from the pipeline crossing were:

1. For turbidity values less than 40 FNU, a 6-FNU increase in turbidity detected downstream from the pipeline crossing, relative to the associated turbidity value upstream from the pipeline crossing, sustained for no less than 1 hour, or

2. For turbidity values greater than or equal to 40 FNU, a 15-percent increase in turbidity detected downstream from the pipeline crossing, relative to the associated turbidity value upstream from the pipeline crossing, sustained for no less than 1 hour.

The real-time turbidity-input warning system used continuous turbidity data collected by the USGS at the paired upstream and downstream monitors on Indian Creek and the unnamed tributary. Turbidity data were collected every 15 minutes and transmitted hourly to the USGS NWIS Web site. East Tennessee Natural Gas automatically retrieved these turbidity data and compared them to the established thresholds. If a threshold was violated for four consecutive turbidity observations (1 hour), then the on-site manager, overseeing the pipeline construction, received a warning that a potential sediment input was detected downstream from the pipeline crossing. The on-site manager was required to (1) investigate the cause of the threshold exceedence, (2) document whether instream turbidity (sediment derived from the pipeline crossing construction) was the cause of the threshold exceedence, and (3) cease construction activities until the sediment input was corrected. This warning system also was subject to false-positive warnings. A false-positive warning is one that is not caused by sediment input from the pipeline crossing but is caused by a variety of sources that include: instream debris such as leaves and trash that get caught on the downstream turbidity probe; bio-fouling on the downstream turbidity probe; or mechanical malfunction of the downstream turbidity probe.

Water-Quality Patterns in Indian Creek and the Unnamed Tributary

Water-quality data collected during pre-construction, construction, and post-construction phases of the pipeline crossings beneath Indian Creek and through an unnamed tributary are summarized in table 2. Water-quality data include the median and the range (minimum and maximum) for turbidity, pH, specific conductance, and water temperature collected during the three phases of construction. Median values of pH ranged from 8.0 to 9.4 during the duration of the study. The highest median pH values occurred during the construction phase at both the Indian Creek left-bank and right-bank downstream monitors 9.4 and 8.4, respectively. Median values of specific conductance observed in Indian Creek ranged from 198 to 244 microsiemens per centimeter (μS/cm) whereas median values of specific conductance observed in the unnamed tributary ranged from 394 to 499 μS/cm. Specific-conductance values in the unnamed tributary were typically double the values observed in Indian Creek. Water temperature was similar in Indian Creek and the unnamed tributary and reflected the phase of construction during which temperature was measured. The highest water-temperature values were observed during the construction period, for example, which took place during the summer months. Time-series plots for pH, specific conductance, and water temperature collected from Indian Creek and specific conductance and water temperature collected from the unnamed tributary are provided for each monitoring station in Appendixes 1 through 6.

Indian Creek Streamflow

Continuous streamflow data were collected from Indian Creek at the upstream monitoring station (USGS station 03520967) from October 2006 through April 2008 (fig. 7). Given the October 2006 start date, streamflow data were only available during the post-construction phase of the study. Monthly summary statistics for streamflow conditions in Indian Creek, which include the minimum, 25th percentile, median, 75th percentile, and maximum, are presented in table 3. Monthly median values of streamflow in Indian Creek ranged from 0.39 to 61.66 cubic feet per second (ft^3/s) in October 2007 and April 2008, respectively. The extensive drought that affected much of southeastern and mid-Atlantic United States is evident in the Indian Creek streamflow data, with diminished values of streamflow measured from July 2007 through January 2008.

Table 2. Statistical summaries of water-quality data collected at Indian Creek and unnamed tributary water-quality monitoring stations during pre-construction, construction, and post-construction of the Jewell Ridge Lateral natural gas pipeline, Tazewell County, Virginia.

[Values presented are the median and range (minimum and maximum) for each construction period; FNU, Formazin Nephelometric Units; µS/cm at 25 ºC, microsiemens per centimeter at 25 degrees Celsius; ºC, degrees Celsius; US, upstream; DS, downstream; —, no data]

	Turbidity, FNU	pH, standard units	Specific conductance, µS/cm at 25 ºC	Water temperature, ºC
Indian Creek, Pre-Construction				
US left bank	3.2 (1.6−94)	8.1 (7.8−9.1)	198 (146−231)	13.9 (9.8−24.1)
US right bank	3.0 (1.4−89)	8.1 (7.8−9.0)	202 (146−236)	13.0 (9.9−23.0)
DS left bank	3.4 (0.9−94)	8.2 (7.9−9.2)	199 (144−240)	13.9 (9.8−24.0)
DS right bank	3.6 (1.8−86)	8.1 (7.7−9.0)	200 (146−233)	13.0 (9.8−23.0)
Unnamed Tributary, Pre-Construction Period				
US	13.0 (0.1−1,060)	—	394 (229−475)	13.1 (9.0−24.1)
DS	14.0 (3.4−1,130)	—	401 (250−467)	13.2 (9.0−25.0)
Indian Creek, Construction Period				
US left bank	4.0 (1.8−540)	8.1 (7.7−8.8)	228 (93−335)	20.0 (13.8−26.2)
US right bank	3.9 (1.4−440)	8.1 (7.6−8.7)	231 (77−331)	20.8 (13.0−25.0)
DS left bank	5.5 (1.8−300)	9.4 (7.9−10.2)	228 (83−333)	20.7 (13.8−26.0)
DS right bank	4.5 (1.3−290)	8.4 (7.8−9.1)	231 (80−336)	20.0 (13.0−26.2)
Unnamed Tributary, Construction Period				
US	11.0 (4.0−1,250)	—	499 (161−556)	19.2 (12.2−26.2)
DS	8.3 (1.5−1,290)	—	487 (178−537)	19.4 (12.3−26.6)
Indian Creek, Post-Construction Period				
US left bank	2.7 (0.0−970)	8.0 (6.8−9.3)	240 (26−441)	10.5 (0.1−26.3)
US right bank	2.6 (0.1−1030)	8.1 (6.6−9.5)	239 (84−437)	10.5 (0.2−26.1)
DS left bank	2.5 (0.0−740)	8.1 (6.2−10.6)	239 (83−445)	10.5 (0.1−27.2)
DS right bank	2.7 (0.1−720)	8.1 (7.3−9.4)	244 (54−439)	10.4 (0.1−27.2)
Unnamed Tributary, Post-Construction Period				
US	10.0 (0.4−2,340)	—	472 (188−905)	10.5 (0.1−25.6)
DS	9.9 (0.4−1,780)	—	471 (188−862)	10.5 (0.1−26.4)
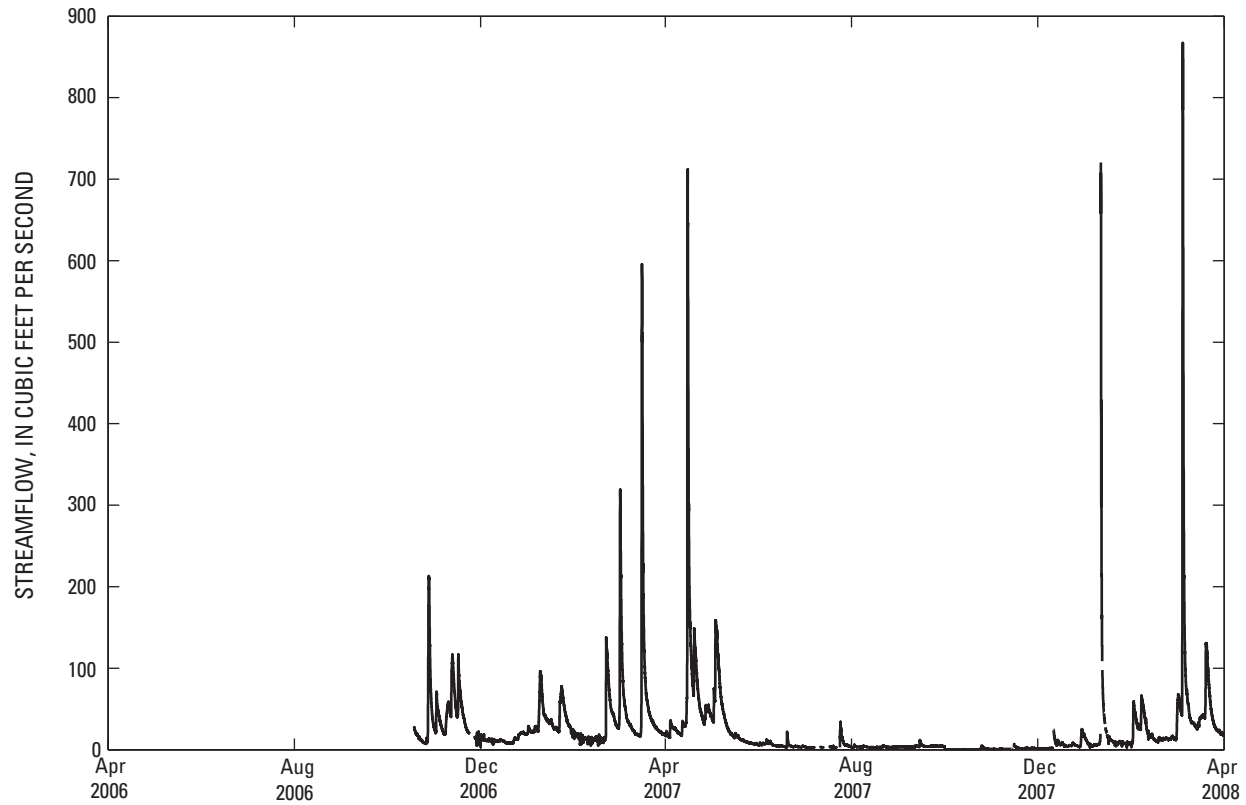
Figure 7. Computed unit values (15-minute) of streamflow collected from Indian Creek near Cedar Bluff, Virginia (Station number 03520967).

Table 3. Statistical summaries of monthly streamflow conditions in Indian Creek near Cedar Bluff, Virginia (Station number 03520967).

[Streamflow is in cubic feet per second]

Date (month/year)	Minimum	25th Percentile	Median	75th Percentile	Maximum
10/2006	7.25	10.00	18.38	32.53	213.10
11/2006	4.73	22.33	39.90	53.81	116.82
12/2006	3.70	10.00	11.81	14.34	22.33
1/2007	13.29	23.75	29.97	42.69	96.23
2/2007	5.01	11.34	14.34	29.97	137.86
3/2007	16.57	22.33	29.97	53.81	595.51
4/2007	14.88	25.23	37.08	66.42	711.91
5/2007	5.60	9.57	17.16	39.00	158.90
6/2007	2.80	3.95	4.73	7.25	22.33
7/2007	2.80	3.01	3.70	5.91	34.31
8/2007	2.80	3.01	3.23	3.46	6.23
9/2007	2.80	3.46	3.95	4.46	11.81
10/2007	0.23	0.33	0.39	0.64	4.96
11/2007	0.53	0.97	1.32	1.90	6.84
12/2007	1.20	1.90	4.96	7.55	25.17
1/2008	3.00	6.17	7.92	11.27	720.34
2/2008	7.55	12.71	14.26	28.29	66.42
3/2008	17.69	28.29	39.00	59.36	867.04
4/2008	14.26	17.69	61.66	102.32	561.61

Instream Turbidity Conditions

Turbidity was the primary water-quality property used to determine if instream water-quality conditions were altered as a result of the Jewell Ridge pipeline crossing beneath Indian Creek and through the unnamed tributary. Turbidity data were collected from each of the six water-quality monitors deployed in Indian Creek and the unnamed tributary and were used to evaluate instream water-quality conditions at various time spans that included: (1) full period of record; (2) the three phases of construction; (3) monthly; and (4) hourly. Results from all time spans were used to formulate a conceptual model for turbidity patterns observed in Indian Creek.

Turbidity values collected during the nearly 24-month period from Indian Creek showed four periods of elevated turbidity: June 2006 through July 2006; September 2006 through November 2006; April 2007 through July 2007; and February 2008 through March 2008 (figs. 8 and 9). These elevated turbidity periods were primarily related to periods of wet weather and increased streamflow, and are fairly consistent between the paired upstream and downstream monitors as well as the left-bank and right-bank monitors. The elevated turbidity observed during March and April 2007, for example, corresponded with the increased streamflow that was measured in Indian Creek during this same period (fig. 7).

Patterns of turbidity measured in the unnamed tributary were much more variable during the 24-month monitoring period (fig. 10), compared with the patterns of turbidity measured in Indian Creek. Turbidity values, measured in the unnamed tributary, were routinely at 1,000 FNU at both the upstream and downstream monitors (fig. 10). Turbidity values measured in the unnamed tributary were two to four times greater than turbidity values measured in Indian Creek (table 2). Turbidity in the unnamed tributary seems to be influenced by other watershed factors, in addition to streamflow, which may potentially include unregulated discharges from local residential and commercial properties as well as the local community working in and around this tributary.

Long-Term Patterns of Turbidity in Indian Creek and the Unnamed Tributary

Exeedance plots were used to graphically compare the turbidity values measured during the pre-construction, construction, and post-construction phases of the pipeline crossing beneath Indian Creek and through the unnamed tributary. Exceedance plots show integrated turbidity data, collected during each phase of construction, as a function of the frequency of occurrence. Indian Creek turbidity values, collected during the three phases of construction, are shown in figures 11 and 12. The initial turbidity patterns from both the left- and right-bank monitors that can be identified from these exceedance plots show that turbidity measured during the construction phase was greater (shifted to the right on the exceedance plot), than turbidity measured during the pre- and

post-construction phases. This pattern of elevated turbidity during the construction phase was consistent at the upstream and downstream monitors; however, the range of turbidity values between the three construction phases was greatest at the downstream monitors (figs. 11 and 12, table 2). These patterns indicate that there was likely a suspended-sediment input (using turbidity as a surrogate) to Indian Creek between the upstream and downstream monitors during the construction period, however, the magnitude of the sediment input between these monitors is relatively small. The observed range in median values, for example, for the three pipeline construction phases at the upstream monitors was 1.3 FNU for each. The range in median values for the construction phases at the downstream monitors increased to 3.0 and 1.8 FNU for the left- and right-bank monitors, respectively. The range in median turbidity values, between the three phases of construction, would be identical for the upstream and downstream monitors if a source of turbidity was not present between the two locations. The input of turbidity, during the active construction phase, is more pronounced at the downstream left-bank monitor compared to the downstream right-bank monitor. The source of the turbidity input between the upstream and downstream monitoring sites during the construction period may be related to the pipeline crossing activities, but other potential turbidity sources between the two monitors such as bank erosion, upstream sediment sources, algal growth, and point inputs from adjoining residential properties cannot be excluded. The discrepancy between the downstream left- and right-bank monitors is discussed further in the "Conceptual Model for Indian Creek Turbidity Patterns" section of this report.

The exceedance plots for turbidity values collected upstream and downstream from the pipeline crossing in the unnamed tributary (fig. 13) exhibit a considerably different pattern than the one observed in Indian Creek (figs. 11 and 12). The major difference is that turbidity values measured during the construction period were generally less than those measured during the pre- and post-construction phases. This pattern also was consistent at both the upstream and downstream monitors. The decrease in turbidity during the construction phase may be related to the diversion of streamflow away from the trenching activity within the active channel. As with Indian Creek, the range of turbidity values between the three construction phases was greatest at the downstream monitors; however, this increased range was directly related to discrepancies between turbidity values at the upstream and downstream monitors collected during the pre-construction phase, not the construction phase. The observed range in median values for the construction phases at the upstream monitor was 3.0 FNU; the range in median values for the construction phases at the downstream monitor was 5.7 FNU (fig. 13, table 2).

The exceedance plots of turbidity data from the unnamed tributary, overall, show that the pipeline crossing was not a substantial source of suspended sediment (using turbidity as a surrogate). A closer look at the turbidity data collected during
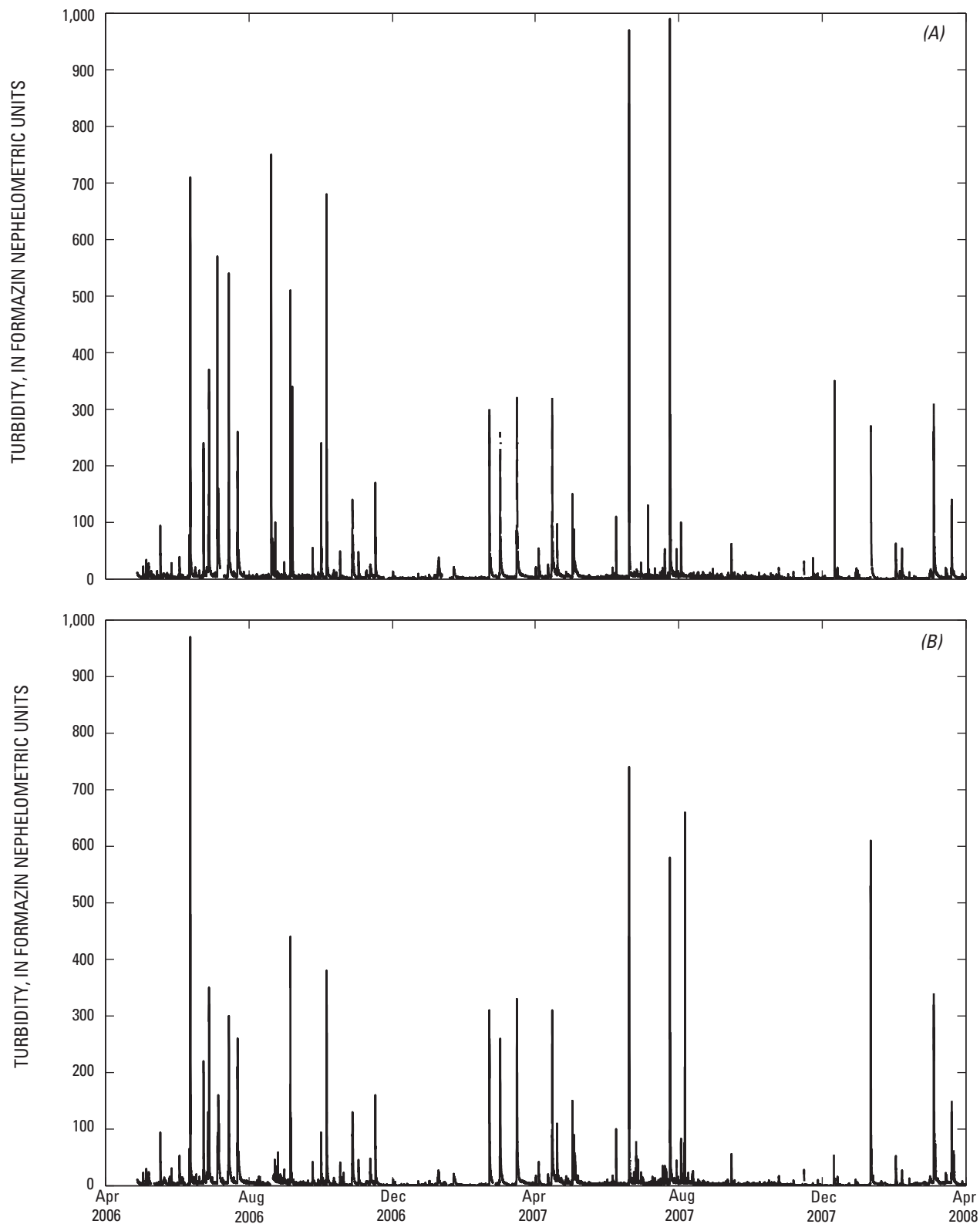
Figure 8.   Turbidity data (15-minute interval) collected from Indian Creek, Tazewell County, Virginia, at the (*A*) upstream (Station number 03520967) and (*B*) downstream (Station number 03520968) left-bank water-quality monitors.
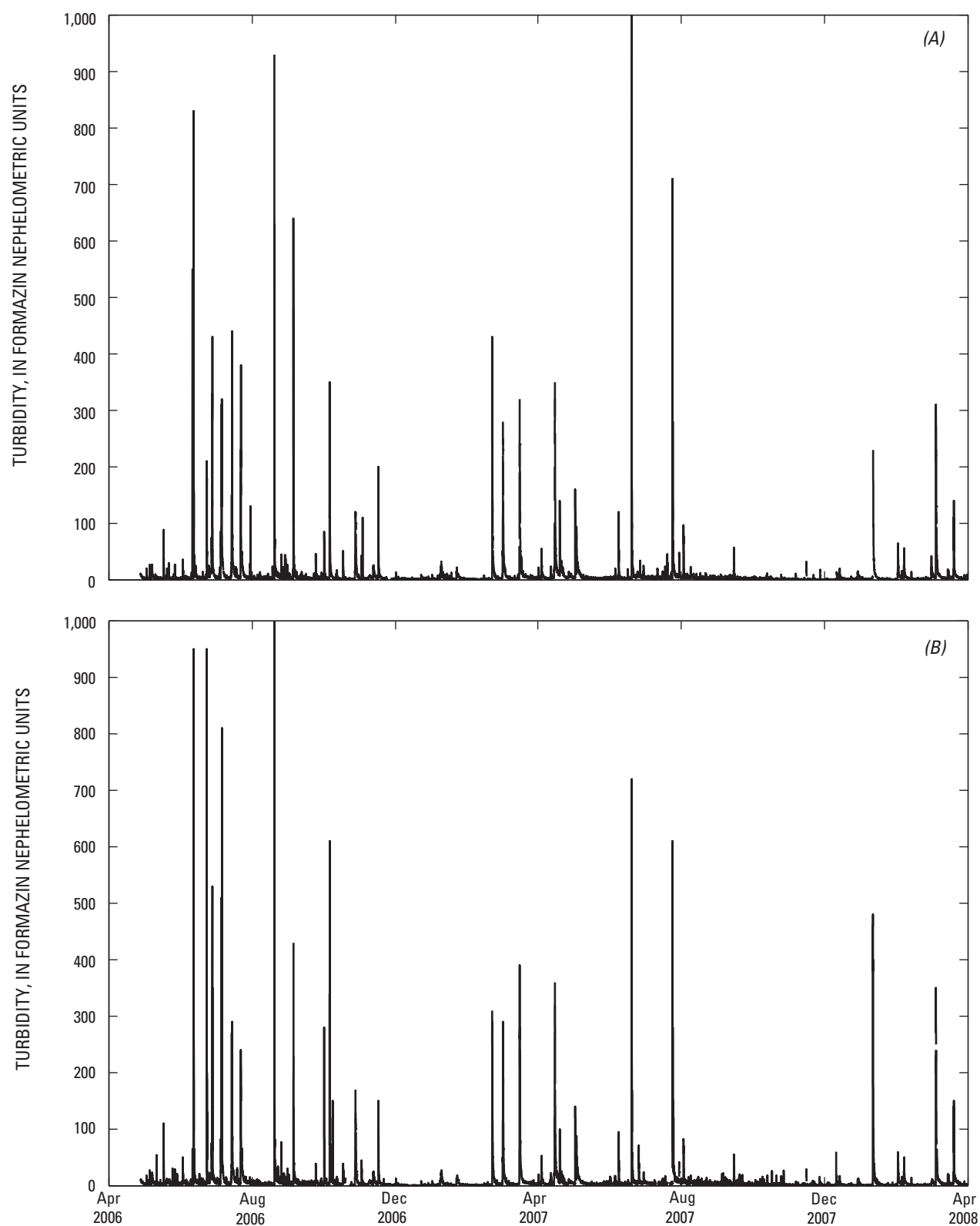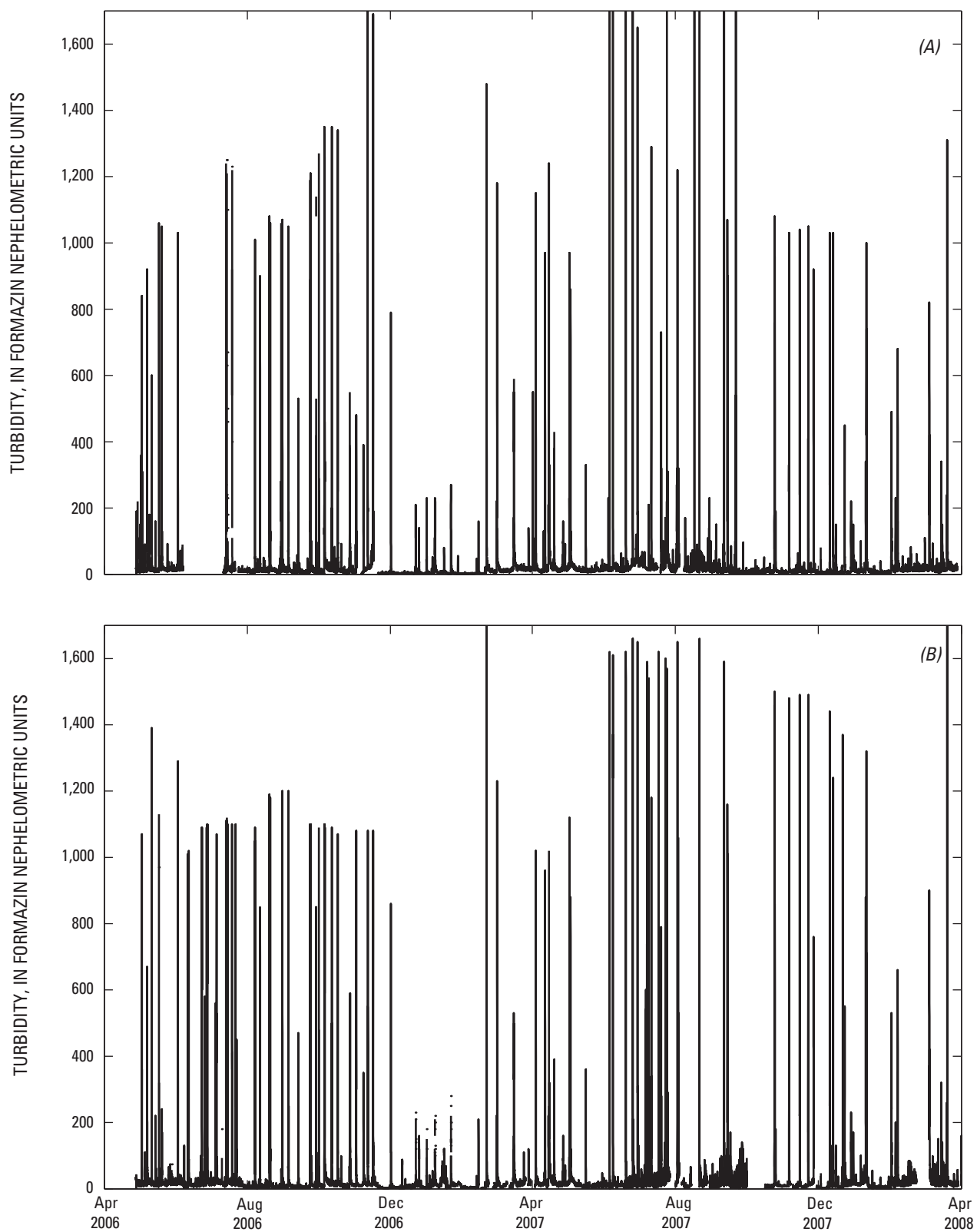
Figure 9.   Turbidity data (15-minute interval) collected from Indian Creek, Tazewell County, Virginia, at the (*A*) upstream (Station number 03520967) and (*B*) downstream (Station number 03520968) right-bank water-quality monitors.

Figure 10. Turbidity data (15-minute interval) collected from the unnamed tributary at the (*A*) upstream (Station number 03520980) and (*B*) downstream (Station number 03520981) water-quality monitors, Tazewell County, Virginia.
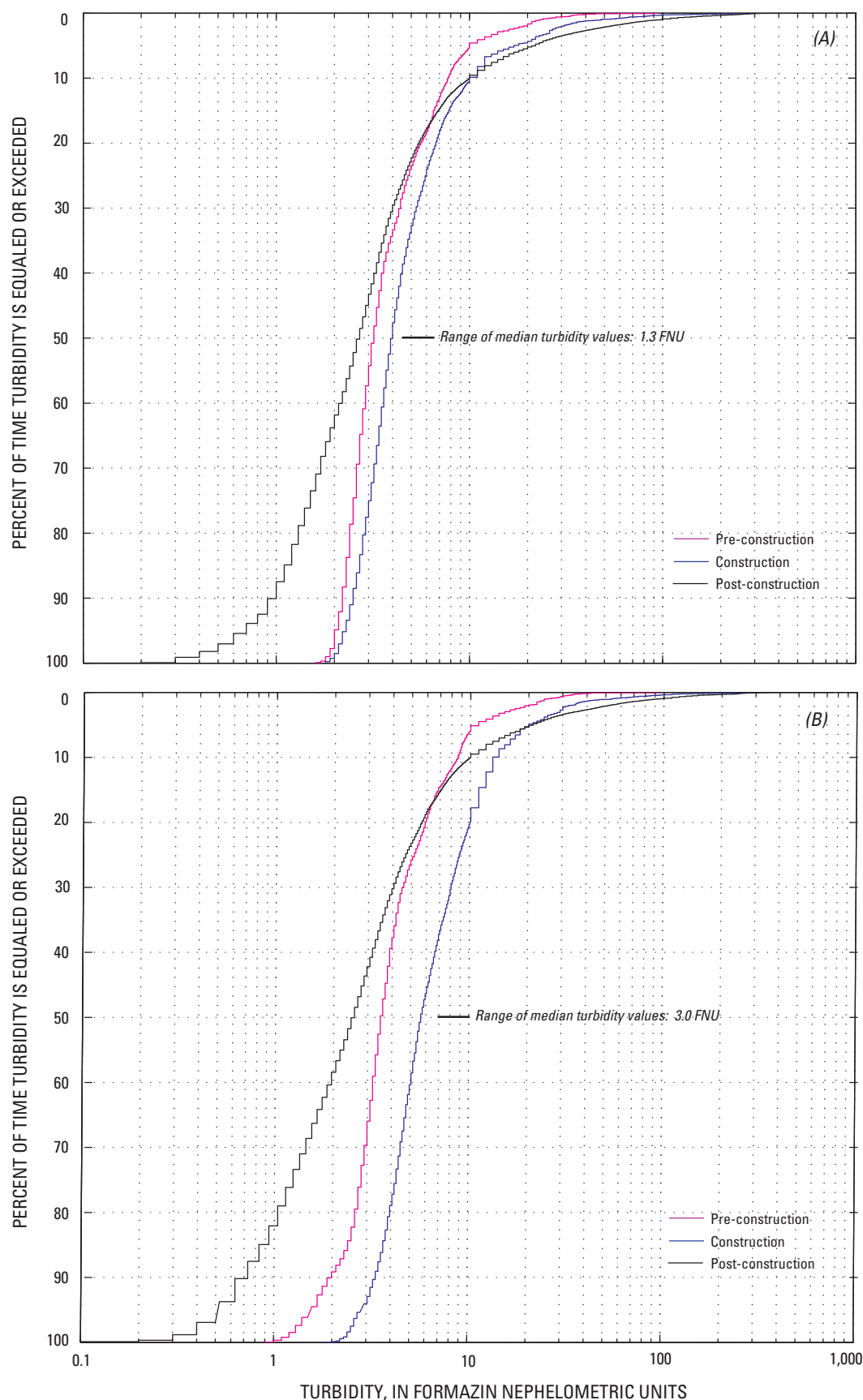
Figure 11. Exceedance plots for left-bank turbidity collected at the (*A*) upstream Indian Creek water-quality monitor (Station number 03520967) and (*B*) downstream Indian Creek water-quality monitor (Station number 03520968) during the pre-construction, construction, and post-construction phases, Tazewell County, Virginia.
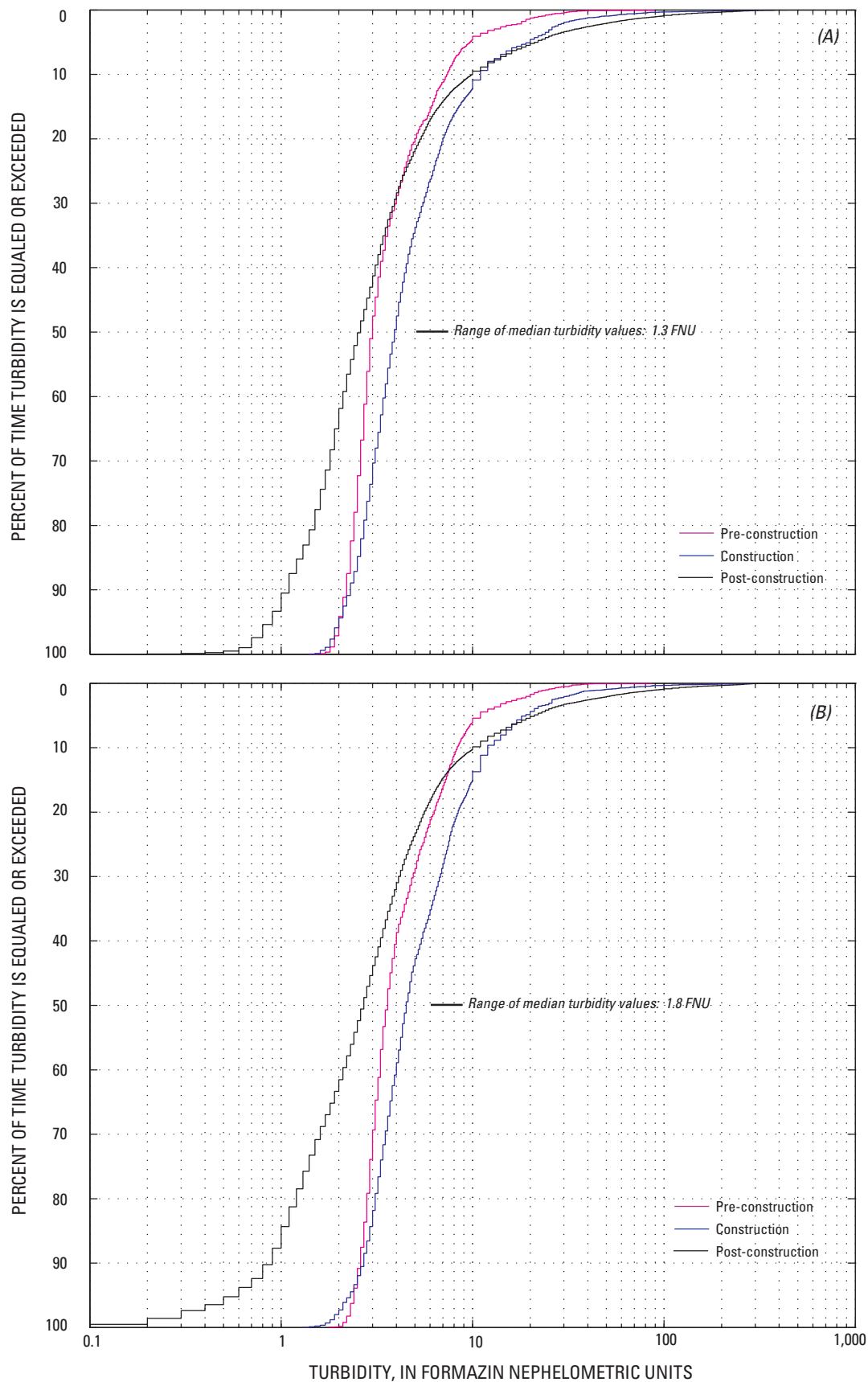
Figure 12. Exceedance plots for right-bank turbidity collected at the (*A*) upstream Indian Creek water-quality monitor (Station number 03520967) and (*B*) downstream Indian Creek water-quality monitor (Station number 03520968) during the pre-construction, construction, and post-construction phases, Tazewell County, Virginia.
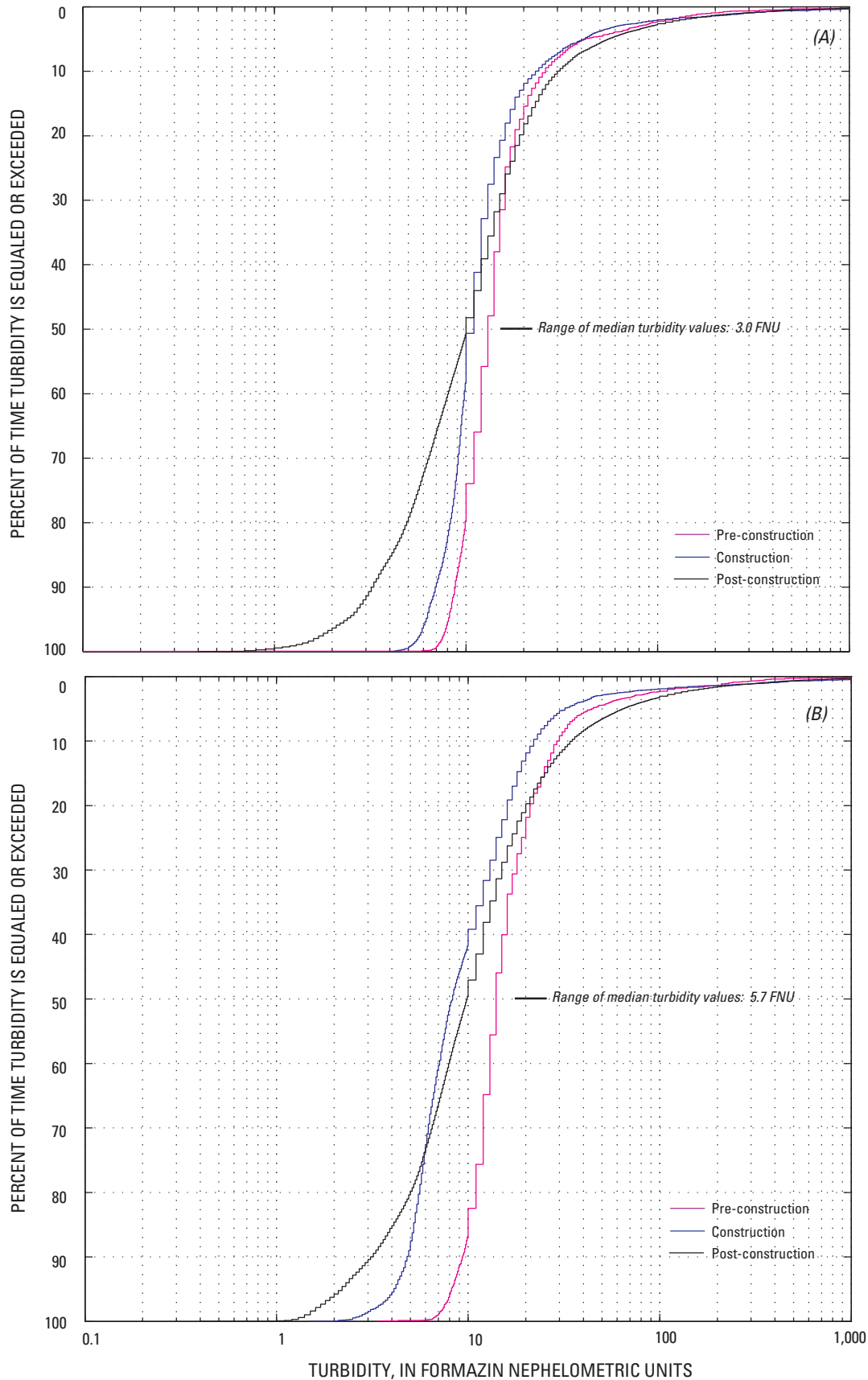
Figure 13. Exceedance plots for turbidity collected at the (*A*) upstream unnamed tributary water-quality monitor (Station number 03520980) and (*B*) downstream unnamed tributary water-quality monitor (Station number 03520981) during the pre-construction, construction, and post-construction phases, Tazewell County, Virginia.

the pipeline crossing activities, (August 4, 2006, through August 7, 2006), however, reveals that turbidity conditions did increase for a short time (fig. 14). On August 4, 2006, the pipeline crossing activities included the installation of flow-control measures and blasting of the pipeline crossing. The installation of the flow-control measures and subsequent channel blasting resulted in one elevated turbidity measurement of 460 FNU and several slightly elevated turbidity values relative to upstream conditions (fig. 14). The channel trenching, pipeline installation, backfilling of the trench, and removal of flow-control measures resulted in the turbidity measurements collected on August 5, 2006 (fig. 14). The elevated turbidity conditions observed following the removal of the flow-control measures were consistent with the literature accounts of the dry-cut pipeline crossing technique (Reid and others, 2002). Although turbidity (suspended sediment) was generated during the construction of the unnamed tributary pipeline crossing, the turbidity values were significantly lower than the turbidity values generated during natural rainfall-runoff events within this tributary (fig. 15). The turbidity values associated with the rainfall-runoff event that occurred on August 7, 2006 are

(1) consistent both upstream and downstream, indicating that the freshly constructed crossing was not a substantial source of sediment during this runoff event, and (2) representative of turbidity values routinely generated during runoff-events.

A signed-rank test was used to directly compare upstream and downstream turbidity values measured during the three phases of pipeline construction. The signed-rank test determines whether the median value of the paired differences of upstream and downstream turbidity values is equal to zero. The results of the signed-rank test are presented in table 4. The signed-rank test on the pre-construction paired differences revealed that the median paired differences for Indian Creek (left bank and right bank) and the unnamed tributary were all significantly different from zero (p < 0.001). The median pre-construction paired differences were –0.3, –0.5, and –1.0 FNU for the Indian Creek left bank and right bank and the unnamed tributary, respectively. The results from the pre-construction paired differences indicate that there is typically a slight increase (1 FNU or less) in turbidity as water passes from the upstream monitors to the downstream monitors. The signed-rank test on the construction paired differences revealed that
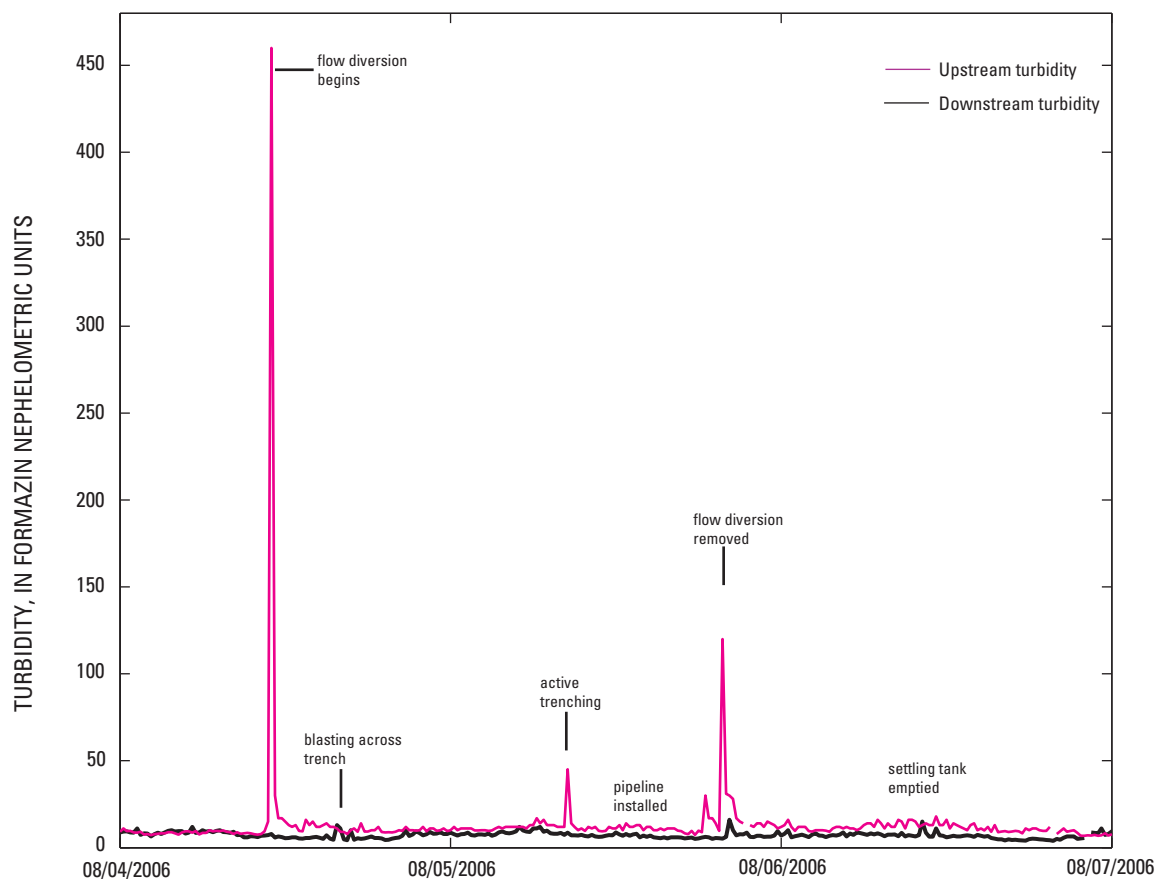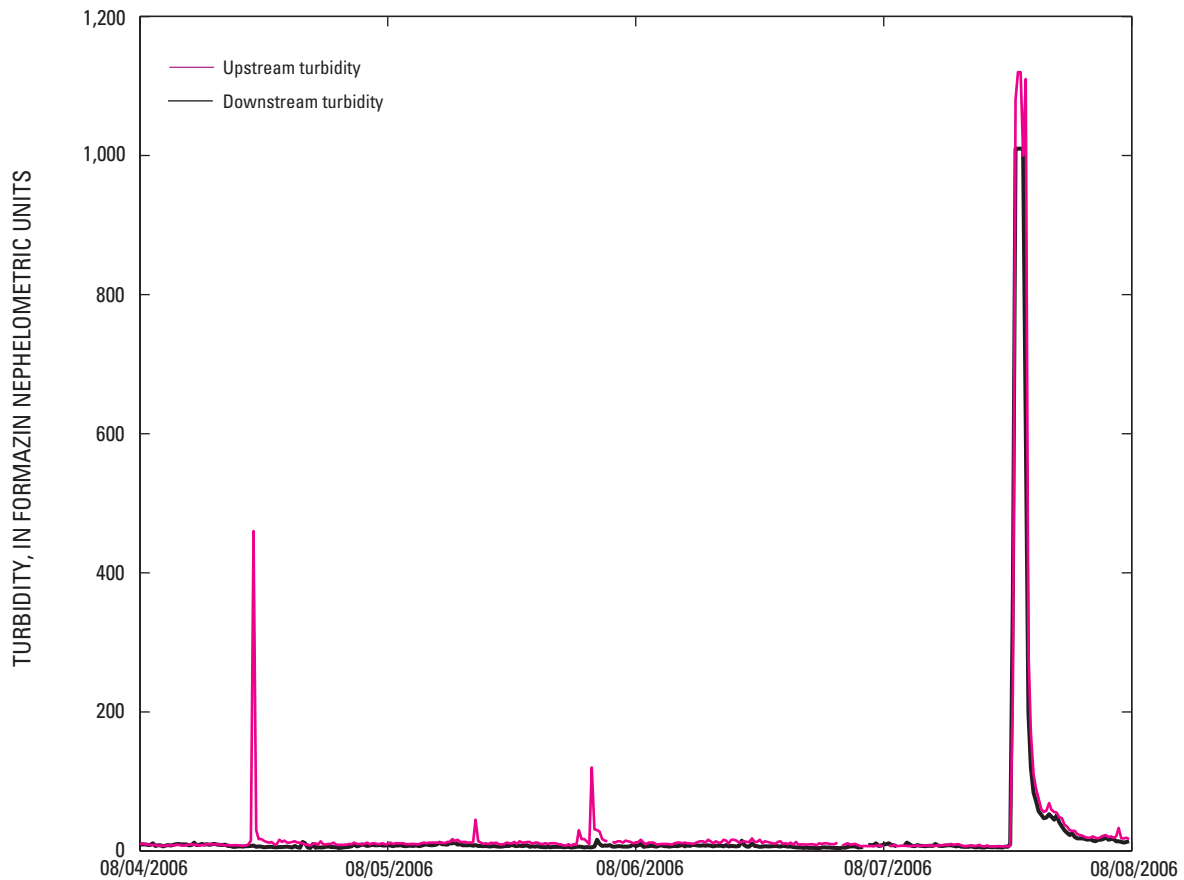

Figure 14.   Turbidity data (15-minute interval) collected from the unnamed tributary at the upstream (Station number 03520980) and downstream (Station number 03520981) water-quality monitors during active pipeline construction August 4–7, 2006, Tazewell County, Virginia.

Table 4. Signed-rank test results for turbidity differences from paired upstream and downstream turbidity values from Indian Creek and unnamed tributary.

[Values presented are the median paired difference in upstream and downstream turbidity, in Formazin Nephelometric Units, and the associated signed-rank test p-value in parentheses]

	Indian Creek left bank	Indian Creek right bank	Unnamed tributary
Pre-Construction	–0.3	–0.5	–1.0
	(< 0.001)	(< 0.001)	(< 0.001)
Construction	–1.3	–0.7	1.7
	(< 0.001)	(< 0.001)	(< 0.001)
Post-Construction	0.2	0.1	0
	(< 0.001)	(< 0.001)	(0.055)

the median percent differences for Indian Creek (left bank and right bank) and the unnamed tributary were all significantly different from zero (p < 0.001). The median construction paired differences values were –1.3, –0.7, and 1.7 FNU for the Indian Creek left bank and right bank and the unnamed tributary, respectively. The result from the construction period paired differences from the Indian Creek left-bank monitors indicates that turbidity values increased 1 FNU as water moved below the pipeline construction. This same pattern in construction paired differences from the right-bank monitors was observed; however, the difference relative to the pre-construction median paired difference was only 0.2 FNU. Conversely, the signed-rank test results for the unnamed tributary indicate that turbidity values decreased 1.7 FNU downstream from the upstream monitor, which is a shift of 2.7 FNU relative to pre-construction conditions. The signed-rank test on the post-construction paired differences revealed that the median of the paired differences for Indian Creek (left bank and right bank) were all significantly different from zero. The median post-construction paired differences were 0.2 and 0.1 FNU for the Indian Creek left bank and right bank, respectively. The signed-rank test on the unnamed tributary post-construction paired differences revealed that the median of the paired differences was not significantly different from zero. The median post-construction paired difference was 0.0 FNU for the unnamed tributary. These post-construction turbidity conditions were similar to the observed pre-construction conditions.

Figure 15. Turbidity data (15-minute interval) collected from the unnamed tributary at the upstream (Station number 03520980) and downstream (Station number 03520981) water-quality monitors during active pipeline construction August 4–8, 2006, Tazewell County, Virginia.

The results from the signed-rank test analysis help to determine whether the pipeline crossing affected downstream sediment conditions in Indian Creek and the unnamed tributary. In Indian Creek, the paired differences of upstream and downstream turbidity values and the associated signed-rank test all indicate that more sediment entered the study reach during the construction phase than during the pre-construction and post-construction phases. The signed-rank test results also indicate that a more pronounced sediment source exists between the upstream and downstream left-bank monitors. Although this result is significant, the magnitude of the difference is small. The discrepancy between the downstream left- and right-bank monitors is discussed further in the "Conceptual Model for Indian Creek Turbidity Patterns" section of this report. In the unnamed tributary, the pipeline crossing did not increase turbidity conditions downstream from the pipeline crossing on the basis of the signed-rank test analysis of the three construction periods.

Boxplots of the paired differences for each month of the study were generated for the Indian Creek and unnamed tributary monitors. These boxplots show the distribution of the monthly paired differences (represented by the 10th, 25th, 50th, 75th, and 90th percentiles). For comparison, the monthly differences for the paired turbidity values collected at the two upstream Indian Creek monitors (left and right bank) are

presented in figure 16. The black horizontal line that passes through all of the monthly boxplots is the locally weighted scatterplot smoothing (LOWESS) (Helsel and Hirsch, 1992) best fit of the monthly medians. The LOWESS best-fit line was used to identify temporal patterns between the monthly medians. This boxplot of the upstream paired differences indicates that the majority of the monthly paired differences, for the entire study period, occurred between 2.0 and –2.0 FNU. This result strongly indicates that the combination of variability between the instruments and the natural variability in the channel accounts for ± 2 FNU. Paired differences within the ± 2 FNU range should be considered environmental and instrument noise, whereas values outside of this range may indicate a measurable change in turbidity. The boxplot of monthly paired differences for the Indian Creek left bank (upstream minus downstream) shows that most of the paired differences occur within the ± 2 FNU range; however, June 2006 through August 2006 had paired differences that exceeded this –2.0 FNU, indicating a sustained sediment input downstream from the upstream Indian Creek monitors (fig. 17*A*). This pattern of sediment input from June 2006 through August 2006 was observed in the paired differences from the upstream and downstream right-bank monitors (fig. 17*B*). The vast majority of the right-bank turbidity paired differences are within the ± 2 FNU range. The boxplot of
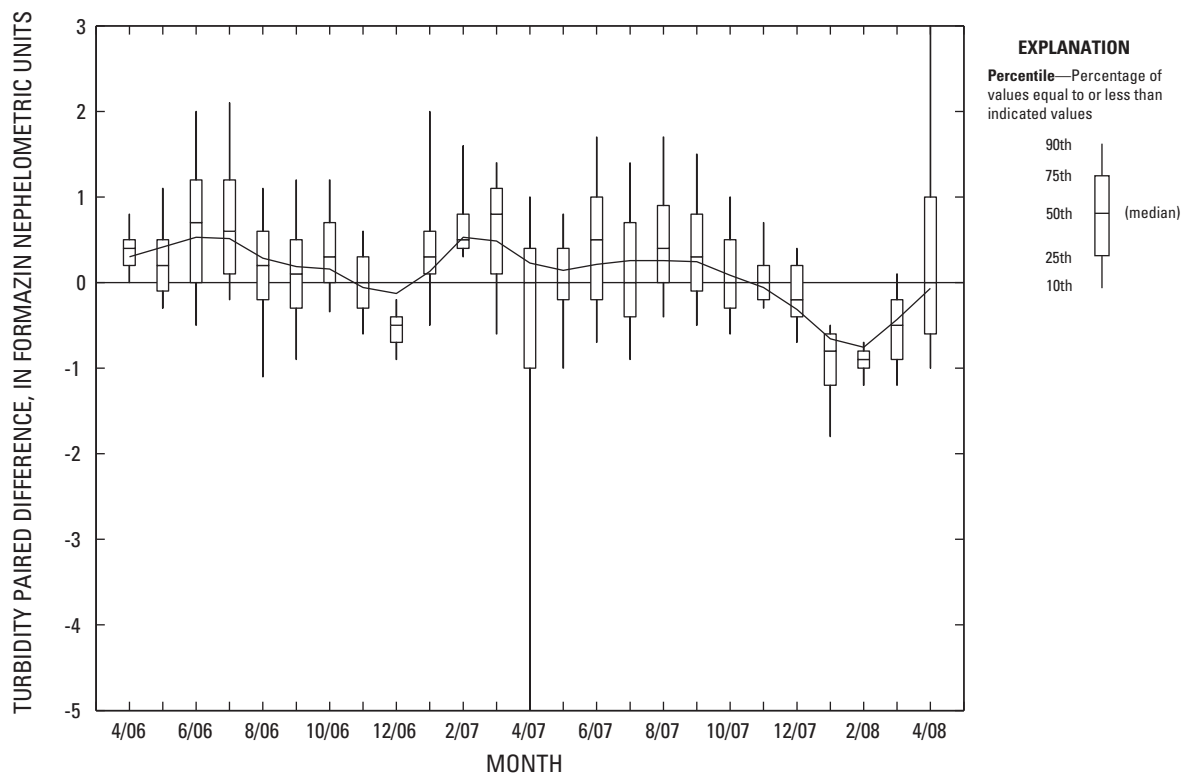

Figure 16.   Monthly differences for paired turbidity values collected at the left-bank and right-bank upstream Indian Creek water-quality monitors (Station number 03520967, fig. 3), Tazewell County, Virginia. Turbidity paired difference equals left-bank turbidity minus right-bank turbidity. The black line represents the LOWESS smoothed fit line through the monthly medians.
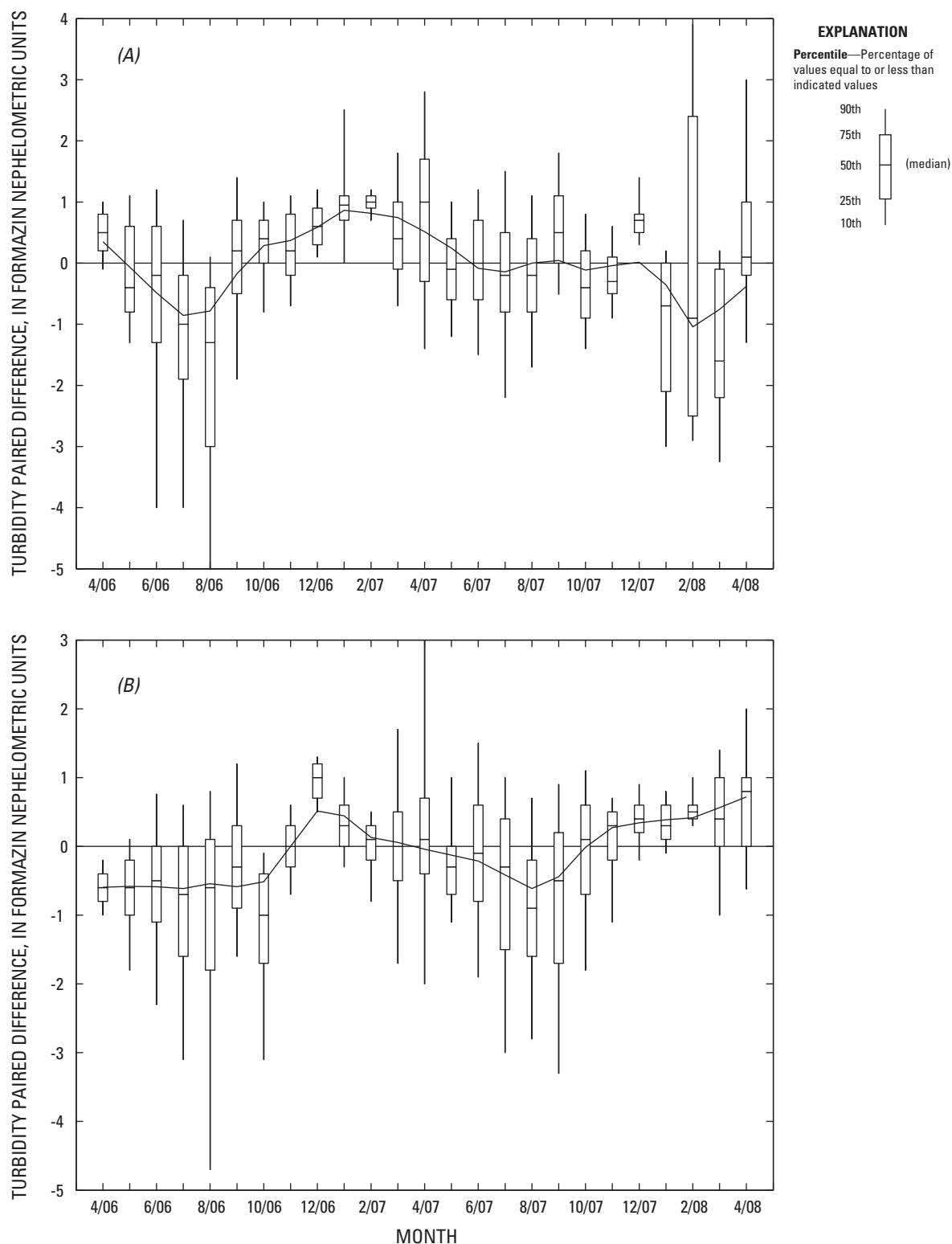
Figure 17.   Monthly differences for paired turbidity values collected at the (*A*) left-bank and (*B*) right-bank monitors located upstream (Station number 03520967, fig. 3) and downstream (Station number 03520968) of the pipeline crossing under Indian Creek, Tazewell County, Virginia. Turbidity paried difference equals left-bank upstream turbidity minus left-bank downstream turbidity. The black line represents the LOWESS smoothed fit line through the monthly medians.

monthly paired differences for the unnamed tributary show that turbidity in the tributary is highly variable compared to turbidity paired differences for Indian Creek, with a range that typically extends ± 10 FNU (fig. 18). The monthly paired differences indicate that turbidity conditions improved (that is, turbidity decreased at the downstream monitor) during the pipeline construction and that the construction paired differences are indistinguishable from the remaining monthly paired differences.

As part of the assessment of long-term turbidity patterns, exceedance plots of measured turbidity values, signed-rank test of turbidity paired differences, and monthly boxplots of turbidity paired differences were used to determine whether the Indian Creek and unnamed tributary pipeline crossings resulted in increased turbidity levels downstream from the crossings. These three analytical evaluations of the measured turbidity patterns provided consistent results for turbidity conditions for both Indian Creek and the unnamed tributary. In Indian Creek, turbidity significantly increased downstream from the pipeline crossing. The greatest increase in downstream turbidity occurred during the construction phase. Although the results for left- and right-bank turbidity patterns were consistent, the turbidity patterns were most pronounced along the left bank. This discrepancy between the left- and right-bank turbidity patterns is discussed further in the "Conceptual Model for Indian Creek Turbidity Patterns" section of this report. In the unnamed tributary, turbidity values downstream from the pipeline crossing were measurably elevated for short durations during active pipeline-crossing construction, August 4–6, 2006; however, the sediment generated during this period, as indicated by the increase in turbidity, was substantially lower than the turbidity levels that are generated during typical runoff events. On the unnamed tributary, the long-term patterns in turbidity, collected during the construction phase, indicate that turbidity significantly decreased downstream from the pipeline crossing.

Utility of the Turbidity-Input Warning System

The turbidity-input warning system required by the USFWS and subsequently established by East Tennessee Natural Gas and the USGS was instrumental in ensuring the integrity of the ecology of Indian Creek and the unnamed tributary. A turbidity warning occurred when downstream turbidity was either 6 FNU, or 15 percent (see "Turbidity-Input Warning System" section for additional details) greater than the corresponding upstream turbidity value, sustained for
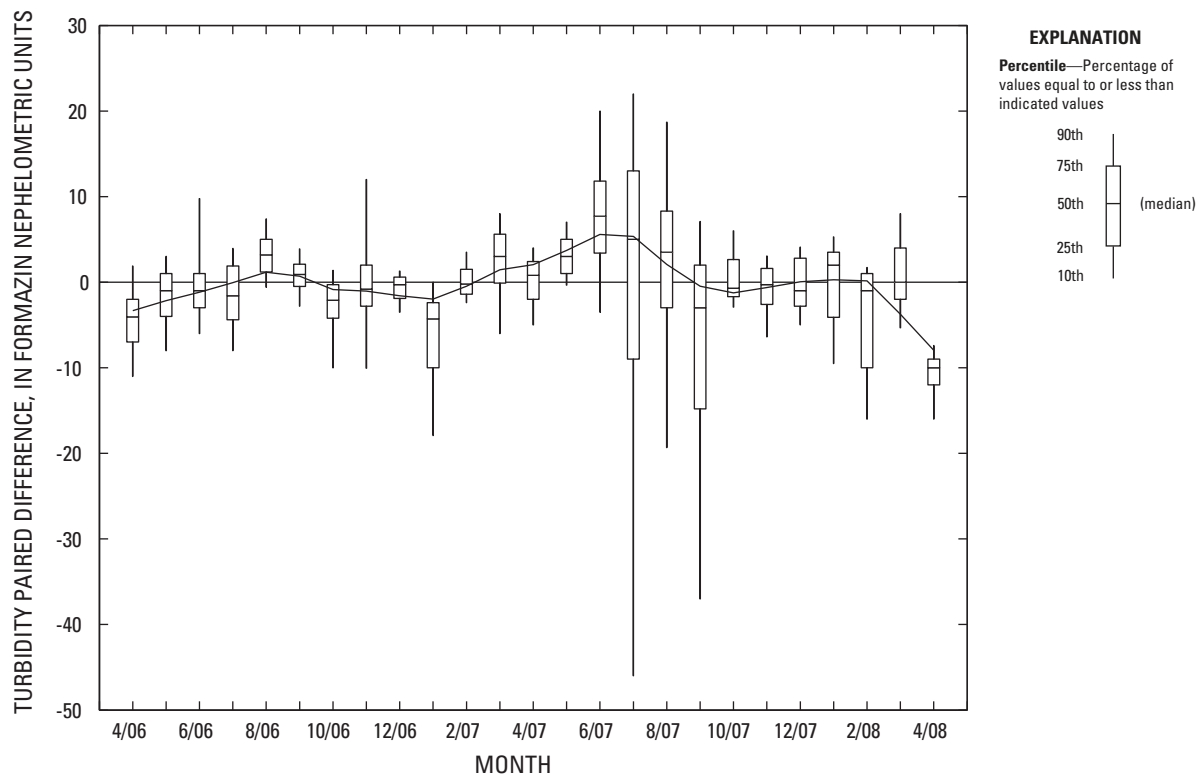

Figure 18.   Monthly differences for paired turbidity values collected at the upstream (Station number 03520980) and downstream (Station number 03520981, fig. 3) unnamed tributary water-quality monitors, Tazewell County, Virginia. Turbidity paired difference equals upstream turbidity minus downstream turbidity. The black line represents the LOWESS smoothed fit line through the monthly medians.

a period of 1 hour. Once a threshold was exceeded, the on-site manager for East Tennessee Natural Gas would investigate Indian Creek below the upstream monitors for incoming sediment. If incoming sediment was not present, then East Tennessee Natural Gas would contact the USGS to check for turbidity-equipment problems such as fouling from the accumulation of debris on the water-quality monitoring sonde. An example of the warnings received each month for exceeding the downstream-turbidity thresholds is provided in figure 19. This figure shows that during each month, between 0 and 38 warnings (0 to 1.45 percent of the collected turbidity unit values) occurred throughout the period of study. During the construction phase, 16 to 38 alarms occurred each month, and were subsequently investigated. Most of the warnings were determined to be caused by fouling of the turbidity probe.

On August 19, 2006, the turbidity-input warning system captured a substantial sediment-input event. An intensive rainfall event in the Indian Creek watershed caused upland surface-water runoff and associated sediment transport from the Jewell Ridge pipeline right-of-way. Although

sediment- and erosion-control measures were in place, this runoff and sediment transport overwhelmed the existing controls and entered an ephemeral unnamed tributary approximately 350 feet upstream from the right-bank monitor on Indian Creek. This runoff event delivered substantial amounts of suspended sediment into Indian Creek. Turbidity values measured at the upstream left- and right-bank monitors peaked at 930 and 750 FNU, respectively, whereas turbidity reached 1,220 FNU at the downstream right-bank monitor. The downstream left-bank monitor was not functioning during this sediment-input event.

The turbidity-warning system allowed real-time detection of sediment/turbidity input within the study reach. The ability for watershed managers to detect sediment input as it happened allowed for rapid-response corrective actions. The turbidity-input warning system successfully detected episodic exceedences of the established turbidity threshold, and helped to prevent occurrences of chronic long-term input of turbidity. One limitation of the turbidity-input warning system is that the conservative nature of the turbidity thresholds make the system highly susceptible to false-positive warnings.
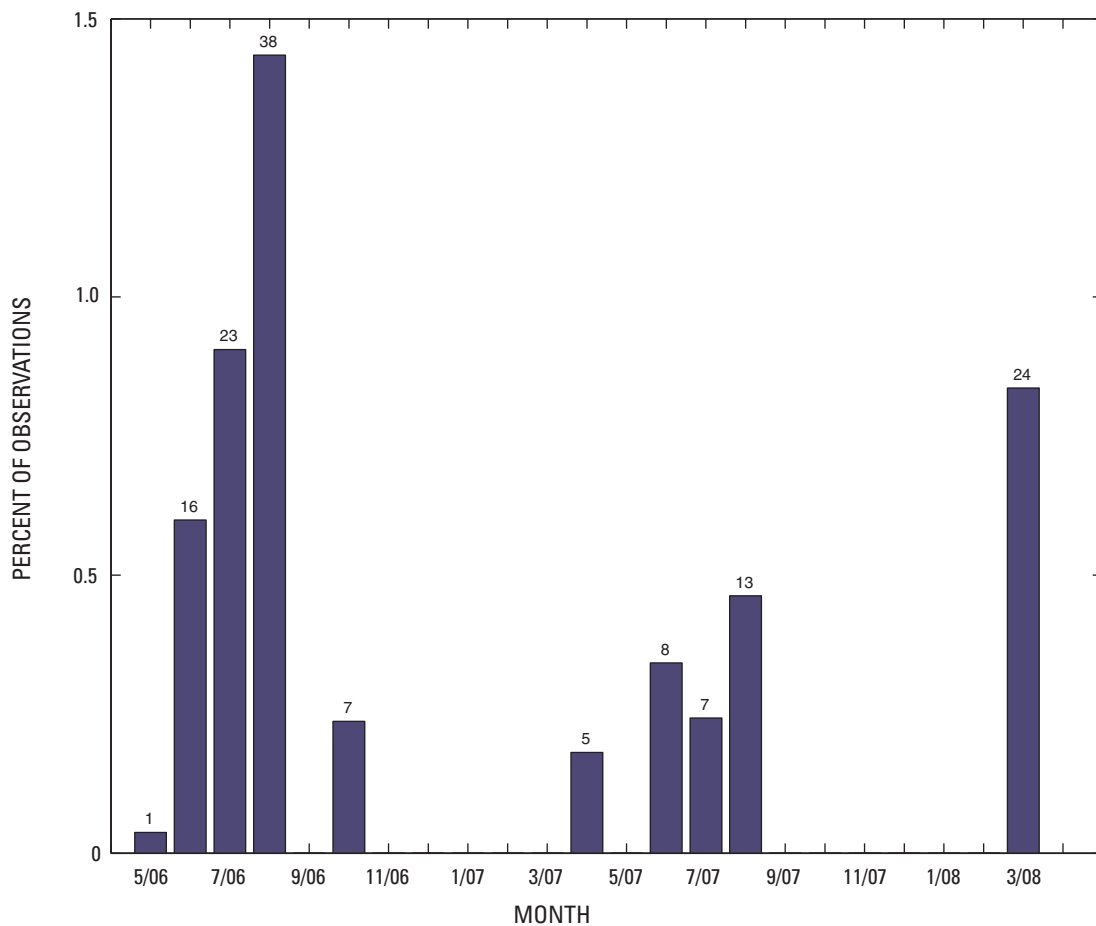

Figure 19. Monthly bar plot showing the percentage of turbidity paired differences that resulted in a warning for exceeding the turbidity threshold along the left bank of Indian Creek, Tazewell County, Virginia. The number above each bar plot represents the actual number of warnings.

Conceptual Model for Indian Creek Turbidity Patterns

This study was designed to evaluate whether the Jewell Ridge pipeline crossing and associated pipeline construction resulted in increased turbidity levels, thus increasing suspended-sediment concentrations during the construction phase, and to detect both real-time and long-term changes in turbidity conditions within the pipeline-crossing easement. Results obtained from all statistical and graphical analyses indicate that turbidity levels increased within the Indian Creek pipeline-crossing easement, and that these increases in turbidity were small in magnitude but occurred over a prolonged time period. Although these results were consistent for all upstream to downstream analyses, the pattern of increased turbidity was always more pronounced along the left side of the channel compared to the right side of the channel. An investigation into these left- and right-channel inconsistencies, coupled with the occurrence of the August 19, 2006, right-of-way slope failure and subsequent sediment transport, led to the development of an alternative conceptual model for turbidity patterns measured during the construction phase. The initial conceptual model, which was tested during this study, was that the pipeline crossing and nearby adjacent trenching activities would transport sediment directly into the Indian Creek monitoring reach. The alternative conceptual model was that transport of sediment from the pipeline construction right-of-way into an ephemeral unnamed tributary and subsequently into Indian Creek served as the primary source of turbidity/sediment detected during the construction phase. For the remainder of this section, data are presented that support the development of this alternative conceptual model.

The ephemeral unnamed tributary (which should not be confused with the unnamed tributary monitored as part of this study) discharges into Indian Creek along the right bank, approximately 350 feet above the upstream water-quality monitors (fig. 20). The path of the Jewell Ridge pipeline crosses the headwaters of the ephemeral unnamed tributary (fig. 20). The effects of this ephemeral unnamed tributary on sediment delivery to Indian Creek were considered during the development phase of this study; however, the study was designed to focus on the Indian Creek pipeline crossing and it was anticipated that this ephemeral unnamed tributary would not be a source of construction sediment. The design of the monitoring network (paired upstream, downstream, left-bank, and right-bank monitors) was chosen to isolate the Indian Creek pipeline crossing and to account for incoming sediment from this ephemeral unnamed tributary; however, the August 19, 2006, sediment transport event showed that the pipeline construction activity was a substantial source of sediment in the ephemeral unnamed tributary. The design of the water-quality network that was implemented and associated data analyses allowed for the determination that sediment derived from this ephemeral unnamed tributary may in fact be the primary source of sediment that was detected within the Indian Creek pipeline-crossing easement.

Analysis of turbidity data collected at the upstream Indian Creek monitors revealed that variability between turbidity data collected at the left- and right-bank monitors increased during pipeline construction. Results from a paired differences analysis (left-bank minus right-bank turbidity value) of the 50th, 75th, 80th, 90th, 95th, and 99th percentiles for turbidity data collected at both upstream Indian Creek turbidity monitors are presented in figure 21. The 50th though the 99th percentiles represent turbidity values that ranged from 3 to 100 FNU during the entire period of study. During pre-construction, paired differences from these specified percentiles ranged from 0.2 to 1.4 FNU, which indicates that turbidity values were slightly greater at the left-bank monitor. This pre-construction result shifted during the construction phase to a range of 1.0 to –3.0 FNU. The paired differences for the 75th, 80th, 90th, and 95th percentiles were all negative, indicating that turbidity values were greater at the right-bank monitor. This result indicates that during elevated turbidity conditions within the construction period, which were typically associated with runoff events, the right side of the Indian Creek channel was more turbid than the left side of the channel. Also, this shift from positive paired differences during the pre-construction phase to negative paired differences during the construction phase indicates that a new sediment source was contributing to Indian Creek turbidity. The ephemeral unnamed tributary discharges to the right bank of Indian Creek 350 feet above the upstream monitors thereby allowing very little distance for mixing, which would generate the negative paired differences that were observed. Additionally, Indian Creek is considered completely mixed upstream from the confluence with the ephemeral unnamed tributary. The paired differences returned to all positive values during the post-construction phase. The post-construction paired differences ranged from 0 to 4 FNU, and the observed range for the 50th to 95th percentiles was 0.0 to 0.1 FNU. The consistent and small observed ranges in pre- and post-construction paired differences indicate that Indian Creek is well mixed as it flows by the upstream monitors. Conversely, the negative paired differences observed during the construction phase indicate that sediment delivered from the ephemeral unnamed tributary primarily was detected by the right-bank monitor, and that the contributions from this tributary dissipated during the post-construction phase.

The results of the paired differences analysis performed on the paired upstream left- and right-bank turbidity percentiles explain the discrepancy observed in the long-term analysis of left- and right-bank paired upstream and downstream data. The long-term analysis of these paired differences indicates that turbidity increased within the pipeline-crossing easement during construction; however, these results were more pronounced along the left channel compared to the results for the right side of the channel. This discrepancy is explained by the turbidity patterns observed at the upstream monitors during the construction phase. Most of the long-term analyses relied on paired differences of upstream and downstream turbidity data to detect change. Because turbidity
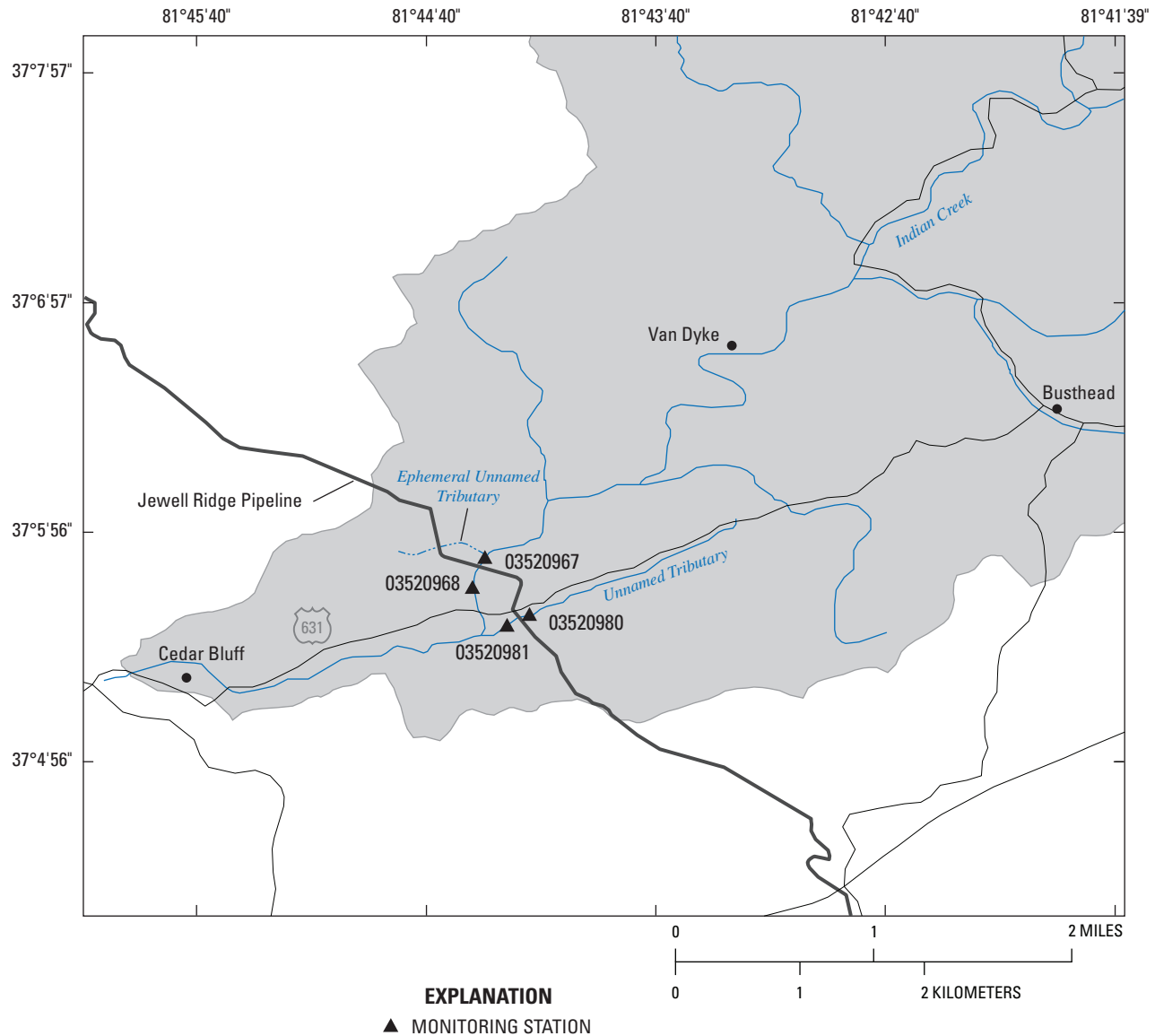
Figure 20.   The Indian Creek and unnamed tributary monitoring network as well as the ephemeral unnamed tributary, Tazewell County, Virginia.

at the upstream right-bank monitor was elevated during the construction phase, the difference between the upstream and downstream right-bank monitors was minimized. Essentially, the turbidity that was detected by the upstream right-bank monitor was detected by the downstream right-bank monitor. Additionally, the turbidity that passed the upstream right-bank monitor was transported and subsequently mixed across the channel so that the downstream left-bank monitor also detected this turbidity. As the upstream left-bank monitor did not fully detect this incoming turbidity from the ephemeral unnamed tributary, a pronounced and statistically significant result was obtained, which indicated that a sediment input occurred along the left bank.

The following conclusions can be drawn from the alternative conceptual model:

1. Turbidity values significantly increased within the pipeline-crossing easement during the construction phase;

2. The primary source of this turbidity increase can be linked to sediment delivered from the ephemeral unnamed tributary; and

3. The bored pipeline crossing had little to no effect on sediment conditions in Indian Creek, and sediment transport from the upland pipeline right-of-way into the ephemeral unnamed tributary was the primary source for the turbidity increases observed in the pipeline-crossing easement.
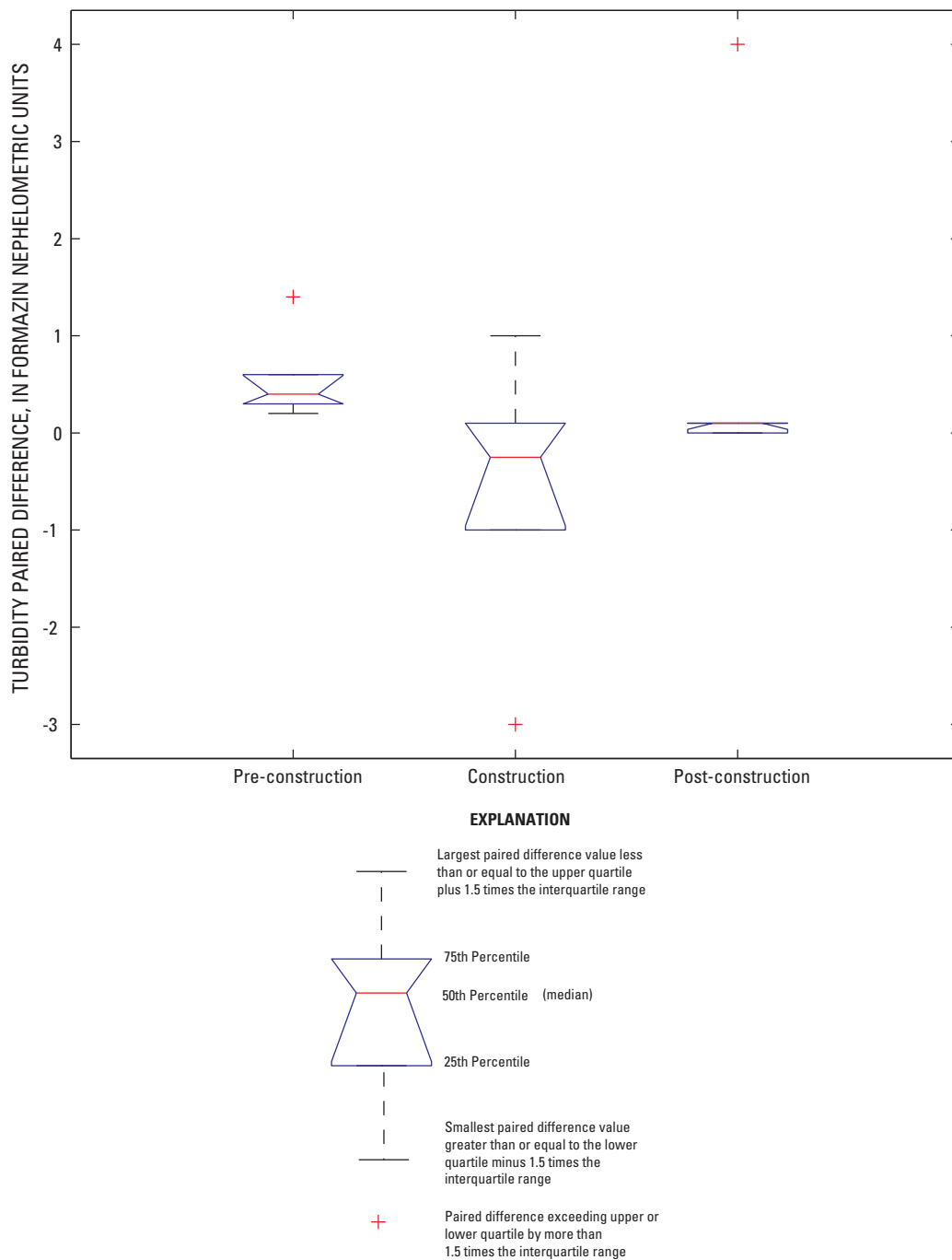
Figure 21. Boxplots of turbidity paired differences for turbidity collected at the left-bank and right-bank upstream Indian Creek water-quality monitors (Station number 03520967), Tazewell County, Virginia. Turbidity paired difference equals left-bank turbidity minus right-bank turbidity for values at the 50th, 75th, 80th, 90th, 95th, and 99th percentiles.

These conclusions are consistent with those in the literature regarding the effect of the HDD technique on downstream suspended-sediment conditions. The HDD technique has been shown to have little to no impact on downstream suspended-sediment conditions (Reid and others, 2002; Lévesque and Dubé, 2007). The HDD technique bores a pipeline crossing at least 5 feet beneath the bottom of the stream. The area of the boring is bordered by extensive silt fencing and hay bails, which also reduce the likelihood that sediment will be transported into the crossing. No sediments were ever observed to directly wash off the Indian Creek pipeline crossing construction site. Conversely, it has been shown that the greatest risk associated with sediment transport during the application of HDD is the runoff and associated sediment transport from the upland pipeline right-of-way into nearby drainages (Reid and others, 2002; Lévesque and Dubé, 2007).

Study Limitations

Although the establishment of the turbidity-monitoring network enabled short-term and long-term evaluation of the pipeline crossing beneath Indian Creek and through the unnamed tributary, several confounding factors affected the statistical analysis to identify changes in turbidity conditions. These factors include (1) an abbreviated pre-construction monitoring period, (2) loss of turbidity data through fouling, (3) uncontrolled sediment sources upstream from the monitoring reach, and (4) routing of extracted bore water downstream from the monitoring reach.

Pre-construction monitoring was a critical component in determining the overall influence of the pipeline crossing on downstream water-quality conditions. The objective of the pre-construction monitoring period was to quantify the extent of environmental and instrument variability in instream water-quality properties. Ideally, the pre-construction monitoring period would have been long enough to capture a wide range of hydrologic conditions. The pre-construction monitoring period was limited to 34 days, however, during which no substantial runoff event occurred within the Indian Creek Basin. As a result, the natural and instrument variability associated with turbidity in Indian Creek is representative of the 34-day pre-construction monitoring period but underrepresents the complete range of conditions.

The use of continuously collected turbidity data was essential to the real-time monitoring of water-quality conditions in Indian Creek and the unnamed tributary. During the study period, turbidity conditions were intensively monitored at an average rate of 2,600 and 2,400 turbidity observations per month from Indian Creek and the unnamed tributary, respectively. The turbidity monitoring instrument, however, was prone to fouling caused by several factors including instream debris (leaves and sediment), biofouling (algal growth and presence of macro-invertebrates), and electronic drift. Fouling of the Indian Creek and the unnamed tributary monitors resulted in an average monthly loss of turbidity data

of 10 and 20 percent, respectively. The USGS, in response to the elevated rate of fouling on the unnamed tributary monitors, increased the maintenance to once every 2 weeks instead of once every 4 weeks. Additionally, the occurrence of turbidity-instrumentation fouling typically resulted in an exceedence of the established turbidity threshold, which had to be investigated to ensure the warning was not a result of sediment input.

On August 19, 2006, excessive runoff and associated sediment transport from the upland Jewell Ridge pipeline construction right-of-way overwhelmed the upland slope and entered an ephemeral unnamed tributary, which brought substantial amounts of suspended sediment into Indian Creek 350 feet upstream from the monitoring site. The primary concern regarding the influence of this sediment input on the success of the monitoring effort is that it occurred upstream from the upstream turbidity monitors. The Indian Creek monitoring network was designed to evaluate the effects of the pipeline crossing on downstream values of turbidity; the upstream monitors were intended to represent non-pipeline-derived turbidity. There is no way to determine how long this sediment-input event influenced the analysis of the differences of paired-turbidity values.

During the construction of the Indian Creek pipeline crossing, HDD was used to drill under Indian Creek. As part of the drilling, water and associated sediment were pumped from the drill site and stored in a series of two on-site settling tanks. Most of the suspended material settled out within the first settling tank. This water was then passed to a second settling tank where additional deposition of particulate constituents occurred. The stored water was then released through a filter bag onto a grassy field that drained into Indian Creek. The discharge location selected for the release in the grassy field caused the release water to flow into Indian Creek downstream from the downstream monitor. Thus, it cannot be determined whether this activity affected water-quality conditions in Indian Creek.

Summary and Conclusions

In 2006, the USGS, in cooperation with East Tennessee Natural Gas and USFWS, began a study to monitor the effects of construction of the Jewell Ridge Lateral natural gas pipeline on suspended-sediment concentrations below the pipeline crossing beneath Indian Creek and through an unnamed tributary to Indian Creek in Tazewell County, Virginia. The Biological Opinion, prepared by the USFWS, required that turbidity conditions be intensively monitored below the pipeline crossings because of the presence of threatened and endangered mussel species. Indian Creek is listed as one of the Virginia Department of Game and Inland Fisheries' designated Threatened and Endangered Species Waters and contains federally designated critical habitat for two endangered freshwater mussel species, purple bean (*Villosa perpurpurea*) and rough rabbitsfoot (*Quadrula cylindrical strigillata*).

Additionally, Indian Creek contains the last known reproducing population of the tan riffleshell (*Epioblasma florentina walkeri*). The primary objective of the USGS monitoring effort was to identify whether the construction of the Indian Creek pipeline crossing would adversely impact the suspended-sediment concentrations, using turbidity as a surrogate. The specific study objectives were to (1) develop a continuous turbidity monitoring network that attempted to measure real-time changes in suspended-sediment conditions (using turbidity as a surrogate) downstream from the pipeline crossing in Indian Creek and the unnamed tributary to Indian Creek, and (2) provide continuous turbidity data that allow for the development of a turbidity-input warning system and assessment of long-term changes in turbidity conditions.

Water-quality conditions were assessed using continuous water-quality monitors deployed upstream and downstream from the pipeline crossings in Indian Creek and the unnamed tributary. In Indian Creek, two water-quality monitoring sondes were suspended from a boom upstream from the pipeline crossing so that one monitor was submersed near the left bank and the second monitor was submersed near the right bank. Two additional water-quality monitoring sondes were suspended from a boom downstream from the pipeline crossing so that one monitor was submersed near the left bank and the second monitor was submersed near the right bank. These paired upstream and downstream monitors were outfitted with turbidity, pH, specific conductance, and water-temperature sensors. In the unnamed tributary, two water-quality monitoring sondes were deployed upstream and downstream from the pipeline crossing. The paired upstream and downstream monitors were outfitted with turbidity, specific-conductance, water-temperature, and water-level sensors. Water-quality data were collected continuously (every 15 minutes) during three phases of the pipeline construction: pre-construction (April 28, 2006, through May 31, 2006), during construction (June 1, 2006, through August 31, 2006), and post-construction (September 1, 2006, through April 9, 2008), transmitted hourly via satellite transmission, and made publicly available on the USGS NWIS Web page (*http://waterdata.usgs.gov/va/nwis/nwis*).

Continuous turbidity data were evaluated at various time steps to determine if the construction of the pipeline crossings had an effect on downstream suspended-sediment conditions in Indian Creek and the unnamed tributary. Hourly evaluations of paired upstream- and downstream-turbidity data were performed by the on-site managers from East Tennessee Natural Gas to ensure that the difference in the paired turbidity values was within the established threshold. This threshold required that downstream turbidity values could not be 6 FNU, or 15 percent greater than the paired upstream turbidity value. If the established threshold was exceeded for a sustained period of 1 hour, then an on-site inspection was required to ensure sediment was not actively being transported from the construction site. At the monthly and phase-of-construction time step, a signed-rank test was performed on the paired differences of the upstream and downstream turbidity values to

test the null hypothesis that the median paired difference value was equal to zero. If the null hypothesis was accepted, then the construction of pipeline crossing had no effect on downstream sediment conditions; conversely, if the null hypothesis was rejected, then it would be concluded that pipeline construction did affect downstream sediment conditions.

The results of this intensive water-quality monitoring effort indicate that values of turbidity in Indian Creek increased significantly between the upstream and downstream water-quality monitors during the construction of the Jewell Ridge pipeline. The magnitude of the turbidity increase, however, is small (less than 2 FNU). The results from this study indicate that the source of the increased turbidity, detected within the pipeline-crossing easement during construction, primarily can be linked to sediment delivered to Indian Creek from an ephemeral unnamed tributary. The primary source of the sediment in the ephemeral unnamed tributary is from runoff from the upland pipeline construction right-of-way. Conversely, turbidity conditions in the unnamed tributary were not adversely altered during the construction of the pipeline crossing. Turbidity data collected during the active construction of the dry-cut pipeline crossing through the unnamed tributary indicated that turbidity increased downstream; however, the increase in turbidity values was shown to be minimal compared to the turbidity values obtained during natural runoff events.

Acknowledgments

References Cited

Box, J.B., and Mossa, Joann, 1999, Sediment, land use, and freshwater mussels—prospects and problems: Journal of the North American Benthological Society, v. 18, no. 1, p. 99–117.

Buchanan, T.J., and Somers W.P., 1968, Stage measurement at gaging station: U.S. Geological Survey Techniques of Water-Resources Investigations, book 3, chap. A7, 28 p.

Cairns, J., Jr., 1977, Aquatic ecosystem assimilative capacity: Fisheries, v. 2, no. 2, p. 5–7.

Christensen, V.G., 2001, Characterization of surface-water quality based on real-time monitoring and regression analysis, Quivira National Wildlife Refuge, south-central Kansas, December 1998 through June 2001: U.S. Geological Survey Water-Resources Investigations Report 01–4248, 28 p.

Dennison, W.C., Orth, R.J., Moore, K.A., Stevenson, J.C., Carter, Virginia, Kollar, Stan, Bergstrom, P.W., and Batiuk, R.A., 1993, Assessing water quality with submersed aquatic vegetation: BioScience, v. 43, no. 2, p. 86–94.

Fenneman, N.M., 1938, Physiography of Eastern United States: New York, McGraw-Hill Book Company, 714 p.

Griscom, S.B., Fisher, N.S., and Luoma, S.N., 2000, Geochemical influences on assimilation of sediment-bound metals in clams and mussels: Environmental Science & Technology, v. 34, no. 1, p. 91–99.

Hayes, D.C., 1991, Low-flow characteristics of streams in Virginia: U.S. Geological Survey Water-Supply Paper 2374, 69 p.

Helsel, D.R., and Hirsch, R.M., 1992, Statistical methods in water resources: New York, Elsevier, 529 p.

Lenat, D.R., Penrose, D.L., and Eagleson, K.W., 1981, Variable effects of sediment addition on stream benthos: Hydrobiologia, v. 79, no. 2, p. 187–194.

Lévesque, L.M., and Dubé, M.G., 2007, Review of the effects of in-stream pipeline crossing construction on aquatic ecosystems and examination of Canadian methodologies for impact assessment: Environmental Monitoring and Assessment, v. 132, nos. 1–3, p. 395–409.

Lloyd, D.S., Koenings, J.P., and LaPerriere, J.D., 1987, Effects of turbidity in fresh waters of Alaska: North American Journal of Fisheries Management, v. 7, no. 1, p. 18–33.

Madsen, J.D., Chambers, P.A., James, W.F., Koch, E.W., and Westlake, D.F., 2001, The interaction between water movement, sediment dynamics and submersed macrophytes: Hydrobiologia, v. 444, nos. 1–3, p. 61–84.

Phillip, T., Tsui, P., and McCart, P.J., 1981, Effects of stream-crossing by a pipeline on the benthic macroinvertebrate communities of a small mountain stream: Hydrobiologia, v. 79, no. 2, p. 271–276.

Reid, S.M., Ade, F., and Metikosh, S., 2004, Sediment entrainment during pipeline water crossing construction: predictive models and crossing method comparison: Journal of Environmental Engineering and Science, v. 3, p. 81–88.

Reid, S.M., Stoklosar, Scott, Metikosh, Serge, and Evans, Jim, 2002, Effectiveness of isolated pipeline crossing techniques to mitigate sediment impacts on brook trout streams: Water Quality Research Journal of Canada, v. 2, no. 2, p. 473–488.

Ryan, P.A., 1991, Environmental effects of sediment on New Zealand streams—a review: New Zealand Journal of Marine and Freshwater Research, v. 25, p. 207–221.

Tobin, James, 2003, Expansion and change on the U.S. natural gas pipeline network—2002: Energy Information Administration, Office of Oil and Gas May 2003, accessed January 21, 2009, at *http://www.eia.doe.gov/pub/oil_gas/ natural_gas/feature_articles/2003/Pipenet03/pipenet03.html*

True, W.R., 1998, Robust pipeline construction plans threatened by spreading Asian crisis: Oil and Gas Journal, v. 96, p. 37–44.

U.S. Fish and Wildlife Service, 2006 Biological opinion on the Jewell Ridge gas pipeline, East Tennessee Natural Gas, FERC Docket # CP05-413-000, FWS Project # sec7-3511, Smyth and Tazewell Counties, Virginia, accessed August 1, 2008, at *http://www.fws.gov/northeast/endangered/tebo/ PDFs/DukeEnergyIndianCreekBO.pdf*

Wagner, R.J., Mattraw, H.C., Ritz, G.F., and Smith, B.A., 2000, Guidelines and standard procedures for continuous water-quality monitors—Site selection, field operation, calibration, record computation, and reporting: U.S. Geological Survey Water-Resources Investigations Report 00–4252, 53 p.

Walling, D.E., 1977, Assessing the accuracy of suspended sediment rating curves for a small basin: Water Resources Research, v. 13, no. 3, p. 531–538.

Waters, T.F., 1995, Sediment in streams: sources, biological effects, and control: Bethesda Maryland, American Fisheries Society, Bethesda, Maryland, 251 p.

Wolman, M.G., and Miller, J.P., 1960, Magnitude and frequency of forces in the geomorphic processes: Journal of Geology, v. 68, p. 54–74.

Wood, P.J., and Armitage, P.D., 1997, Biological effects of fine sediment in the lotic environment: Environmental Management, v. 21, no. 2, p. 203–217.

Woods, A.J., Omernik, J.M., and Brown, D.D., 1999, Level III and IV Ecoregions of Delaware, Maryland, Pennsylvania, Virginia, and West Virginia: Corvallis, Oregon, U.S. Environmental Protection Agency, accessed August 1, 2008, at *ftp://ftp.epa.gov/wed/ecoregions/reg3/reg3_eco_desc.doc*

Young, R.J., and Mackie, G.L., 1991, Effect of oil pipeline construction on the benthic invertebrate community structure of Hodgson Creek, Northwest Territories: Canadian Journal of Zoology, v. 69, p. 2154–2160.

Zwirn, M., 2002, Pipeline-stream crossing installation—best management practices, accessed August 1, 2008, at *http:// www.wildsalmoncenter.org/pipeline-stream-english.pdf*

Appendixes 1–6

The following appendixes provide graphs showing continuous water-quality data collected from Indian Creek and an unnamed tributary, Tazewell County, Virginia.
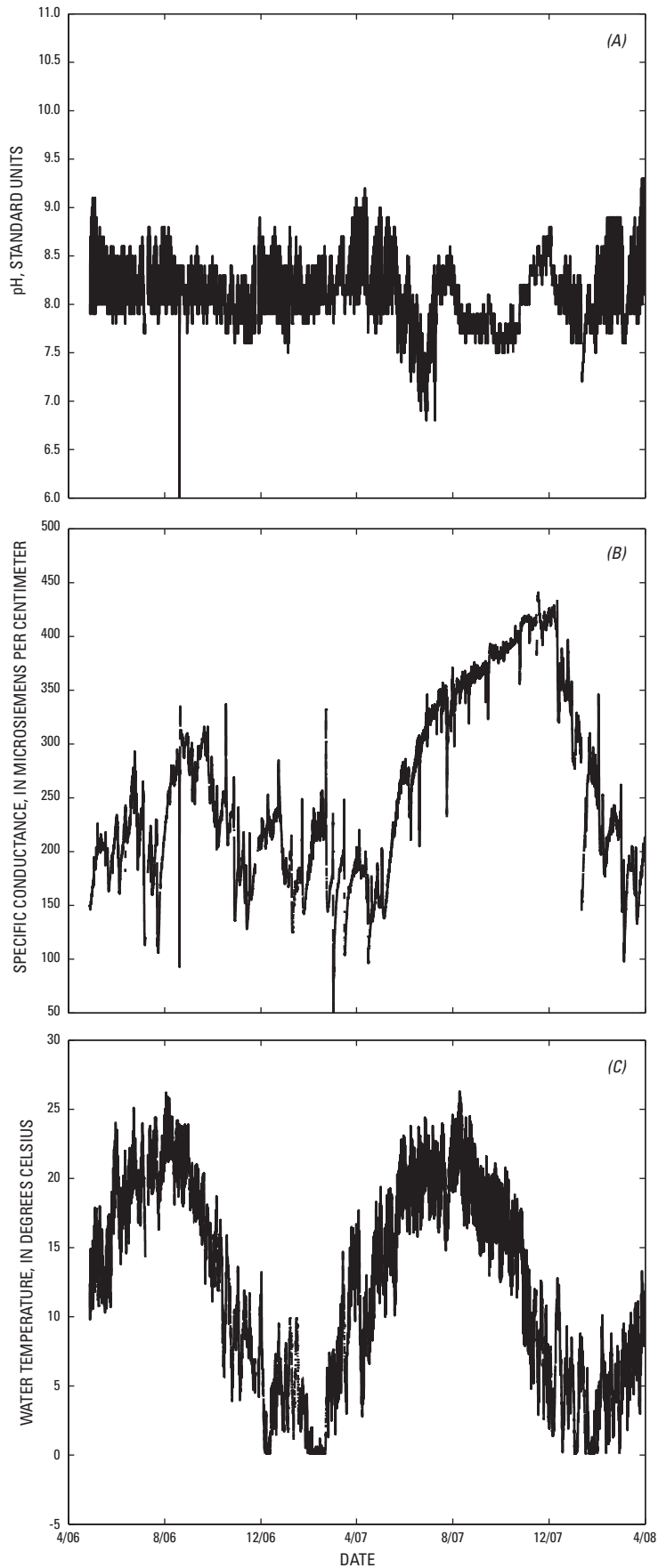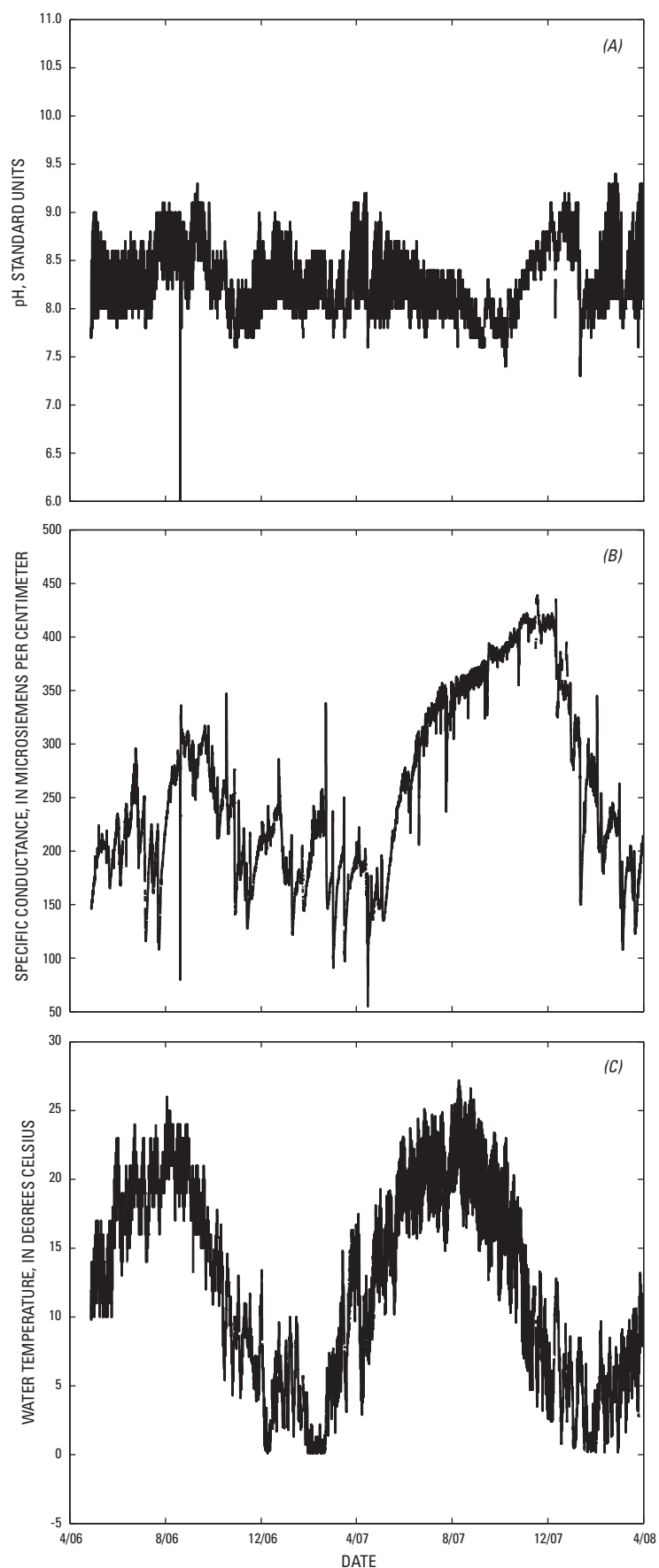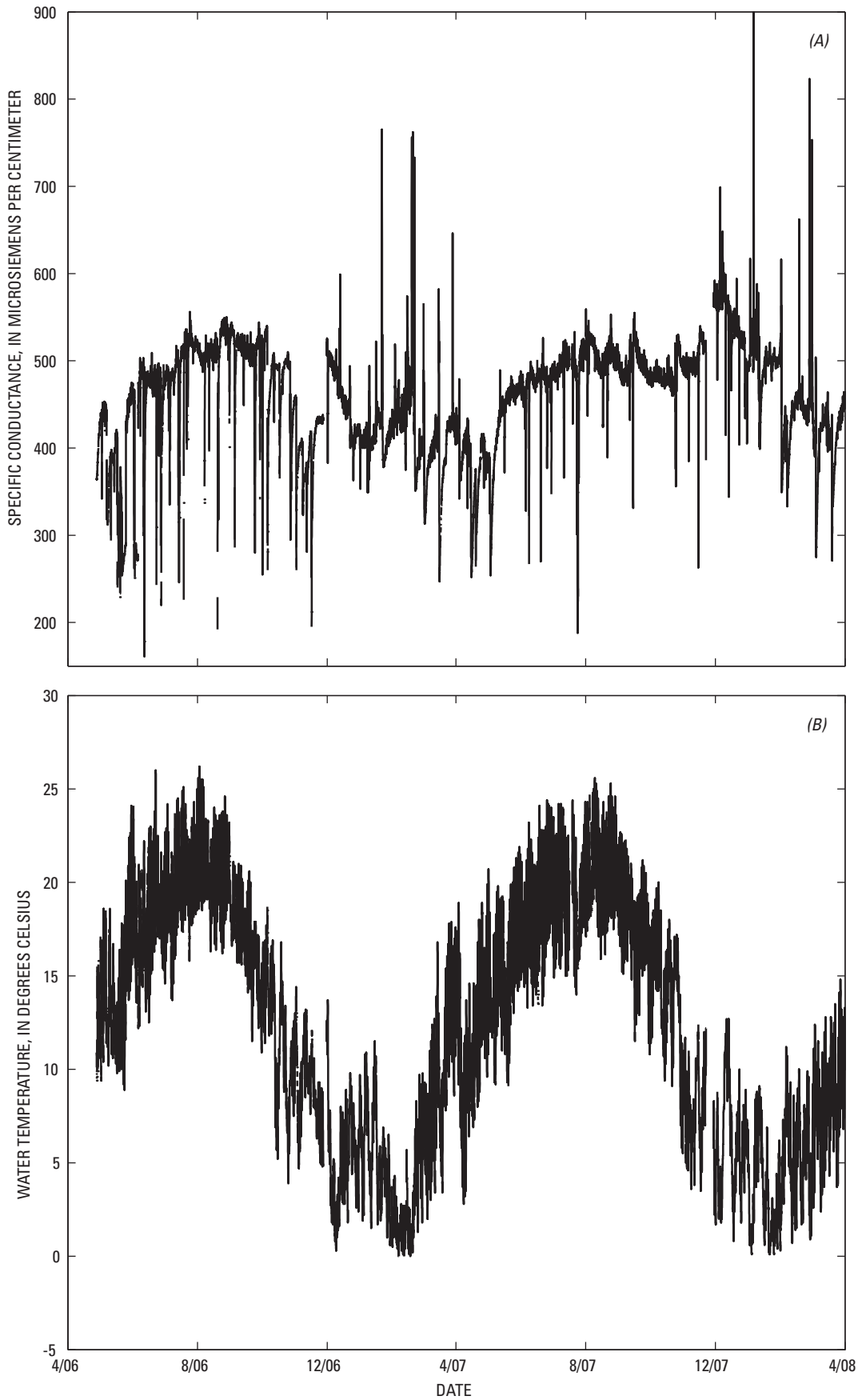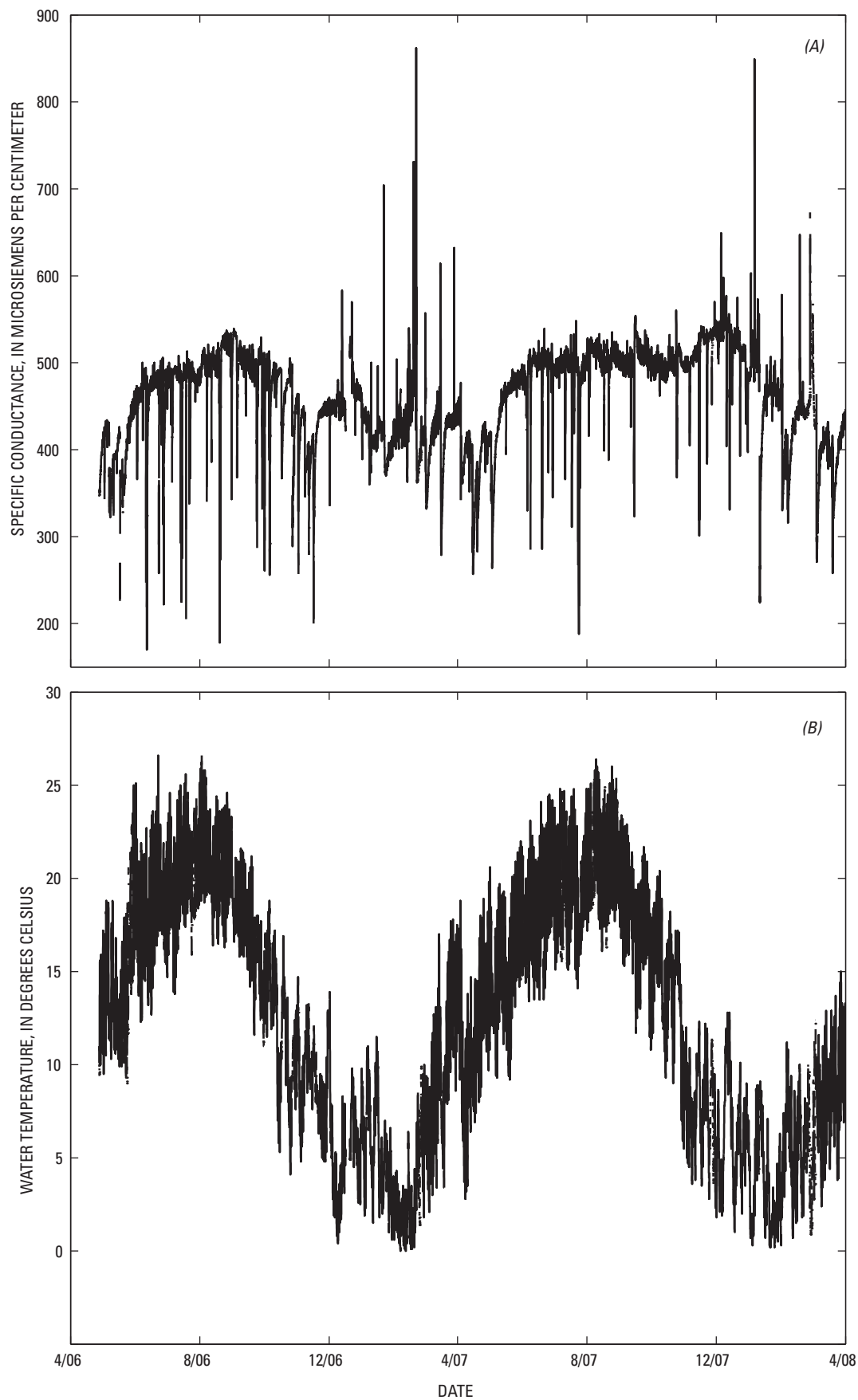
Appendix 1. Continuous water-quality data (15-minute interval) collected from Indian Creek, Tazewell County, Virginia, at the upstream (Station number 03520967) left-bank water-quality monitor: (*A*) pH, (*B*) specific conductance, and (*C*) water temperature.
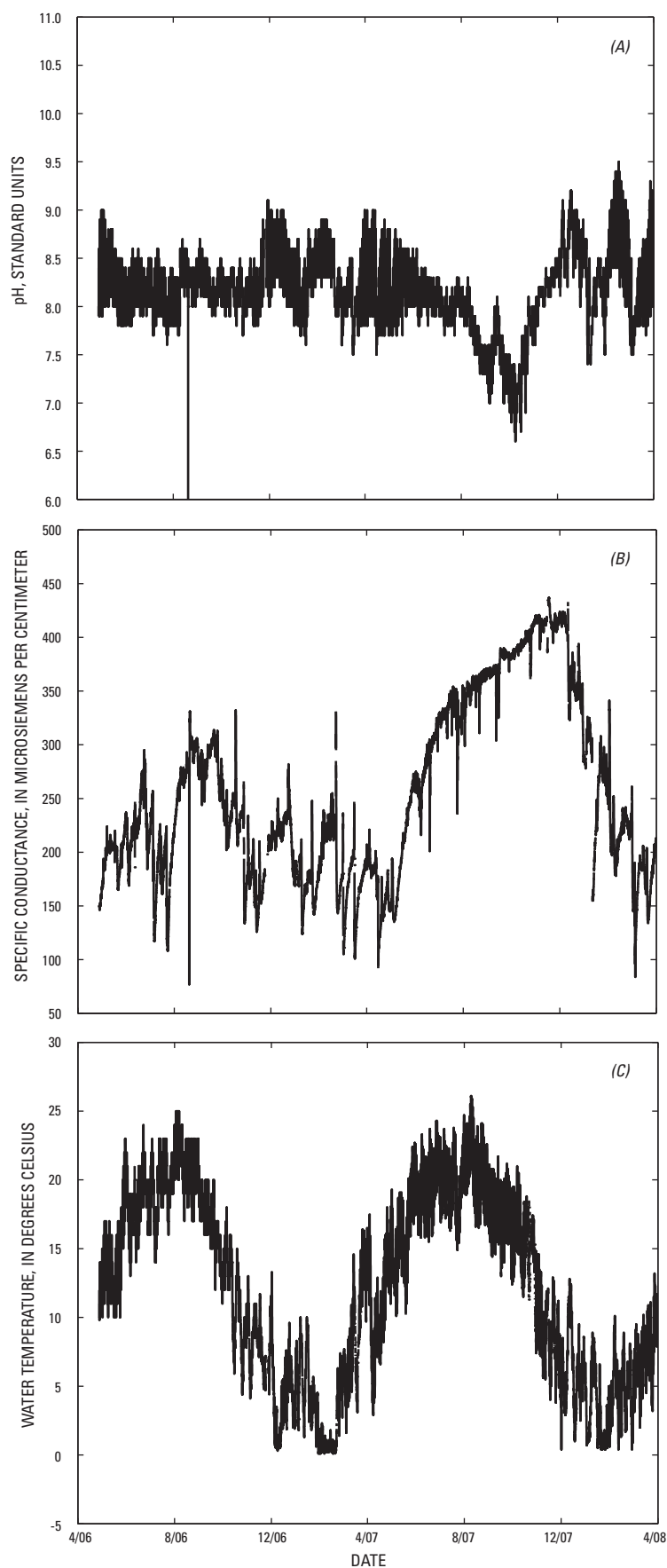
Appendix 2. Continuous water-quality data (15-minute interval) collected from Indian Creek, Tazewell County, Virginia, at the upstream (Station number 03520967) right-bank water-quality monitor: (*A*) pH, (*B*) specific conductance, and (*C*) water temperature.
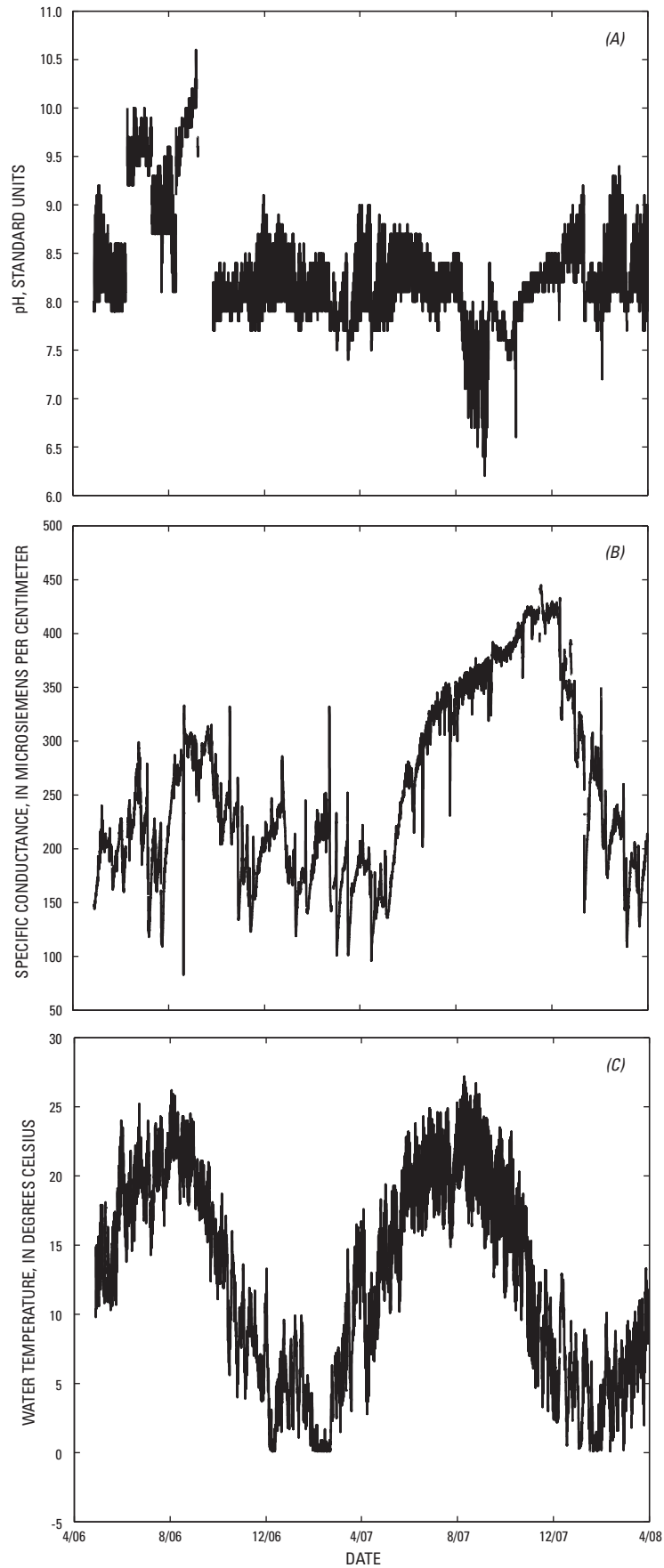
Appendix 3. Continuous water-quality data (15-minute interval) collected from Indian Creek, Tazewell County, Virginia, at the downstream (Station number 03520968) left-bank water-quality monitor: (*A*) pH, (*B*) specific conductance, and (*C*) water temperature.

Appendix 4.   Continuous water-quality data (15-minute interval) collected from Indian Creek, Tazewell County, Virginia, at the downstream (Station number 03520968) right-bank water-quality monitor: (*A*) pH, (*B*) specific conductance, and (*C*) water temperature.

Appendix 5. Continuous water-quality data (15-minute interval) collected from the unnamed tributary, Tazewell County, Virginia, at the upstream (Station number 03520980) water-quality monitor: (*A*) specific conductance and (*B*) water temperature.

Appendix 6. Continuous water-quality data (15-minute interval) collected from the unnamed tributary, Tazewell County, Virginia, at the downstream (Station number 03520981) water-quality monitor: (*A*) specific conductance and (*B*) water temperature.

USGS

Attachment 3

Attachment 4

Mountain Valley

Sedimentation Analysis – Discussion of Erosion and Sedimentation Control Containment Percentage

Field-scale tests represent a compromise between laboratory and field tests, allowing for the ability to incorporate conditions relevant to typical installations while operating in a controlled environment that allows for standardized testing procedures. Field-scale testing has become common practice for the assessment of erosion and sedimentation control best management practices (BMPs) or sediment retention devices because they incorporate full-scale, "as installed" conditions. A recent study involving field-scale testing conducted by Dubinsky (2014) evaluated containment at a variety of slopes and rainfall events and found that overall average projected performance efficiency ranged from 48 to 87 percent with a mean and median of 79 and 86 percent, respectively. The 79% from Dubinsky (2014) represents a reasonable expectation of overall performance efficiency.

In addition, these field-scale tests look exclusively at the performance of the perimeter control in isolation without consideration of other erosion controls and sediment detention devices. Mountain Valley intends to use a variety of BMPs in addition to sediment barriers that will further limit soil erosion and slow and/or pond runoff to encourage sedimentation within the limits of disturbance rather than at the sediment perimeter control. In combination, these measures will reasonably attain a sediment containment of 79% or higher.

Mountain Valley recognizes and understands the variability in sediment control performance as a function of proper installation and maintenance. For that reason Mountain Valley is committed to proper installation, maintenance, and frequent inspections to reduce BMP failures or inadequacies.

Mountain Valley explicitly requires that all Company and Contractor personnel comply with environmental permits authorizing the construction, operation, and restoration of the Project and requires all Company and Contractor personnel to immediately notify the Mountain Valley Environmental Coordinator and the EI when there is the potential for noncompliance, including any visible sedimentation outside of the limits of disturbance, so that the issue can be resolved in a timely and appropriate manner.

It is also important to note that in sensitive areas of the Jefferson National Forest, such as the Craig Creek drainage, Mountain Valley committed to construction during times of the year with minimal rainfall (i.e., low flow time periods). Within the Craig Creek drainage, Mountain Valley committed to an expedited time frame that reduces the chance (through reduced exposure) of a large rainfall event occurring during active construction. These additional conservation measures will help ensure that erosion is minimized, thus limiting sedimentation in adjacent waterbodies.

percent with a mean and median of 79 and 86 percent, respectively. The 79% from Dubinsky (2014) represents a reasonable expectation of overall performance efficiency.

In addition, these field-scale tests look exclusively at the performance of the perimeter control in isolation without consideration of other erosion controls and sediment detention devices. Mountain Valley intends to use a variety of BMPs in addition to sediment barriers that will further limit soil erosion and slow and/or pond runoff to encourage sedimentation within the limits of disturbance rather than at the sediment perimeter control. In combination, these measures will reasonably attain a sediment containment of 79% or higher.

Mountain Valley recognizes and understands the variability in sediment control performance as a function of proper installation and maintenance. For that reason Mountain Valley is committed to proper installation, maintenance, and frequent inspections to reduce BMP failures or inadequacies.

Mountain Valley explicitly requires that all Company and Contractor personnel comply with environmental permits authorizing the construction, operation, and restoration of the Project and requires all Company and Contractor personnel to immediately notify the Mountain Valley Environmental Coordinator and the EI when there is the potential for noncompliance, including any visible sedimentation outside of the limits of disturbance, so that the issue can be resolved in a timely and appropriate manner.

It is also important to note that in sensitive areas of the Jefferson National Forest, such as the Craig Creek drainage, Mountain Valley committed to construction during times of the year with minimal rainfall (i.e., low flow time periods). Within the Craig Creek drainage, Mountain Valley committed to an expedited time frame that reduces the chance (through reduced exposure) of a large rainfall event occurring during active construction. These additional conservation measures will help ensure that erosion is minimized, thus limiting sedimentation in adjacent waterbodies.